ELECTROFUSION
OF CELLS ON CHIP

FROM A STATIC, PARALLEL APPROACH TO A
HIGH-THROUGHPUT, SERIAL, MICRODROPLET PLATFORM

Evelien Kemna

ELECTROFUSION OF CELLS ON CHIP

FROM A STATIC, PARALLEL APPROACH TO A HIGH-THROUGHPUT, SERIAL, MICRODROPLET PLATFORM

Evelien Kemna

November 15th 2013

The research described in this thesis was carried out at the BIOS lab on Chip group of the MESA+ institute for Nanotechnology of the University of Twente, Enschede, The Netherlands. The research was financially supported by European Research Council (ERC) through the ERC advanced grant titled 'Elab$_4$life'.

Members of the committee:

Chairman	Prof.dr. J. Schmitz	University of Twente
Promotor	Prof.dr.ir. A. van den Berg	University of Twente
Assistant promotor	Dr. F. Wolbers	Eindhoven University
Members	Prof. Dr. L.W.M.M. Terstappen	University of Twente
	Prof.dr. H.B.J. Karperien	University of Twente
	Prof. D.A. Weitz	Harvard University
	Prof.dr. I. Vermes	University of Twente
	Prof.W.T.S. Huck	Radboud University

Author	Evelien Kemna
Title	Electrofusion of cells on chip. From a static, parallel approach to a high-throughput, serial, microdroplet platform PhD thesis, University of Twente, The Netherlands
ISBN	978-90-365-0825-4
DOI	10.3990/1.9789036508254
Publisher	Wohrmann Print Service, Zuthphen, The Netherlands
Cover design	Leon Rolefes

ELECTROFUSION OF CELLS ON CHIP

FROM A STATIC, PARALLEL APPROACH TO A HIGH-THROUGHPUT, SERIAL, MICRODROPLET PLATFORM

PROEFSCHRIFT

ter verkrijging van
de graad van doctor aan de Universiteit Twente,
op gezag van de rector magnificus,
prof.dr. H. Brinksma,
volgens het besluit van het College voor Promoties
in het openbaar te verdedigen
op vrijdag 15 november 2013 om 14.45

door

Evelien Willemijn Maria Kemna
geboren op 24 juni 1985
te Almelo

Dit proefschrift is goedgekeurd door:

Promotor	Prof.dr.ir. A. van den Berg
Assistent promotor	Dr. F. Wolbers

ISBN 978-90-365-0825-4

Contents

Page

On chip electrofusion of single human B-cells and mouse myeloma cells

CHAPTER 4

Droplet microfluidics: A review

CHAPTER 5

High-yield cell ordering and deterministic cell-in-droplet encapsulation

CHAPTER 6

Label-free, high-throughput electrical detection of cells in droplets

CHAPTER 7

Electrofusion of cells in droplets

CHAPTER 8

Summary and outlook

CHAPTER 9

AIM AND OUTLINE

CHAPTER 1

The problem description and the goal of this thesis "Electrofusion of cells on chip" are described in this chapter. This project is funded by the European Research Council as part of the ^{e}lab4life grant. A brief introduction of the process of cellular electrofusion is given, followed by our aim. This chapter is concluded with an outline of this thesis.

1.1 Electrofusion of cells

Currently, there is an increasing need for the development of antibodies for research, as well as for diagnostic and therapeutic purposes[1, 2]. The production of monoclonal antibodies primarily relies on the creation of antibody-secreting hybridomas[2, 3]. These hybridoma's are obtained via cell fusion. Cell fusion is a process, fusing two cell types to generate a third cell (hybrid cell)[4, 5]. Since the hybrid cell contains genetic material from two different parent cells, it displays the characteristics of both cells.
The first fusion phenomenon was observed almost two centuries ago, by the German biologist Johannes Muller[6, 7]. An important step in the history of cell fusion was made by Milstein and Kohler in 1975[8, 9]. They developed a hybridoma technology based on the fusion of somatic cells. Activated mouse B lymphocytes, which have a short lifespan *in vitro* and hence produce antibodies only briefly, were fused with mouse myeloma cells, which proliferate rapidly *in vitro* due to their cancer characteristics, and a hybridoma cell was formed, for the prolonged production of antibodies.

There are different methods to fuse cells, *e.g.,* using chemicals, viruses or electrical pulses. The latter one, called electrofusion, is the most efficient method for cell fusion[3, 4, 10-12]. Conventionally, electrofusion occurs in a fusion chamber under the influence of an electric field. However, the lack of control over the process is a severe drawback, since random cell-pairing leads to unwanted fusion products that afterwards must be removed from the functional fusion products. Additionally, commercially available systems often create undefined or poor cell–cell contact which leads to low fusion yields[10, 11, 13-17] and, thus, require working with large cell numbers. Moreover, conventional methods utilizes hundreds of microliters of cell suspension. As a consequence, the fusion of rare cell populations is hardly possible. Furthermore, because of the large distance between the electrodes, an expensive high voltage generator has to be used in order to generate a sufficiently high electrical field. Using conventional electrofusion, it is therefore time-consuming to vary electrical, biological and/or chemical parameters.

To overcome these limitations, microfluidic technology is used to develop microchips for cell electrofusion. These microfluidic devices
provide a high control over cell pairing and the fusion process[18, 19]. Furthermore, microtechnology enables the use of lower quantities of cells and media and allows to work with lower voltages. Hence, due to the increasing need for (human) antibodies, research is driven to find a more efficient method for electrofusion of cells and subsequent antibody producing hybridoma generation.

Due to PhD project of dr A. Valero 'Single cell electroporation on chip'[20-22] at the BIOS group, the company ModiQuest B.V. approached Prof. A. van den Berg with the question if, besides electroporation, electrofusion of cells on chip was possible and could contribute to current methods. As a result, preliminary research was conducted and a PhD project proposal was written.

The ultimate aim of this PhD project is the development of a microdevice to efficiently electrofuse human B-cells with myeloma cells for the high-yield generation of antibody producing hybridoma's. Furthermore, integration of this device with the isolation of B-cells and/or cultivation of the hybridoma's, is preferred. In this thesis, a step towards an efficient and complete electrofusion system is made.
This PhD project is funded by the European Research Council's Seventh Framework Programme as part of the elab4life grant. [e]Lab4life focuses on the development of electrical labs-on-a-chip for health and life sciences.

1.2 Thesis outline

To define a theoretical background for the experimental chapters, the fundamentals of electrofusion and the status of current electrofusion techniques are described in chapter 2. A short historic overview and the principals of electrofusion are given. The conventional technique for electrofusion is described, as well as the drawbacks of this method. At the end of chapter 2, a review of microfluidic devices for electrofusion of cells is presented.

For performing successful and efficient electrofusion on chip, both the microfluidic device and experimental set-up need to meet certain requirements. Therefore, is it of importance to gain insight in all the different parameters, which (might) influence the efficiency of electrofusion. Chapter 3 evaluates, which microfluidic device and experimental set-up are best suited for efficient electrofusion on chip. This entails the cellular requirements as well as the necessary microfluidic requirements, plus the final hybridoma culture and antibody production analysis.

Chapter 4 shows the development and characterization of a static, parallel approach for the demonstration and evaluation of cell electrofusion on chip. After that the subsequent chapters asses the use of a high-throughput, serial, microdroplet platform. But first, a single cell electrofusion chip using traps (static approach) is designed, based on the work of Skelley et al.[18]. This device demonstrated high electrofusion efficiencies in literature[18]. We have optimized and adapted this design for the electrofusion of single B-cells and myeloma cells for hybridoma formation. Moreover, the trap structure is designed such that it provides an optimal electric field distribution regarding cell fusion of different sized cells. The obtained results are reported in chapter 4.

As the described design in chapter 4 is not high-throughput, an alternative method, the droplet-based platform, is introduced. The main advantage of the droplet platform is the high-throughput (kHz) encapsulation of cells in discrete volumes. Droplet-based microfluidic systems have been used for various biotechnology research applications[23-25] in the last years. An introduction to this field is given in chapter 5. This entails the droplet generation mechanisms as well as the droplet manipulation techniques. Different biomedical applications of the droplet platform are discussed, with great potency to improve the current method for hybridoma generation and selection. In order to

generate hybridomas in a high-throughput fashion and with high efficiency, the microfluidic system needs several properties. The microfluidic system should contain high-speed single cell droplet encapsulation, droplet pairing, droplet electrofusion and droplet shrinkage, followed by cell-cell in droplet electrofusion and hybridoma selection.

We encountered that cell encapsulation is dictated by Poisson statistics, so a maximum of 37% of the generated droplets contain a single cell. This strongly influences the efficiency of the final system. Therefore, in chapter 6, we focus on a deterministic encapsulation technique.

Although, the encapsulation efficiency was greatly improved to nearly 80%, it was not possible to obtain 100%. However, the encapsulation efficiency can be improved by coupling the device to an integrated impedance analyser. In chapter 7, we describe a label-free method to detect the presence of cells in droplets for sorting and selection purposes. The presence of viable cells encapsulated in low-conducting buffer is detected by a decrease in impedance. The sensitivity and positive/negative predictive value of the label-free detection method was determined.

The further development of the droplet-based electrofusion device is described in chapter 8. This chapter starts with the encapsulation of cells and subsequent fusion of droplets, to obtain one droplet with two cells. The droplet volume is reduced to induce cell-cell contact, which is critical for electrofusion. Before starting with the electrofusion experiments, it is important to characterize the electric field inside a droplet. Therefore, simulations experiments are performed, followed by the electroporation of cells in droplets. Finally, electrofusion of cells in droplets is shown in detail at a cellular level. Nevertheless, the efficiency remains low and needs further optimization.

In chapter 9, the results of this thesis are summarized, followed by recommendations regarding the further development and improvements of the droplet-based electrofusion platform.

1.3 References

1. Sullivan, S. and K. Eggan, *The potential of cell fusion for human therapy*. Stem Cell Reviews, 2006. **2**(4): p. 341-349.
2. Alkan, S.S., *Landmark - Monoclonal antibodies: the story of a discovery that revolutionized science and medicine*. Nature Reviews Immunology, 2004. **4**(2): p. 153-156.
3. Zimmermann, U., et al., *Electro-fusion of cells: principles and potential for the future*. Ciba Found Symp, 1984. **103**: p. 60-85.
4. Neumann, E., Gerisch, G., Opatz, K., *Cell Fusion Induced by High Electric to Dictyostelium*. Naturwissenschaften, 1980. **67**: p. 414.
5. Weber, H., et al., *Microbiological implications of electric field effects. III. Stimulation of yeast protoplast fusion by electric field pulses*. Z Allg Mikrobiol, 1981. **21**(7): p. 555-62.
6. Ringertz, N.R.a.R.E.S., *Cell Hybrids* 1976 New York: Academic Press.
7. Dimitrov, D.S., *Electroporation and electrofusion of membranes*, in *Handbook of biological physics*, R. Lipowsky, Sackmann, E., Editor. 1995, Elsevier science.

8. Kohler, G. and C. Milstein, *Continuous cultures of fused cells secreting antibody of predefined specificity*. Nature, 1975. **256**(5517): p. 495-7.
9. Abhyankar, V.V., Beebe, D.J., *Human embryonic stem cells & microfluidics*, in *Lab-on-Chips for Cellomics, micro and nanotechnologies for life science*, H. Andersson, van den Berg, A., Editor. 2004, Kluwer Academic Publishers: Dordrecht, The Netherlands.
10. Karsten, U., et al., *Direct comparison of electric field-mediated and PEG-mediated cell fusion for the generation of antibody producing hybridomas*. Hybridoma, 1988. **7**(6): p. 627-33.
11. Steenbakkers, P.G., H.A. Hubers, and A.W. Rijnders, *Efficient generation of monoclonal antibodies from preselected antigen-specific B cells. Efficient immortalization of preselected B cells*. Mol Biol Rep, 1994. **19**(2): p. 125-34.
12. Steenbakkers, P.G.A., F.C.M. Vanmeel, and W. Olijve, *A New Approach to the Generation of Human or Murine Antibody-Producing Hybridomas*. Journal of Immunological Methods, 1992. **152**(1): p. 69-77.
13. Jahn, S., et al., *Establishment of human Ig producing heterohybridomas by fusion of mouse myeloma cells with human lymphocytes derived from peripheral blood, bone marrow, spleen, lymph node, and synovial fluid. Effect of polyclonal prestimulation and cryopreservation*. J Immunol Methods, 1988. **107**(1): p. 59-66.
14. Kwekkeboom, J., C. de Groot, and J.M. Tager, *Efficient electric field-induced generation of hybridomas from human B lymphocytes without prior activation in vitro*. Hum Antibodies Hybridomas, 1992. **3**(1): p. 48-53.
15. Stromberg, A., et al., *Microfluidic device for combinatorial fusion of liposomes and cells*. Anal Chem, 2001. **73**(1): p. 126-30.
16. Trontelj, K., et al., *Optimization of bulk cell electrofusion in vitro for production of human-mouse heterohybridoma cells*. Bioelectrochemistry, 2008. **74**(1): p. 124-9.
17. Vanduijn, G., et al., *High Yields of Specific Hybridomas Obtained by Electrofusion of Murine Lymphocytes Immunized Invivo or Invitro*. Experimental Cell Research, 1989. **183**(2): p. 463-472.
18. Skelley, A.M., et al., *Microfluidic control of cell pairing and fusion*. Nat Methods, 2009.
19. Cao, Y., Yang, J., Yin, Z.Q., Luo, H.Y., Yang, M., Yang, N.H.J., Huo, D.Q., Hou, C.J., Jiang, Z.Z., Zhang, R.Q., Xu, R., Zheng, R.L., *Study of high-throughput cell electrofusion in a microelectrode-array chip*. Microfluid Nanofluid, 2008. **5**(5): p. 669-675.
20. Valero, A., et al., *Gene transfer and protein dynamics in stem cells using single cell electroporation in a microfluidic device*. Lab on a Chip, 2008. **8**(1): p. 62-67.
21. Valero, A., et al., *Apoptotic cell death dynamics of HL60 cells studied using a microfluidic cell trap device*. Lab on a Chip, 2005. **5**(1): p. 49-55.
22. Valero, A., *Single cell electroporation*, in *BIOS Lab-on-a-Chip group of the MESA+ Institute for Nanotechnology*. 2006, University of Twente: Enschede, The Netherlands. p. 209.
23. Teh, S.Y., et al., *Droplet microfluidics*. Lab Chip, 2008. **8**(2): p. 198-220.
24. Wheeler, A.R., et al., *Digital microfluidics for cell-based assays*. Lab on a Chip, 2008. **8**(4): p. 519-526.
25. Whitesides, G.M., *The origins and the future of microfluidics*. Nature, 2006. **442**(7101): p. 368-73.

ELECTROFUSION OF CELLS: FUNDAMENTALS AND CURRENT STATUS

CHAPTER 2

In this chapter the fusion of cells, using electrical fields, is presented. This is referred to as electrofusion. An historical overview, principles and possible application of cell fusion are shown. The ability to perform single cell electrofusion using microtechnology is discussed and a review is given on current microfluidic electrofusion devices for the fusion of liposomes and cells.

2.1 Introduction

All animal and plant tissues consist of cells and these cells are the integral units of life. It is believed that the fusion of cells is of central importance for development, repair of tissues and the pathogenesis of disease[1]. Cell fusion was originally discovered *in vivo* in animal cells as a natural phenomenon[2]. It is involved in a variety of life processes today, i.e. during fertilization, development of skeletal muscle and bone[1, 3]. The fusion products are believed to possess enhanced functions compared to their unfused progenitors[4, 5]. Furthermore, cell-to-cell fusion can also be induced *in vitro,* which plays an important role in areas such as biotechnology and medicine[6-8]. In this chapter the focus lies on the generation of monoclonal antibody (Ab)-secreting hybridomas using cell fusion.

Firstly, cell fusion and its history, is reviewed briefly (section 2.2 and 2.3). This is followed by principles of electrofusion and the effects of an electric field on cells in section 2.4. Next, the conventional bulk electrofusion (section 2.5) is shown. In section 2.6, the contribution of microfluidics to the current electrofusion technology is discussed. In section 2.7, an overview of electrofusion microdevices that are currently available is given. Finally, concluding remarks are made in section 2.8.

2.2 Historical overview of cell fusion

The first fusion phenomenon was observed almost two centuries ago, by the German biologist Johannes Muller[2, 9]. He discovered multinucleated giant cells and raised the question whether these originated from successive mitoses or from mononucleated cell fusion. Later, cell fusion was clearly established as the mode of formation of the multinucleated giant cells, but it was not until the 1960s, when the studies of fusion expanded significantly[9]. A number of interesting fusion phenomena were discovered during a short period of time[10, 11 12]. An important step was made by Milstein and Kohler in 1975[13, 14]. They developed a B lymphocyte hybridoma technology based on the fusion of somatic cells. Activated mouse B lymphocytes, which have a short lifespan *in vitro*, were fused with mouse myeloma cells, which proliferate rapidly *in vitro,* and a hybridoma cell was formed. Fusion was induced using virus based methods. The resulting hybridoma not only retained the rapidly proliferating capacity of the myeloma cells, but also inherited the antibody synthesizing and secretory capacity of the B lymphocytes. Therefore, it could secrete antibodies for longer periods. They were awarded with a Nobel Prize for this revolutionary technology[11]. Due to the great potential of this technology in the biological, medical and pharmaceutical fields, many physicists, electronic engineers and biologists devoted themselves to the development of a good cell-fusion method.

2.3 Cell fusion

Cell fusion is a process, fusing two cell types to generate a third cell (hybrid cell) (figure 2.1)[15, 16]. Since the hybrid cell contains genetic matter from two different parent cells, it

displays characteristics of both cells. Cell fusion plays a central role in biotechnology, with applications including, cloning of mammals, determining the genetic make-up of organisms or vaccination against cancer[17]. Moreover, cell fusion plays a crucial role in the generation of monoclonal Ab-secreting hybridomas[9, 18-24].

For complete cell fusion, the membranes have to be in close contact. The resulting cell still contains two separate nuclei, therefore nuclear fusion the next step (figure 2.1). Membrane fusion can be induced by several methods. However, nuclear fusion is a random process which cannot be influenced and occurs 1-2 weeks after membrane fusion. The resulting cell has to recombine the genetic make-up and this results in a hybrid cell.

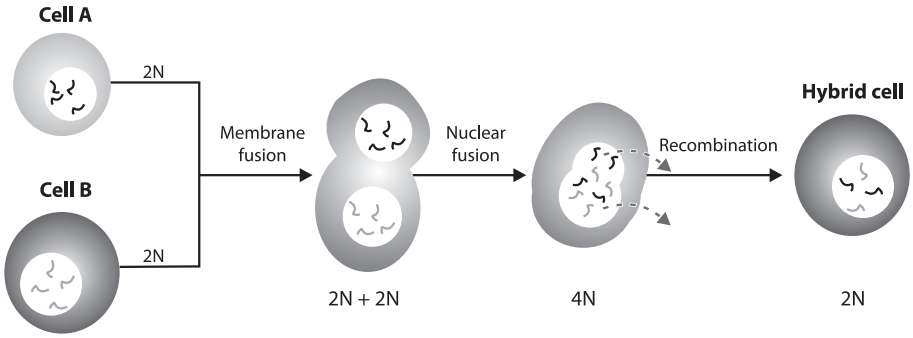

Figure 2.1: Schematic overview of cell-cell fusion, generating a hybrid cell. Cells of different lineages fuse to form a cell with double nuclei (2N+2N). Next, nuclear fusion occurs and the fused nucleus initially contains the complete chromosomal content of both fusion partners (4N). Ultimately chromosomes are cast out and/or re-sorted and a hybrid cell is formed displaying characteristics of both cell A and B.

2.3.1 Fusion methods

Up till now, several approaches have been carried out to induce cell fusion. As mentioned before, chemical and virus-based fusion methods were developed in the earlier years.

Chemical fusion is based on the application of chemical fusogens, such as polyethylene glycol (PEG)[25-27]. PEG induces cell agglutination and cell-cell contact, leading to subsequent cell fusion. The detailed mechanism underlying PEG-mediated cell fusion is not fully known. However, studies indicate that small perturbations in lipid packing within contacting membranes are necessary and probably sufficient to promote membrane fusion[28, 29]. For virus-based fusion several different fusogenic viruses, such as Epstein Barr were used[30 31]. Also virus based fusion mechanisms are not fully elucidated. It is described that several cell surface proteins, including members of the ADAM (a disintegrin and metalloproteinase) gene family, have emerged as candidate adhesion/fusion proteins[32]. Furthermore, the use of focused laser beams (laser-induced

fusion) was developed[33]. However, all these methods have been associated with several limitations such as toxicity to cells, batch to batch variability, and low efficiency (both fusion and functional hybridoma generation).

In the late 1970s, it was reported that cell fusion can also be induced by external electric fields, referred to as electrofusion[15, 16, 34]. Electrofusion overcomes the mentioned limitations of conventional chemical or virus-based cell fusion and has several advantages[35, 36]. Firstly, electrofusion is a physical method and can be applied to a much wider selection of cell types with high post-fusion viability. Secondly, it is an easy and reproducible fusion technique[15, 37].

2.4 Electrofusion

The first publication on electrofusion was published by Senda et al[38]. In this paper plant protoplast were fused using electrical fields. By then it was already well established that high-voltage fields could induce (1) reversible breakdown of the electrical resistance of the cell membrane, (2) transient loss of semi-permeability, and (3) the exchange of intracellular and extracellular materials. In the early 1980s, Zimmermann's group[37, 39] utilized dielectrophoresis (DEP) to facilitate cell-cell contact, hence making the electrofusion method more widely useful and gaining higher fusion efficiencies than traditional chemical or virus-based methods. Moreover, besides electrofusion of plant cells, fusion between mammalian cells was shown[40]. A large amount of today's work is based on those early papers of Zimmerman[8, 37, 39-43].

Even though electrofusion experiences increasing use, the fusion mechanism is still poorly understood. It can be stated that electrofusion is a multistep process and requires close contact between the membranes. There are several approaches regarding the explanation of electrofusion reported in literature[37, 40, 44-52]. It is generally accepted that the phenomenon of electrofusion is closely related to that of electroporation[18, 53-55]. Furthermore, destabilization of the membranes followed by appropriate rearrangements of the lipid matrix is thought to be involved in electrofusion. Still, the molecular mechanisms are unknown and new approaches are needed for their elucidation[9]. Understanding the mechanisms of electrofusion is not only of practical importance for its optimization but is of help in understanding the fundamentals of *in vitro* fusion.

Overall, electrofusion has developed into an efficient method for the fusion of mammalian cells, and has been widely used in biological experiments, from the formation of hybridomas[22] to the production of cloned offspring, like the sheep Dolly[56]. In this thesis the focus lies on the generation of monoclonal Ab-secreting hybridomas. Despite of the wide use of electrofusion, the fusion efficiency regarding hybridoma generation still remains very low[20-22, 36, 57-59], and is in the order of 0.001%.

Next, the underlying principles of electrofusion regarding mammalian cells are elucidated.

2.4.1 Electrofusion principles

Generally, the electrofusion process is composed of three phases: cell alignment (pairing), electroporation and fusion (figure 2.2). Firstly, cell alignment is achieved by suspending the cell mixture in a weakly conductive fusion medium. Next, this cell mixture is subjected to a non-uniform alternating-current field (AC field) of moderate intensity (around 100–300 V/cm) and high-frequency (around 1–3 MHz) to bring the fusion partners into close contact by DEP. This is one of the most widely used and convenient way to induce cell-cell contact, called pearl chain formation (figure 2.3). Secondly, one or more short-duration (around 10–100 µs) and high-strength (around 1–10 kV/cm) direct-current (DC) pulses are applied to induce pore formation (electroporation) in the contact zones, which subsequently initiates fusion of adjacent cells. Finally, post-alignment using DEP ensures the cell-cell contact during the closure of the pores. Coupled to the closure of the pores, the cell membrane is reconstructed and the contacted cells are fused to form a hybrid cell[60]. The parameters for electrofusion are cell specific, and therefore for example dependent of cell size and cell type[33]. Furthermore, it is known that a number of chemical (*e.g.* buffer composition) and electrical factors (*e.g.* number of pulses) affect the yield of electrofusion[37, 44, 61]. Learning what factors have major or minor effects on the fusion process will provide clues to the mechanism and will optimize the electrofusion efficiency of the cells of interest.

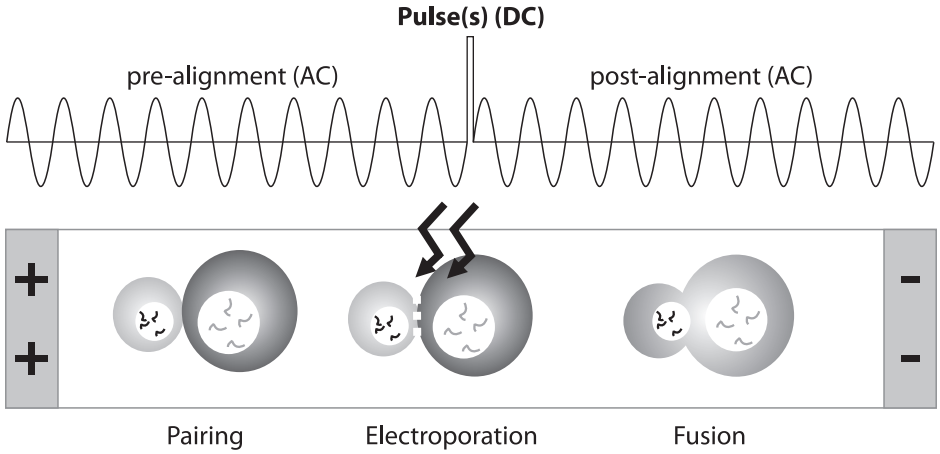

Figure 2.2: Basic theory of cell electrofusion.: Cell electrofusion is composed of three continuous processes: cell alignment (pairing), electroporation and fusion, all induced by a series of electrical signals

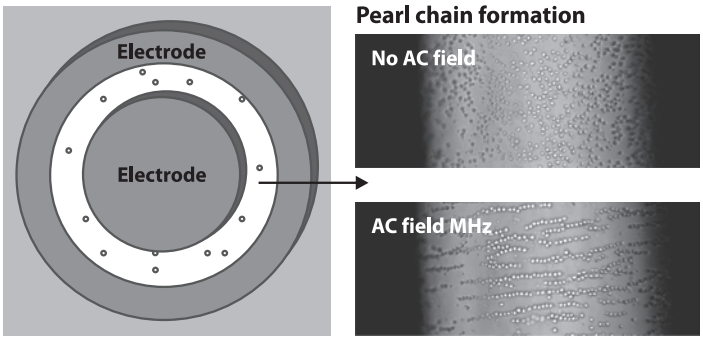

Figure 2.3: Pearl chain formation of a cell suspension under influence of a AC field in the order of MHz [62]

2.4.2 Polarization of cells in an electric field

When subjected to an electric field, dielectric particles, such as cells, experience a range of electrokinetic forces, pressures and torques[63]. An external electric field can induce formation of pores in cell membranes, move cells by DEP and fuse membranes[64]. These effects are based on the electrostatic interactions of the induced cell dipole with the applied field.

The dielectric properties of cells are described by the permittivity ε and the conductivity σ. The permittivity is defined as ability of a material to permit the formation of an electric field. In other words, permittivity is the charge density in response to an electric field. The conductivity is how strongly a given material opposes the flow of electric currents. In other words, conductivity is the current density in response to an electrical field[65].

When examining the frequency scale, it is found that different dispersions occur at different frequencies (figure 2.4 A). The α-dispersion, around a frequency of 10^2 Hz, is caused by the ionic diffusion effects. At the range of 10^4 – 10^7 Hz, the operation range of electrofusion, interfacial polarization (β-dispersion) is occurring[66, 67]. β-Dispersion arises when a heterogeneous dielectric system is subjected to an electric field, *e.g.* a biological cell in medium. The γ-dispersion is seen around 10^9 Hz and is caused by the dipolar orientation of water [65].

Electric fields exert forces on mobile- and surface-charges and accumulate at the interface of the dielectrics. The free motion of charge depends on the conductivity (ability of the material to conduct an electrical current to move through the material), while the charge redistribution in a limited space is characterized by its permittivity[9]. Figure 2.4 B illustrates schematically how a cell can be polarized due to the restricted motion of ions imposed by the plasma membrane. The induced dipole is a function of the dielectric properties of the cell and the medium, as well as the frequency of the AC electric field, which is described in more detail in 2.4.3.

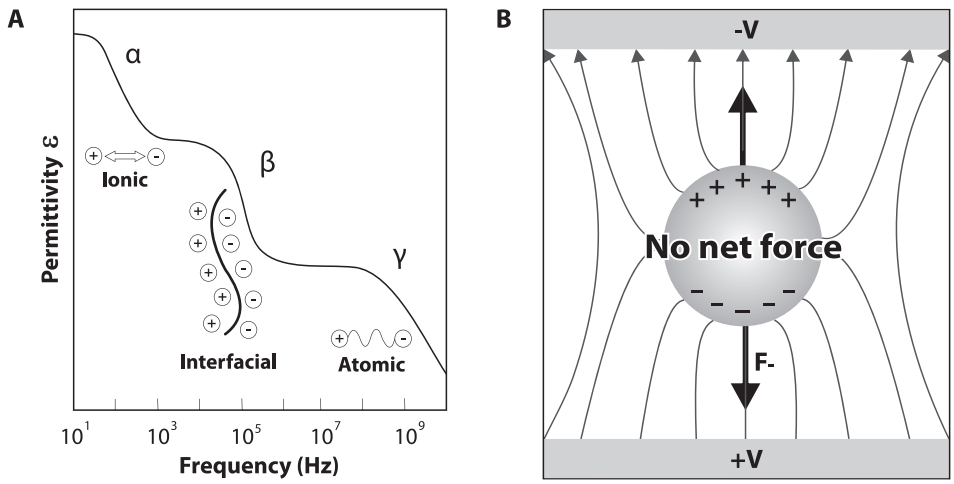

Figure 2.4: A) Diagram of the dielectric dispersion regions (modified from[65]) B) The polarization of a neutral particle in a uniform electric field, no net force present ($F_- = F_+$)

Furthermore, in order to interpret experimental results in AC electrokinetics and impedance measurements (chapter 7), shelled-models have been widely used to model the dielectric properties of cells in suspension[64, 68, 69]. A mammalian cell is usually modeled as a single-shell model with a conductive interior (cytoplasm), encapsulated by a thin insulator layer (cell membrane, figure 2.5)[69, 70].

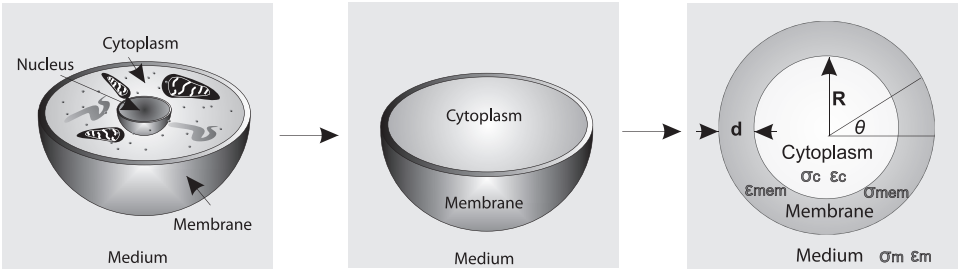

Figure 2.5: Model used for a mammalian cell in an electric field, the cell is modeled as a spherical structure with a conductive interior (cytoplasm) encapsulated in a thin insulator layer (membrane). $\sigma_{c/mem/m}$ are conductivities of the cytoplasm, membrane and medium, respectively. $\varepsilon_{c/mem/m}$ are the permittivity's of the cytoplasm, membrane and medium respectively. R represents the radius of the cell and d the membrane thickness.

2.4.3 Di-electrophoretic force and cell alignment

In cell electrofusion, two cells are brought into contact by DEP. This is the motion of dielectric particles, in this case mammalian cells, within an non-uniform AC electric field. As mentioned in the previous paragraph, a cell polarizes upon the induced electrical field. The interaction of the induced dipole with the electric field generates a DEP force (F_{DEP}), which is proportional to the cell volume $(\propto R^3)$, field gradient ∇E_0 and real part Claussius-Mossotti (CM) factor, K(ω). F_{DEP} is given by[67, 71, 72]:

$$F_{DEP} = 2\pi R^3 \varepsilon_m \nabla E_0^2 \operatorname{Re}[K(\omega)] \qquad [2.1]$$

where ε_m is the dielectric permittivity of the medium surrounding the cell, r the cell radius, Re the real part of the CM factor, E_0 the electric field strength, ω the angular frequency of the electric field and K(ω) the complex CM equation. And describes the relationship between the dielectric constants of the cell and medium[67, 73], and is defined as

$$K(\omega) = \frac{\varepsilon_p^* - \varepsilon_m^*}{\varepsilon_p^* + 2\varepsilon_m^*} \qquad [2.2]$$

$$\varepsilon_p^* = \varepsilon_{mem}^* \frac{\gamma^3 + 2\left(\dfrac{\varepsilon_c^* - \varepsilon_{mem}^*}{\varepsilon_c^* + 2\varepsilon_{mem}^*}\right)}{\gamma^3 - \left(\dfrac{\varepsilon_c^* - \varepsilon_{mem}^*}{\varepsilon_c^* + 2\varepsilon_{mem}^*}\right)} \quad \text{with} \quad \gamma = \frac{R+d}{R} \qquad [2.3]$$

Equation 2.3 shows the complex permittivity of the cell (ε_p^*). This is a function of the dielectric properties of the cell membrane ε_{mem}^* ($\varepsilon_{mem}^* = \varepsilon_{mem} + \sigma_{mem}/[j\omega]$) and internal properties ε_c^* ($\varepsilon_c^* = \varepsilon_c + \sigma_c/[j\omega]$) of the cell, and j is $\sqrt{-1}$. The complex permittivity of the medium, ε_m^* is a function of the dielectric property of the medium ε_m^*, where $\varepsilon_m^* = \varepsilon_m + \sigma_m/(j\omega)$ [74 75, 76].

Concluding, the absolute value of the DEP force on a particle depends on ∇E_0^2, as well as on the real part of K(ω). Re[K(ω)] is the in-phase component of the particle's effective polarizability. The imaginary part of K(ω) relates to the electro rotational force[70]. Examining the expression, the real part of K(ω) is bounded by the limits $-½ < \operatorname{Re}[K(\omega)] < 1$ and varies with the frequency of the applied field and the conductivity of the medium.

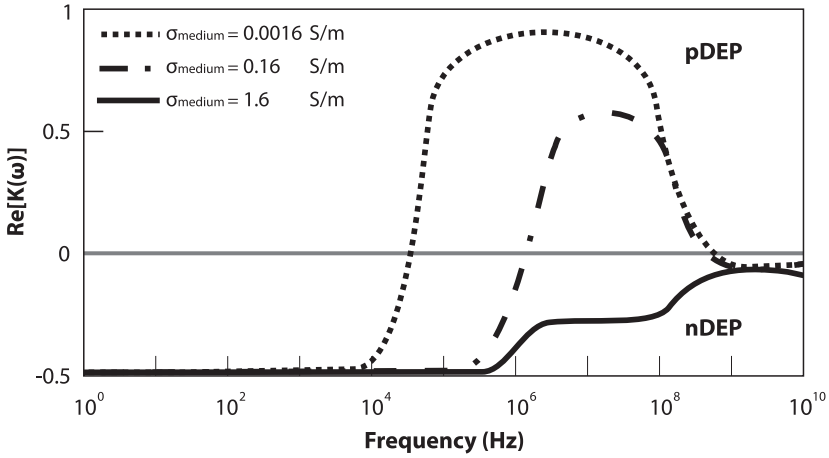

Figure 2.6: Plot showing a schematic spectrum of the real part of the CM factor for a cell in an electrolyte with different suspending medium conductivities. Adapted from[70]

In figure 2.6 several features can be observed. Firstly, the CM factor is a function of frequency. This is due to the fact that internal compartments of the cell contribute differently to the polarizability, each having unique kinetics. For instance, at low frequencies (<100 kHz), the cell appears insulating and therefore less polarizable than typical ionic media (>0.16 S/m). Hence a cells will experience negative DEP (Re[K(ω)] < 0). Which means that, the cell aligns against the field and is repelled from regions of high electric field, see figure 2.7. However, when using low conductive media(~0.0016 S/m), positive DEP will occur (Re[K(ω)] > 0). Hence, with positive DEP, the cell aligns towards the region of the highest electric field, see figure 2.7.

At higher frequencies (~1–100 MHz), the field bridges the membrane and the CM factor will compare the cytoplasm and the media permittivity's, resulting in nDEP at higher solution conductivities and positive DEP at low solution conductivities[63, 68-70]. Finally, high frequencies (>1 GHz) results in nDEP, likely due to cytoplasmic proteins that impart a net permittivity lower than surrounding medium[63].

In electrofusion experiments, frequencies for DEP are 1-100 MHz. Due to the use of low conductive fusion buffer, positive DEP is generated which favors close cell-cell contact[34, 54, 58].

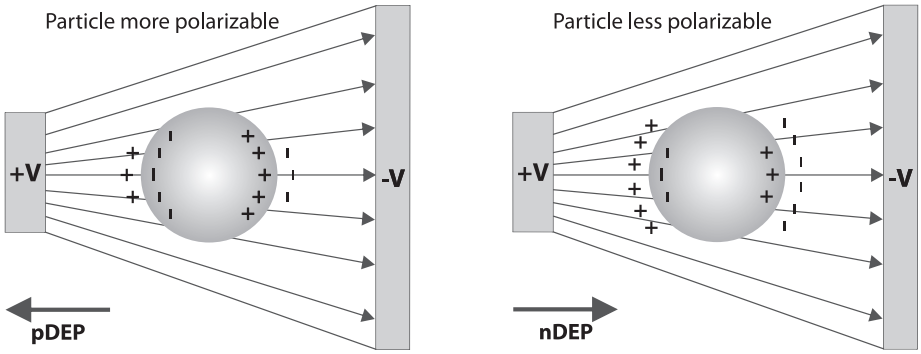

Figure 2.7 A schematic drawing of a polarizable cell subjected to an AC field. When the cell polarises, the interaction between the dipolar charges with the local electric field produces a force. Due to the inhomogeneous nature of the electric field, the force is greater at the side facing the point than that on the side facing the plane, and there is net motion towards or away from the smaller electrode. This effect is respectively called positive and negative DEP.

2.4.4 Membrane fusion using electric pulses

After cell alignment and pairing, high intensity pulses for short periods of time need to be applied to induce fusion[53, 77, 78]. Membrane breakdown occurs when the membrane electric voltage (V_m) reaches its critical value V_C at room temperature[53]. Experimental studies showed that the threshold for electroporation is 300-350 mV in mammalian cells[79]. An important parameter for electrofusion is the transition between reversible and irreversible breakdown. An induced transmembrane potential around the reversible breakdown can result in electrofusion of cells[18, 55, 80-82]. The V_m of an isolated spherical cell under the influence of an electric field, E_0, is given by[80, 83, 84]:

$$V_m = 1.5\ R\ E_0 \cos(\theta)(1 - \exp[-\tau/\tau_m]) \qquad [2.3]$$

Where, R is the cell radius, θ is the angle between the normal to the membrane and the electric field vector and τ_m is the time constant of membrane charging. When the pulse duration is 5-10*τ_m, the membrane charging is completed and equation [2.3] simplifies to the well-known equation [2.4].

$$V_m = 1.5\ R\ E_0 \cos(\theta) \qquad [2.4]$$

The induced membrane potential is proportional to the cell radius (R). Often, cells of different sizes are electrofused. Large cells experience a high voltage drop across the membrane and are more likely to be irreversibly damaged by the electrical treatment. Conversely, small cells experience a low voltage drop across the membrane, and they have less chance to be porated. Following the DC pulse, it is essential to keep the cells in contact with each other for a while in order to obtain high fusion efficiency (post-alignment).

2.5 Conventional electrofusion

Currently, electrofusion of large number of cells occurs in a fusion chamber with parallel electrodes (conventional bulk electrofusion). It requires the exposure of cells to an electric field and short pulses, as explained in the previous paragraphs. This means that the minimum requirements include a chamber, a strong electric field and a pulse generator[85]. Figure 2.3 shows a schematic representation of a conventional electrofusion electrofusion chamber with pearl chain formation. And figure 2.8 shows a commercially available electrofusion chamber.

Using a conventional electrofusion chamber, electrofusion efficiencies of the same cell type can go up to 40%[87, 88]. For hybridoma generation, two different sized cell types need to be electrofused (B-lymphocyte with myeloma cells). As a result the efficiency, regarding solely the fusion efficiency of lymphocytes and myeloma cells lowers to 5-10%[71, 86]. Moreover, the efficiency of generating antibody producing hybridomas is drastically low[22, 59], with efficiencies of 4×10^{-4} (average of 4 hybridomas on 100000 cells). Hence, the conventional bulk electrofusion has many limitations and drawbacks.

Figure 2.8: Conventional commercially available electrofusion apparatus from Eppendorf [87]

2.5.1 Limitations of conventional electrofusion

Main cause for the low electrofusion efficiencies is the fact that the conventional technique has no ability to manipulate and fuse individual cell pairs. Furthermore, it utilizes hundreds of microliters of cell suspension. Moreover, because of the large distance between the electrodes an expensive high voltage generator has to be used in order to generate a sufficiently high electrical field. Using conventional electrofusion, it is time-consuming to vary electrical, biological and/or chemical parameters. As said above, the efficiency of generating antibody producing hybridomas is drastically low[22, 59] and a large number of cells are of no use[36, 58].

Overall, despite this wide use of electrofusion in biotechnology regarding hybridoma generation the final fusion efficiency still remains very low. Therefore, it is of great interest and central importance to develop a good and efficient cell-fusion method.

2.6 Why the move to on chip electrofusion?

To overcome the drawbacks of bulk electrofusion, several approaches were developed to achieve cell pair selection prior to fusion, for example flow cytometry[88] and laser-based single cell manipulation[89]. However, these methods are laborious and do not offer high-throughput electrofusion of cells. Due to advances in microfluidics, especially the rapid development of on-chip electroporation[54, 90] and dielectrophoretic control of cells[91-93], research of cell-fusion has been carried out on microdevices[61, 94]. As a result, higher pairing precision and fusion throughput can be achieved[86].

In the nineties the term micro total analysis systems was introduced, to describe a complete microsystem integrating sample handling, analysis and detection into a single device, also called a Lab-on-a-Chip (LOC) device[95]. Cell handling and manipulation are easier, as the channels are comparable to the sizes of the cells (10-100 µm). Furthermore, LOC provides low fluid volume consumption, less waste, lower reagents costs and less cell suspension volumes[54, 61]. In addition, microelectronic pattern techniques decrease the distances between the electrodes. As a result, electrofusion microdevices can achieve a necessary electric field strength with a much lower applied voltage, avoiding the potential risks of using high voltage and the use of expensive high voltage pulse generators. Moreover, heat dissipation occurs faster due to its large surface/volume ratio[54,95, 95-97]. Moreover, the fusion process can be followed in detail and possibly long term, using microdevices.

Overall, to overcome the limitations in existing cell electrofusion methods, today's research focuses on on-chip electrofusion. In the following section, an outline is given of currently existing microfluidic devices for low and high-throughput cell electrofusion. Finally, its future development is discussed.

2.7 Current status of electrofusion using microfluidic devices

As mentioned before, electrofusion has many applications throughout biotechnology. And the use of microfluidic technology to realize cell electrofusion on a microchip platform has gained more and more interest[57, 61, 71, 98-100]. The focus of this thesis is the efficient generation of antibody producing hybridomas. Nevertheless, below an overview is given on currently existing microfluidic devices regarding electrofusion, focusing generally on electrofusion of cells and liposomes, and specifically on hybridoma generation for Ab production.

The overview is divided in static and flow through approaches for electrofusion on chip, with a focus on cell pairing, electrofusion and detection analysis.

2.7.1 Static electrofusion on chip

Very early work on cell-cell electrofusion in a micromachined system was addressed by Masuda *et al.* [101]. This device consisted of two micropumps, each supplying one species

of cells, and a fusion chamber. This was the onset of increasing research and development regarding cell fusion using microfluidic devices.

In 2001 Stromberg *et al.* showed electrofusion by a micromanipulator-controlled microelectrode[57]. Optical trapping was used to transport individual liposomes and cells through the microchannels into the fusion container. In the fusion container, selected pairs of liposomes were fused together using microelectrodes. Fusion yields of about 20% were accomplished for hybrid cell production. However, the throughput was very low, since fusion was induced pairwise.

The next generation of electrofusion chips included the use of sidewall microelectrodes. One of the first papers was by Tresset *et al.* 2004[94](figure 2.9 A). This paper reports a microfabricated device with high aspect-ratio electrodes, with liposome electrofusion yield of 75%.

A cell-electrofusion chip, with microelectrodes on a silicon substrate, was designed by Cao *et al.*[71] (figure 2.9 B). Here, a fusion efficiency of 40% was reached using plant protoplast. A similar, dense continuous microelectrode array, was used by Qu *et al.*[102]. Here, comparable fusion efficiencies of 40% were achieved, using 3T3 cells (fibroblast). Recently, a similar approach for cell electrofusion on chip was developed by Hu *et al.*[103] (figure 2.9 C). The device contains a serpentine-shaped microchannel with discontinuously patterned vertical sidewall microelectrodes in the microchannel. This device showed 3T3 cell fusion with an efficiency above 40%. However, all three devices offer no control on cell pairing of different cell types. Hence, these devices are not of interest regarding the electrofusion of B-lymphocytes and myeloma cells for the generation of hybridomas.

An electric cell fusion chip with an embedded cell delivery function, driven by surface tension was presented by Ju *et al.*[104]. The chip consists of a microchannel with a fusion chamber and gold–titanium electrodes. The electrofusion of cells was successfully carried out under AC field for cell alignment and DC pulse to induce fusion. Even though it was possible to remove the fused cells with a micropipette, the fusion efficiency did not exceed 3-5%. Moreover, this device was only tested for electrofusion of plant protoplast.

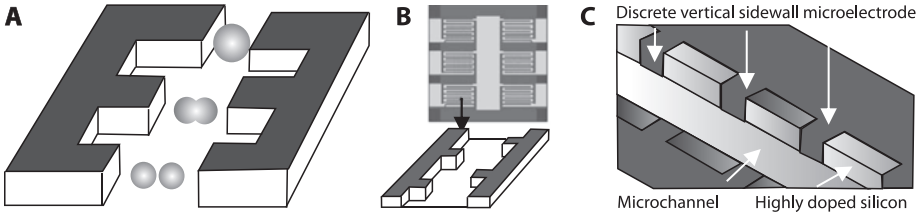

Figure 2.9: A) Schematic view of the device and protocol to fuse liposomes. Several electrode gaps were designed for liposome alignment during static situation (AC voltage) followed by membrane breakdown (DC pulses) and fused into a hybrid vesicle. Adapted from [94]. B) The layout of microchannel and microelectrodes on the chip with a 3D schematic diagram of the microchannel and microelectrodes. Adapted from [71]. C) A 3D schematic diagram of the microfluidic chip with discrete vertical sidewall microelectrodes. Adapted from [103].

Higher electrofusion yields where achieved by the group of Voldman *et al.*[86]. They fabricated a microfluidic device, which uses traps to pair thousands of cells for electrofusion (figure 2.10 A). Using this device, different mammalian cell types were paired, using a two-step protocol, achieving pairing efficiencies up to 70%[86, 105]. Electrical fusion of 3T3 cells was more efficient than chemical fusion, achieving fusion yields up to 90%. Electrofusion of B- and myeloma cells was shown, however no trapping or fusion efficiency were mentioned, therefore information about functional antibody producing hybridomas is unknown. Furthermore, the trapped cells were not able to be removed from the device.

Techaumnat *et al.*[106] presented an electric-field constriction, created by a microfabricated structure to realize high-yield electrofusion of biological cells. The device is shown schematically in figure 2.10 B. Membrane breakdown takes place nowhere but in the orifice. Experiments were performed with plant protoplast and human lymphoblasts and showed a yield higher than 90%[106]. However, no different sized cell fusion was shown. Recently, Kimura *et al.*[107] presented a massively parallel electrofusion system using the micro-orifice platform by Techaumnat *et al.*[106]. Here, a fusion yield of 79% was achieved for different sized cell types, namely HL60 with K562 cells. No cell retrieval was mentioned and it was not possible to follow the fusion process. Another publication based on similar construction shows similar fusion yields regarding stem-somatic cell fusion[102].

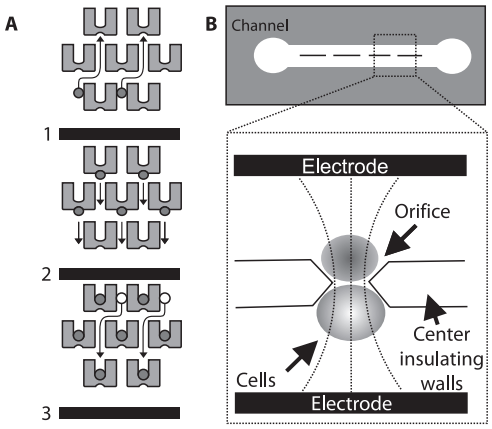

Figure 2.10: A) Three-step cell-loading protocol. 1. Cells are loaded 'up' toward the smaller back-side capture cup 2. The direction of the flow is reversed, and the cells are transferred 'down' into the larger front-side capture cup 3. The second cell type is loaded from the top and cells are captured in front of the first cell typ. Adapted from [86]. B) Schematic overview of electrofusion device. Top view showing principle of field constriction in more detail. Working principle of micro orifice based cell fusion. Attraction of cells in to the micro orifice array located in an insulating membrane between electrodes, this induces cell pairing and contact formation between cells, followed by cell fusion with a DC pulse. Adapted from[106]

2.7.2 Continuous electrofusion on chip

While the majority of the described devices use trapping geometries or DEP for cell alignment, it is also possible to use continuous DC current in combination with geometric variation of the chip. A cell to cell electrofusion technique using a common DC current power supply was designed by Wang *et al.* (figure 2.11 A). Firstly, cells had to be conjugated based on biotin-streptavidin interaction. The electrofusion was then conducted by running the linked cells through a microfluidic channel with geometric variation under continuous DC field. A fusion efficiency between CHO cells of 30% was shown. However, the requirement to chemical link the cells is a drawback of the device. Furthermore, the properties of the fused cells should be characterized and electrofusion of different sized cells was not shown[100].

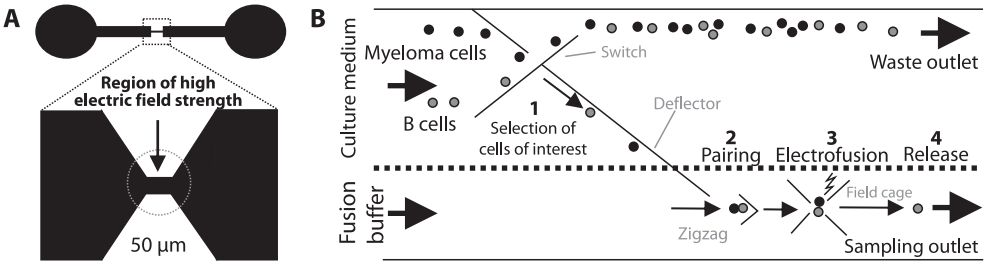

Figure 2.11: Continuous electrofusion on chip. A) Layout of a single-pulsed microfluidic device for cell electrofusion. As shown in the inset, the narrow section indicates the section where the high intensity pulse was generated using the geometric variation. Adapted from[100]. B) Microfluidic configuration. Myeloma cells and B cells enter the chip through two separate inlets in two parallel laminar flows. Unprocessed cells leave the chip through the waste outlet. In the central channel, two separate flows of cell culture medium and hypo-osmolar fusion buffer are generated. By means of consecutive deflection and switch electrodes, individual cells are selected from their respective flows, transferred into the fusion buffer and directed to a zigzag electrode for pairing. The pair is then forwarded to the DEP field cage, where a fusogenic voltage pulse is applied. After that, the processed cells are released from the fluidic system into standard cell culture equipment for further cultivation and analysis, adapted from [108].

Electrofusion of individually selected cells in DEP field cages was recently shown by Kirschbaum *et al.*[108] (figure 2.11 B), showing fusion efficiencies of more than 30% for individual pairs of mouse myeloma and B cell blasts. Furthermore, three days after fusion, proliferating ability was shown in 22% of the hybrid cells. This was not using selection media, hence no information on the functionality and genetic make-up of the proliferating hybridomas was shown. Furthermore, the throughput of this technique was very low, since cells were selected and trapped in the DEP cage, after which the flow stopped and fusion was induced. This indicates a semi-continuous electrofusion method, with one fusion product every 3-10 min.

2.8 Conclusion

The devices, which are reviewed, were tested with animal cells, plant cells or liposomes. Only two studies show fusion between myeloma cells and lymphocytes[86] or B-lymphoblast[108], where only the latter also shows cell survival. Presumably, the difference in cell size complicates the electrofusion process, as mentioned before. This could explain the lack of data and results in the area of antibody producing hybridoma generation, while the demand for better, more efficient electrofusion method is increasing. Hence, after reviewing the current available methods, we are able to identify certain criteria and requirements regarding our electrofusion chip for hybridoma generation.

2.8.1 Cell pairing

Several different strategies to achieve cell alignment in the discussed microfluidic devices, are AC field, cell traps, focusing current into small flow constriction and optical trapping. The first approach was applied by the majority of the authors[71, 94, 104, 106].

For generating hybridomas, it is of utmost importance to fuse one B-cell with one myeloma cell. This makes the use of selective cell pairing using trapping geometries most attractive. However, this directly rules out flow through method and implies a static approach. Static designs are generally used for single cell fusion[57, 86, 106], facilitating the introduction of a cell suspension, cell alignment and finally fusion. The cell is retained at a defined place, subsequently a fusion pulse can be applied and the process can be followed. With flow-through devices, the advantage is the continuous flow of cells, which are aligned and subsequently electrofused[100, 108]. However, the flow-through should be high enough to compete with static approach. And it is difficult to follow the fusion process.

2.8.2 Electrofusion

Different electrofusion efficiencies in microfluidic devices were reported, ranging from 3-90%[86, 104, 106]. However, only two studies showed fusion between myeloma cells and lymphocytes[86] or B-lymphoblast[108]. The latter only mentioned fusion efficiency (30%) and showed cell survival (22%) This could be due to the difference in cell size which complicates the electrofusion process as mentioned before. Initially, we will base our microfluidic design on the approaches which have shown high electrofusion efficiencies in previous literature and then optimize this further for the specific electrofusion of B-cells and myeloma cells towards hybridoma formation.

2.8.3 Detection and analysis

Detecting and analyzing the fusion efficiency is performed in several different ways, but optical detection is performed most often. The majority of the studies solely rely on image acquisition during electrofusion, followed by careful analysis [71 39, 99, 106]. In order to

improve optical detection, fluorescent dyes were used, such as calcein. This enables determination of pairing and fusion efficiencies based on fluorescence exchange[86, 100]. Furthermore, a membrane fluorescent dye can be used to analyze membrane reorganizations during the electrofusion process[57]. However, it has to be kept in mind that only cytoplasmic fusion can be imaged using the detection mechanism. Nuclear fusion occurs spontaneously, after 1-2 weeks and is therefore difficult to detect. Furthermore, the device should be designed with an optimal electric field distribution regarding different sized cell fusion, while being able to follow the fusion process and regain the fusion products for further analysis (viability, antibody production). Or even better culture and analyze the fused product on chip.

Overall, for performing efficient cell electrofusion on chip, for hybridoma generation, the microfluidic device and the experimental set-up both have to meet certain requirements. The microfluidic chip should enable the efficient electrofusion of B-cells en myeloma cells, using an easy to handle experimental set-up. Our ultimate goal is to gain high efficiency electrofusion, followed by a high yield of antibody producing hybridomas. Therefore, the next chapter will investigate which microfluidic device and experimental set-up are best suited to meet our ultimate goal.

2.9 References

1. Ogle, B.M., M. Cascalho, and J.L. Platt, *Biological implications of cell fusion.* Nat Rev Mol Cell Biol, 2005. **6**(7): p. 567-75.
2. Ringertz, N.R.a.R.E.S., *Cell Hybrids* 1976 New York: Academic Press.
3. Lin, H.P., et al., *Bimolecular fluorescence complementation analysis of eukaryotic fusion products.* Biol Cell, 2010. **102**(9): p. 525-37.
4. Chen, E.H. and E.N. Olson, *Unveiling the mechanisms of cell-cell fusion.* Science, 2005. **308**(5720): p. 369-373.
5. Larsson, L.I., B. Bjerregaard, and J.F. Talts, *Cell fusions in mammals.* Histochem Cell Biol, 2008. **129**(5): p. 551-61.
6. Sullivan, S. and K. Eggan, *The potential of cell fusion for human therapy.* Stem Cell Rev, 2006. **2**(4): p. 341-9.
7. Alkan, S.S., *Landmark - Monoclonal antibodies: the story of a discovery that revolutionized science and medicine.* Nature Reviews Immunology, 2004. **4**(2): p. 153-156.
8. Zimmermann, U., et al., *Electro-fusion of cells: principles and potential for the future.* Ciba Found Symp, 1984. **103**: p. 60-85.
9. Dimitrov, D.S., *Electroporation and electrofusion of membranes*, in *Handbook of biological physics*, R. Lipowsky, Sackmann, E., Editor. 1995, Elsevier science.
10. Barski, G., S. Sorieul, and F. Cornefert, *Hybrid Type Cells in Combined Cultures of 2 Different Mammalian Cell Strains.* Journal of the National Cancer Institute, 1961. **26**(5): p. 1269-&.
11. Capers, C.R., *Multinucleation of skeletal muscle in vitro.* J Biophys Biochem Cytol, 1960. **7**: p. 559-66.

12. Colwin, L.H. and A.L. Colwin, *Formation of sperm entry holes in the vitelline membrane of Hydroides hexagonus (Annelida) and evidence of their lytic origin.* J Biophys Biochem Cytol, 1960. **7**: p. 315-20.
13. Kohler, G. and C. Milstein, *Continuous cultures of fused cells secreting antibody of predefined specificity.* Nature, 1975. **256**(5517): p. 495-7.
14. Abhyankar, V.V., Beebe, D.J., *Human embryonic stem cells & microfluidics*, in *Lab-on-Chips for Cellomics, micro and nanotechnologies for life science*, H. Andersson, van den Berg, A., Editor. 2004, Kluwer Academic Publishers: Dordrecht, The Netherlands.
15. Neumann, E., Gerisch, G., Opatz, K., *Cell Fusion Induced by High Electric to Dictyostelium.* Naturwissenschaften, 1980. **67**: p. 414.
16. Weber, H., et al., *Microbiological implications of electric field effects. III. Stimulation of yeast protoplast fusion by electric field pulses.* Z Allg Mikrobiol, 1981. **21**(7): p. 555-62.
17. Yang, J.Y., et al., *Dendritic cells fused with allogeneic hepatocellular carcinoma cell line compared with fused autologous tumor cells as hepatocellular carcinoma vaccines.* Hepatology Research, 2010. **40**(5): p. 505-513.
18. Bates, G.W., Saunders, J.A. Sowers, A.E., *Electrofusion: principles and applications*, in *Cell fusion*, A.E. Sowers, Editor. 1987, Plenum Press: New York.
19. Glassy, M.C., et al., *UC 729-6, a human lymphoblastoid B-cell line useful for generating antibody-secreting human-human hybridomas.* Proc Natl Acad Sci U S A, 1983. **80**(20): p. 6327-31.
20. Jahn, S., et al., *Establishment of human Ig producing heterohybridomas by fusion of mouse myeloma cells with human lymphocytes derived from peripheral blood, bone marrow, spleen, lymph node, and synovial fluid. Effect of polyclonal prestimulation and cryopreservation.* J Immunol Methods, 1988. **107**(1): p. 59-66.
21. Kwekkeboom, J., C. de Groot, and J.M. Tager, *Efficient electric field-induced generation of hybridomas from human B lymphocytes without prior activation in vitro.* Hum Antibodies Hybridomas, 1992. **3**(1): p. 48-53.
22. Steenbakkers, P.G., H.A. Hubers, and A.W. Rijnders, *Efficient generation of monoclonal antibodies from preselected antigen-specific B cells. Efficient immortalization of preselected B cells.* Mol Biol Rep, 1994. **19**(2): p. 125-34.
23. Trevor, K.T., et al., *Generation of dendritic cell-tumor cell hybrids by electrofusion for clinical vaccine application.* Cancer Immunol Immunother, 2004. **53**(8): p. 705-14.
24. Weise, J.B., et al., *A dendritic cell based hybrid cell vaccine generated by electrofusion for immunotherapy strategies in HNSCC.* Auris Nasus Larynx, 2004. **31**(2): p. 149-53.
25. Ahkong, Q.F., et al., *Proteinases and cell fusion.* FEBS Lett, 1978. **95**(1): p. 147-52.
26. Davidson, R.L., K.A. O'Malley, and T.B. Wheeler, *Polyethylene glycol-induced mammalian cell hybridization: effect of polyethylene glycol molecular weight and concentration.* Somatic Cell Genet, 1976. **2**(3): p. 271-80.
27. Poste, G. and A.C. Allison, *Membrane fusion reaction: a theory.* J Theor Biol, 1971. **32**(1): p. 165-84.
28. Jian, Y.a.M.H., Shen, *Polyethylene Glycol-Mediated Cell Fusion*, in *Methods in Molecular Biology: Nuclear Reprogramming: Methods and Protocols*, S. Pells, Editor. 2006, Humana Press Inc., Totowa, NJ.

29. Lee, J. and B.R. Lentz, *Outer leaflet-packing defects promote poly(ethylene glycol)-mediated fusion of large unilamellar vesicles.* Biochemistry, 1997. **36**(2): p. 421-31.
30. Sorem, J., T.S. Jardetzky, and R. Longnecker, *Cleavage and secretion of Epstein-Barr virus glycoprotein 42 promote membrane fusion with B lymphocytes.* J Virol, 2009. **83**(13): p. 6664-72.
31. White, J., K. Matlin, and A. Helenius, *Cell fusion by Semliki Forest, influenza, and vesicular stomatitis viruses.* J Cell Biol, 1981. **89**(3): p. 674-9.
32. Hernandez, L.D., et al., *Virus-cell and cell-cell fusion.* Annual Review of Cell and Developmental Biology, 1996. **12**: p. 627-661.
33. Wiegand, R., et al., *Laser-induced fusion of mammalian cells and plant protoplasts.* J Cell Sci, 1987. **88 (Pt 2)**: p. 145-9.
34. Senda, M.T., J., Abe, S., Nakamura, T., *Induction of cell fusion of plant protoplasts by electrical stimulation* Plant Cell Physiology, 1979. **20**(7): p. 1441-1443.
35. Orentas, R.J., et al., *Electrofusion of a weakly immunogenic neuroblastoma with dendritic cells produces a tumor vaccine.* Cell Immunol, 2001. **213**(1): p. 4-13.
36. Karsten, U., et al., *Direct comparison of electric field-mediated and PEG-mediated cell fusion for the generation of antibody producing hybridomas.* Hybridoma, 1988. **7**(6): p. 627-33.
37. Zimmermann, U. and J. Vienken, *Electric field-induced cell-to-cell fusion.* J Membr Biol, 1982. **67**(3): p. 165-82.
38. Senda, M., et al., *Induction of Cell-Fusion of Plant-Protoplasts by Electrical-Stimulation.* Plant and Cell Physiology, 1979. **20**(7): p. 1441-1443.
39. Zimmermann, U., *Electric field-mediated fusion and related electrical phenomena.* Biochim Biophys Acta, 1982. **694**(3): p. 227-77.
40. Pilwat, G., H.P. Richter, and U. Zimmermann, *Giant culture cells by electric field-induced fusion.* FEBS Lett, 1981. **133**(1): p. 169-74.
41. Zimmerman, U., Pilwat, G., *Electric field-mediated cell fusion.* Journal Biol. Phys. , 1982. **10**: p. 43-50.
42. Zimmermann, U. and P. Scheurich, *Fusion of Avena sativa mesophyll cell protoplasts by electrical breakdown.* Biochim Biophys Acta, 1981. **641**(1): p. 160-5.
43. Zimmermann, U., et al., *Electrofusion: a novel hybridization technique.* Adv Biotechnol Processes, 1985. **4**: p. 79-150.
44. Neumann, V., F. Siegemund, and B. Baessler, *Electrically induced fusion of different human cell types.* J Neurol, 1986. **233**(3): p. 153-6.
45. Abidor, I.G. and A.E. Sowers, *Kinetics and mechanism of cell membrane electrofusion.* Biophys J, 1992. **61**(6): p. 1557-69.
46. Huang, S.K. and S.W. Hui, *Chemical co-treatments and intramembrane particle patching in the poly(ethylene glycol)-induced fusion of turkey and human erythrocytes.* Biochim Biophys Acta, 1986. **860**(3): p. 539-48.
47. Mehrle, W., et al., *Effects of microgravitation on electrofusion of plant cell protoplasts.* Plant Physiol, 1989. **89**: p. 1172-7.
48. Poo, M., *In situ electrophoresis of membrane components.* Annu Rev Biophys Bioeng, 1981. **10**: p. 245-76.
49. Sowers, A.E., *A long-lived fusogenic state is induced in erythrocyte ghosts by electric pulses.* J Cell Biol, 1986. **102**(4): p. 1358-62.

50. Sowers, A.E. and C.R. Hackenbrock, *Rate of lateral diffusion of intramembrane particles: measurement by electrophoretic displacement and rerandomization.* Proc Natl Acad Sci U S A, 1981. **78**(10): p. 6246-50.
51. Stenger, D.A. and S.W. Hui, *Kinetics of ultrastructural changes during electrically induced fusion of human erythrocytes.* J Membr Biol, 1986. **93**(1): p. 43-53.
52. Wilschut, J. and D. Hoekstra, *Membrane fusion: lipid vesicles as a model system.* Chem Phys Lipids, 1986. **40**(2-4): p. 145-66.
53. Chang, D.C., Saunders, J.A., Chassy, B.M., Sowers, A.E., *Overview of electroporation and electrofusion*, in *Guide to electroporation and electrofusion*, D.C. Chang, Saunders, J.A., Chassy, B.M., Sowers, A.E., Editor. 1992, Academic Press Limited: London.
54. Valero, A., *Single cell electroporation*, in *BIOS Lab-on-a-Chip group of the MESA+ Institute for Nanotechnology*. 2006, University of Twente: Enschede, The Netherlands. p. 209.
55. Weaver, J.C., *Theory on electroporation*, in *Electroporation and electrofusion in cell biology*, E. Neumann, Sowers, A.E., Jordan, C.A., Editor. 1989, Plenum Press: New York. p. 111-126.
56. Evans, M.J., et al., *Mitochondrial DNA genotypes in nuclear transfer-derived cloned sheep.* Nature Genetics, 1999. **23**(1): p. 90-93.
57. Stromberg, A., et al., *Microfluidic device for combinatorial fusion of liposomes and cells.* Anal Chem, 2001. **73**(1): p. 126-30.
58. Trontelj, K., et al., *Optimization of bulk cell electrofusion in vitro for production of human-mouse heterohybridoma cells.* Bioelectrochemistry, 2008. **74**(1): p. 124-9.
59. Vanduijn, G., et al., *High Yields of Specific Hybridomas Obtained by Electrofusion of Murine Lymphocytes Immunized Invivo or Invitro.* Experimental Cell Research, 1989. **183**(2): p. 463-472.
60. *Guide to electroporation and electrofusion*, ed. C. Chang B. M., J. A. Saunders, Sowers A.E. 1992, San Diego: Academic Press.
61. Chiu, D.T., *A microfluidics platform for cell fusion.* Curr Opin Chem Biol, 2001. **5**(5): p. 609-12.
62. Modiquest, *Generating Hybridomas By Electrofusion*. 2008: Enschede.
63. Voldman, J., *Electrical forces for microscale cell manipulation.* Annu Rev Biomed Eng, 2006. **8**: p. 425-54.
64. Morgan, M.N.G.G., *AC Electrokinetic: Colloids and Nanoparticles (Microtechnologies and Microsystems)*. 2002: institute of physichs publishing.
65. Foster, K.R. and H.P. Schwan, *Dielectric-Properties of Tissues and Biological-Materials - a Critical-Review.* Critical Reviews in Biomedical Engineering, 1989. **17**(1): p. 25-104.
66. Schwan, H.P., *Mechanisms responsible for electrical properties of tissues and cell suspensions.* Med Prog Technol, 1993. **19**(4): p. 163-5.
67. Morgan, H., Green, N.G., *AC electrokinetics: colloids and nanoparticles*. 2002, Philadelphia: Research Studies Press.
68. Morgan, H., Sun, T., *AC electrokinetic particle manipulation in microsystems*, in *microfluidics based microsystems: fundametnals and applications*, S. Kakac, Kosoy, B., Li, D, Pramuanjaroenkij, A., Editor. 2010.
69. Pethig, R., *Dielectrophoresis: using inhomogeneous AC electrical fields to separate and manipulate cells.* Critical Reviews in Biotechnology 1996. **16**: p. 331-348.

70. Sun, T. and H. Morgan, *Single-cell microfluidic impedance cytometry: a review.* Microfluidics and Nanofluidics, 2010. **8**(4): p. 423-443.
71. Cao, Y., Yang, J., Yin, Z.Q., Luo, H.Y., Yang, M., Yang, N.H.J., Huo, D.Q., Hou, C.J., Jiang, Z.Z., Zhang, R.Q., Xu, R., Zheng, R.L., *Study of high-throughput cell electrofusion in a microelectrode-array chip.* Microfluid Nanofluid, 2008. **5**(5): p. 669-675.
72. Pohl, H.A. and J.S. Crane, *Dielectrophoresis of cells.* Biophys J, 1971. **11**(9): p. 711-27.
73. Hughes, M.P., *AC Electrokinetics: Applications for Nanotechnology* Nanotechnology 2000. **11**: p. 124–132.
74. Ramos, A., et al., *Ac electrokinetics: a review of forces in microelectrode structures.* Journal of Physics D-Applied Physics, 1998. **31**(18): p. 2338-2353.
75. Sukhorukov, V.L., et al., *A biophysical approach to the optimisation of dendritic-tumour cell electrofusion.* Biochem Biophys Res Commun, 2006. **346**(3): p. 829-39.
76. Kua, C.H., et al., *Cell motion model for moving dielectrophoresis.* Anal Chem, 2008. **80**(14): p. 5454-61.
77. Gross, D., *Electromobile surface charge alters membrane potential changes induced by applied electric fields.* Biophys J, 1988. **54**(5): p. 879-84.
78. Pliquett, U., et al., *High electrical field effects on cell membranes.* Bioelectrochemistry, 2007. **70**(2): p. 275-82.
79. Gabriel, B. and J. Teissie, *Direct observation in the millisecond time range of fluorescent molecule asymmetrical interaction with the electropermeabilized cell membrane.* Biophys J, 1997. **73**(5): p. 2630-7.
80. Zimmermann, U., *Electrical breakdown, electropermeabilization and electrofusion.* Rev Physiol Biochem Pharmacol, 1986. **105**: p. 176-256.
81. Gaynor, P.T., Bodger, P.S., *Electrofusion processes: theoretical evaluation of high electric field effects on cellular transmembrane potentials* IEE Proc.-Sci. Meas. Technol., 1995. **142**(2).
82. Stenger, D.A., Hui, S.W., *Electrofusion kinetics*, in *Electroporation and electrofusion in cell biology*, E. Neumann, Sowers, A.E., Jordan, C.A., Editor. 1989, Plenum Press: New York. p. 167-192.
83. Washizu, M. and B. Techaumnat, *Polarisation and membrane voltage of ellipsoidal particle with a constant membrane thickness: a series expansion approach.* IET Nanobiotechnol, 2008. **2**(3): p. 62-71.
84. Cole, K.S., *Membrane watching.* J Gen Physiol, 1968. **51**(5): p. Suppl:1S-7S.
85. Sowers, A.E., *Fusion events and nonfusion contents mixing events induced in erythrocyte ghosts by an electric pulse.* Biophys J, 1988. **54**(4): p. 619-26.
86. Skelley, A.M., et al., *Microfluidic control of cell pairing and fusion.* Nat Methods, 2009.
87. Eppendorf, *Multitalent for transfection and cell fusion - eppendorf multiporator.* 2007-2010.
88. Bakker Schut, T.C., et al., *Selective electrofusion of conjugated cells in flow.* Biophys J, 1993. **65**(2): p. 568-72.
89. Stromberg, A., et al., *Manipulating the genetic identity and biochemical surface properties of individual cells with electric-field-induced fusion.* Proc Natl Acad Sci U S A, 2000. **97**(1): p. 7-11.

90. Zhan, Y.H., et al., *Electroporation of Cells in Microfluidic Droplets.* Analytical Chemistry, 2009. **81**(5): p. 2027-2031.
91. Archer, S., et al., *Cell reactions to dielectrophoretic manipulation.* Biochem Biophys Res Commun, 1999. **257**(3): p. 687-98.
92. Holmes, D., M. Thomas, and H. Morgan, *Dielectrophoretic separation/isolation of rare particles/cell types form a heterogeneous suspension within a microfluidic system.* Micro Total Analysis Systems 2000, Proceedings, 2000: p. 115-118.
93. Morgan, H., et al., *Trapping single human osteoblast-like cells from a heterogeneous population using a dielectrophoretic microfluidic device.* Biomicrofluidics, 2010. **4**(2).
94. Tresset, G., Takeuchi, S., *A microfluidic device for electrofusion of biological membranes.* Seisan-kenkyu, 2004. **56**(1).
95. Andersson, H., van den Berg, A., *Microfluidic devices for cellomics - a general overview of the field*, in *Lab-on-Chips for Cellomics, micro and nanotechnologies for life science*, H. Andersson, van den Berg, A., Editor. 2004, Kluwer Academic Publishers: Dordrecht, The Netherlands.
96. Yi, C., Li, C.S., Ji, S., Yang, M., *Microfluidics technology for manipulation and analysis of biological cells.* Analytica Chimica Acta 2006. **560** p. 1-23.
97. Bao, N., J. Wang, and C. Lu, *Recent advances in electric analysis of cells in microfluidic systems.* Anal Bioanal Chem, 2008. **391**(3): p. 933-42.
98. Tan, W.H. and S. Takeuchi, *A trap-and-release integrated microfluidic system for dynamic microarray applications.* Proc Natl Acad Sci U S A, 2007. **104**(4): p. 1146-51.
99. Tresset, G. and S. Takeuchi, *A microfluidic device for electrofusion of biological vesicles.* Biomed Microdevices, 2004. **6**(3): p. 213-8.
100. Wang, J., Lu, C., *Microfluidic cell fusion under continuous direct current voltage.* Applied physics letters 2006. **89**.
101. Masuda, S., Washizu, M., Nanba, T., *Novel method of cell fusion in field constriction area in fuid integrated circuit.* IEEE Transactions on industry applications, 1989. **25**(4).
102. Qu, Y., et al., *Somatic and stem cell pairing and fusion using a microfluidic array device.* Microfluidics and Nanofluidics, 2011. **11**(5): p. 633-641.
103. Hu, N., et al., *A cell electrofusion microfluidic chip using discrete coplanar vertical sidewall microelectrodes.* Electrophoresis, 2012. **33**(13): p. 1980-1986.
104. Ju, J., Ko, J.M., Cha, H.C., Park, J.Y., Im, C.H., Lee, S.H., *An electrofusion chip with a cell delivery system driven by surface tension.* Journal of Micromechanics and Microengineering 2009. **19**.
105. Skelley, A.M., Kirak, O., Jaenisch, R., Voldman, J., *Studying reprogramming of somatic cells via fusion with embryonic stem cells: a massively parallel device for cell fusion*, in *Eleventh International Conference on Miniaturezed Systems for Chemistry and Life Sciences.* 2007: Paris, France.
106. Techaumnat, B., et al., *High-yield electrofusion of biological cells based on field tailoring by microfabricated structures.* IET Nanobiotechnol, 2008. **2**(4): p. 93-9.
107. Kimura, Y., et al., *Dielectrophoresis-assisted massively parallel cell pairing and fusion based on field constriction created by a micro-orifice array sheet.* Electrophoresis, 2011. **32**(18): p. 2496-2501.

108. Kirschbaum, M., et al., *Highly controlled electrofusion of individually selected cells in dielectrophoretic field cages.* Lab on a Chip, 2012. **12**(3): p. 443-450.

ELECTROFUSION CONDITONS AND CHIP REQUIREMENTS

CHAPTER 3

For performing successful and efficient electrofusion on chip, both the microfluidic device and experimental set-up need to meet certain requirements. Our ultimate goal is to generate antibody producing hybridomas in high-yield. Therefore, we need to investigate which microfluidic device and experimental set-up are best suited for efficient electrofusion on chip. This entails the cellular requirements (*e.g.*, cell isolation, nutrients and buffer compositions) as well as the necessary microfluidic requirements, plus the final hybridoma culture and antibody production analysis (*e.g.*, fluorescent dyes and selection media). In this chapter different microfluidic designs and approaches are evaluated to select the methods and parameters which best fits our criteria.

3.1 Introduction

This chapter focuses on the development of a microfluidic platform to efficiently perform electrofusion. Our ultimate goal is to electrofuse B-cells and myeloma cells for the generation of hybridomas. This device would provide us with an efficient method to produce human antibodies for therapy or many other applications, as stated in chapter 2.

It is of utmost importance to investigate the different aspects of electrofusion on chip. There are several parameters which play a key role in successful fusion. On the one hand, the electrofusion conditions including for example the buffer composition and the fusion settings. On the other hand, the design of the microfluidic device (static or flow-through) and the electrical geometry and configuration. Various requirements need to be implemented in the microfluidic platform to be able to perform cell electrofusion on chip. In the next sections, these different requirements are discussed in an itemized form, as well as the different microfluidic platforms that were analyzed.

Firstly, we discuss the electrofusion requirements regarding electrical settings and buffer parameters. Secondly, the chip requirements are reviewed, mainly focusing on the device materials. Next, different cell pairing approaches are discussed for their feasibility and efficiency. Subsequently, the first electrofusion results are shown together with the obtained information derived from those first results. Lastly, the detection and selection requirements regarding electrofusion are studied.

3.2 Electrofusion conditions

An important technique in bulk electrofusion is dielectrophoresis (DEP). Therefore, several microfluidic approaches were also based on cell pairing via DEP[1-4]. In order to use DEP, either for cell pairing or to increase membrane susceptibility for pulses prior to fusion, it is of importance to investigate the parameters which are involved, such as field strength, frequency and conductivity. In order to investigate these parameters, we use a semi-microfluidic approach. In this device, platinum electrodes were sputtered on a glass slide to create locally a high electric field (figure 3.1). This platform was used to gain insights in the electrical parameters which influence electrofusion (*e.g.*, AC voltage, frequency, pulse strength and duration) and the effect of various buffer compositions. In these experiments DEP was used for cell-alignment to promote close cell-cell contact and DC pulses to induce cell fusion.

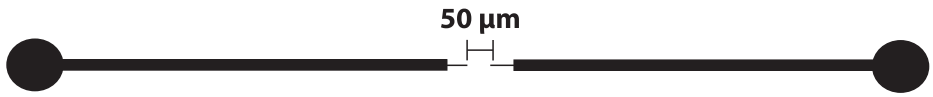

Figure 3.1: Overview of a glass slide with platinum electrodes, at a distance of 50 µm.

3.2.1 Electrical parameters

Cell pairing is the first important step to achieve successful electrofusion of different cells. As mentioned above DEP is a widely used method. However, when applied in bulk liquid (*e.g.* a cuvette) this approach results in completely random cell pairing (chapter 2.4.1, figure 2.3), as the cells arbitrarily line up in pearl chains.
This lining-up in 'pearl-chains' only occurs at certain frequencies, dependent on the fusion buffer conductivity (figure 2.7 chapter 2). So, it is of importance to realize that the buffer of choice also influences the electrical parameters of DEP. Furthermore, low frequencies (less than 10 KHz) should not be used because of undesirable electrolysis and electrophoresis effects[5]. Hence, in electrofusion experiments, frequencies for DEP are 1-100 MHz. Due to the use of low conductive fusion buffer, positive DEP is generated which favors close cell-cell contact.

Another important parameter that controls the electrofusion yield is the specification of the electric field pulse in terms of its strength E_0 and duration[6-8]. Duration must be accurately specified, because exponentially decaying pulses have longer decay half-time ($t_{½}$) compared to square wave pulses. Adjustment of these factors can have at least a two-order of magnitude effect on the fusion yield[9]. Membrane breakdown occurs when the membrane electric voltage (V_m) reaches its critical value V_C of 1 V at room temperature[7]. The V_m of an isolated spherical cell under the influence of an electric field, E_0, is given by[10-12]:

$$V_m = 1.5\ R\ E_0 \cos(\theta) \qquad [3.1]$$

The induced membrane potential is proportional to the cell radius (R). Hence, the range of Vc at which the membrane breakdown is observed varies from cell to cell, and this relationship has to be taken into consideration when cells of different origins are fused[13]. Large cells experience a high voltage drop across the membrane and are more likely to be irreversibly damaged by the electrical treatment. Conversely, small cells have a low voltage drop across the membrane, and have therefore less chance to be porated. Both specification of the electric field pulse in terms of its strength E_0 and duration are extensively discussed in section 2.4.4 and section 4.1.1. With given diameters for B- and myeloma cells the pulse strength and length is in the order of several kV/cm and 50 µs or longer, respectively. Overall, the frequency used for DEP, the pulse amplitude and duration used for fusion must be optimized regarding the cells used for electrofusion[14].

3.2.2 Buffer parameters

There are several parameters which are important to discuss regarding the electrofusion buffer. The conductivity, presence of cations and the osmolality of the buffer all have influence on the electrofusion efficiency.

Conductivity

DEP and pearl-chain formation usually have to be performed in a virtually nonconductive solution (conductivity less than 10^{-4} ohm/cm)[15]. This is because the presence of electrolytes creates heating problems, which results in turbulences and disruption of pearl-chain formation and the fusion process[16]. Furthermore, low conducting buffer promotes the required pDEP (figure 3.2). Hence, electrofusion needs to be performed in low conducting buffer. The use of low conducting buffer has successfully been used by Steenbakkers et al.[17] regarding bulk electrofusion of B-cells and myeloma cells.

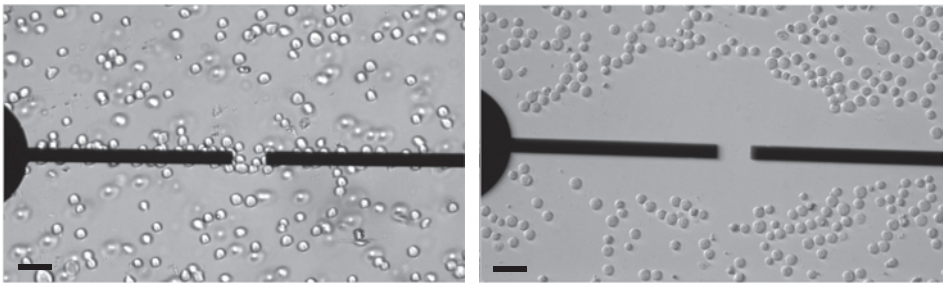

Figure 3.2: pDEP is shown in the left picture using low conducting buffer at 2 MHz. At the same frequency nDEP is demonstrated using high conducting buffer. Scale bar is 50 µm and black parts represent electrodes.

Cations

The presence of divalent cations (Ca^{2+} and Mg^{2+}) and pretreatment of cells with protease are factors known to improve the fusion yield[3, 12]. Divalent cations have a stimulating effect on the viability of the electrofused cells, and therefore on the fusion yield. A concentration of around 0.1mM of Ca^{2+} is optimal for generation hybridoma's[18]. A lower or higher concentration of these ions results in a dramatically decreased hybrid yield[19]. This critical level of Ca^{2+}in the fusion buffer presumably arises from the interaction of this divalent cation with intracellular and membrane components after electroporation[19, 20].

Osmolality

The osmolality of the fusion buffer is a critical parameter in electrofusion. It is said that the fusion yield increases significantly if carried out in hypotonic media or if cells are pretreated briefly in hypotonic media then returned to isotonic media for fusion[21]. Extensive hypotonic preswelling of cells improves membrane contact due to smoothing of the cell surface. Moreover, electrofusion also benefits from the increased mobility of membrane components and dissolution of the cytoskeleton in hypotonically swollen cells[22]. In addition, hypotonic swelling enhances both cell alignment and membrane breakdown simply because the DEP force and induced membrane voltage scale linearly with the cell volume and radius, respectively. To ensure the optimal efficiency of hypotonic electrofusion, several factors have to be considered. The initial cell swelling

can activate various volume-sensitive pathways in the cell membrane that mediate the efflux of cytoplasmatic ions and osmotically driven water loss, to restore normal cell volume. This process, known as regulatory volume decrease (RVD), can abolish the beneficial effects of hypotonic swelling on electrofusion by restoring the cell size and initiating excessive leakage of cytoplasmatic ions[23]. Sorbitol, inositol or sucrose are usually used to adjust the osmolality of the fusion buffer.

In our experiments, commercially available hypotonic electrobuffer from Eppendorf, Westbury, NY was used. To analyze the effect of hypotonic buffer on the size increase and viability, human B-cells were pretreated with hypotonic buffer for 5 min. Human B-cells responded well to this hypotonic medium (11% non-viable cells) vs. isotonic (280 mOsmol/Kg) (4% non-viable cells) and culture medium (8% non-viable cells). Furthermore, a diameter increase was observed from 7.5 um to 10.3 µm (figure 3.3). In isotonic fusion buffer, the diameter of B-cells remained unchanged. This diameter increase is beneficial, because it decreases the difference in cell size dependent parameters between the smaller B-cells and larger myeloma cells, such as the pulse strength and length. However, when investigating the effect of hypotonic buffer on myeloma cells (NS-1 cells), we found a unfavorable effect. Hypotonic buffer was detrimental to NS-1 cells, causing 25% non-viable cells, compared to 10% non-viable cells in isotonic buffer and 3% non-viable cells in culture medium. This could be explained by the RVD effect and significant loss of cytoplasmic ions as mentioned above.

In conclusion, we chose to use low conducting (0.009 S/m), hypotonic/isotonic buffer, containing cations (Ca^{2+} and Mg^{2+}) in our electrofusion experiments.

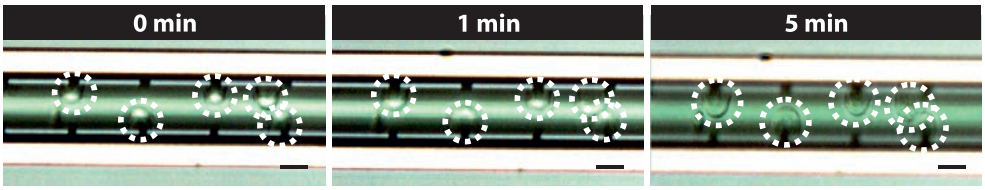

Figure 3.3: Trapped B-cells before and after changing to hypotonic medium. Scale bars are 10 µm.

3.2.3 Electrofusion

In our initial electrofusion experiments, we used the low-throughput DEP-based device, as presented in figure 3.1. The knowledge we obtained about the importance of the electrical and chemical conditions for efficient electrofusion, provides us with valid guidelines for our experiments. However, these conditions vary widely between cell types, and the optimal conditions for carrying out electrofusion between B-cells and myeloma cells need to be found empirically. Electrofusion was observed both in hypotonic and isotonic, low conducting buffer. When human promyelocytic leukemic cells (HL60) were pretreated with hypotonic buffer for 5 minutes, they became more sensitive to pulses (µs) and experienced higher pDEP. Furthermore, multiple and longer pulses (>100 µs), was in majority of these experiments detrimental to the cells (78%

death cells). Cells required mostly 1 pulse of 100 µs (~2.5 kV/cm), or 2-3 short pulses of 10-40 µs to be fused. With low conducting isotonic buffer, multiple pulses – with similar strength and length - were needed. However, most successful fusion events were achieved in isotonic, low conducting buffer (figure 3.4). Pre-alignment was achieved using AC 0.4 kV/cm, 30 s, 2 MHz. With subsequent application of 3 DC pulses of 2 kV/cm and 100 µs. The post-alignment settings were similar to pre-alignment settings. Even though electrofusion was successfully demonstrated, the fusion process is still uncontrollable, has a low success rate and is not high-throughput. So, there is the need to improve and control the cell pairing and increase the throughput. Next, the chip requirements to obtain these goals are discussed.

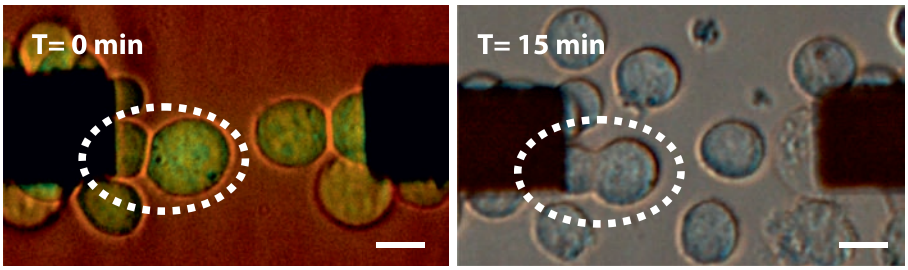

Figure 3.4: Electrofusion of HL60 cells. T=0 HL60 cells in isotonic low conducting buffer. AC 0.4 kV/cm, 30 s, 2 MHz - DC pulses 3x 100 µs 2 kV/cm - AC 0.4 kV/cm, 30 s. T=15 minutes, cell fusion was observed at left electrode, highlighted with dashed circle. Scale bars are 10 µm.

3.3 Chip requirements

3.3.1 Device materials

There are different aspects to take into account when selecting the materials for the device and electrodes, such as biocompatibility and configuration These important issues are described in this paragraph.

Chip material

Glass-silicon devices have the advantage to achieve high aspect ratio and high precision structures, of which the alignment of channels and electrodes is easy. However, the fabrication process is expensive and not advantageously regarding disposability and long-term cell culture and cell recovery. Polymers (*e.g.*, PDMS polydimethylsiloxane) as a substrate material are a good candidate for our experiments. PDMS has proven its use, since a lot of microfluidic electrofusion devices are already polymer-based or partially polymer-based[2, 3, 24]. PDMS is cheap, transparent, gas permeable and biocompatible, overall very well suited as a material for electrofusion on chip[25, 26].

Electrode material and configuration

The incorporation of electrodes in a microfluidic device entails different aspects. The choice of the electrode material and the way it is incorporated.. The effects of

electrochemical processes, such as electrolysis of the medium, free radical generation, and release of ions from the electrodes, are very often neglected[27]. To avoid these reactions, platinum electrodes are commonly used, since platinum electrodes are chemically inert[28]. Furthermore, platinum has a low affinity for protein absorption, in contrast to gold. Low frequencies (less than 10 KHz) should not be used because of undesirable electrolysis and electrophoretic effects[21]. Indium tin oxide (ITO) is also of interest because of its transparency. ITO could be useful in top-bottom electrode designs.

It is important to realize that the electrode configuration is just as important as the choice of material. The electrical field distribution regarding cell position should be optimal. It is desirable that the smaller B-cell experiences a relatively large electric field, since the critical voltage is higher compared to the larger myeloma cells. Furthermore, electrodes should be placed in close proximity to avoid high voltages (~10V instead of ~1000V).

3.3.2 Controlled cell pairing

The several different strategies to achieve cell alignment are DEP, cell traps, focusing current into small flow constrictions and optical trapping [3, 29-31]. DEP was applied by the majority of the authors[1-4] and we have also used a DEP-based, low-throughput method in our first electrofusion experiments. This has given us insights in the various important experimental parameters.

For generating functional hybridomas, it is of utmost importance to fuse one B-cell with one myeloma cell. This makes trapping geometries for selective and controlled cell pairing attractive. Static designs are generally used for single cell fusion[3, 29, 32], facilitating the introduction of a cell suspension, cell alignment and finally fusion. Here, the cell is retained at a defined place when the fusion pulse is applied.

Initially, we will also base our microfluidic design on this static approach. The presented devices have already shown high efficiencies regarding electroporation[33]. We have adapted these designs for the application of electrofusion, with a special focus on controlled cell pairing.

Single cell electrofusion (SCEF) chip

To induce controllable pairing of the cells and achieve medium- throughput electrofusion, the SCEF chip was designed, consisting of glass-silicon (figure 3.5 A and B). Cells were loaded and trapped using pressure differences at the inlets and outlets. HL60 cells (figure 3.5 C) or B-cells and myeloma cells (figure 3.5 E) were trapped and pulsed to induce fusion. Figure 3.5 D shows the electric field distribution using Comsol simulation. Because of the cell size difference, the trap size for B-cells was smaller, 3x4 µm, compared to the larger myeloma cell trap, 5 x 4 µm. As a result the local electric field at the B-cell trap was increased. However, cells were not fused, but electroporated and/or destroyed. Pulses with a length of 100-1000 µs (2.5 kV/cm) showed either no effect, or

resulted in apoptotic cells. Hence, there was no consistent effect on cells after DC pulsing and traps were easily clogged, which resulted in a disturbed electric field. Furthermore, there was a low success rate of trapping living B-cells and myeloma cells, due to shear stress on the cells during loading and trapping.

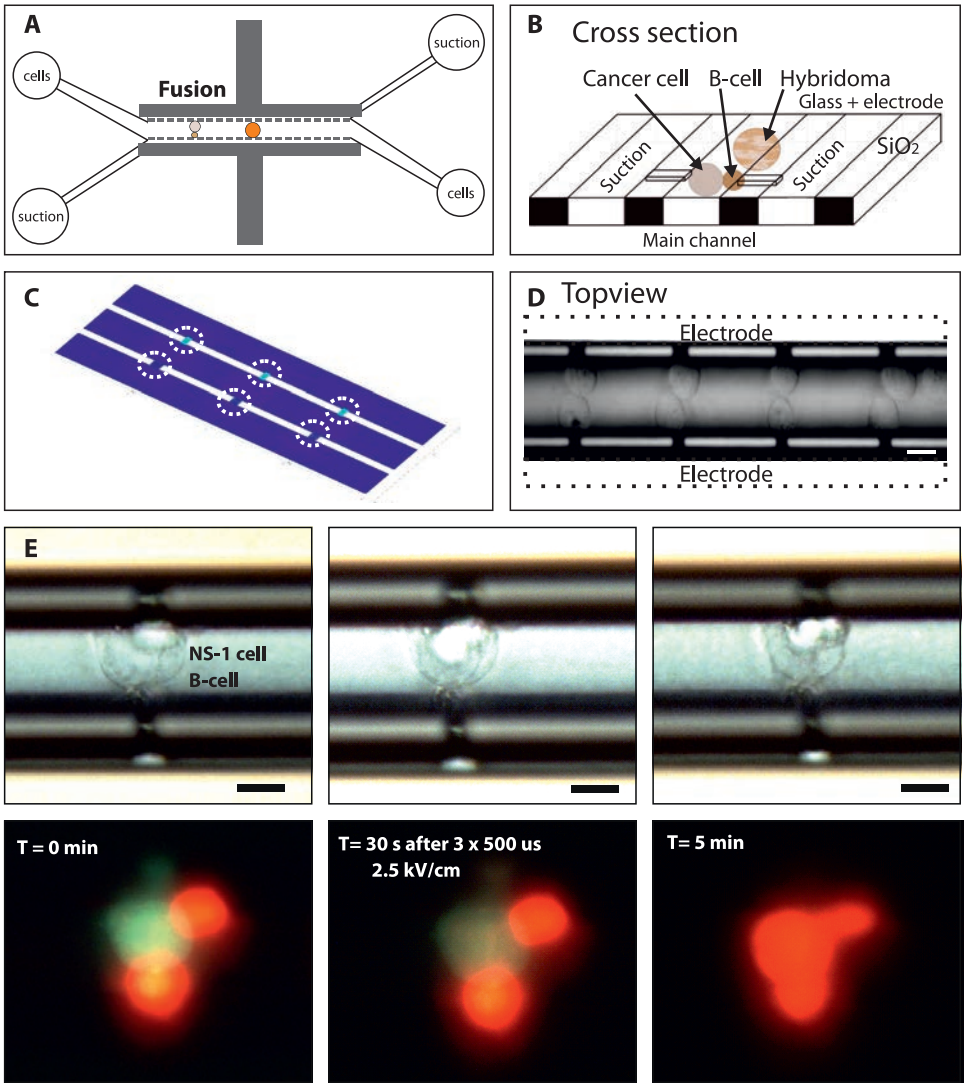

Figure 3.5: Layout of the SCEF chip. A) Schematic overview of the chip with in/outlets and suction channels. Black bars represent the electrodes. B) A cross-section of the SCEF chip. The main channel and suction channels are of silicon (SiO_2). In the main channel, the B-cells and myeloma cells are paired. The chip is covered with a glass slide, containing the sputtered electrodes. C) Comsol simulation of the SCEF chip with top B-cell trap(3x 4 µm) and bottom larger NS-1 myeloma cell trap (5x4 µm) D) Trapped HL60 cells. Scale bar is 10 µm. E) Trapped B-cells and NS-1 cells before and after DC pulses. red; propidium iodide, apoptotic cell stain, green; cytoplasmic cell stain. Scale bars are 10 µm.

Because of the disturbed electric field due to clogging and rough silicon channels, the chip material was changed to glass-PDMS, as shown in figure 3.6. As a result, the viability of the cells after trapping was improved. However, efficient one-to-one trapping remained low and the essential cell-cell contact was difficult to establish. Another practical problem was the alignment of the channels and the electrode structure during the assembly of this design. In conclusion, this approach was not successful for efficient B-cell en myeloma cell fusion.

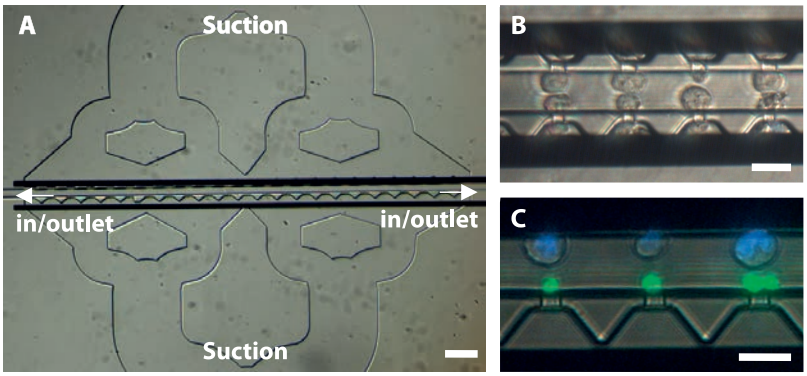

Figure 3.6: PDMS version of SCEF chip. Black structures represent electrodes A) Overview. Scale bar is 80 µm. B) HL60 cells trapped. Scale bar is 20 µm. C) B cells (green CFDA staining) and myeloma (blue Hoechst staining) cells trapped. Scale bar is 20 µm.

High-throughput flow through fusion chip

A flow through fusion chip (glass-silicon) was designed to test the possibility of flowing single cells through a long straight channel with opposing electrodes (ITO) on the side to form cells pairs for subsequent fusion. ITO was chosen for it transparency as a future plan was to use top-bottom electrodes, for an uniform electric field (figure 3.7). However, ITO oxidized and turned opaque, presumably because of anionic binding, resulting in a high resistivity.

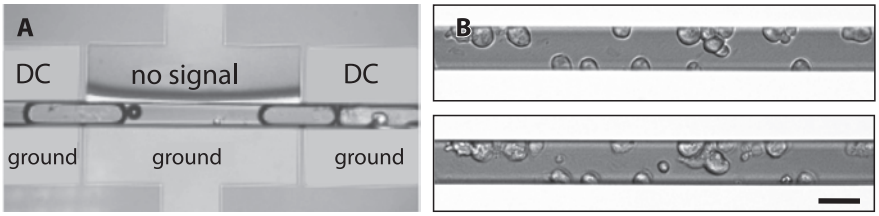

Figure 3.7: A) overview of the flow through design. The middle top electrode was damaged after applying a DC pulse on the other electrodes of 5-10 V, but not when an AC field of 10 V, 2 MHz was put on for long term. B) HL60 cells before (top) and after (bottom) an AC field of 0.625 kV/cm followed by 3 DC pulses of 300 µs 2.5 kV/cm. Scale bars are 40 µm.

Furthermore, platinum electrodes also did not work, as it showed no flow through effect. No pearl chains were formed, cells did not pair up, but instead the cells got stuck to the

channel walls and electrodes. To show that there was an electrical field present, 3 DC pulses of 300 µs were applied. As a result, as shown in figure 3.7 B, the cells did not survive these pulses.

In conclusion, a flow-through approach was not successful and fusion results were achieved using a static approach. Furthermore, cell pairing was achieved using the SCEF chip, however the trap geometry was not optimal for cell-cell contact and electric field distribution. Overall, the device should enable efficient single cell pairing with an optimal electric field distribution. Hence, the recommendation is to choose cell traps which provide optimal cell–cell contact and electric field distribution for B- and myeloma cell fusion. Next, the detection and selection component of the electrofusion chip is discussed.

3.3.3 Detection and selection

Detecting and analyzing the fusion efficiency can be performed in different ways, but optical detection is performed most often. The majority of the studies solely rely on image acquisition during electrofusion, followed by careful analysis[1, 3, 4]. In order to facilitate optical detection, fluorescent dyes are used, such as the cytoplasmic dye calcein. Cytoplasmic dyes enable the determination of pairing and fusion efficiencies based on fluorescence exchange[24, 29]. Furthermore, a membrane fluorescent dye can be used to analyze membrane reorganizations during the electrofusion process[32]. However, it has to be kept in mind that only cytoplasmic fusion can be imaged. Nuclear fusion occurs spontaneously, after 1-2 weeks and is therefore difficult to detect.

Membrane marker

In first experiments, we tried a membrane marker, mainly to gain more insight in the fusion process (figure 3.8). However, when using this dye, we observed no cell fusion. It is known that membrane markers can interfere with cell fusion[34].

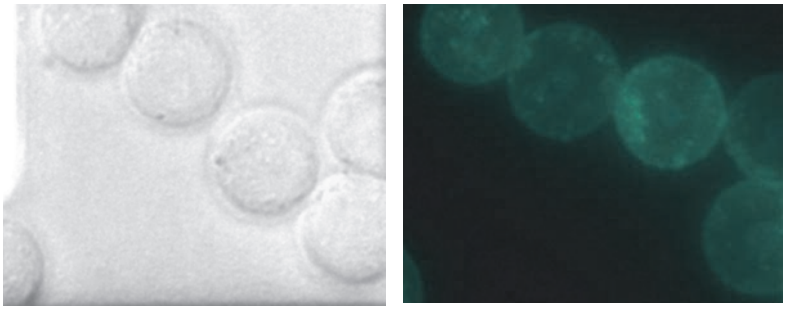

Figure 3.8: HL60 cells stained with the membrane dye PKH67 (10 µM).

Cytoplasmic marker

To avoid interference of the fluorescent dye with the cell fusion process, we tried a cytoplasmic stain (CFDA-SE, carboxyfluorescein diacetate succinimidyl ester). Figure 3.9 shows isolated B-cells with CFDA staining 4 µM (left) and NS-1 cells (right) were stained with Hoechst staining, which is a nuclear staining. The CFDA staining in suitable for cell tracking, therefore also for following the fusion process, while retaining viability throughout the process, Hoechst staining is not.

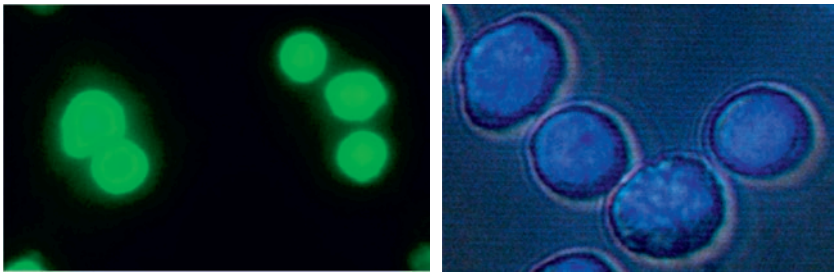

Figure 3.9: Left B-cells 4 µM CFDA staining, right NS1 cells Hoechst staining (2.5 µg/ml).

Hybridoma selection

After the detection of cell electrofusion, it is crucial to analyze the fusion products and select the hybridomas. When fusing B- cells and myeloma cells, the selection of the correct fusion product is done by culturing the fused products in selection medium, called HAT medium[17, 35, 36]. This HAT medium contains hypoxanthine, aminopterin and thymidine. During DNA synthesis, normal cells synthesize purine nucleotides and thymidylate in a pathway requiring tetrahydrofolate. Aminopterin blocks the activation of tetrahydrofolate and inhibits the synthesis of purines in this pathway. Aminopterin treated cells can use an alternative pathway to synthesize purine nucleotides if hypoxanthine is supplied externally (as is done when culturing in HAT medium)[37]. The enzyme present in cells that catalyzes the alternative pathway is hypoxanthine-guanine phosphoribosyltransferase (HGPRT)[38]. The used myeloma cells (NS-1) are HGPRT deficient and therefore cannot use this alternative pathway. Therefore, the myeloma cells will die in HAT medium. However, if B-cells are fused with NS-1 myeloma cells, the B-cells provide the necessary enzymes, so that the hybridoma cells can grow in HAT medium. Unfused B-cells cannot survive for more than 1-2 weeks, because they are not immortalized[37] HAT medium therefore provides the ideal environment for the selection of hybridomas. After several days, the medium is replaced by HT medium to avoid the unnecessary longer use of the toxic aminopterin[39]. The final stage is to select the hybridomas, which produce the right antibody.

3.4 Conclusion

For performing efficient cell electrofusion on chip, intended to generate hybridomas, the microfluidic device and the experimental set-up both have to meet certain requirements. In this chapter, we carefully reviewed and tested the important parameters for cell electrofusion. Furthermore, low-throughput electrofusion of HL60 cells was shown. This provided us with insights into some critical parameters. Below some recommendations are highlighted, regarding the chip design and electrofusion parameters.

Platinum electrodes will be used for providing the DC pulses and if needed an AC field. Furthermore, the use of a low conducting buffer prevents electrode degradation and heating during experiments. As mentioned in section 3.2.2., an isotonic buffer will be used, containing Ca^{2+} and Mg^{2+}.

The most critical part of the electofusion device will be the controlled cell pairing combined with the electric field distribution. The recommendation is to choose cell traps which provide optimal electric field distribution for B- and myeloma cell fusion.

We think the use of a cytoplasmic dye is a good trade-off between being able to visualize the cell fusion and avoiding interfering with the fusion process. Although the membrane stain could give interesting information on membrane fusion, we were not able to fuse membrane-stained cells. This suggests interference of this dye during the fusion process. Although antibody formation is the gold standard, we first focus on the selection of the hybridomas using HAT selection medium, since the latter method is the first and more practical proof of hybridoma generation.

In conclusion, the proposed device should enable efficient single cell pairing with an optimal electric field distribution, while being able to follow the fusion process and regain the fusion products for further analysis (viability, antibody production). Finally, our ultimate goal is to gain high efficiency electrofusion, followed by a high-yield of antibody producing hybridomas.

In the next chapter, we characterize and analyze a single cell electrofusion chip using traps (static approach). This microfluidic design is based on the work of Skelley et al.[29], which have shown high electrofusion efficiencies in literature. We have optimized and adapted this design for the electrofusion of single B-cells and myeloma cells for hybridoma formation. Moreover, the trap structure is designed such that it provides an optimal electric field distribution regarding cell fusion of different sizes cells.

Although, it has to be kept in mind that this is a good approach for characterization and optimizing B- and myeloma cell fusion on chip, it is not a high-throughput approach. Hence, after achieving static electrofusion of B-cell and myeloma cells, we finally move to the microfluidic droplet platform to obtain high-throughput cell fusion (chapter 5-8).

3.5 References

1. Cao, Y., Yang, J., Yin, Z.Q., Luo, H.Y., Yang, M., Yang, N.H.J., Huo, D.Q., Hou, C.J., Jiang, Z.Z., Zhang, R.Q., Xu, R., Zheng, R.L., *Study of high-throughput cell electrofusion in a microelectrode-array chip.* Microfluid Nanofluid, 2008. **5**(5): p. 669-675.
2. Ju, J., Ko, J.M., Cha, H.C., Park, J.Y., Im, C.H., Lee, S.H., *An electrofusion chip with a cell delivery system driven by surface tension.* Journal of Micromechanics and Microengineering 2009. **19**.
3. Techaumnat, B., et al., *High-yield electrofusion of biological cells based on field tailoring by microfabricated structures.* IET Nanobiotechnol, 2008. **2**(4): p. 93-9.
4. Tresset, G., Takeuchi, S., *A microfluidic device for electrofusion of biological membranes.* Seisan-kenkyu, 2004. **56**(1).
5. MacDonald, S.J., Bodger, P.S., Elder, P.A., *Biological cell alignment for electrofusion.* IEE PROCEEDINGS-A, , 1992. **39**(3).
6. Gross, D., *Electromobile surface charge alters membrane potential changes induced by applied electric fields.* Biophys J, 1988. **54**(5): p. 879-84.
7. Chang, D.C., Saunders, J.A., Chassy, B.M., Sowers, A.E., *Overview of electroporation and electrofusion*, in *Guide to electroporation and electrofusion*, D.C. Chang, Saunders, J.A., Chassy, B.M., Sowers, A.E., Editor. 1992, Academic Press Limited: London.
8. Pliquett, U., et al., *High electrical field effects on cell membranes.* Bioelectrochemistry, 2007. **70**(2): p. 275-82.
9. Sowers, A.E., *Mechanisms of electroporation and electrofusion*, in *Guide to electroporation and electrofusion*, D.C. Chang, Saunders, J.A., Chassy, B.M., Sowers, A.E., Editor. 1992, Academic Press limited: London.
10. Washizu, M. and B. Techaumnat, *Polarisation and membrane voltage of ellipsoidal particle with a constant membrane thickness: a series expansion approach.* IET Nanobiotechnol, 2008. **2**(3): p. 62-71.
11. Zimmermann, U., *Electrical breakdown, electropermeabilization and electrofusion.* Rev Physiol Biochem Pharmacol, 1986. **105**: p. 176-256.
12. Cole, K.S., *Membrane watching.* J Gen Physiol, 1968. **51**(5): p. Suppl:1S-7S.
13. Neumann, V., F. Siegemund, and B. Baessler, *Electrically induced fusion of different human cell types.* J Neurol, 1986. **233**(3): p. 153-6.
14. Chiu, D.T., *A microfluidics platform for cell fusion.* Curr Opin Chem Biol, 2001. **5**(5): p. 609-12.
15. Zimmermann, U. and J. Vienken, *Electric field-induced cell-to-cell fusion.* J Membr Biol, 1982. **67**(3): p. 165-82.
16. Neumann, E., Sowers, A.E., Jordan, C.A., *electroporation and electrofusion in cell biology*, ed. E. Neumann, Sowers, A.E., Jordan, C.A. 1989: Plenum press, NY.
17. Steenbakkers, P.G., H.A. Hubers, and A.W. Rijnders, *Efficient generation of monoclonal antibodies from preselected antigen-specific B cells. Efficient immortalization of preselected B cells.* Mol Biol Rep, 1994. **19**(2): p. 125-34.
18. Ohno-Shosaku, T. and Y. Okada, *Electric pulse-induced fusion of mouse lymphoma cells: roles of divalent cations and membrane lipid domains.* J Membr Biol, 1985. **85**(3): p. 269-80.

19. Dimitrov, D.S., *Membrane fusion kinetics* in *Guide to Electroporation and Electrofusion,*, B.M.C. D.C. Chang, J.A. Saunders and A.E. Sowers, Editor. 1992, Academic Press: San Diego. p. 155–166.
20. Dimitrov, D.S., *Electroporation and electrofusion of membranes*, in *Handbook of biological physics*, R. Lipowsky, Sackmann, E., Editor. 1995, Elsevier science.
21. Zimmermann, U., Neil, G.A., *Electrofusion of cells: State of the art and future directions*, in *Electromanipulation of Cells* 1996, CRC-Press.
22. Schmitt, J.J., U. Zimmermann, and P. Gessner, *Electrofusion of osmotically treated cells. High and reproducible yields of hybridoma cells.* Naturwissenschaften, 1989. **76**(3): p. 122-3.
23. Sukhorukov, V.L., et al., *Surviving high-intensity field pulses: strategies for improving robustness and performance of electrotransfection and electrofusion.* J Membr Biol, 2005. **206**(3): p. 187-201.
24. Wang, J., Lu, C., *Microfluidic cell fusion under continuous direct current voltage.* Applied physics letters 2006. **89**.
25. Ismagilov, R.F., et al., *Experimental and theoretical scaling laws for transverse diffusive broadening in two-phase laminar flows in microchannels.* Applied physics letters, 2000. **76**(17): p. 2376-2378.
26. Wolbers, F., et al., *Viability study of HL60 cells in contact with commonly used microchip materials.* Electrophoresis, 2006. **27**(24): p. 5073-80.
27. Marszalek, P., D.S. Liu, and T.Y. Tsong, *Schwan equation and transmembrane potential induced by alternating electric field.* Biophys J, 1990. **58**(4): p. 1053-8.
28. Al Mamun, N.H. and P. Dutta, *Patterning of platinum microelectrodes in polymeric microfluidic chips.* Journal of Microlithography Microfabrication and Microsystems, 2006. **5**(3).
29. Skelley, A.M., et al., *Microfluidic control of cell pairing and fusion.* Nat Methods, 2009.
30. Tresset, G. and S. Takeuchi, *Utilization of cell-sized lipid containers for nanostructure and macromolecule handling in microfabricated devices.* Analytical Chemistry, 2005. **77**(9): p. 2795-2801.
31. Stromberg, A., et al., *Manipulating the genetic identity and biochemical surface properties of individual cells with electric-field-induced fusion.* Proceedings of the National Academy of Sciences of the United States of America, 2000. **97**(1): p. 7-11.
32. Stromberg, A., et al., *Microfluidic device for combinatorial fusion of liposomes and cells.* Anal Chem, 2001. **73**(1): p. 126-30.
33. Valero, A., *Single cell electroporation*, in *BIOS Lab-on-a-Chip group of the MESA+ Institute for Nanotechnology*. 2006, University of Twente: Enschede, The Netherlands. p. 209.
34. Nickoloff, *Plant Cell Electroporation And Electrofusion Protocols*, H. Jones, Editor. 1994.
35. Kua, C.H., et al., *Cell motion model for moving dielectrophoresis.* Anal Chem, 2008. **80**(14): p. 5454-61.
36. Zimmermann, U., et al., *Efficient hybridization of mouse-human cell lines by means of hypo-osmolar electrofusion.* J Immunol Methods, 1990. **134**(1): p. 43-50.
37 . Pandey, S., *Hybridoma technology for production of monoclonal antibodies.* International Journal of Pharmaceutical Sciences Review and Research, 2010.
38. Hiatt, A.C., *Monoclonal antibodies, hybridoma technology and heterologous production systems.* Curr Opin Immunol, 1991. **3**(2): p. 229-32.

39. Golestani, R., A.A. Pourfathollah, and S.M. Moazzeni, *An extreme strategy for the production of hybridoma*. Hybridoma (Larchmt), 2009. **28**(2): p. 139-44.

ON CHIP ELECTROFUSION OF SINGLE HUMAN B-CELLS AND MOUSE MYELOMA CELLS*

CHAPTER 4

This chapter describes the development and full characterization of a microfluidic chip for electrofusion of human peripheral blood B-cells and mouse myeloma (NS-1) cells to generate hybridomas. The chip consists of an array of 783 traps, with dimensions that were optimized to obtain a final cell pairing efficiency of 33 ± 6%. B-cells were stained with a cytoplasmic stain to assess the different stages of cell fusion, i.e., dye transfer to NS-1 cells (initiating fusion) and membrane reorganization (advanced fusion). 6 DC pulses of 100 μs (2.5 kV/cm) combined with an AC field (30 s, 2 MHz, 500 V/cm) and pronase treatment resulted in the highest electrofusion efficiency of paired cells (51 ± 11%). Hybridoma formation, with a yield of 0.33% and 1.2%, was observed after culturing the fused cells for 14 days in conditioned medium. This work provides valuable leads to improve the current electrofusion protocols for the production of human antibodies for diagnostic and therapeutic applications.

*modified from: E. Kemna. F. Wolbers, I. Vermes, A. van den Berg. Electrophoresis, 2011, 32(22) 3138-46

4.1 Introduction

The rapid increase in use of antibodies necessitates the development of efficient antibody production technologies. Today, this production of relevant antibodies primarily relies on the cell fusion of human B-cells with myeloma cells (chapter 2). In cell fusion, two cell types are fused to generate a third cell type, which displays the combined characteristics of both cells[1-3]. Apart from its use in the generation of antibody-secreting hybridomas, cell fusion is also used for other applications such as, cloning of mammalian cells and therapeutic purposes[4-6].

As mentioned in chapter 2, there are several methods to achieve fusion *in vitro*, including chemical (PEG)[7], viral (Epstein-Barr)[8] and physical methods (electric fields). Electrofusion is the most commonly used approach, as it shows the highest fusion efficiency[9].

For therapeutic applications, such as cancer immunotherapy, human antibodies, and hence human B-cells, are a prerequisite[10, 11]. A human IgM-producing hybridoma can be generated via the fusion of a human B-cell with a mouse myeloma cell[11-13]. Furthermore, readily accessible human peripheral blood $CD19^+$ B-cells are known to generate a high number of antibody secreting hybridomas[14].

The goal of this study is to efficiently fuse human $CD19^+$ B-cells with mouse myeloma cells on chip to generate hybridomas. These hybridomas are able to produce human antibodies, which can be used for therapeutic applications. For this, a microfluidic PDMS chip with an array of 783 traps is developed for selective cell pairing, based on the design presented by Skelley et al.[15] (figure 4.1 A and B). Cell loading was achieved by subsequently loading B-cells, followed by NS-1 cells, as schematically shown in figure 4.1 B. After applying the electrical pulses, the process of fusion between B-cells and NS-1 cells could be observed in detail at a single cell level in real-time.

Microelectronic patterning techniques have been applied to decrease the distance between the electrodes enabling the use of low voltages (10V). Firstly, the microfluidic chip was characterized regarding B-cell and mouse myeloma cell trapping and COMSOL simulations were performed to simulate the electric field gradient. Secondly, the electrofusion parameters were set and cells were stained with fluorescent dyes to assess cell fusion. Lastly, to determine hybridoma formation, fused cells were checked for viability after 14 days of conditioned culturing.

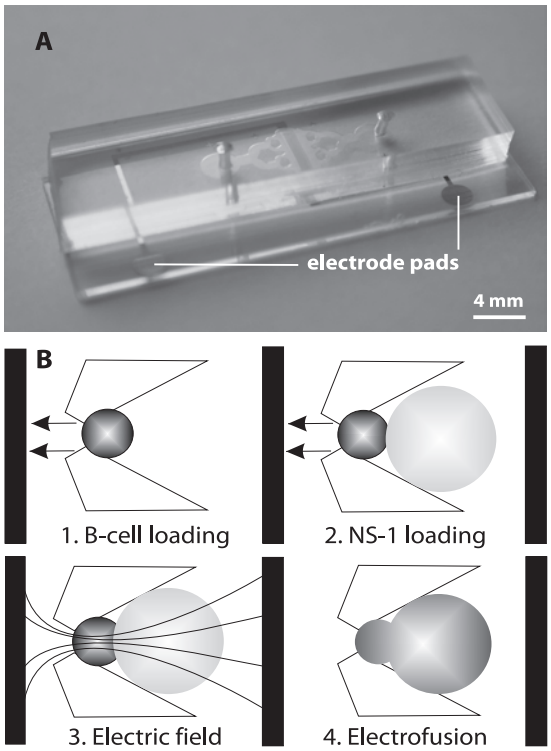

Figure 4.1: A) Photo of microfluidic device. B) Schematic overview of B- and NS-1 cell loading in one trap of the array, followed by electric field pulses and fusion.

4.1.1 Theory

A biological cell, with radius *R*, is usually modelled as having a conductive interior (cytoplasm) encapsulated by a thin insulating layer (plasma membrane). The membrane electric voltage (V_m) of an isolated spherical cell under the influence of a uniform electric field (E_0), is defined as[16]:

$$V_m = 1.5\ R\ E_0 \cos(\theta)(1 - \exp[-\tau/\tau_m]) \qquad [4.1]$$

The voltage generated across the plasma membrane of a spherical cell grows exponentially with time. θ is the angle between the normal to the membrane and the electric field vector and τ_m is the time constant of membrane charging, given by

$$\tau_m = R * C_m \left(\frac{1}{\sigma_c} + \frac{1}{2\sigma_m}\right) \qquad [4.2]$$

in which σ_c and σ_m are the cell's interior and exterior conductivity. C_m is the membrane capacitance per unit area (F/m^2). A typical value of C_m is 10 mF/m^2[2,17]. When the pulse

duration is 5-10*τ_m, the membrane charging is completed and equation [4.1] simplifies to the well-known equation

$$V_m = 1.5\ R\ E_0 \cos(\theta) \qquad [4.3]$$

Membrane breakdown occurs when V_m reaches its critical value (V_c) of 1 V at room temperature[18]. Using the parameters of the cells of interest, the pulse strength and duration can be calculated with above described equations.

4.2 Materials and Methods

4.2.1 Microfluidic chip design and fabrication

The microfluidic chip (figure 4.2) consists of a trap array (5100 µm x 1800 µm) containing 11 rows of 87 traps, in which the first two rows act as a filter. Hence, the trap array has a total of 783 effective traps. The rows are separated at a distance of 50 µm, and the distance between the traps (d_t) is varied. Electrodes are 30 µm in width and the distance between the electrodes is 40 µm. The total chip depth is 26 µm. A single trap consists of a large trap, which has a V-shape (width = 25-29 µm; length = 20-21 µm) with in the middle a small trap with varying depths (d_s = 3 or 6 µm). A silicon master design was drawn in Clewin (version 4.01) and fabricated using standard UV-lithography. SU-8 2-25 (Microchem) was spun on the silicon master. Firstly, a layer with a thickness of 3 or 6 µm was spun in combination with second layer of 26 µm thick, to generate the small traps with a depth of 3 or 6 µm. As a final step, FDTS (1H,1H,2H,2H perfluorodecyltrichlorosilane) was spin coated on the master. The trap array was made in PDMS (Sylgard 184, Dow Corning, Midland, MI, USA). Curing and base agent were mixed at a ratio of 1:10 and degassed. PDMS was poured on the FDTS-coated patterned silicon wafer, degassed, and cured at 60 °C for 24 hours. FDTS coating was applied to increase the hydrophobicity of the wafer and to make it less proned for sticking of PDMS on the SU-8 structures after curing.

After curing, in- and outlets were punctured using an EFD dispensing tip (Nordson, Westlake, Ohio, USA; inner Ø 1.36 mm, outer Ø 1.65 mm) and the PDMS trap array was carefully cleaned with isopropanol for 10 minutes in an ultrasonic bath, rinsed in deionized water and dried with nitrogen. Subsequently, the PDMS trap array was sealed to a Pyrex glass slide with patterned Pt electrodes using oxygen plasma. The PDMS and Pyrex surfaces were placed in the plasma oxygenator (Harrick PDC001) for 45 seconds at a RF (radio frequency) of 29.6 W and a pressure of 400 mTorr. The oxygen flow was 2 sccm. After sealing, the chip was put for 30 minutes at 60 °C, after which PBS was introduced into the chip to preserve the hydrophilicity of the PDMS and facilitate cell loading.

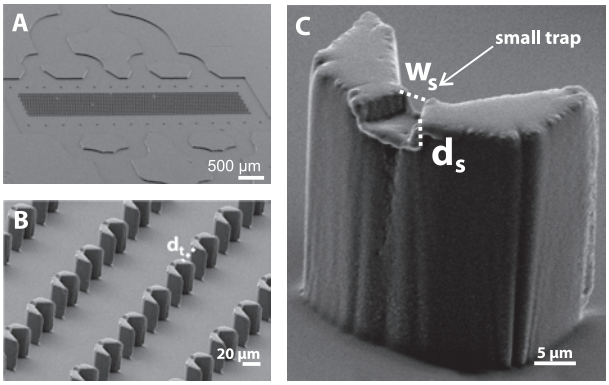

Figure 4.2: Microfluidic device for cell pairing and electrofusion. A) Scanning electron micrograph (SEM) of the PDMS chip. B) Magnified SEM image of the trap array, d_t represents the distance between the traps. C) Detailed zoom of one trap structure, highlighting the large and small trap; w_s and d_s represent the width and depth of the small trap.

4.2.2 Cell culture

Mouse myeloma cells

The mouse myeloma cell line NS-1 was a kind donation from ModiQuest, The Netherlands. Cells were grown in DMEM/F12 medium (Invitrogen, Grand Island, NY, USA), supplemented with 10 % (v/v) fetal bovine serum (FBS; Invitrogen), 100 U/ml penicillin (Invitrogen), 100 µg/ml streptomycin (Invitrogen), 2 mM L-glutamine (Invitrogen), 20 µM ethanolamine (Sigma, St. Louis, MO, USA), 2.6 pM sodium selenite (Sigma) and 30 µM 2-mercaptoethanol (Sigma) (= DMEM$^+$ medium). Cell cultures were sustained in a 5 % CO_2 humidified atmosphere at 37 °C. NS-1 cells were split every 3-4 days at a ratio of 1:10 after treatment with 0.2 mM EDTA in PBS. NS-1 cells were in exponential state when used for electrofusion experiments.

Human B-cells

For isolation of CD19$^+$ B-cells, 4 ml of EDTA peripheral blood from anonymous healthy donors was used. Peripheral blood mononuclear cells (PBMC) were isolated with Ficoll–Hypaque (GE healthcare, Eindhoven, The Netherlands) gradient centrifugation. The PBMC were washed twice in calcium- and magnesium-free PBS and resuspended in RPMI-1640 medium with phenol red (Invitrogen), supplemented with 10 % FBS (v/v), 100 U/ml penicillin, 100 µg/ml streptomycin, 2 mM L-glutamine, 2 mM sodium-pyruvate (Lonza, Verviers, Belgium) and 50 µM 2-mercapthoethanol (= RPMI$^+$ medium). PBMC were cultured in the presence of 20 µg/ml lipoprotein saccharide (LPS; Sigma), for B-cell stimulation, in a 5 % CO_2 humidified atmosphere at 37 °C. After 3-4 days of LPS stimulation, the PBMC were collected and the B-cells were isolated with anti-CD19 antibody-coupled supramagnetic beads (Invitrogen) at a ratio of 1:50. After 20 minutes of incubation at 4 °C, bound cells were isolated magnetically, washed three times with PBS, supplemented with 1 % w/v BSA and 2 mM EDTA to remove cells that bound unspecifically to the beads, and resuspended in 200 µl RPMI$^+$ medium. The magnetic

beads were removed from bound cells by incubation for 45 minutes at room temperature with 25 µl DetachaBead (Invitrogen). In experiments, B-cells were used within two days after isolation.

4.2.3 Electrofusion experimental set-up

Cell preparation

B-cells were stained with 4 µM carboxyfluorescein diacetate succinimidyl ester (CFDA-SE) (Cell Tracer Kit, Molecular Probes) for 15 minutes at 37 °C, to stain the cytoplasm. After incubation, the B-cells were centrifuged and resuspended in prewarmed $RPMI^+$ medium and incubated for another 30 minutes to ensure complete modification of the CFDA dye. Subsequently, the B-cells were washed again in $RPMI^+$ medium and resuspended in the desired concentration and volume.

In some experiments, NS-1 cells were treated with 0.5 mg/ml pronase (Sigma), a membrane stabilizing agent, for 3 minutes at 37 °C in isoosmolar electrofusion buffer. Isoosmolar electrofusion buffer consisted of deionized water, supplemented with 280 mM inositol (Sigma), 0.1 mM calcium acetate (Sigma), 0.5 mM magnesium acetate (Sigma) and 1 mM l-histidine (Sigma). The conductivity was adjusted, using deionized water, to 0.009 S/m. The effect of pronase was halted after adding FBS. The NS-1 cells were washed and resuspended in $DMEM^+$ medium for further experimental use.

Set-up

The microfluidic chip was mounted on to an X-Y-Z translation stage of an inverted wide fluorescence microscope (Leica DM IRM, Leica Microsystems, Wetzlar, GmbH, Germany). The microscope was equipped with a mercury lamp as an excitation source for fluorescence measurements. In addition, a computer-controlled CCD camera (Leica DFC300 FX) was mounted on to the microscope for image recording, using the accompanied Leica Application Suite Software (version 2.3.4 R2). The outlet of the microfluidic chip was punctured with PEEK tubing, (Vici, Schenkon, Switzerland, inner Ø 0.5 mm and outer Ø 1.59 mm) and connected to a glass gastight syringe (Hamilton, Bonaduz, Switzerland). Probes were used (SUSS MicroTec PH100, Germany) for connection to the electrode pads on the Pyrex glass.

Electrofusion experiment

The microfluidic chip was conditioned with 3 % w/v BSA for a minimum of 30 minutes, this is to prevent sticking of cells throughout the chip on places other than the cell trap. Both cell types were filtered (40 µm filter) before cell loading, ensuring a homogeneous cell suspension. Cell loading was accomplished by manually placing ~200 µl cell suspension in the inlet reservoir and drawing the cells through the device at 10 µl/min (65 - 130 µm/s) using a syringe pump (KdScientific 101). The isolated B-cells were used in a concentration of ~1 x 10^6 cells/ml in $RPMI^+$ medium. When B-cell trapping was accomplished, the cell solution was exchanged with a cell solution containing NS-1 cells (~2 x 10^6 cells/ml in $DMEM^+$ medium). After cell pairing, the medium was exchanged for

200 µl isoosmolar electrofusion buffer. Subsequently, pulses were applied according to the pulse scheme, as specified in table 4.1, using in house software, based on LabVIEW, which uses a Data Acquisition Card for generating the AC and DC pulses.

Table 4.1: Overview of the pulse scheme. In every experiment, the applied DC voltage was set at 10V. + refers to 'with AC', - refers to 'no AC'.

Pulse length (µs)	50						100						200					
DC pulses (#)	1		3		6		1		3		6		1		3		6	
+/- AC	-	+	-	+	-	+	-	+	-	+	-	+	-	+	-	+	-	+

In every experiment, the applied DC voltage was set at 10 V (2.5 kV/cm) at various pulse lengths, of 50, 100 and 200 µs. In some experiments, an AC field of 2 V, 2 MHz and 30 seconds was applied, before and after the DC pulses.

4.2.4 Hybridoma culture and analysis

15 minutes after applying the final DC pulse, the isoosmolar electrofusion buffer was exchanged for HAT selection medium, consisting of DMEM$^+$ medium, supplemented with 100 µM hypoxanthine (Sigma), 0.4 µM aminopterin (Sigma), 16 µM thymidin (Sigma) and 100 U/ml hIl-6 (Sigma). The microfluidic chip, covered with HAT medium, was put at 37 °C in the incubator overnight. The next day, the cells were removed from the chip by peeling of the PDMS. The collected cell suspension was transferred to a 96 well plate and placed back in the incubator for hybridoma culture. After 5-6 days, the HAT selection medium was replaced by HT medium (= HAT selection medium without aminopterin). The HT medium was refreshed every 3 days. 14 days after the electrofusion experiments, the cells were analyzed for hybridoma growth. Hybridoma growth is in these experiments defined as the presence of viable cells after 14 days of culturing in selection medium. This selection medium only allows for hybridoma cell survival, as discussed in chapter 3. Hybridoma viability was checked after 30 minutes of incubation with 2 µM calcein AM (Invitrogen).

4.2.5 Image acquisition and analysis

Membrane reorganisation and CFDA dye transfer were determined optically with light and fluorescence microscopy. The complete array was imaged at t = 0 minutes (= before DC pulse) and at t = 15 minutes and t = 30 minutes after DC pulse. The obtained data was analyzed using CorelDRAW X3 to determine trapping and pairing efficiencies (= number of traps occupied with one pair of a single B-cell and single NS-1 cell) and fusion efficiency (based on fluorescence exchange and membrane reorganization). For one single trapping experiment, the average trapping and pairing efficiency was based on a minimum of 300 analyzed traps. For the electrofusion experiments, all cell pairs in the array were analyzed.

4.2.6 COMSOL simulation

Using COMSOL 3.5 Multiphysics, a 3D electric field profile of one trap with at both sides electrodes, was simulated. The module, which was used, was conductive media DC (emdc). In addition, the conductivity of the medium was set at 0.009 S/m and the PDMS as insulating. One electrode was set as ground, as the other was set to a potential of 10 V.

4.3 Results and discussion

4.3.1 Characterization of the microfluidic device

The microfluidic chip (figure 4.1 A) consists of one inlet branching into four channels to promote even cell distribution (figure 4.2 A). The chip consists of a densely packed trap array (figure 4.2 B), with a total of 783 traps. The cell trap (figure 4.2 C) is designed in such a way that an optimal electrical field for fusion of different sized cells, i.e. human B-cells with mouse NS-1 cells, is ensured. This electrical field is simulated using COMSOL.

Electric field distribution

Using COMSOL, a 3D electric field profile of a trap with a d_s of 6 µm, a w_s of 5 µm and an electrode distance of 40 µm was simulated (figure 4.3 A). The normalized electric field gradient along the path from one electrode to the other electrode was analyzed (cross-section A-A' in figure 4.3 A). Figure 4.3 B shows the normalized electric field inside the trap array when a pulsed DC square wave (10 V) was applied at the electrodes. The simulation shows that the electrical field density increased in the small trap, which captures the B-cell, as compared to the large trap, which traps the NS-1 cell. This is favorable as the larger NS-1 cell is more sensitive to the electric field than the smaller B-cell. In this design the B-cell will therefore experience a relatively larger field strength.

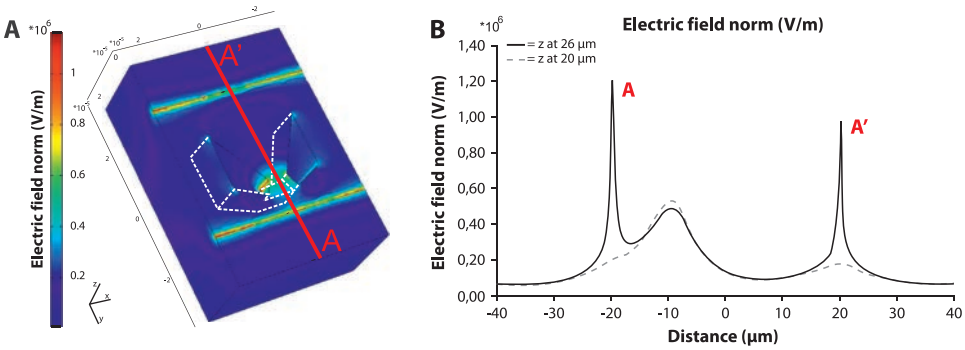

Figure 4.3: Electric field profile. A) Normalized electrical field in a single trap B) Graph of the normalized electric field intensity gradient along the cross section A-A' at a depth of 0 and 6 µm.

Cell trapping and pairing

Different trap structures and distances were analyzed for efficient cell trapping and pairing. The small trap was tested for two different depths (d_s = 3 µm and 6 µm). A d_s of 3 µm showed a B-cell trapping efficiency (= one B-cell per trap) of 42 ± 20 % (w_s=4 µm, n=4, 166/400 traps), which is significantly lower (two sided T-test, $p<0.05$) compared to the 6 µm trap depth, 77 ± 2.3 % (w_s=4 µm, n=6, 464/600 traps). Hence, the 3 µm trap was too small for efficient B-cell trapping. The distance between the traps, d_t, was varied at 20-25-30 µm (d_s = 6 µm). Here, the critical factor was the NS-1 cell, which has a diameter of 14.2 ± 1.6 µm (n=20). A d_t of 25 µm showed the highest trapping efficiency of NS-1 cells (83.3 ± 3.5 %, n=3, 250/300). This is not in accordance with the results obtained by Skelley et al.[15], who stated that a separation distance of 1 to 1.5 of the cell diameter between traps is optimal. A d_t of 20 µm and 30 µm showed trapping efficiencies of respectively 56.4 ± 6.5 % (n=4, 225/400) and 71.3 ± 2.5 % (n=4, 285/400). Furthermore, a d_t of 20 µm resulted in clogging of the device.

Next, the cell pairing of both cell types was tested varying the width of the small trap (w_s). A w_s of 4 µm, 5 µm and 6 µm, combined with a d_s of 6 µm and a d_t of 25 µm, resulted in a pairing efficiency of 32.9 ± 6.4 % (n=6, 195/600), 30.8 ± 9.3 % (n=6, 154/600) and 19 ± 4.9 % (n=3, 57/300), respectively. Pairing efficiency was defined as the percentage of traps occupied by exactly one B-cell and one NS-1 cell (figure 4.4).

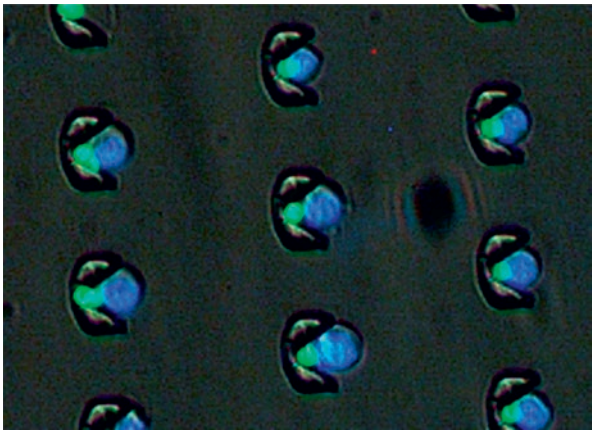

Figure 4.4: Array of traps with captured green fluorescent B-cells (CFDA staining) and blue fluorescent NS-1 cells (Hoechst staining).

In the next electrofusion experiments, the dimensions of the small trap were set at a w_s of 4 µm and a d_s of 6 µm, with a d_t of 25 µm, as this resulted in the highest pairing efficiency. The device by Skelley et al.[15] achieved a pairing efficiency of 70 %. This higher pairing efficiency was shown with equal sized cell types, whereas our traps are designed and optimized for different sized cells.

4.3.2 Electrofusion experiments

Firstly, the electrical parameters for electrofusion of B-cells and NS-1 cells were determined.

Calculation of the critical field strength

The critical field strength E_{crit} (V/cm) required for the breakdown of the membrane at the sites facing the electrodes ($\cos\theta = 1$) was estimated from equation [4.3]. The applied electric field E_0, is equivalent to E_{crit}, when the permeation voltage V_m reaches ~1 V [18]. The average cell radius, R, of a B-cell and a NS-1 cell in isoosmolar electrofusion buffer, was 7.5 ± 1.2 µm and 15.4 ± 1.8 µm, respectively. This gave rise to an E_{crit} value of 1.8 kV/cm for B-cells and 865 V/cm for NS-1 cells. Based on the observations that the most favorable field strength of breakdown pulses is 1 to 3 times E_{crit} [19], the further electrofusion experiments were restricted to a field strength of 2.5 kV/cm (~3 x 865V) [20]. However, as shown in figure 4.3A, the electrical field varies in the trap due to the specific geometry. In the small trap, the B-cell, which is captured first, experiences a higher electrical field (~3-5 kV/cm), followed by a decrease in the field strength in the larger trap (~1-2 kV/cm), which captures the NS-1 cell.

Furthermore, equation [4.1] shows that the optimal duration of a breakdown pulse is dictated by the time required to charge the membrane (τ_m). The induced membrane voltage (V_m) reaches a stationary level after 5 to 10 times τ_m , see equation [4.3]. Using equation [4.2] with a C_m of 10 mF/m^2, resulted in a τ_m of 4.4 µs for the NS-1 cell and 2.1 µs for the B-cell. Accordingly, the minimum pulse length was set at 50 µs [21].

Characterization of fusion

In our microfluidic device, the process of fusion between B-cells and NS-1 cells was observed in detail at a single cell level in real-time. Fusion efficiencies for all experiments were determined by imaging and analyzing both the fluorescent dye exchange and plasma membrane reorganization between cell pairs. Fluorescent dye exchange is an indication of cell-cell contact, electroporation of cell membranes and exchange of the cytosols. Plasma membrane reorganization indicates advanced fusion. Fusion efficiency was defined as the sum of the correct cell pairs that show initiating fusion (dye transfer) and/or advanced fusion (membrane reorganization), divided by the total number of cell pairs.

Figure 4.5 shows the temporal sequence of cell fusion between a human B-cell and a mouse NS-1 cell. Before (t = 0 min) and immediately after applying the electric pulses, two distinct membranes were visible and the fluorescent dye CFDA was still localized in the B-cell. After 15 minutes, green NS-1 cells were observed, indicating that the cytosols of the two cells had connected and fusion was initiated. After 30 minutes, advanced fusion, with membrane reorganization had occurred at the sites where the two cells connected, creating a hybridoma, clearly visible in the brightfield images. Advanced fusion, obtaining a hybrid cell, containing the nuclei of both cells, is needed in order to

generate a functional hybridoma. However, initiative fusion can also progress to advanced fusion at a later time point.

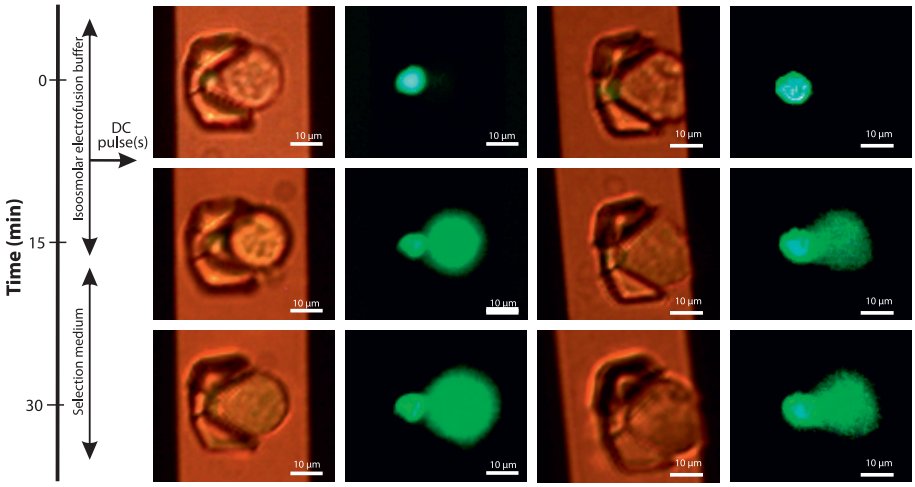

Figure 4.5: Temporal sequence of electrofusion between a CFDA stained B-cell and an unstained NS-1 cell. Bright field and fluorescent images before (t = 0 minutes), t= 15 minutes and t = 30 minutes after applying 3 DC pulses of 50 µs with AC (left columns) and 6 x 100µs with AC (right columns).

Fusion efficiency using different electric parameters

The fusion efficiency between B-cells and NS-1 cells using different electrofusion parameter settings, as described in table 4.1, was determined. Fluorescent dye exchange and/or membrane reorganization was determined by manually inspecting and evaluating the images of the properly paired cells in the array. Results show that applying multiple pulses resulted in a higher fusion efficiency (figure 4.6). This is in agreement with the results described in literature[13, 15, 22]. However, pulses of 200 µs directly initiated cell death. Furthermore, a significant increase* ($p<0.01$) in the fusion efficiency was observed when applying an AC field before and after a DC pulse of 50-100 µs in comparison to no AC field (figure 4.6). The use and effect of AC fields on the fusion efficiency has been a point of discussion for a long time[23]. On one hand, it is believed that an AC field can prone the plasma membrane for electrofusion by generating protein-free areas in the cell membrane [24-26]. On the other hand, observations of Sowers [23] contradict the need for an AC field, showing that cells can be fused by DC pulses alone. However, these results are not based on mammalian cells. Overall, our obtained results indicate the need for an AC field for successful electrofusion of human B-cells and NS-1 cells.

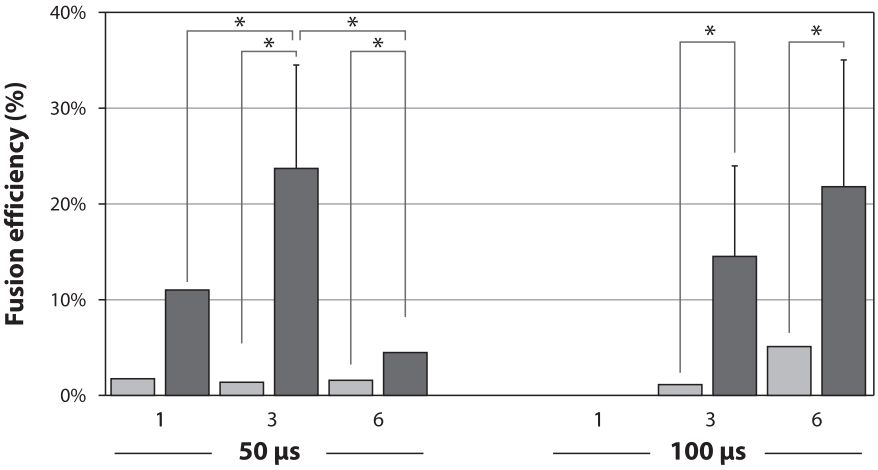

Figure 4.6: Comparison of the fusion efficiencies with and without AC and different pulse parameters (1-3-6x 50 µs and 1-3-6 x 100 µs). Dark grey bars are with AC; Light grey bars represent electrofusion without AC. The fusion efficiency for each electrical parameter was calculated (± SD), *p<0.05 (two sided T-test).

Figure 4.7 shows the results of the electrical parameters with the highest fusion efficiencies. All experiments were performed 3 times in the presence of an AC field. Three DC pulses of 50 µs gave a fusion efficiency of 23.6 ± 10.8 % (72/264), whereas 6 DC pulses of 100 µs resulted in a fusion efficiency of 21.7 ± 13.2 % (55/276). In both cases, more cell pairs showed only the initiating steps of fusion (dye transfer), with no clear membrane reorganization. These conditions were used to further optimize the fusion efficiency, by treating the larger NS-1 cell with pronase, a membrane stabilizing agent.

Fusion efficiency using pronase treated NS-1 cells

Treating NS-1 cells with pronase significantly decreased the fusion efficiency when applying 3 DC pulses of 50 µs pulses with AC ($p<0.05$; figure 4.7). Probably the membranes of the NS-1 cells became too stable and therefore insensible to the applied pulses. However, pronase had an increasing effect on the fusion efficiency when applying 6 DC pulses of 100 µs with AC ($p<0.02$; figure 4.7). This condition gave overall the highest fusion efficiency of 50.6 ± 11.1% (103/198). This can be explained by the fact that in the presence of pronase, NS-1 cells are stabilized against higher field strengths and longer exposure times, which resulted in a higher survival rate when 6 DC pulses of 100 µs were applied. This is in agreement with previous results, showing that pronase treatment can greatly enhance electrofusion yields of mammalian cells [25-27]. Moreover, figure 4.7 shows that, in the presence of pronase, in more cell pairs membrane reorganization (advanced fusion) occurred in comparison with no pronase treatment, however dye transfer (initiative fusion) still had the overhand. The shown electrofusion efficiency of 50.6 ± 11.1 %, is comparable to or even higher than previous reported fusion yields (initiative and advanced) of other cell types in microfluidic chips [15, 22, 28, 29].

Moreover, the shown electrofusion efficiency using this microfluidic device is significantly higher than fusion efficiencies achieved by conventional electrofusion methods of other cell types [15].

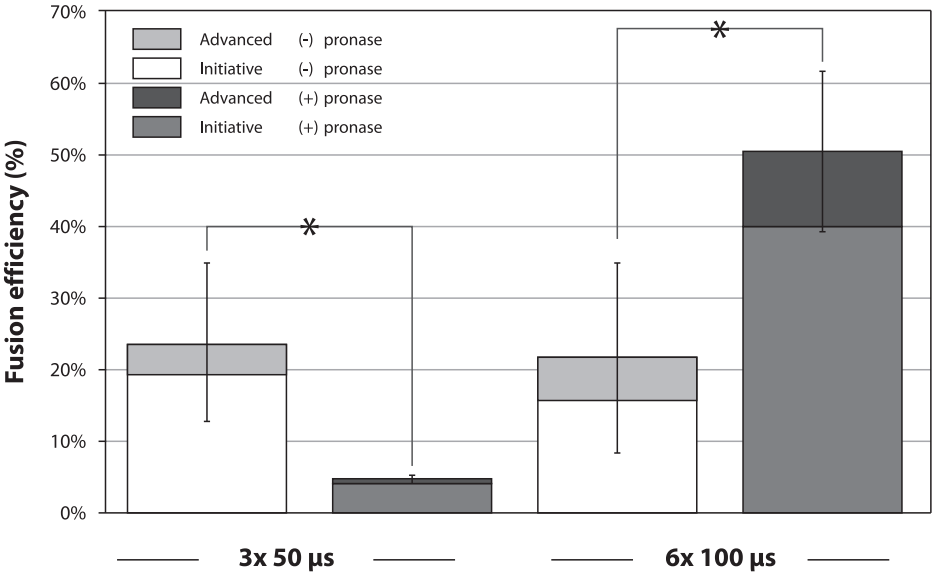

Figure 4.7: Comparison of the fusion efficiencies with and without pronase treatment and different pulse parameters (3x 50 µs and 6 x 100 µs with AC. White and light grey bars are without pronase treatment; Middle and dark grey bars represent electrofusion with pronase treatment. In all the bars, the lower part refers to dye transfer (initiating fusion) and the upper part to membrane reorganization (advanced fusion). The fusion efficiency for each electrical parameter was calculated from 3 individual experiments (± SD), *$p<0.05$ (two sided T-test).

4.3.3 Demonstration of hybridoma generation

The golden standard for hybridoma growth is to determine whether the fused cells from the chip can survive in conditioned culture. A functional hybridoma is formed when after membrane reorganization, the nuclei of both cells fuse and functional antibodies are produced. Nuclear fusion occurs spontaneously 1-3 weeks after fusion[3]. In our experiments, the fused cells were analyzed for their viability after 14 days of culture in hybridoma specific medium. In this medium, only the hybridomas survive. Viable hybridomas, with a yield of 0.33% (1/302 cell pairs), were observed after applying 6 DC pulses of 50 µs (n=1), with AC field and without pronase treatment (figure 4.8 A). Secondly, viable hybridomas were observed after applying 6 DC pulses of 100 µs (n=1), with a yield of 1.2% (2/166 cell pairs), also with AC field and without pronase treatment (figure 4.8 B-C).

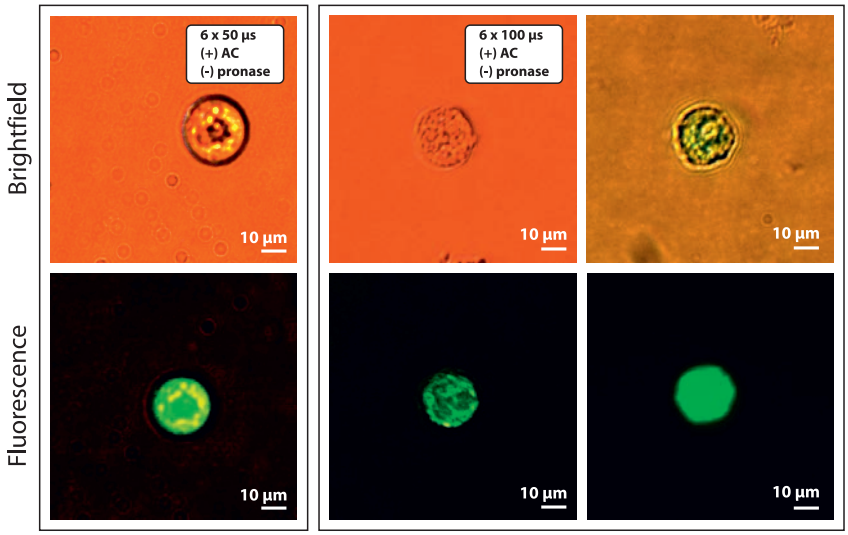

Figure 4.8: Hybridoma formation after applying 6 DC pulses of 50 µs A) or 100 µs (B-C) with AC and without pronase, followed by 14 days of conditioned culturing. Hybridomas were stained with 2 µM Calcein to analyze the viability.

Though very low, these hybridoma yields are higher than the yields reported in literature, regarding conventional bulk electrofusion, which is in the range of 0.001%[13, 30]. Kirschbaum et al.[29] showed cell survival (22%) after fusing B-cells with myeloma cells, however this was not using selection media, hence no information on the functionality and genetic make-up of the proliferating hybridomas was shown.

Furthermore, using AC fields during electrofusion experiments showed to be advantageous regarding fusion efficiency. Our initial results suggest a positive effect regarding hybridoma generation. Moreover, it is thought that frequencies around 2-4 MHz have the advantage that intracellular DEP of the nuclei can be induced, which results in a positioning of the nuclei of the two attached cells close to the contact zone[31, 32] (as mentioned chapter 3). This could influence the hybridoma efficiency, even though nuclear fusion occurs spontaneously. More research and experiments needs to be performed to analyze this possible phenomenon.

In future experiments, the hybridomas need to be tested for antibody production, which serves as the ultimate control regarding successful fusion and optimal gene recombination.

4.4 Conclusion

Today, there is a huge interest for human antibodies for diagnostic and therapeutic applications. The electrofusion of a human B-cell with a myeloma cell can meet this need, as the formed hybridoma produces large amounts of a selected antibody. Conventionally, these electrofusion experiments are performed in bulk with extremely low efficiencies. With microfluidic technology, the electrofusion efficiency can be

increased and the process of electrofusion can be analyzed in detail, enabling discrimination between initiating fusion and advanced fusion. This was the first time on chip electrofusion of a human B-cell with a mouse myeloma cell was shown, with subsequent hybridoma generation. The microfluidic device, as presented in this chapter, showed an electrofusion efficiency of 50.6 ± 11.1%, which is comparable or even higher than previous reported fusion yields in microfluidic chips. Culturing these fused cells led to a hybridoma yield of 0.33% or more, which is higher than the yields reported in literature.

In conclusion, these results provide us with valuable leads to improve the current electrofusion protocols. However, the approach remains static and provides only limited throughput. One could increase the number of traps in the array, however, this would be still batch-to-batch fusion. So, although we have demonstrated the principle feasibility of realizing single cell fusion and hybridoma creation using microfluidic techniques, we conclude that the multiple-trap device is not the ideal platform to realize large scale hybidoma production. Therefore, in the next chapter we will evaluate the possibility to use the microdroplet platform as an alternative.

4.5 References

1. Neumann, V., F. Siegemund, and B. Baessler, *Electrically induced fusion of different human cell types.* J Neurol, 1986. **233**(3): p. 153-6.
2. Weber, H., et al., *Microbiological implications of electric field effects. III. Stimulation of yeast protoplast fusion by electric field pulses.* Z Allg Mikrobiol, 1981. **21**(7): p. 555-62.
3. Kohler, G. and C. Milstein, *Continuous cultures of fused cells secreting antibody of predefined specificity.* Nature, 1975. **256**(5517): p. 495-7.
4. Sullivan, S. and K. Eggan, *The potential of cell fusion for human therapy.* Stem Cell Rev, 2006. **2**(4): p. 341-9.
5. Alkan, S.S., *Landmark - Monoclonal antibodies: the story of a discovery that revolutionized science and medicine.* Nature Reviews Immunology, 2004. **4**(2): p. 153-156.
6. Larsen, J., et al., *Extending the light-harvesting properties of transition-metal dendrimers.* Chemphyschem, 2007. **8**(18): p. 2643-2651.
7. Hu, Z., et al., *Anti-tumor effects of fusion vaccine prepared by renal cell carcinoma 786-O cell line and peripheral blood dendritic cells of healthy volunteers in vitro and in human immune reconstituted SCID mice.* Cell Immunol, 2010. **262**(2): p. 112-9.
8. Sorem, J., T.S. Jardetzky, and R. Longnecker, *Cleavage and secretion of Epstein-Barr virus glycoprotein 42 promote membrane fusion with B lymphocytes.* J Virol, 2009. **83**(13): p. 6664-72.
9. Karsten, U., et al., *Direct comparison of electric field-mediated and PEG-mediated cell fusion for the generation of antibody producing hybridomas.* Hybridoma, 1988. **7**(6): p. 627-33.

10. Weise, J.B., et al., *A dendritic cell based hybrid cell vaccine generated by electrofusion for immunotherapy strategies in HNSCC.* Auris Nasus Larynx, 2004. **31**(2): p. 149-53.
11. Grunow, R., H.D. Volk, and R. von Baehr, *[Diagnostic and therapeutic use of monoclonal antibodies].* Z Gesamte Inn Med, 1985. **40**(18): p. 529-31.
12. Jahn, S., et al., *Establishment of human Ig producing heterohybridomas by fusion of mouse myeloma cells with human lymphocytes derived from peripheral blood, bone marrow, spleen, lymph node, and synovial fluid. Effect of polyclonal prestimulation and cryopreservation.* J Immunol Methods, 1988. **107**(1): p. 59-66.
13. Trontelj, K., et al., *Optimization of bulk cell electrofusion in vitro for production of human-mouse heterohybridoma cells.* Bioelectrochemistry, 2008. **74**(1): p. 124-9.
14. Schmidt, E., et al., *CD19+ B lymphocytes are the major source of human antibody-secreting hybridomas generated by electrofusion.* J Immunol Methods, 2001. **255**(1-2): p. 93-102.
15. Skelley, A.M., et al., *Microfluidic control of cell pairing and fusion.* Nat Methods, 2009.
16. Zimmermann, U., Neil, G.A., *Electrofusion of cells: State of the art and future directions*, in *Electromanipulation of Cells* 1996, CRC-Press.
17. Cao, Y., Yang, J., Yin, Z.Q., Luo, H.Y., Yang, M., Yang, N.H.J., Huo, D.Q., Hou, C.J., Jiang, Z.Z., Zhang, R.Q., Xu, R., Zheng, R.L., *Study of high-throughput cell electrofusion in a microelectrode-array chip.* Microfluid Nanofluid, 2008. **5**(5): p. 669-675.
18. Chang, D.C., Saunders, J.A., Chassy, B.M., Sowers, A.E., *Overview of electroporation and electrofusion*, in *Guide to electroporation and electrofusion*, D.C. Chang, Saunders, J.A., Chassy, B.M., Sowers, A.E., Editor. 1992, Academic Press Limited: London.
19. Zimmermann, U., Friedrich, U., Mussauer, H., Gessner, P., Hamel, K., Sukhoruhov, V., *Electromanipulation of mammalian cells: fundamentals and application.* IEEE TRans Plasma Scie, 2000. **28**: p. 72-82.
20. ModiQuest, *Generating Hybridomas By Electrofusion*. 2008, ModiQuest Therapeutics BV: Enschede, The Neterlands.
21. Sukhorukov, V.L., et al., *A biophysical approach to the optimisation of dendritic-tumour cell electrofusion.* Biochem Biophys Res Commun, 2006. **346**(3): p. 829-39.
22. Wang, J., Lu, C., *Microfluidic cell fusion under continuous direct current voltage.* Applied physics letters 2006. **89**.
23. Sowers, A.E., *Membrane electrofusion: a paradigm for study of membrane fusion mechanisms.* Methods Enzymol, 1993. **220**: p. 196-211.
24. Huang, S.K. and S.W. Hui, *Chemical co-treatments and intramembrane particle patching in the poly(ethylene glycol)-induced fusion of turkey and human erythrocytes.* Biochim Biophys Acta, 1986. **860**(3): p. 539-48.

25. Zimmermann, U. and J. Vienken, *Electric field-induced cell-to-cell fusion.* J Membr Biol, 1982. **67**(3): p. 165-82.
26. Stenger, D.A. and S.W. Hui, *Kinetics of ultrastructural changes during electrically induced fusion of human erythrocytes.* J Membr Biol, 1986. **93**(1): p. 43-53.
27. Pilwat, G., H.P. Richter, and U. Zimmermann, *Giant culture cells by electric field-induced fusion.* FEBS Lett, 1981. **133**(1): p. 169-74.
28. Bakker Schut, T.C., et al., *Selective electrofusion of conjugated cells in flow.* Biophys J, 1993. **65**(2): p. 568-72.
29. Kirschbaum, M., et al., *Highly controlled electrofusion of individually selected cells in dielectrophoretic field cages.* Lab on a Chip, 2012. **12**(3): p. 443-450.
30. Yu, X., et al., *An optimized electrofusion-based protocol for generating virus-specific human monoclonal antibodies.* J Immunol Methods, 2008. **336**(2): p. 142-51.
31. Bertsche, U., A. Mader, and U. Zimmermann, *Nuclear membrane fusion in electrofused mammalian cells.* Biochim Biophys Acta, 1988. **939**(3): p. 509-22.
32. Ohno-Shosaku, T. and Y. Okada, *Electric pulse-induced fusion of mouse lymphoma cells: roles of divalent cations and membrane lipid domains.* J Membr Biol, 1985. **85**(3): p. 269-80.

DROPLET MICROFLUIDICS: A REVIEW

CHAPTER 5

Droplet-based microfluidics is a rapidly growing subgroup of microfluidics. It combines chemistry, cell biology, physics and microsystems engineering. The basis of a droplet microfluidic platform is the formation of homogenous droplets using two immiscible fluids. The presence of an extensive range of technologies for droplet generation and manipulation, in combination with fast analysis tools, has enabled the applications of droplet microfluidics in a wide variety of fields, ranging from single cell analysis to material synthesis. In this chapter, we summarize the available droplet generation techniques as well as the droplet manipulation techniques. Finally, the recent advances of the droplet platform for cell experimentation and analysis are discussed.

5.1 Introduction

In recent years, performing biological studies on a single cell basis is of increasing interest[1 2]. And since its advent in 2000s[3, 4] droplet microfluidics has become enormously popular and a quickly evolving research field regarding biological studies[5-9]. Droplets facilitate high-throughput single cell analysis within micrometer-sized droplets[10], which are physically and (bio)chemically isolated[11,12]. Using microfluidic devices, monodisperse droplets can be generated, merged, and sorted at kHz rates, enabling high-throughput single cell screening[2,12].

Unlike continuous flow systems, droplet-based systems focus on creating discrete volumes with the use of immiscible phases[13, 14]. Droplet-based microfluidic systems are sometimes referred to as "digital microfluidics". This term aims to underline the use of discrete and distinct volumes of fluids[15]. In this chapter we will use "droplet-based microfluidic systems" to refer to the field.

The main focus of this chapter is to shed light on the basic techniques for droplet generation and manipulation. First, a general introduction on the droplet formation is given. Followed by an overview of the operations methods that are developed to manipulate droplets. Finally, the use of these droplet techniques in the biomedical engineering field is illustrated with applications for (single) cell analysis.

5.2 Droplet formation

Conventional methods for making droplets involve agitation of multiphase fluids[16]. In these systems, there is no way to control the homogeneity of the stresses involved in droplet breakup, therefore the droplet size is highly polydisperse. However, when using microfluidic devices it is possible to control the flow rates of two immiscible phases in microchannels with given geometry and dimension. As a result, the droplet breakup is highly repeatable and hence it is feasible to generate droplets with a dispersity as low as 1–3%[6, 17]. One method to form droplets is using two immiscible liquids such as water and oil[18-20]. However, air-liquid droplets systems have also been studied[21-23]. Water (or medium) in oil droplets are mostly used when performing biological related studies. The oil phase is referred to as the continuous phase and the water phase as the dispersed phase.

Droplet-based microfluidic systems can produce highly monodisperse droplets in the nano- to femtoliter range, at rates up to twenty thousand per second[24,25]. Furthermore, this platform has dimensional scaling benefits that enables controlled and rapid mixing of fluids in the droplet, resulting in decreased reaction times[26]. Droplet-based microfluidic systems have been shown to be compatible with many chemical and biological reagents and capable of performing a variety of fluidic operations[27]. This, combined with the precise generation and repeatability of droplet operations, has made the droplet-based microfluidic system a potent high-throughput platform for biomedical research and applications.

In the next paragraph, the underlying principles and physics of droplet formation is discussed. Followed by a review of available droplet generators.

5.2.1 Capillary number

The mechanism for droplet breakup in immiscible shearing flows has been thoroughly investigated[3, 16, 28-32]. Essentially, droplet breakup occurs when the viscous stress exerted by the continuous phase induces a critical asymmetric stress on the droplet causing an imbalance of the surface tension. This is generally described by the capillary number[15 26, 33 34]. This dimensionless capillary number, *Ca*, plays a key role in determining droplet dynamics. The capillary number characterizes the relative importance of viscous stresses and capillary pressure. The capillary number for microfluidic droplet formation is defined in terms of the continuous phase that acts to deform the droplet:

$$Ca = \frac{\mu_c * v}{\sigma} \qquad [5.1]$$

In which μ_c represents the viscosity of the continuous phase, *v* the velocity of the continuous phase ($Q_c/(w*h)$), and σ the interfacial tension between both the continuous and dispersed phase[34]. This definition is consistent with classical experiments examining the deformation and breakup of isolated droplets in linear flows[35, 36]. When the *Ca* becomes greater than the critical capillary number (Ca_{cr}), droplet breakup occurs[34]. It is important to note that the critical capillary number is system dependent as different values have been reported by various groups using different geometries[34,37,38,39]. In microfluidic droplet formation, capillary numbers typically range from $Ca \sim 10^{-3}$ to 10^{1} for flow rates generated via syringe pumps[17, 36]. Previous studies on symmetric breakup conditions and the critical capillary number were performed by Link et al.[39]. A low value of *Ca* indicates that the stresses due to interfacial tension are strong compared to the viscous stresses. Droplets flowing under such a condition minimise their surface area. In the opposite situation of a high *Ca*, viscous effects dominate and one can observe large deformations of the droplets and asymmetric shapes[17].

An additional dimensionless parameter that is important in microfluidic droplet formation is the ratio of the volumetric flow rates φ, given by[36]

$$\varphi = Q_c / Q_d \qquad [5.2]$$

in which Q_c is the volumetric flow rate of the continuous phase (μl/min) and Q_d of the dispersed phase. The ratio of the volumetric flow rates of the different phases also influences the droplet size.

In summary, the droplet breakup process in microfluidic channels can be described in terms of the two dimensionless parameters describing the flow: the capillary number and the volumetric flow rate ratio. Nevertheless, the geometry of the device (5.2.2), described by several different aspect ratios including the ratio of the widths of the inlet channels, are important parameters regarding the process of droplet breakup process and droplet size[40]. Moreover, the size of the generated droplets depends on the flow

rates of the two phases, the dimensions of the channels[23], the relative viscosity between the two phases[29] and the use of surfactants and their concentrations[41 42].

Due to all of these parameters, it difficult to predict the behavior of droplet generation on forehand.

5.2.2 Microfluidic geometries

Besides producing a regular and stable monodisperse droplet stream, the microfluidic device should also be flexible in providing droplets of a prescribed size at a prescribed rate. In the recent years of research, a wide variety of techniques have been developed for droplet generation[43]. There are droplet generation techniques based on electrohydrodynamics[44], such as electrowetting on dielectric (EWOD)[45]. This technique is based on the power of an electric field to change the interfacial energy between a fluid and the contact surface. As a result the contact angle is affected and causes the fluid to wet the surface. Hence, by changing hydrophobicity, using an electric field, droplets are generated. Another commonly used droplet generation method is based on DEP, pulling the droplets from a fluid reservoir[46, 47].

However, the two most widely used microfluidic geometries to form droplets are either the T-junction or the flow focusing[15]. These two main approaches utilize different geometries at the droplet production zone: (i) breakup in T-junction (figure 5.1 A) (ii) breakup in flow focus junction (figure 5.1 B)

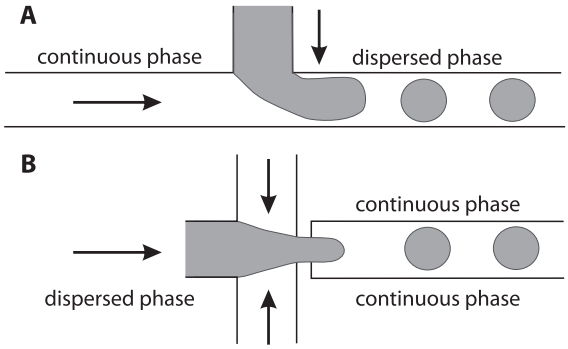

Figure 5.1: Schematic representation of the two main droplet generation mechanisms. A) T-junction. B) Flow focussing junction.

T-junction

The first controllable production of a single stream of monodisperse droplets in a microfluidic channel was demonstrated using a T-junction[3]. The T-junction comprises an inlet channel, containing the dispersed phase, which perpendicularly intersects the main channel, containing the continuous phase[3, 23, 48].[37] As the fluid flow of dispersed phase continues, the tip of the dispersed phase enters the main channel, where both phases form an interface. The shear forces, generated by the continuous phase, and the consequent pressure gradient, causes the tip of the dispersed phase to extend into the main channel until the neck of the dispersed phase thins and eventually breaks the dispersed phase into a droplet (figure 5.1 A)[15, 49]. The dimensions of the droplets can be

changed by the relative viscosity between the two phases and also by the flow rate ratio. T-junctions are not limited to single inlets as more complicated schemes have been used for performing chemical reactions[50] and generating droplets of alternating composition.

Three main regimes can be distinguished for droplet formation at a T-junction (figure 5.2): (a) squeezing, (b) dripping, and (c) jetting[42]. The squeezing mechanism arises as the emerging dispersed phase blocks the flow of the continuous phase, causing the pressure to rise. This pressure rise allows the continuous phase to squeeze on the dispersed phase, pinching off a droplet in the process. The dripping mechanism occurs when the shear stress overcomes the interfacial tension, and droplet break up is caused by the shearing of the dispersed phase by the continuous phase. Finally, the jetting mechanism is characterized by the formation of long threads, which are broken due to the Plateau–Rayleigh instability[51]. There is also an alternative version of jetting shown in figure 5.2 D. This is referred to as 'uncontrolled jetting', which produces relatively large polydisperse droplets. There are no general scaling laws that can predict the transitions between the described regimes.

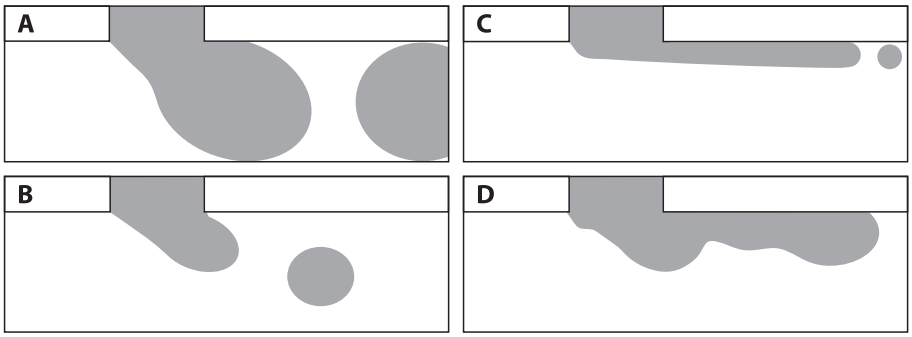

Figure 5.2: Main flow regimes of droplet formation at a T-junction. A) Squeezing. B) Dripping. C) Jetting. D) 'Uncontrolled jetting'.

Flow focusing junction

In the flow focusing configuration (figure 5.1 A), both the dispersed and continuous phases are forced through a narrow region in the microfluidic device[15, 49, 52, 53]. This design entails symmetric shearing by the continuous phase on the dispersed phase, which enables controlled and stable generation of droplets.

Four different droplet generation regimes have been identified in flow focusing geometries, as shown in figure 5.3: squeezing, dripping, jetting and 'uncontrolled' or widening jetting[53], as described previously by for the T-junction. Again, here are also no general scaling laws that can predict the transitions between these regimes[54]. This is due to the large number of variable parameters[42].

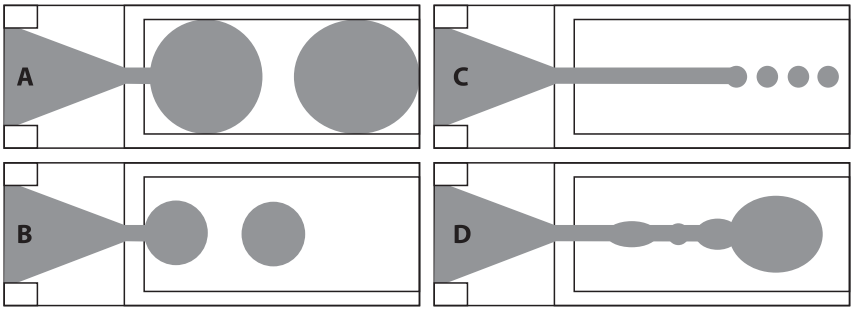

Figure 5.3: Main flow regimes of droplet formation at a flow focusing junction. A) Squeezing. B) Dripping. C) Jetting. D) 'Uncontrolled jetting'.

Comparison

Both the T-junction and the flow focusing are able to change the size and frequency of the droplets by varying the mentioned parameters *e.g.* the flow rate ratio. However, the flow focusing configuration allows to generate droplets, which are smaller than the orifice size[38]. This is attractive when small sized droplets are required. The T-junction has a simpler channel design. Further detailed discussions on the hydrodynamic features of the two droplet generation techniques are summarized in recent reviews[12, 17, 36, 55, 56].

Flow focusing is one of the most frequently used techniques to generate droplets in microfluidic devices[12]. Compared with a T-junction, the flow focusing geometry typically offers better monodispersity and superior frequency of the droplet generation. Flow focusing also seems to have a slight preferences if delicate objects such as cells or primary emulsion droplets are encapsulated in the droplets[12, 57,58].

5.3 Droplet manipulation

For useful microfluidic processes, it is crucial that the generated trains of monodisperse droplets can be consistently manipulated downstream. In the next section, we will review different universally used techniques to perform droplet manipulation in microfluidic devices.

5.3.1 Droplet splitting

Droplet splitting, also referred to as fission or shrinkage, is a critical operation that can enhance the effectiveness of droplet-based microfluidic systems[6]. As each droplet serves as a vessel for reagents, splitting a single droplet into two or more droplets, easily scales up the experimental capacity. In addition to increasing the experimental throughput, droplet splitting can also be used as a method to control the droplet content concentration or reduce droplet volume.[33]

Song et al.[59] first proposed the splitting of a droplet in a constricted T-shaped channel as shown in figure 5.4 A. They demonstrated that when a droplet flowed towards the junction, it was stretched in that region. If the initial droplet was large enough, it thinned at its center and split into two daughter droplets as it passed the

junction. Moreover, asymmetrical splitting was also attainable by altering the lengths of the two branching channels. Subsequently, Link et al.[39] comprehensively investigated the process of droplet-splitting in a T-shaped channel. Furthermore, passive droplet splitting at junctions of arbitrary angles was investigated[60].

The splitting of droplets depends on the effective flow resistance of each channel or around obstacles[39], provided that the flow velocity is sufficiently high. More active control of droplet splitting, in which the size of the two daughter droplets was regulated, was also demonstrated[61-63]. Nie et al.[61] reported asymmetrical droplet splitting as a method for sampling small amounts from larger droplets (figure 5.4 B). In this device, droplets were pumped into a loop where they split according to the flow resistance. The loop structure prevents changes in flow resistance over time, caused by accumulation of plugs in downstream collector capillaries, from interfering with the split ratio.

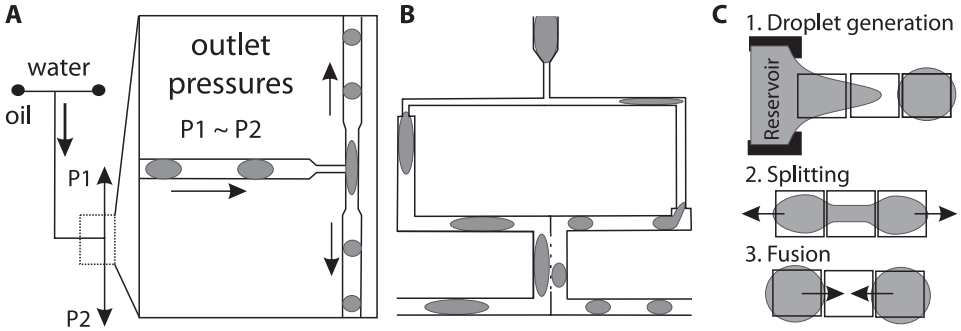

Figure 5.4: Splitting of droplets. A) Splitting of droplets using a T-junction. Adapted from[59]. B) splitting of droplets using a T-junction with loop structure. Adapted from[61]. C) EWOD based droplet generation, splitting and fusion. Adapted from[64].

In contrast to the passive splitting methods described above, active fission relies on external power or electrical control of the droplet splitting. EWOD is for example a technology several groups have used to generate droplets[65,66], but also to actively divide a droplet into smaller droplets[64]. Splitting is achieved when the surfaces near the opposite ends of a droplet are activated, and the surface central to the droplet is grounded. The activated regions pull the droplet towards its respective ends, causing the droplet to divide in the middle[64] (figure 5.4 C). Thermally induced surface gradients can also be used to assist droplet splitting or even sorting[67]. Increased temperature lowers the viscosity and interfacial tension of liquids, therefore this concept can be applied to attract an aqueous plug into a heated channel[15].

5.3.2 Droplet fusion

Controlled fusion of droplets is a fundamental operation unit for droplets used as microreactors. Fusion enables to combine different reagents or cells and initiate chemical and biological reactions in microfluidic devices in a confined space. Furthermore, droplet fusion is demanded to concentrate or dilute reactants in a droplet

or to add reagents in a droplet[11, 68]. In fusion, two separately generated droplets are brought into contact and merged. Fusion occurs due to fluctuations in the surface tension on the droplet surface, which cause destabilization of the interface between the continuous and dispersed phase[69]. As with previous fluidic operations for droplet splitting, there are passive and active methods of controlling droplet fusion. Channel geometry variations and electrodes were implemented for respectively passive and active fusion.

Passive fusion

The passive method to fuse two droplets is to bridge and break the film in between the droplets and enabling the droplets to merge via modulating the geometric design of the microchannel[33, 50,44, 70]. One example of passive fusion is shown in figure 5.5 A. This design, presented by Niu et al.[71] induced droplet fusion by means of a pillar structure. The droplets flowed into a chamber containing a comb-shaped pillar array and, while the first droplet was squeezed through the pillar array, and slowed down, the following droplet caught up and fused with it. Bremond et al.[72] designed a channel of 'decompression merging' (100 fusion events/s) as shown in figure 5.5 B. The widening of the channel slows down the first droplet and this droplet fused with the second droplet when this second droplet overtook the first one. The principle is comparable with Niu et al. Recently, an easy passive fusion method, combined with droplet splitting, using 3D microstructures was shown by Chen et al.[26] (figure 5.5 C).

Besides passive fusion using variations in the channel geometry, fusion methods based on tuning channel surface energy or liquid interfacial tension were also proposed. For example, Fidalgo et al.[73] presented droplet fusion based on changing the wettability of the PDMS microchannel, as shown in figure 5.5 D. A hydrophilic patch was mounted within a hydrophobic PDMS channel, which caused the passing droplets to fuse at about 160 Hz. Furthermore, Mazutis et al. [74] proposed a passive method (figure 5.5 E) based on the injection of surfactant stabilized emulsion droplets into a microfluidic device with subsequent one-to-one fusion with droplets generated on-chip (with low surfactant concentration). The obtained fusion rate was in the kHz range, which has not yet been obtained with other passive methods (20-160 Hz). However, it does involve the injection of previously generated droplets, adding to the complexity. Furthermore the use of high concentrations of surfactant is needed.

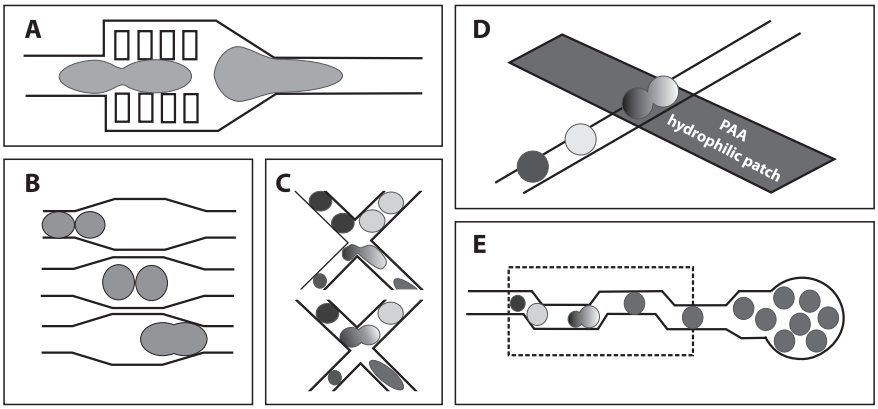

Figure 5.5: Passive droplet fusion devices. A) Pillar assisted droplet fusion. Adapted from[71]. B) Passive droplet fusion using widening of the channel. Adapted from[72]. C) Passive droplet fusion and splitting using 3D microstructures. Adapted from[26]. D) Droplet fusion based on surface energy patterning. Adapted from[73]. E) Fusion based on changing the concentration of surfactant. Adapted from[74].

Active fusion

Next to the passive methods for droplet fusion, the research on active droplet fusion is growing. The fusion of individual droplet pairs by electrocoalescence was shown by Chabert et al.[75] in 2005. This was in a static approach. One of the first applications of electrocoalescence of continuously flowing trains of droplets was demonstrated by Tan and co-workers[76]. In their approach, a widening chamber was incorporated, in which the precedent droplet slowed down, providing a chance for a second droplet to catch up (figure 5.6 A). Electrocoalescence was initiated via two embedded electrodes perpendicular to the flow of the droplets. An AC field (30-280 kV/m) was applied across the chamber to facilitate the droplet fusion.

Several variations on the geometry presented by Tan et al. were used to induce electrocoalescence in a microfluidic settings[11, 77, 78]. One example is shown in figure 5.6 B, designed by Brouzes et al.[11]. Moreover, the (variations) on the geometry of Tan et al. was used to study the coalescence behaviour[12, 79]. Many reports can be found that describe several mechanisms of electrocoalescence[75, 80-82]. The common idea is that electrocoalescence mechanism is based on accumulation of charges at the droplet interface, which induces droplet coalescence. Whereas the attraction of individual droplets in an applied electric field is readily explained, the mechanism leading to droplet coalescence was elucidated not too long ago. It is thought to be based on the spinodal breakup of a thin oil lamella between two conducting droplets in the presence of an electric field. Further information about the exact mechanism can be found in several articles[83-85].

Electrocoalescence can also be achieved by directly contacting the droplets with electrodes[86]. Ahn et al.[87] proposed an electrocoalescence device (figure 5.6 C), which relied on pair-wise synchronizing droplets via their size-dependent flow velocities.

Additionally, Link et al.[88] showed a way to use electric force to fuse droplets (figure 5.6 E). Two streams of oppositely charged droplets were generated simultaneously. Subsequent fusion occurred when these droplets came into contact with each other. Furthermore, droplet fusion using optical trapping and fusion was shown by Lorentz[89].

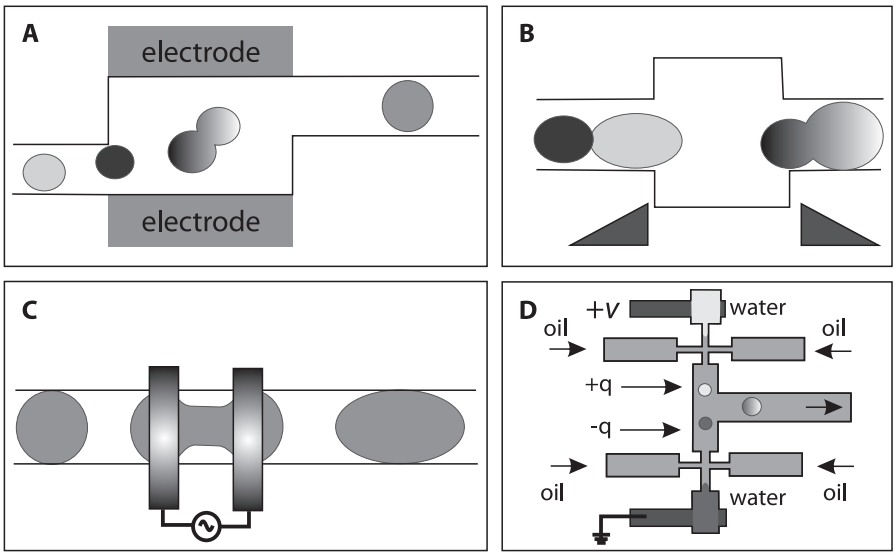

Figure 5.6: Active droplet fusion devices. A) Electrocoalescence between to droplets by applying an external AC field. Adapted from[76]. B) Electrocoalescence by externally placed electrodes. Adapted from[11]. C) Electrocoalescence by directly placing electrodes in the main channel. Adapted from[87]. D) Electrocoalescence of droplets by oppositely charging the droplets. Adapted from[88].

5.3.3 Droplet sorting

Droplet generation, splitting and fusion, as discussed in the previous sections, are important manipulation techniques for droplets. Another essential component for high-throughput screening applications is droplet sorting. Droplet sorting enables the separation of the droplets of interest from a large population of droplets. In the following section, we will summarize commonly used techniques to passively or actively sort droplets.

Passive sorting

Tan et al.[34] described a method for passive droplet sorting. The smaller satellite droplets were sorted into a side channel, whereas the larger primary droplets flowed through the main channel. This concept is based on different flow rates at different channel positions. Due to their smaller surface area, the satellite droplets were exposed to the flow projected from only the side channel, whereas the larger droplet perceived the higher velocity flow stream of the main channel. This allowed sorting of droplets by size.

Another method is gravity-driven size-based sorting. Huh et al.[90] developed a microfluidic sorting device, which combined gravity-based sorting with a specific

channel design to purify perfluorocarbon droplets from a polydispersed emulsion. The essence of this sorting principle is that the sedimentation velocity of larger particles is greater than that of smaller particles at a given density. This difference results in the separation of larger droplets from smaller droplets. The presented device was able to sort virtually all small (< 6μm diameter) perfluorocarbon droplets out of a polydispersed sample.

The group of prof Lee[91] demonstrated passive hydrodynamic droplet sorting in microfluidic channels based on intrinsic viscoelastic fluid properties. Sorting was achieved by tuning the droplets' intrinsic viscous and viscoelastic properties relative to the continuous oil phase. This resulted in a positive or negative lateral migration towards high or low shear gradients in the channel. Sorting of droplets was achieved at 200 Hz.

Active sorting

A convenient way of selecting droplets is by means of electric fields that are applied locally in the channel. Since the dielectric constant of aqueous droplets is typically above the dielectric constant of most non-polar (oil) liquids, uncharged droplets can be drawn into the direction of increasing electric field strength by DEP[12, 96]. This dielectrophoretic effect was first introduced for high-speed droplet sorting by Ahn et al.[92] (figure 5.7 A). The location and shape of the electrodes were designed such to maximize the field gradient and effectiveness in deflecting the droplets. In addition, it was possible to select a single droplet out of the entire stream of droplets at a generation rate of 1.6 kHz.

Recently, Cao et al.[93] presented a deflection mechanism based on the use of a solenoid valve (figure 5.7 B). By passing droplets through a narrow interrogation channel, the encapsulated particles were detected individually by fluorescence. The number of encapsulated particles was determined and a sorting decision either led to actuation of the solenoid valve or not.

Robust droplet fusion and sorting for two parallel trains of droplets was shown by Xu et al.[95]. Droplet pairs were synchronized through a railroad-like channel and electrically fused. The fused droplets transited to the middle guiding track towards the middle channel; non-synchronized and non-fused droplets were discarded into the side waste channels by following their own guiding tracks (figure 5.7 D). The combined droplet fusion and sorting technology, as shown in this example, has widespread application in droplet-based microfluidics, however the through-put of this design was very low (~10 Hz)[95].

Finally, there are also other methods for droplet sorting, such as using a magnetic field[97], the application of surface acoustic waves (figure 5.7 C)[94] or EWOD[64]. However, these methods are complex, with a low throughput, which limit their applications[6].

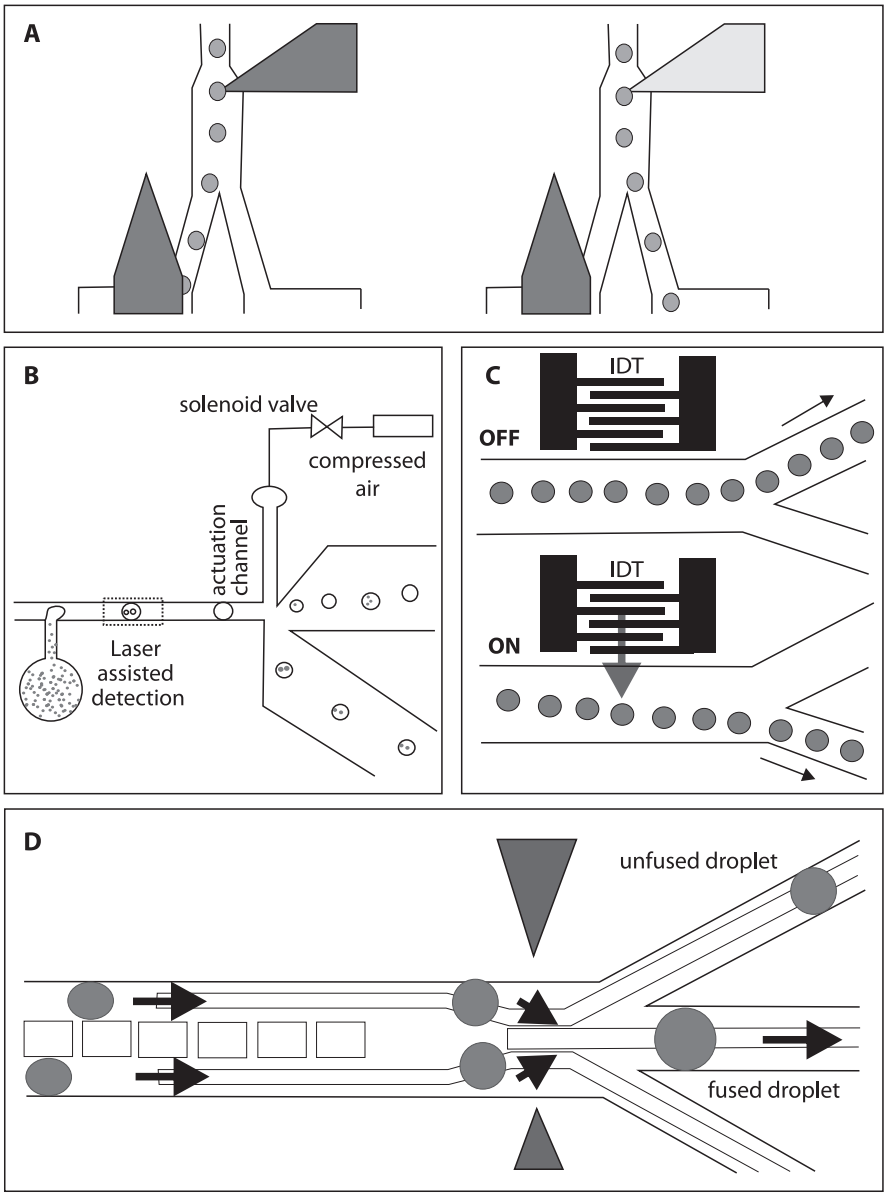

Figure 5.7: Droplet sorting. A) Droplet sorting using DEP. Adapted from[92]. B) Droplet sorting using laser assisted detection of cells/particles in droplets and sorting using a solenoid valve. Adapted from[93]. C) Droplet sorting based on surface acoustic waves. Adapted from [94]. D) droplet fusion followed by sorting using railroad-like structures. Adapted from[95].

5.4 Droplet-based techniques for single cell applications

Droplet-based microfluidics to study biological systems are very promising. The ability to generate precise picoliter sample volumes in high-throughput, combined with advanced sample handling, dramatically increases the productivity of bioassays. The droplet content can be varied systematically during droplet generation and can be modified subsequently by droplet splitting and fusion. Droplet content ranges from bacteria[98,99] to yeast[100] and to mammalian cells[5]. Suspension and adherent cells, as well as multicellular organisms, survive for long times in a droplet and can be recovered and re-cultivated with comparable viability to conventional cell culturing[10, 12].

Single cell encapsulation

Normally, encapsulation of single cells from a solution results in a Poisson distribution with empty droplets as well as one or more cells in the droplet. The number of cells inside each droplet can be estimated using the Poisson distribution[101], $P(\lambda;k) = \lambda^k \exp(-\lambda)/k!$, in which k is the number of cells in the droplet and λ is the average number of cells per droplet, which is adjusted by controlling the cell density. Very low loading densities are required to minimize the number of droplets that contain multiple cells. This effect leads to a large fraction of empty droplets and reduction in effective throughput[33]. Hence, the majority of the droplets are empty and the efficiency of the single cell encapsulation is drastically decreased. This inefficiency has stimulated the development of new methods to increase the single cell encapsulation efficiency. In the next chapter, we will highlight this crucial component for droplet-based single cell experimentation.

Droplet analysis

The analysis of the droplet content is still mainly performed using optical methods, primarily using a laser-setup. Laser-induced fluorescence enables the high-throughput analysis of single cells and/or their encapsulated product. One of the first uses of this approach was demonstrated by detecting the expression of a fluorescent protein in individual cells with simultaneous measurement of droplet size and cell occupancy[102].

The detection of fluorescence emission is similar to flow cytometry. Encapsulation in droplets does, however, provide benefits over conventional flow cytometry, as the droplet can serve as a picoliter vessel for secreted molecules, such as antibodies from hybridomas[33, 103]. Hence, the secreted biomolecules are then available for analysis by droplet-based homogeneous assays, while maintaining the genotype–phenotype link to the cell. However, a great disadvantage is the requirement of cell labeling[104]. One appealing option is to label-free detect the droplet content via impedance measurements (chapter 7).

Enzyme analysis of single cells

The analysis and characterization of enzyme expression is one of the earliest uses of droplet microfluidics. Griffiths et al.[105] developed a emulsion platform for enzyme analysis at the end of the 90s and referred to it as *in vitro* compartmentalization (IVC). IVC is based on partitioning reactions in droplets. The cell-like volumes of these droplets in combination with the ability to regulate their content provided the basis for a range of new, high-throughput, cell-free technologies[106]. A large number of reports on enzyme characterization were published, in which in vitro expressed or purified enzymes were analyzed[66, 104, 107, 116].

Droplet-based enzyme screening for cell-based expression has a role in a directed evolution research[108]. Directed evolution is a powerful method for developing new/better variants of enzymes and proteins in general[109, 110]. A recent report by Agresti et al.[111] demonstrated the benefits of droplet-based systems for directed evolution, by improving the activity of the horseradish peroxidase (HRP) enzyme, expressed on the surface of S. Cerevisiae, 12-fold after two rounds of mutation (figure 5.8 A)[111]. This system combined fluorescence detection with droplet selection by DEP.

Drug Screening in Droplets

A particularly challenging area is the droplet-based screening of drug candidates. In these assays, cell containing droplets are incubated, often for long periods of time, with a wide range of molecules with varying chemical characteristics. In a recent study, Griffiths and coworkers[112] coupled droplet generation to automated sampling to perform a fully automated screen of hundreds of chemical compounds for inhibition of the enzyme tyrosine phosphatase 1B. This approach produced dose–response curves with extremely high resolution by analyzing 10000 droplets for each compound[104].

Brouzes et al.[11] designed a microfluidic device for cytotoxicity screening of encapsulated single cells. The drug concentration library was emulsified with a fluorescent optical code and fused to droplets containing single cells. After 24 hours of incubation, the encapsulated cells were reinjected in a second device. Here, a droplet viability assay was performed, quantitatively scoring the cell viability and growth of the encapsulated cells. The throughput of this assay was 100 cells/s (figure 5.8 B).

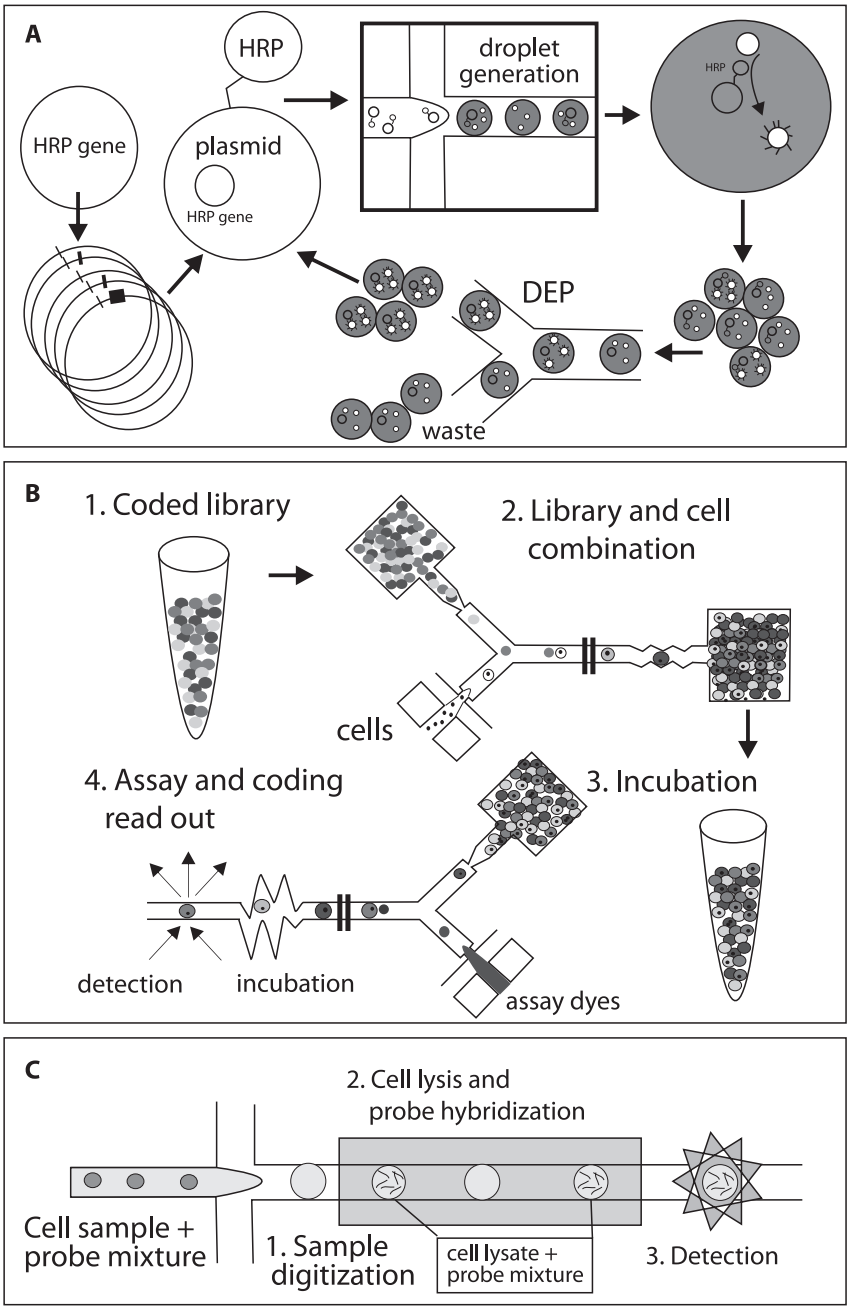

Figure 5.8: Examples of droplet platforms for cell analysis. A) Directed evolution of the HRP gene. Adapted from[111]. B) Cytotoxicity screening of encapsulated single cells. Adapted from[11]. C) Genetic detection of single cells using fluorescent beacons. Adapted from[113].

Baret et al.[114] reported the use of a droplet-based assay for nuclear receptor activation screening in adherent cells at different hormone concentrations. This study demonstrated concurrent analysis of thousands of single cells with ten optically coded hormone concentrations.

In summary, these studies show that drug screening assays on cells can be performed in microfluidic droplets[11, 114]. In contrast to flow cytometry analysis, the screened compounds are added to compartmentalized single cells as opposed to a group of cells. The generation of these large-scale droplet libraries is one of the significant challenges for drug screening. This concept will ultimately determine whether droplet microfluidics offers throughput and financial advantages over automated drug screening in microtiter plates[104].

Single cell genetic analysis in droplets

Genetic analysis of single cells requires the lysis of encapsulated cells for DNA extraction, followed by subsequent DNA amplification and detection using a polymerase chain reaction (PCR). PCR produces many copies of a DNA template, and is therefore crucial for analyzing small amounts of molecules or cells. One way to access the cell contents is via on-chip cell lysis in droplets, using an electric field.

Zhang et al.[115] described a microfluidic device for performing single copy, reverse transcriptase (RT)-PCR within agarose droplets. Efficient RNA/cell encapsulation and RT-PCR at the single copy level was achieved in agarose-in-oil droplets, which, after amplification, were solidified into agarose beads for further analysis. Two different cell lines were studied by this single cell RT-PCR method, and the results confirmed differences in the expression level between these two cell lines.

Amplification-free single cell genetic analysis in droplets was reported by Rane et al.[113]. The device streamlined multiple functionalities to carry out sample digitization, cell lysis and probe–target hybridization for subsequent fluorescent detection (figure 5.8 C). A dilute mixture of pathogenic cells and peptide nucleic acid (PNA) beacons were encapsulated in droplets, which were then incubated at elevated temperatures to facilitate cell lysis and beacon–target hybridization. In this settings, the ribosomal RNA content of a single cell within a droplet, was detected with fluorescence.

Overall, droplet microfluidics enables whole genome sequencing of rare single cells from complex environmental samples[110]

5.5 Conclusion

In this chapter, a short overview was given about the current status of droplet-based microfluidics. Different droplet manipulation techniques were discussed and applications for single cell analysis were shown. Our aim is to use droplet-based microfluidics to fuse a B-cell with a myeloma cell to form an Ab-producing hybridoma in a droplet. For this, we need to consider some important aspects.

The first important consideration for any droplet manipulation mechanism is the throughput and efficiency. Some presented methods here demonstrated a high fusion

efficiency, while the throughput of the system was much lower than a system in which the fusion efficiency was not as high. Both a high efficiency and a high-throughput are desirable, however it may be necessary to find a middle ground in order to satisfy the demands of the intended application.

Second consideration is the use of surfactants regarding droplet fusion, since adding a surfactant is common to stabilize the droplets[11, 12, 15]. However, the presence of surfactant makes droplet fusion more difficult. Furthermore, the use of surfactants, oil and aqueous phase should be biocompatible, especially when longer incubation times are required. Additionally, retaining viability of biological material might be a concern in active fusion, splitting and sorting methods were electric fields are used. Passive fusion, splitting and sorting methods often carry a lower risk of contamination and are more biocompatible, however they generally have a lower throughput[26, 72] than active methods[116, 69]. Passive techniques are limited by the rate at which natural phenomena, such as surface tension fluctuations occur, and are therefore often slower than most active techniques.

We believe the droplet platform can greatly improve the current method for hybridoma generation and selection. We already showed on-chip electrofusion of a human B-cell and a mouse myeloma cell (NS-1), with subsequent hybridoma formation (chapter 4), however not in high-throughput. Hence, the next step is to electrofuse cells in droplets towards a complete electrofusion droplet platform as shown in figure 5.9.

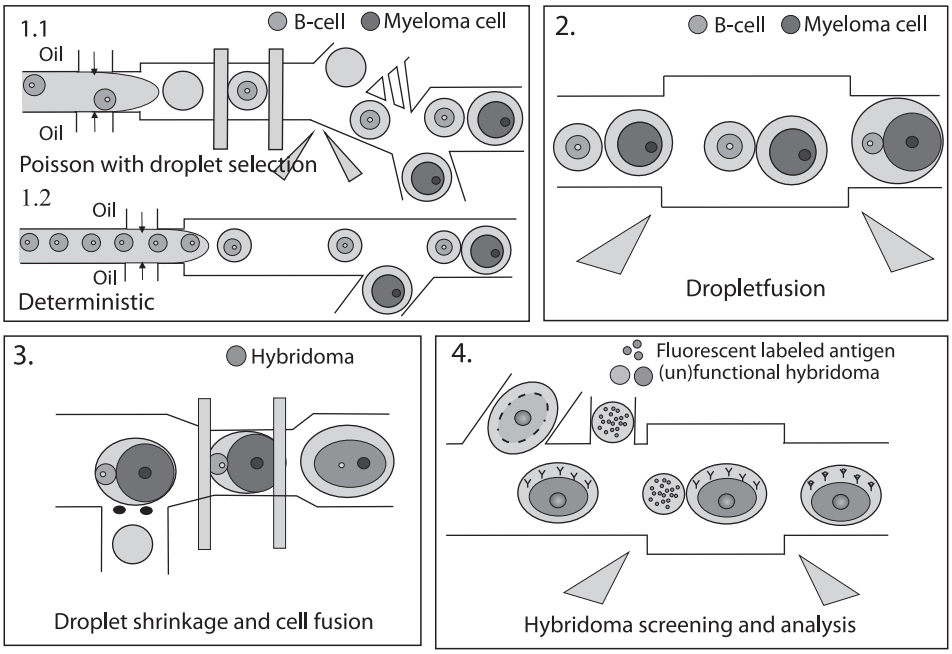

Figure 5.9: Lab-on-a-chip system. 1) Cell encapsulation (1.1 Poisson; 1.2 Deterministic) and selection, 2) Droplet fusion. 3) Droplet shrinkage and electrofusion 4) Screening and analysis of hybridomas.

The first component of the droplet-based platform for electrofusion of cells is cell encapsulation. To obtain high fusion efficiencies, it is important to generate large amounts of single cell containing droplets. We used two approaches, based on deterministic encapsulation (chapter 6) and label-free, electrical, cell in droplet detection (chapter 7). Secondly, active droplet fusion needs to be established to obtain a single droplet with one B-cell and one myeloma cell. Subsequently, the most critical part of the electrofusion device is the cell fusion inside a droplet using electrodes placed inside the main channel. If needed, droplet shrinkage is applied to promote cell-cell contact during pulsing. The final part of the electrofusion platform is the incubation of the hybridomas followed by selection of the desired hybridomas. Obtaining and validating monoclonal cultures typically takes 10–12 weeks. Droplet microfluidics can bypass the repeated culturing and screening steps by encapsulating and analyzing single antibody-producing hybridomas directly

Keeping all considerations in mind, the next chapter focuses on the development of a high-throughput, efficient, single cell encapsulation technique for electrofusion application downstream.

5.6 References

1. Weitz, D.A., et al., *Drop-based microfluidic devices for encapsulation of single cells.* Lab on a Chip, 2008. **8**(7): p. 1110-1115.
2. Um, E., S.G. Lee, and J.K. Park, *Random breakup of microdroplets for single-cell encapsulation.* Applied physics letters, 2010. **97**(15).
3. Thorsen, T., et al., *Dynamic pattern formation in a vesicle-generating microfluidic device.* Physical Review Letters, 2001. **86**(18): p. 4163-4166.
4. Anna, S.L., N. Bontoux, and H.A. Stone, *Formation of dispersions using "flow focusing" in microchannels.* Applied physics letters, 2003. **82**(3): p. 364-366.
5. Koster, S., et al., *Drop-based microfluidic devices for encapsulation of single cells.* Lab Chip, 2008. **8**(7): p. 1110-5.
6. Zeng, S., et al., *Basic technologies for droplet microfluidics.* Top Curr Chem, 2011. **304**: p. 69-90.
7. Bhagat, A.A., et al., *Inertial microfluidics for sheath-less high-throughput flow cytometry.* Biomed Microdevices, 2010. **12**(2): p. 187-95.
8. Edd, J.F., et al., *Controlled encapsulation of single-cells into monodisperse picolitre drops.* Lab on a Chip, 2008. **8**(8): p. 1262-1264.
9. Koltay, P., et al., *Inkjet-like printing of single-cells.* Lab on a Chip, 2011. **11**(14): p. 2447-2454.
10. Clausell-Tormos, J., et al., *Droplet-based microfluidic platforms for the encapsulation and screening of Mammalian cells and multicellular organisms.* Chem Biol, 2008. **15**(5): p. 427-37.
11. Brouzes, E., et al., *Droplet microfluidic technology for single-cell high-throughput screening.* Proceedings of the National Academy of Sciences of the United States of America, 2009. **106**(34): p. 14195-14200.
12. Seemann, R., et al., *Droplet based microfluidics.* Rep Prog Phys, 2012. **75**(1): p. 016601.

13. Atencia, J. and D.J. Beebe, *Controlled microfluidic interfaces.* Nature, 2005. **437**(7059): p. 648-655.
14. Stone, H.A., A.D. Stroock, and A. Ajdari, *Engineering flows in small devices: Microfluidics toward a lab-on-a-chip.* Annual Review of Fluid Mechanics, 2004. **36**: p. 381-411.
15. Teh, S.Y., et al., *Droplet microfluidics.* Lab on a Chip, 2008. **8**(2): p. 198-220.
16. Briscoe, B.J., C.J. Lawrence, and W.G.P. Mietus, *A review of immiscible fluid mixing.* Advances in Colloid and Interface Science, 1999. **81**(1): p. 1-17.
17. Baroud, C.N., F. Gallaire, and R. Dangla, *Dynamics of microfluidic droplets.* Lab on a Chip, 2010. **10**(16): p. 2032-2045.
18. Kobayashi, I., K. Uemura, and M. Nakajima, *CFD analysis of generation of soybean oil-in-water emulsion droplets using rectangular straight-through microchannels.* Food Science and Technology Research, 2007. **13**(3): p. 187-192.
19. Le Reverend, B.J.D., M.S. Taylor, and I.T. Norton, *Design and application of water-in-oil emulsions for use in lipstick formulations.* International Journal of Cosmetic Science, 2011. **33**(3): p. 263-268.
20. Zhu, Y., et al., *A double-emulsion microfluidic platform for in vitro green fluorescent protein expression.* Journal of Micromechanics and Microengineering, 2011. **21**(5).
21. Gunther, A., et al., *Transport and reaction in microscale segmented gas-liquid flow.* Lab on a Chip, 2004. **4**(4): p. 278-286.
22. Hashimoto, M., et al., *Formation of bubbles and droplets in parallel, coupled flow-focusing geometries.* Small, 2008. **4**(10): p. 1795-805.
23. Garstecki, P., et al., *Formation of droplets and bubbles in a microfluidic T-junction-scaling and mechanism of break-up.* Lab Chip, 2006. **6**(3): p. 437-46.
24. Tang, S.K., et al., *A multi-color fast-switching microfluidic droplet dye laser.* Lab Chip, 2009. **9**(19): p. 2767-71.
25. Kobayashi, I., K. Uemura, and M. Nakajima, *Formulation of monodisperse emulsions using submicron-channel arrays.* Colloids and Surfaces a-Physicochemical and Engineering Aspects, 2007. **296**(1-3): p. 285-289.
26. Chen, Y.T., et al., *Fission and fusion of droplets in a 3-D crossing microstructure.* Microfluidics and Nanofluidics, 2012. **13**(2): p. 239-247.
27. Zeng, Y., M. Shin, and T. Wang, *Programmable active droplet generation enabled by integrated pneumatic micropumps.* Lab Chip, 2013. **13**(2): p. 267-73.
28. de Bruijn, R.A., *Tipstreaming of drops in simple shear flows.* Chemical Engineering Science, 1993. **48** (2): p. 277–284.
29. Tice, J.D., A.D. Lyon, and R.F. Ismagilov, *Effects of viscosity on droplet formation and mixing in microfluidic channels.* Analytica Chimica Acta, 2004. **507**(1): p. 73-77.
30. Tice, J.D., et al., *Formation of droplets and mixing in multiphase microfluidics at low values of the Reynolds and the capillary numbers.* Langmuir, 2003. **19**(22): p. 9127-9133.
31. Janssen, J.M.H. and H.E.H. Meijer, *Droplet Breakup Mechanisms - Stepwise Equilibrium Versus Transient Dispersion.* Journal of Rheology, 1993. **37**(4): p. 597-608.
32. Garstecki, P., et al., *Formation of droplets and bubbles in a microfluidic T-junction - scaling and mechanism of break-up.* Lab on a Chip, 2006. **6**(3): p. 437-446.

33. Mazutis, L., et al., *Single-cell analysis and sorting using droplet-based microfluidics.* Nat Protoc, 2013. **8**(5): p. 870-91.
34. Tan, Y.C., et al., *Design of microfluidic channel geometries for the control of droplet volume, chemical concentration, and sorting.* Lab Chip, 2004. **4**(4): p. 292-8.
35. Stone, W.E., J.H. Crocket, and M.E. Fleet, *Light-Rare Earth Element-Rich Minerals Associated with Platinum-Group Element Mineralization in the Archean Boston Creek Flow, Ontario.* Mineralogy and Petrology, 1994. **51**(1): p. 85-109.
36. Christopher, G.F. and S.L. Anna, *Microfluidic methods for generating continuous droplet streams.* Journal of Physics D-Applied Physics, 2007. **40**(19): p. R319-R336.
37. Nisisako, T., S. Okushima, and T. Torii, *Controlled formulation of monodisperse double emulsions in a multiple-phase microfluidic system.* Soft Matter, 2005. **1**(1): p. 23-27.
38. Anna, S.L. and H.C. Mayer, *Microscale tipstreaming in a microfluidic flow focusing device.* Physics of Fluids, 2006. **18**(12).
39. Link, D.R., et al., *Geometrically mediated breakup of drops in microfluidic devices.* Physical Review Letters, 2004. **92**(5).
40. Christopher, G.F., et al., *Experimental observations of the squeezing-to-dripping transition in T-shaped microfluidic junctions.* Physical Review E, 2008. **78**(3).
41. Baret, J.C., et al., *Kinetic aspects of emulsion stabilization by surfactants: a microfluidic analysis.* Langmuir, 2009. **25**(11): p. 6088-93.
42. Gu, H., M.H. Duits, and F. Mugele, *Droplets formation and merging in two-phase flow microfluidics.* Int J Mol Sci, 2011. **12**(4): p. 2572-97.
43. Abate, A.R. and D.A. Weitz, *Air-bubble-triggered drop formation in microfluidics.* Lab Chip, 2011. **11**(10): p. 1713-6.
44. Ahmed, R. and T.B. Jones, *Dispensing picoliter droplets on substrates using dielectrophoresis.* Journal of Electrostatics, 2006. **64**(7-9): p. 543-549.
45. Cho, S.K., Y. Zhao, and C.J. Kim, *Concentration and binary separation of micro particles for droplet-based digital microfluidics.* Lab Chip, 2007. **7**(4): p. 490-8.
46. Ahmed, R., et al., *Dispensing picoliter droplets using dielectrophoretic (DEP) microactuation.* Microscale Thermophysical Engineering, 2004. **8**(3): p. 271-283.
47. Wang, K.L., T.B. Jones, and A. Raisanen, *DEP actuated nanoliter droplet dispensing using feedback control.* Lab Chip, 2009. **9**(7): p. 901-9.
48. Priest, C., S. Herminghaus, and R. Seemann, *Generation of monodisperse gel emulsions in a microfluidic device.* Applied physics letters, 2006. **88**(2).
49. Eslamian, M., Ashgriz, N., *Chapter 25 - Drop on demand droplet generators*, in *handbook of atomization and sprays*, N. Ashgriz, Editor. 2011, springer science.
50. Hung, L.H., et al., *Alternating droplet generation and controlled dynamic droplet fusion in microfluidic device for CdS nanoparticle synthesis.* Lab Chip, 2006. **6**(2): p. 174-8.
51. De Menech, M., et al., *Transition from squeezing to dripping in a microfluidic T-shaped junction.* Journal of Fluid Mechanics, 2008. **595**: p. 141-161.
52. Romero, P.A. and A.R. Abate, *Flow focusing geometry generates droplets through a plug and squeeze mechanism.* Lab on a Chip, 2012. **12**(24): p. 5130-5132.
53. Sullivan, M.T. and H.A. Stone, *The role of feedback in microfluidic flow-focusing devices.* Philos Transact A Math Phys Eng Sci, 2008. **366**(1873): p. 2131-43.
54. Ward, T., et al., *Microfluidic flow focusing: drop size and scaling in pressure versus flow-rate-driven pumping.* Electrophoresis, 2005. **26**(19): p. 3716-24.

55. Squires, T.M. and S.R. Quake, *Microfluidics: Fluid physics at the nanoliter scale.* Reviews of Modern Physics, 2005. **77**(3): p. 977-1026.
56. Ong, W.L., et al., *Experimental and computational analysis of droplet formation in a high-performance flow-focusing geometry.* Sensors and Actuators a-Physical, 2007. **138**(1): p. 203-212.
57. Xu, Q.B., et al., *Preparation of Monodisperse Biodegradable Polymer Microparticles Using a Microfluidic Flow-Focusing Device for Controlled Drug Delivery.* Small, 2009. **5**(13): p. 1575-1581.
58. Hindson, B.J., et al., *High-throughput droplet digital PCR system for absolute quantitation of DNA copy number.* Anal Chem, 2011. **83**(22): p. 8604-10.
59. Song, H., J.D. Tice, and R.F. Ismagilov, *A microfluidic system for controlling reaction networks in time.* Angewandte Chemie-International Edition, 2003. **42**(7): p. 768-772.
60. Menetrier-Deremble, L. and P. Tabeling, *Droplet breakup in microfluidic junctions of arbitrary angles.* Phys Rev E Stat Nonlin Soft Matter Phys, 2006. **74**(3 Pt 2): p. 035303.
61. Nie, J. and R.T. Kennedy, *Sampling from Nanoliter Plugs via Asymmetrical Splitting of Segmented Flow.* Analytical Chemistry, 2010. **82**(18): p. 7852-7856.
62. Yamada, M., et al., *Hydrodynamic control of droplet division in bifurcating microchannel and its application to particle synthesis.* Journal of Colloid and Interface Science, 2008. **321**(2): p. 401-407.
63. Christopher, G.F. and S.L. Anna, *Passive breakup of viscoelastic droplets and filament self-thinning at a microfluidic T-junction.* Journal of Rheology, 2009. **53**(3): p. 663-683.
64. Cho, S.K., H.J. Moon, and C.J. Kim, *Creating, transporting, cutting, and merging liquid droplets by electrowetting-based actuation for digital microfluidic circuits.* Journal of Microelectromechanical Systems, 2003. **12**(1): p. 70-80.
65. Ren, H., R.B. Fair, and M.G. Pollack, *Automated on-chip droplet dispensing with volume control by electro-wetting actuation and capacitance metering.* Sensors and Actuators B-Chemical, 2004. **98**(2-3): p. 319-327.
66. Mazutis, L., et al., *Multi-step microfluidic droplet processing: kinetic analysis of an in vitro translated enzyme.* Lab on a Chip, 2009. **9**(20): p. 2902-2908.
67. Ting, T.H., et al., *Thermally mediated breakup of drops in microchannels.* Applied physics letters, 2006. **89**(23).
68. Xiong, B., et al., *Gas-solid flow in an integrated external heat exchanger for CFB boiler.* Powder Technology, 2010. **202**(1-3): p. 55-61.
69. Simon, M.G., Lee, A.P., *Microfluidic Droplet Manipulations and Their Applications*, in *Microdroplet Technology: Principles and Emerging Applications in Biology and Chemistry, Integrated Analytical Systems,*, P. Day, Editor. 2012.
70. Liu, K., et al., *Droplet-based synthetic method using microflow focusing and droplet fusion.* Microfluidics and Nanofluidics, 2007. **3**(2): p. 239-243.
71. Niu, X., et al., *Pillar-induced droplet merging in microfluidic circuits.* Lab on a Chip, 2008. **8**(11): p. 1837-1841.
72. Bremond, N., A.R. Thiam, and J. Bibette, *Decompressing emulsion droplets favors coalescence.* Physical Review Letters, 2008. **100**(2).
73. Fidalgo, L.M., C. Abell, and W.T.S. Huck, *Surface-induced droplet fusion in microfluidic devices.* Lab on a Chip, 2007. **7**(8): p. 984-986.

74. Mazutis, L., J.C. Baret, and A.D. Griffiths, *A fast and efficient microfluidic system for highly selective one-to-one droplet fusion.* Lab on a Chip, 2009. **9**(18): p. 2665-2672.
75. Chabert, M., K.D. Dorfman, and J.L. Viovy, *Droplet fusion by alternating current (AC) field electrocoalescence in microchannels.* Electrophoresis, 2005. **26**(19): p. 3706-3715.
76. Tan, W.H. and S. Takeuchi, *Timing controllable electrofusion device for aqueous droplet-based microreactors.* Lab on a Chip, 2006. **6**(6): p. 757-763.
77. Gu, H., et al., *A microfluidic platform for on-demand formation and merging of microdroplets using electric control.* Biomicrofluidics, 2011. **5**(1).
78. Wang, W., C. Yang, and C.M. Li, *On-demand microfluidic droplet trapping and fusion for on-chip static droplet assays.* Lab on a Chip, 2009. **9**(11): p. 1504-1506.
79. Thiam, A.R., N. Bremond, and J. Bibette, *Breaking of an Emulsion under an ac Electric Field.* Physical Review Letters, 2009. **102**(18).
80. Eow, J.S. and M. Ghadiri, *Motion, deformation and break-up of aqueous drops in oils under high electric field strengths.* Chemical Engineering and Processing, 2003. **42**(4): p. 259-272.
81. Zagnoni, M. and J.M. Cooper, *On-chip electrocoalescence of microdroplets as a function of voltage, frequency and droplet size.* Lab on a Chip, 2009. **9**(18): p. 2652-2658.
82. Young, P.M. and K. Mohseni, *Calculation of DEP and EWOD forces for application in digital microfluidics.* Journal of Fluids Engineering-Transactions of the Asme, 2008. **130**(8).
83. Vrij, A., *Possible Mechanism for Spontaneous Rupture of Thin Free Liquid Films.* Discussions of the Faraday Society, 1966(42): p. 23-&.
84. Herminghaus, S., *Dynamical instability of thin liquid films between conducting media.* Physical Review Letters, 1999. **83**(12): p. 2359-2361.
85. Priest, C., S. Herminghaus, and R. Seemann, *Controlled electrocoalescence in microfluidics: Targeting a single lamella.* Applied physics letters, 2006. **89**(13).
86. Zagnoni, M., C.N. Baroud, and J.M. Cooper, *Electrically initiated upstream coalescence cascade of droplets in a microfluidic flow.* Physical Review E, 2009. **80**(4).
87. Ahn, K., et al., *Electrocoalescence of drops synchronized by size-dependent flow in microfluidic channels.* Applied physics letters, 2006. **88**(26).
88. Link, D.R., et al., *Electric control of droplets in microfluidic devices.* Angewandte Chemie-International Edition, 2006. **45**(16): p. 2556-2560.
89. Lorenz, R.M., et al., *Vortex-trap-induced fusion of femtoliter-volume aqueous droplets.* Analytical Chemistry, 2007. **79**(1): p. 224-228.
90. Huh, D., et al., *Gravity-driven microfluidic particle sorting device with hydrodynamic separation amplification.* Analytical Chemistry, 2007. **79**(4): p. 1369-1376.
91. Hatch, A.C., et al., *Passive droplet sorting using viscoelastic flow focusing.* Lab on a Chip, 2013. **13**(7): p. 1308-1315.
92. Ahn, K., et al., *Dielectrophoretic manipulation of drops for high-speed microfluidic sorting devices.* Applied physics letters, 2006. **88**(2).
93. Cao, Z.N., et al., *Droplet sorting based on the number of encapsulated particles using a solenoid valve.* Lab on a Chip, 2013. **13**(1): p. 171-178.

94. Franke, T., et al., *Surface acoustic wave (SAW) directed droplet flow in microfluidics for PDMS devices.* Lab on a Chip, 2009. **9**(18): p. 2625-2627.
95. Xu, L.F., et al., *Fusion and sorting of two parallel trains of droplets using a railroad-like channel network and guiding tracks.* Lab on a Chip, 2012. **12**(20): p. 3936-3942.
96. Wang, L., et al., *Dielectrophoresis switching with vertical sidewall electrodes for microfluidic flow cytometry.* Lab on a Chip, 2007. **7**(9): p. 1114-1120.
97. Zhang, K., et al., *On-chip manipulation of continuous picoliter-volume superparamagnetic droplets using a magnetic force.* Lab on a Chip, 2009. **9**(20): p. 2992-2999.
98. Boedicker, J.Q., et al., *Detecting bacteria and determining their susceptibility to antibiotics by stochastic confinement in nanoliter droplets using plug-based microfluidics.* Lab on a Chip, 2008. **8**(8): p. 1265-1272.
99. Shim, J.U., et al., *Simultaneous Determination of Gene Expression and Enzymatic Activity in Individual Bacterial Cells in Microdroplet Compartments.* Journal of the American Chemical Society, 2009. **131**(42): p. 15251-15256.
100. Westman, J.O., et al., *Effects of encapsulation of microorganisms on product formation during microbial fermentations.* Applied Microbiology and Biotechnology, 2012. **96**(6): p. 1441-1454.
101. Papoulis, A., *Estimation of Average Density of a Nonuniform Poisson Process.* Ieee Transactions on Communications, 1974. **22**(2): p. 162-167.
102. Huebner, A., et al., *Quantitative detection of protein expression in single cells using droplet microfluidics.* Chemical Communications, 2007(12): p. 1218-1220.
103. El Debs, B., et al., *Functional single-cell hybridoma screening using droplet-based microfluidics.* Proceedings of the National Academy of Sciences of the United States of America, 2012. **109**(29): p. 11570-11575.
104. Joensson, H.N. and H.A. Svahn, *Droplet Microfluidics-A Tool for Single-Cell Analysis.* Angewandte Chemie-International Edition, 2012. **51**(49): p. 12176-12192.
105. Tawfik, D.S. and A.D. Griffiths, *Man-made cell-like compartments for molecular evolution.* Nature Biotechnology, 1998. **16**(7): p. 652-656.
106. Griffiths, A.D. and D.S. Tawfik, *Miniaturising the laboratory in emulsion droplets.* Trends in Biotechnology, 2006. **24**(9): p. 395-402.
107. Bringer, M.R., et al., *Microfluidic systems for chemical kinetics that rely on chaotic mixing in droplets.* Philosophical Transactions of the Royal Society of London Series a-Mathematical Physical and Engineering Sciences, 2004. **362**(1818): p. 1087-1104.
108. Fallah-Araghi, A., et al., *A completely in vitro ultrahigh-throughput droplet-based microfluidic screening system for protein engineering and directed evolution.* Lab on a Chip, 2012. **12**(5): p. 882-891.
109. Petrounia, I.P. and F.H. Arnold, *Designed evolution of enzymatic properties.* Current Opinion in Biotechnology, 2000. **11**(4): p. 325-330.
110. Guo, M.T., et al., *Droplet microfluidics for high-throughput biological assays.* Lab on a Chip, 2012. **12**(12): p. 2146-2155.
111. Agresti, J.J., et al., *Ultrahigh-throughput screening in drop-based microfluidics for directed evolution.* Proceedings of the National Academy of Sciences of the United States of America, 2010. **107**(9): p. 4004-4009.

112. Miller, O.J., et al., *High-resolution dose-response screening using droplet-based microfluidics.* Proc Natl Acad Sci U S A, 2012. **109**(2): p. 378-83.
113. Rane, T.D., et al., *Droplet microfluidics for amplification-free genetic detection of single cells.* Lab on a Chip, 2012. **12**(18): p. 3341-3347.
114. Baret, J.C., et al., *Quantitative Cell-Based Reporter Gene Assays Using Droplet-Based Microfluidics.* Chemistry & Biology, 2010. **17**(5): p. 528-536.
115. Zhang, H.F., et al., *Massively Parallel Single-Molecule and Single-Cell Emulsion Reverse Transcription Polymerase Chain Reaction Using Agarose Droplet Microfluidics.* Analytical Chemistry, 2012. **84**(8): p. 3599-3606.
116. Aranda, M.A.G., et al., *Coherent X-ray diffraction investigation of twinned microcrystals.* Journal of Synchrotron Radiation, 2010. **17**: p. 751-760.

HIGH-YIELD CELL ORDERING AND DETERMINISTIC CELL-IN-DROPLET ENCAPSULATION*

CHAPTER 6

In this chapter, high-yield (77%) and high-speed (2700 cells/s) single cell droplet encapsulation is described using Dean-coupled inertial ordering of cells in a simple curved continuous microchannel. By introducing the Dean force, particles order to one equilibrium position after less than 1 cm travelled. We use a planar curved microchannel structure in PDMS to spatially order two types of myeloid leukemic cells (HL60 and K562 cells), enabling deterministic single cell encapsulation in picolitre droplets. A single cell encapsulation efficiency of up to 77% is reached, overcoming the limitations imposed by Poisson statistics for random cell loading, which yields only 37% of droplets containing a single cell. Furthermore, we confirm that >90% of the cells remain viable. The small footprint (~0.4 cm^2), simple planar structure and high-throughput provided by this passive microfluidic approach makes it attractive for implementation in Lab on a Chip (LOC) devices for single cell applications using droplet-based platforms.

* modified from: E.W.M. Kemna, R.M. Schoeman, F. Wolbers, I. Vermes, D.A. Weitz and A. van den Berg. Lab Chip, 2012, 12, 2881-2887

6.1 Introduction

Droplet-based microfluidic systems have been used for various biotechnology research applications[1-3], such as cell-based assays[4], polymerase chain reactions[5], proteome analysis[6] and cell printing technologies[7] and have become a standard platform for high-throughput single cell experimentation and analysis[8,9]. Encapsulation of single cells within picolitre-sized droplets enable quantitative studies of large populations of single cells[10, 11]. The droplets serve as microvessels, which entrap the secretion products of the individual cells and prevent mixing with other cells. In addition, uptake of trace chemicals can be probed due to their depletion within the confined droplet. Using microfluidic devices, monodisperse droplets can be generated, merged, and sorted at kilohertz rates, enabling high-throughput single cell screening[12]. However, the platform suffers from one fundamental limitation, the variability in the number of cells per droplet[13]. Typically, cells are loaded in the droplets by diluting suspensions of the cells and randomly encapsulating them into the droplets; the distribution is thus dictated by Poisson statistics[14]:

$$P(\lambda;k) = \lambda^k \exp(-\lambda)/k! \qquad [6.1]$$

where k is the number of cells in the droplet and λ is the average number of cells per droplet, which is adjusted by controlling the cell density[11]. Very low loading densities are required to minimize the number of droplets that contain multiple cells. Hence, the majority of the droplets are empty and the efficiency of the single cell encapsulation is drastically decreased[12, 15]. This inefficiency has stimulated the development of new methods to increase single cell encapsulation efficiency, such as using a laser[16], hydrodynamic focusing and sorting[17] and on-demand impedance-based cell encapsulation[10, 17, 18]. However, these approaches suffer from disadvantages such as reduced throughput[16-18], the use of sophisticated optical equipment or extensive input from the user[16]. Recently, Edd et al.[10] demonstrated efficient single cell encapsulation by ordering cells using inertial migration in a 6 cm straight channel. Unfortunately, this method suffers from a lack of robustness, requires high flow rates and is difficult to implement in microfluidic LOC devices.

We overcome these drawbacks with a fast, easy and novel approach to deterministically encapsulate single cells in droplets using inertial ordering in a curved microchannel. The curvature introduces a second force, the Dean force[19], which causes particles to focus at a single equilibrium position. The device shows a wider dynamic range, regarding particle size and number of equilibrium positions. Moreover, it has a small footprint, making it compatible for microfluidic LOC devices. Furthermore, curved microchannels show faster cell ordering than straight channels[20]. Inertial ordering of particles in curved microchannels is used in sorting and filtration applications[21-24], but not for single cell encapsulation.

The microfluidic chip presented here (figure 6.1), consists of a curved microchannel which combines inertial ordering with Dean forces to evenly space the cells. By

matching the periodicity of the cell flow with the droplet generation, we increase the efficiency of single cell encapsulation. This deterministic encapsulation method reduces the number of empty and multi-cell droplets, while increasing the number of droplets containing a single cell.

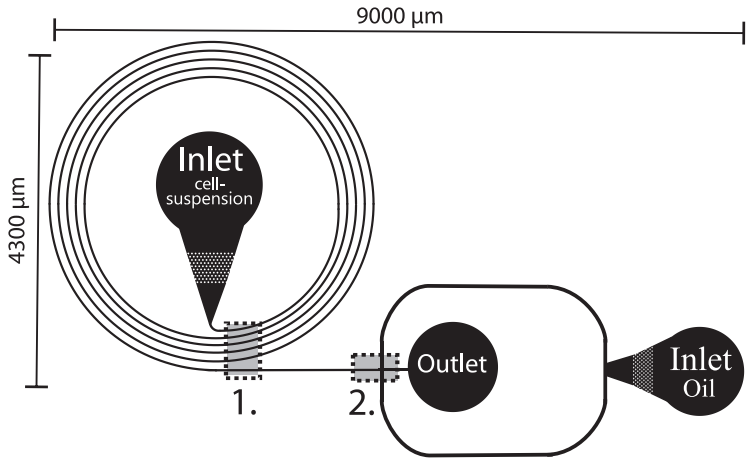

Figure 6.1: Schematic drawing of the microfluidic chip consisting of a curved microchannel (1) to induce cell ordering, followed by an encapsulation part (2).

6.2 Theoretical background

Fluid flowing through a straight rectangular microchannel experiences primary a Poiseuille flow with a parabolic velocity profile. This parabolic velocity results in a fluidic shear-gradient-induced inertial lift force (F_{IL}); this causes particles in the flow to move away from the centerline. However, as the particles move towards the walls of the microchannel, a wall-induced inertial lift force (F_{WL}) pushes the particles away from the wall, due to the asymmetric wake induced around the particles. This causes F_{WL} to increase as the particles approach the wall. Because F_{IL} and F_{WL} are opposing lift forces, which vary in magnitude across the cross-section of the microchannel, particles are forced to occupy positions where the two forces cancel out (figure 6.2). Hence, in a straight rectangular microchannel, there are up to *four* equilibrium positions present[25-27], depending on channel dimensions and volume fraction[10, 28].

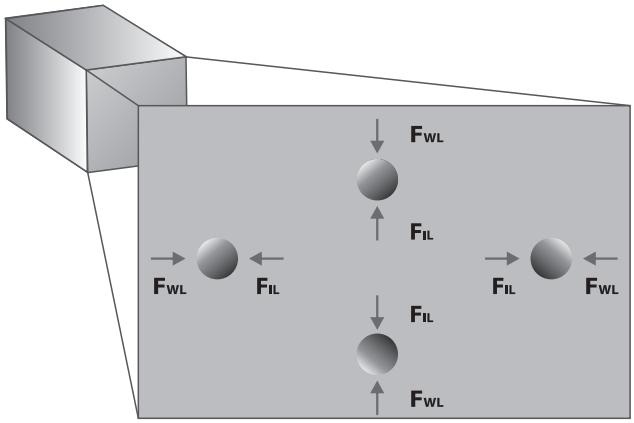

Figure 6.2: A schematic overview of the four equilibrium positions induced in a straight channel by F_{WL} and F_{IL}.

However, for single-particle encapsulation we are interested in ordering of particles with a steady axial particle-particle distance. Because stable equilibrium position combined with steady particle-particle distance makes single particle encapsulation in droplets possible. Due to hydrodynamic interactions and Stokes flow, particles find equilibrium positions at a certain distance from each other. One can imagine that when there are up to four equilibrium positions the particle interactions increase and steady axial particle-particle distance compared to *e.g.* a single equilibrium position is increasingly comprised. In the later situation, a single equilibrium position, particle distance is only dependent on the particle 'in front and behind' the middle particle and the distance is thought to be more stable. Making it easier to adapt the droplet generation frequency to the passing particle train. Moreover, particle ordering occurs faster in a curved microchannel compared to a straight channel[26].

In a continuous curved rectangular microchannel, there is a secondary flow due to the difference between the downstream velocity of the fluid in the center and that near the wall. Thus, fluid elements have larger inertia in the center of the microchannel than near the walls. This produces a pressure gradient in the radial direction of the microchannel, as the fluid tends to flow outward around the curve, leading to the formation of two counter rotating vortices at the top and bottom halves of the microchannel (figure 6.3). F_L is the net lift force, which is a combination of the shear-gradient-induced inertial lift force (F_{IL}), and the wall-induced lift force (F_{WL})

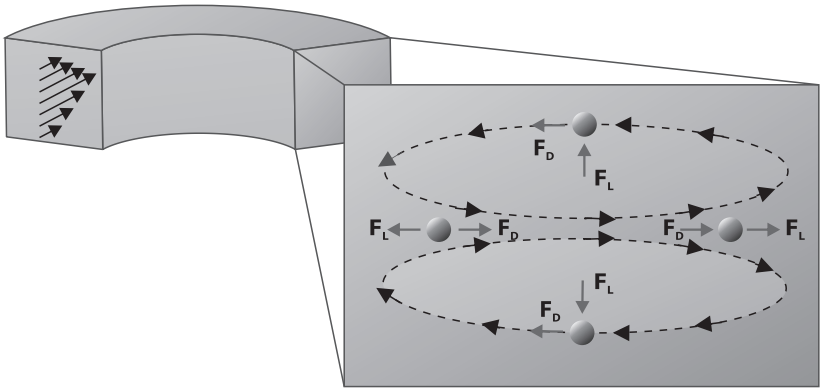

Figure 6.3: Schematic illustration of a continuous curved rectangular microchannel in which both the Dean force (F_D) and lift force (F_L) are shown. The directions of their applied force on the particles, result in a single equilibrium position at the inner wall of the microchannel, where both forces operate in opposite direction.

The magnitude of these secondary flows is quantified by the Dean number[21, 24]:

$$De = Re \cdot \sqrt{\frac{D_h}{2 \cdot R}} \qquad [6.2]$$

in which R is the radius of the curvature (m) of the path of the channel, D_h is $2 \cdot w \cdot h / w+h$, in which w (m) and h (m) are the width and height of the channel, and Re is the flow Reynolds number, $Re = Uf \cdot Dh / (\mu/\rho)$. U_f is the flow velocity of the fluid (m/s), μ is the viscosity of the fluid (kg/m·s) and ρ the fluid density (kg/m^3). The secondary flows, called Dean flows (U_D, m/s), are flows with a range of lateral velocities, which are dependent on the position in the cross-section of the channel. The average velocity can be calculated by an expression formulated by Ookawara et al.[29] at a given De number[30, 31]:

$$U_D = 1.8 \times 10^{-4} \cdot De^{1.63} \qquad [6.3]$$

The Dean flows are capable of applying a drag force on the particles present in the fluid. The maximum value of this drag force (F_D) can be estimated by Stokes drag [29, 30]:

$$F_D = 3 \cdot \pi \cdot \mu \cdot U_D \cdot a_p = 5.4 \times 10^{-4} \cdot \pi \cdot \mu \cdot De^{1.63} \cdot a_p \qquad [6.4]$$

in which a_p is the particle diameter (m). The radius of the curvature of the microchannel has to be minimized to create a large Dean number, and hence a large Dean force, thereby causing the particles to equilibrate faster. Depending on the particle size, F_D constrains the particles to follow the path of the Dean flows, causing them to circulate either at the top or bottom half of the channel. Moreover, in addition to the F_D, another force is present in the channel acting on the particles. As mentioned, this force is the net lift force, F_L (a combination of F_{IL} and F_{WL}) [21, 24, 30]:

$$F_L = \frac{2 \cdot \rho \cdot U_f^2 \cdot C_L \cdot a_p^4}{D_h^2} \quad [6.5]$$

C_L is the lift coefficient, which is a function of the particle position across the cross section of the microchannel and has an average value of 0.5 [27, 30]. Figure 6.3 schematically illustrates the Dean flows, F_D and F_L as well as their directions on the particles. The balance between F_L and F_D determines the preferred location of particles in microchannels with a curved geometry. The additional force, F_D, does not create particle ordering, but instead acts in a different direction than F_L, reducing the number of equilibrium positions. Depending on the relative magnitude of F_D and F_L acting on a particle, focusing (dominant lift force) or mixing (dominant Dean force) occurs[24]. The particles will circulate in the Dean flows until they have all reached an equilibrium position. This equilibrium position is at the inside of the curved microchannel, where F_L and F_D work in opposite direction on the particle. However, this preferential focusing of particles can only be achieved when the $a_p/D_h \geq 0.07$[27, 30, 32]. In addition, F_L dominates the particle behavior only when the particle Reynolds number, $Re_p = Re \cdot a_p^2/D_h^2$, is in the order of 1[26].

Particle spacing

As stated, in a straight channel the number of equilibrium positions of particles can be determined by adjusting the channel dimensions and the volume fraction of particles in the solution[28]:

$$\frac{m \cdot a_p}{l} = \frac{6 \cdot \phi \cdot w \cdot h}{\pi \cdot a_p^2} \quad [6.6]$$

In which m is the number of equilibrium positions present in the channel, l is the longitudinal distance between two particles (m), ϕ is the volume fraction of particles in the solution.

The longitudinal distance l, between particles on the same side of the channel, does not depend on the volume fraction. Though, adjusting the flow rate of the fluid, the channel dimensions, the volume fraction, and the particle diameter, it is possible to align particles at a single equilibrium position, all with similar longitudinal distances. This enables encapsulation of single particles in droplets in a straight channel. Furthermore, it is likely that a similar relationship between Re_p and l pertains in a continuous curved rectangular microchannel. Moreover, there probably will be a relationship between the volume fraction and the number of equilibrium positions.

6.3 Experimental setup

6.3.1 Microfluidic chip design and fabrication

The microfluidic chip consists of a 5-loop curved microchannel, with one inlet for the cell suspension and one inlet for the oil. Several chip designs were used with varying parameters which are specified when discussing the results.

A silicon master design was drawn in Clewin (version 4.0.1) and fabricated using standard UV-lithography. SU-8 (Microchem, Berlin, Germany) was spun on the silicon master with a thickness of 29 µm. The chip was made in PDMS (Sylgard 184, Dow Corning, Midland, MI, USA). Curing and base agent were mixed at a ratio of 1:10 and degassed. PDMS was poured onto a silicon wafer, degassed, and cured at 60 °C for 24 hours. After curing, in- and outlets were punched using a dispensing tip (Nordson EFD, Maastricht, the Netherlands, inner Ø 1.36 mm and outer Ø 1.65 mm). Subsequently, the PDMS was sealed to a microscope slide (VWR, Leuven, Belgium) using an oxygen plasma (Harrick PDC-001, NY, USA). After sealing, the chip was placed at 60 °C for a minimum of 30 minutes. Before use, Aquapel (Vulcavite, the Netherlands) was introduced into the channels to ensure hydrophobic channel walls.

6.3.2 Materials

Two types of myeloid leukemic cells where used: HL60 (human promyelocytic leukemic cells) and K562 (human erythromyeloblastoid leukemic cells). Both cell types were grown in RPMI medium (Invitrogen, Grand Island, NY, USA), supplemented with 10% (v/v) fetal bovine serum (FBS; Invitrogen), 100 U/ml penicillin (Invitrogen), 100 µg/ml streptomycin (Invitrogen) and 2 mM L-glutamine (Invitrogen) (= $RPMI^+$ medium). Cell cultures were sustained in a 5% CO_2 humidified atmosphere at 37 °C. Cell cultures were split every 3-4 days at a ratio of 1:10. In the experiments, cells were suspended at the desired volume fraction, ranging from 1 to 2.2 %, in $RPMI^+$ medium prior to use. Polystyrene beads (Polysciences Inc, Germany) with a diameter of 6 and 10 µm were used for initial experiments and optimization. Subsequently, the experiments with the cells were performed. For the continuous phase, FC-40 (3M, St. Paul, MN, USA) was used with 1% (w/w) oil-phase biocompatible fluorosurfactant supplied by Ralph Sperling (Harvard).

6.3.3 Experimental set-up

The bead or cell suspensions and oil were separately introduced into the microfluidic chip using two 3 ml plastic syringes (BD, Breda, the Netherlands), and connected to the two inlets with PEEK tubing (Vici, Schenkon, Switzerland, inner Ø 0.5 mm and outer Ø 1.59 mm). PEEK tubing was also connected to the outlet of the device and routed into a collection tube. Flow was driven at a constant volume rate by a syringe pump (neMESYS dosing units, Cetoni GmbH, Germany). A magnetic stir bar was inserted to the syringe to prevent suspension settling during injection. The flow rate of the continuous phase was

30-43 µL/min and the aqueous flow rate, containing the cells or beads, was set to 10-20 µL /min.

The microfluidic chip was mounted on an X-Y-Z translation stage of an inverted wide fluorescence microscope (Leica DM IRM, Leica Microsystems, Wetzlar, GmbH, Germany). For image recording, a computer-controlled high-speed camera (Photron SA-3, West Wycombe, United Kingdom) was mounted onto the microscope, using the accompanied Photron software (Photron Fastcam Viewer). Illumination was supplied by a fiber optic illuminator (Leica KL 1500 LCD).

6.3.4 Image acquisition and analysis

Videos and images of cell ordering in the curved microchannel and subsequent cell encapsulation were captured using the high-speed camera at a frame rate of 3000-18181 frames per second and a shutter time of 5-30 µs. All videos and images captured were analyzed with the image processing program ImageJ (National Institute of Health, MD, USA). To determine the encapsulation efficiency, the number of droplets containing 0, 1, or more cells was divided by the total number of droplets counted.

6.4 Results and discussion

Using equations [6.2-5], the microfluidic chips with the different dimensions were characterized for their ordering capacity. Firstly, to gain insight into the different parameters (e.g. particle size, chip dimensions, Dean and lift forces) we started with bead experiments. The 6 µm beads are used to mimick the B-cell dimensions, and the 10 µm beads correspond to the larger, widely available leukocytes (HL60 and K562).

6.4.1 Characterization of the microfluidic chip - bead ordering

Chips with different dimensions regarding width and height were analyzed for their Dean and lift forces on different sized particles. Subsequently, the ordering capacity was analyzed. Table 6.1 shows how the flow rate (U_f) and the channel dimensions influence the Reynolds number (Re), the Reynolds particle number (Re_p), the Dean number (De), and the apparent Dean (F_D) and lift forces (F_L) using 6 µm and 10 µm beads.

Table 6.1: Summary of the Dean force (F_D), lift force (F_L) and Re_p acting on 6 or 10 µm bead for varying Dean numbers

w x h	Chip 1: 25 x 25 (µm)		Chip 2: 50 x 25 (µm)	
R (µm)	1700			
a_p (µm)	6		10	
U_f (µL/min)	10	20	10	20
Re	6.67	13.33	4.44	8.88
Re_p	0.38	0.77	0.4	0.8
De	0.57	1.14	0.44	0.88
F_L (N)	2.95×10^{-10}	1.18×10^{-9}	3.2×10^{-10}	1.28×10^{-9}
F_D (N)	4.09×10^{-12}	1.27×10^{-11}	4.45×10^{-12}	1.37×10^{-11}

The Dean forces acting on the 6 µm beads in chip 1 and the 10 µm beads in chip 2, at the two flow rates are less than the corresponding lift forces. Hence, for both chip 1 and 2, the lift forces dominate, which predicts that ordering will occur and the beads will focus along the one equilibrium position at the inner wall as illustrated in figure 6.2.

Bead ordering

Besides, the channel dimension, the ratio between particle and channel dimension and the domination of F_L over F_D, the bead concentration is of essential importance in order to achieve bead alignment in a curved microchannel. In chip 1, 6 µm beads were used with concentrations ranging from 0.1% w/v to 1% w/v. Figure 6.4 A shows that a concentration of 1% w/v is too high to achieve alignment and the beads were not forced in the single equilibrium position as expected. However, at a concentration of 0.5% w/v, alignment is shown (figure 6.4 B). These results demonstrate the strong impact of particle concentration on the ordering capacity. The minimal flow rate to achieve alignment was 10 µL/min and alignment occured, in the second coil, after 0.91 cm (54 ms). The distance between the beads was 25.7 ± 5.5 µm (n=20). Furthermore, particles with a diameter >10 µm could not be ordered using chip 1. Even though the restriction regarding particle and channel dimension, $a_p/D_h \geq 0.07$, is met ordering does not occur. This is probably explained by to the upper limit of a_p/D_h ratio. Where the ratio of the particle diameter of 10 µm and the channel width and height of 25 µm is too large. Furthermore, all other requirements regarding Dean number, particle Reynolds number and F_L and F_D are met.

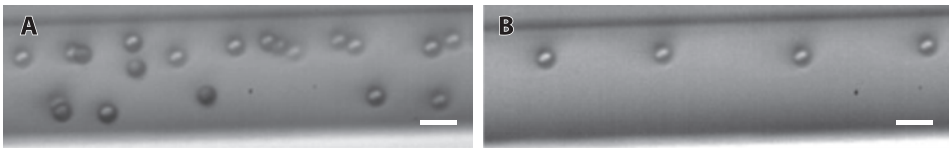

Figure 6.4: 6 µm bead ordering in chip 1. A) No alignment at a concentration of 1% w/v and a flow rate of 20 µL/min. B) Alignment at concentration of 0.5% w/v and a flow rate of 20 µL/min. Scale bars are 10 µm.

Next, in chip 2, alignment of 10 µm beads occurred at a flow rate of 20 µL/min, as shown in figure 6.5. The alignment took place at a single equilibrium position at the inner side of the wall. The distance between the beads was 31.4 ± 2.9 µm (n=20). However, in some experiments, an interesting phenomenon was observed regarding the equilibrium positions of the beads in chip 2. There was a second stable equilibrium position for the 10 µm beads in chip 2, as shown in figure 6.5 B. This double equilibrium positions occurred at all tested flowrates up till 40 µL/min. This suggest that the incidence of a double equilibrium position is independent of the flow rate.

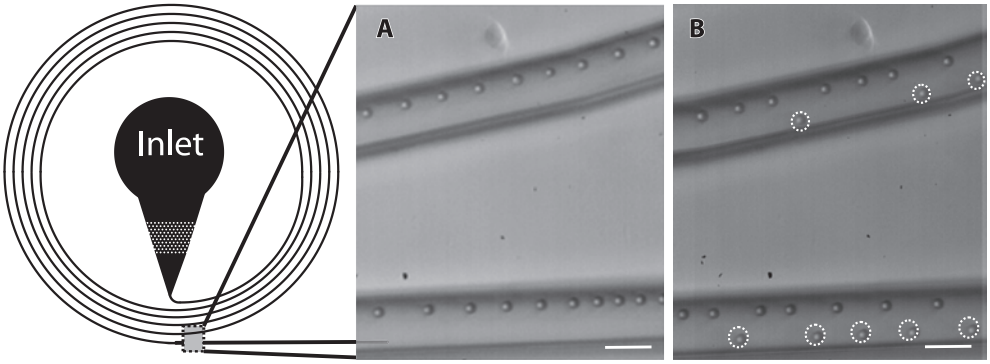

Figure 6.5: 10 µm bead ordering in chip 2. A) Alignment of 10 µm beads at a single equilibrium position, concentration of 0.8% w/v and at a flow rate of 20 µL/min. B) Alignment of 10 µm beads at a double equilibrium position, concentration of 0.8% w/v and at a flow rate of 20 µL/min. Scale bars are 50 µm.

Furthermore, a curved microchannel with a width of 50 µm and a height of 48 µm (chip 3) was tested for alignment of 6 µm beads at a flow rate of 30 µl/min. Here, the equilibrium position was in the middle of the channel (figure 6.6 A), which differs from the equilibrium positions observed in chip 1 and 2. Interestingly, a second equilibrium position was observed (figure 6.6 A) at different heights in the middle of the channel. The distance between the 6 µm beads on a single height was 20.3 ± 3.5 µm (n=20). It is logical that regarding de double equilibrium position, the distance in the x-direction would be half. Figure 6.6 B shows the alignment of 10 µm beads in chip 3 at 30 µl/min,

resulting in only one equilibrium position. The distance between the 10 µm beads was 30.6 ± 2.7 µm.

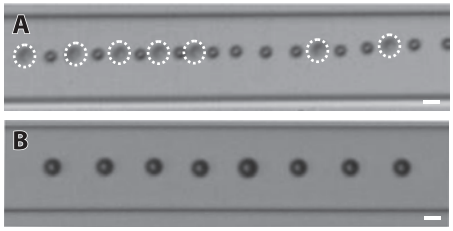

Figure 6.6: Bead ordering in chip 3. A) Alignment of 6 µm beads at two equilibrium positions at a concentration of 1% w/v and a flow rate of 30 µL/min. B) Alignment of 10 µm beads at one equilibrium position at a concentration of 1% w/v and a flow rate of 30 µL/min. Scale bars are 10 µm.

Double equilibrium position

In our experiments, both observations, in chip 2 and 3, regarding the double equilibrium positions were unrelated to flow rate. Equation 6.6 defines the influence of the particle diameter on the number of equilibrium position. Figure 6.6 A and B show the effect of an increase from 6 µm to 10 µm beads in chip 3. The double equilibrium position was shown with 6 µm beads but not with 10 µm beads. This is in correspondence with equation 6.6. Increasing the particle diameter decreases *m*, the number of equilibrium positions. It has to be kept in mind that this equation applies for straight channels, its use in curved channels is unknown. Using equation 6.6, the calculated equilibrium position value (*m*) for 6 µm particles, in a 50 µm x 48 µm curved microchannel, using a volume fraction of 1% and a longitudinal distance between the particles at the similar side of the channel of 20.3 µm is 4.3. This indicates multiple equilibrium positions. *m* has a value of 1.4 for 10 µm particles in the same curved microchannel at similar volume fraction and a *l* of 30.6 µm. The obtained data suggests that equation 6.6 also applies for curved microchannels. However, in chip 2 there are simultaneously single and double equilibrium positions with a *m* of 0.75. These obtained results emphasizes the strong effect of (local) particle concentration on the equilibrium position.

Finally, it has been suggested by di Carlo et al.[20, 25-27] that an inertial force ratio, $R_f = ap^2 \cdot R/H^3$, in which H is the smallest dimension of the curved microchannel, is useful in predicting particle behavior[19]. Here, R_f describes the order of magnitude scaling between F_L and F_D. It was proposed that equilibrium positions can be modified by the secondary flow at intermediate $R_f > 0.04$[20,26]. For chip 2, with 10 µm beads, R_f is 9.6. Additionally, for chip 3 with 6 µm or 10 µm beads, Rf is 0.48 and 1.35 respectively. According to di Carlo et al.[25] this could lead to interesting new ordering modes, as shown in figure 6.5 B and 6.6 A, for a continuous curved microchannel.

Although R_f provides a parameter to help simplify the use and understanding of the ordering modes (F_L vs F_D), the exact mechanism and location of interactions between secondary flow and lift effects is complex and unknown experimentally and theoretically. The observed second equilibrium positions in the z-direction in our

devices, has been reported before by Russom[24]. They also agree that the interaction of secondary and lift forces across the channel is of importance, but the functional form of magnitude change is not known.

However, our results do support the speculations by Di Carlo et al.[25] about the existence of the combined behavior of F_L and F_D (figure 6.7). In this review, the existence of two different equilibrium positions in symmetrical curved microchannels (figure 6.7) were discussed. In our experiments we have two different situations to discuss. Firstly, an a-symmetrical curved microchannel (chip 2: 50 x 25 µm) and secondly, a symmetrical curved microchannel (chip 3: 50 x 48 µm).

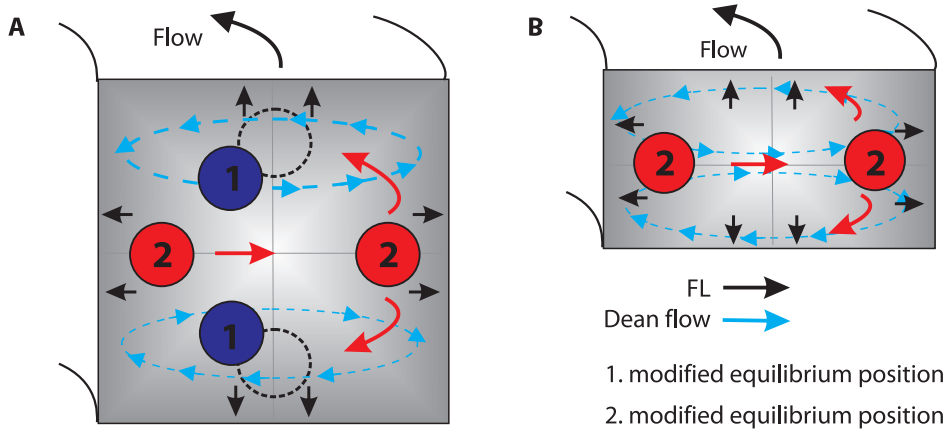

Figure 6.7: Schematic representation of the lift force, FL (black) and Dean flow (blue) in curved channels. Presumed stable and unstable equilibrium positions are indicated. Stable focusing positions in straight channels are shown as red solid circles and black dashed circles. Modified from[25].

Based on the theory presented by di Carlo we think modified equilibrium positions arise, as shown in figure 6.7 A and B. In the symmetrical chip 3 (figure 6.6) modified stable equilibrium positions at number 1 are shown. These equilibrium positions are biased in chip 2, by the decreased channel height and resulting in the equilibrium positions at number 2 (figure 6.5B) at both sides of the channel wall. It is suggested by di Carlo et all that the equilibrium position at number 1 are more stable compared to position 2. This would correlate with the observation in chip 2, where the stable positions (1) are biased by both, the decreased channel height and larger particle dimension (10 µm vs 6 µm), resulting in the move to less stable equilibrium positions (2) at both sides of the channel walls.

Furthermore, 10 µm particles show also a modified single equilibrium position towards the middle of the channel in chip 3 (figure 6.6 B), also suggesting modified single equilibrium position of number 1 in figure 6.7. As we would expect the particles to align at the channel wall. Moreover, increasing particle diameter would move the particles towards the channel wall, since the effect of particle diameter is a third power

larger in the F_L than in F_D (equation 6.4 and 6.5). To gain more insight in these new ordering modes, one should study the ordering behavior using different combinations of particle and channel dimension.

Overall, we suggest that both the particle concentration and R_f (channel dimension and particle diameter) are the important parameters modifying and influencing the equilibrium positions in the continuous curved microchannel.

Lower limit of particle ordering

The lower limit of the particle diameter which can still be ordered was determined in various chip designs (table 6.2). To achieve ordering of particles in the range of 1-3 µm, we used curved channels with varying channel widths and channel heights. Table 6.2 shows how the flow rate (U_f) and the channel dimensions influence the Reynolds number (Re), the Reynolds particle number (Re_p), the Dean number (De), and the apparent Dean (F_D) and lift forces (F_L) using 2 µm and 3 µm beads.

Table 6.2: Summary of the Dean force (F_D), lift force (F_L) and Re_p acting on 2 or 3 µm bead for varying Dean numbers

w x h (µm)	10 x 10	10 x 20	25 x 10	25 x 29
R (µm)	1500			
a_p (µm)	2	2	3	3
U_f (µL/min)	6.7	8	6.7	10
Re	11.2	8.88	6.4	6.17
Re_p	0.44	0.2	0.28	0.08
De	0.64	0.59	0.44	0.58
F_L (N)	4×10^{-10}	4.05×10^{-10}	3.13×10^{-11}	1.19×10^{-11}
F_D (N)	1.66×10^{-12}	2.17×10^{-12}	8.9×10^{-13}	2.12×10^{-12}

The Dean and lift forces were calculated using equations 6.2-5 and accordingly were sufficient for particle ordering. We used 1-2-3 µm beads in the devices with varying channel height and width of 10 µm, as described in table 6.2. No ordering occurred in any of the combinations regarding chip design and particle diameters. Figure 6.8 shows three examples of the absence of ordering. We also tried to order 5 µm beads in the device of 25 µm width and 29 µm height, however no ordering occurred. For ordering, the lower limit particle diameter is 6 µm.

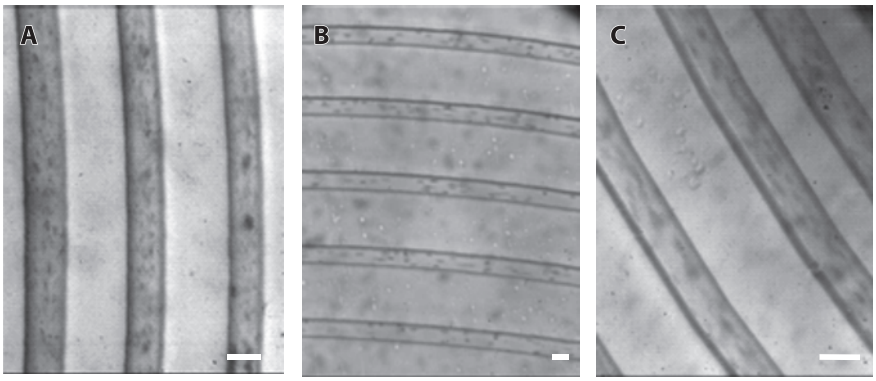

Figure 6.8: 1, 2 and 3 µm beads in curved microchannels. A) 1 µm beads 0.8% w/v at a flow rate of 6.7 µl/min. Channel width 10 µm x height 10 µm. Scale bar 10 µm. B) 2 µm beads 0.8% w/v at a flowrate of 6.7 µl/min. Channel width 10 µm x height 20 µm . Scale bar 10 µm. C) 3 µm beads 1% w/v at a flowrate of 10 µl/min. Channel height of 25 µm x height 29 µm. Scale bar 25 µm.

Even though the F_L was sufficiently higher than F_D, particle ordering did not occur. These results emphasize that there are more important factors playing a role, as mentioned before. The *Ap/Dh* ratio is sufficient, however, the Reynolds particle number is not approaching 1 and the Dean number is also low. Furthermore, another key factor is the volume fraction. This volume fraction is very important regarding the ordering capability of the device. When the volume fraction is too high, ordering cannot be expected due to steric interactions between particles [25]. In the described experiments volume fractions of 0.1-1% were used. However, when the diameter of the particle decreases, more diluted suspensions (~0.1%) should be used. This is true in straight channels[25], it is therefore not guaranteed that a similar relation exist for curved channels. However, it could be the reason why ordering small beads in these experiments did not work.

Overall, in this section, we presented the bead ordering capacity of the curved microchannel devices with varying widths and heights. Moreover, we discussed the behavior of these beads and their individual equilibrium positions in the microchannels.

The best results for ordering particles of 6 µm, similar size to B-cells, was achieved using a curved microchannel with a channel width of 25 µm and height of 25 µm. However, particles ≥ 10 µm could not be ordered using this device. For ordering cells with a diameter of 10 µm, the curved microchannel with a channel width of 50 µm and a height of 25 µm needs to be used. This showed the best results regarding 10 µm bead ordering. Using chip 3 with the increased channel height increases the droplets size, which is therefore not of interest.

Up till now we only showed the ordering capacity of the curved microchannels for beads. The next paragraph is focused on cell ordering, followed by single cell encapsulation. The essential part is to utilize the cell ordering for efficient single cell encapsulation. By matching the periodicity of the cell flow with the droplet generation,

we ought to increase the efficiency of single cell encapsulation. This deterministic encapsulation method reduces the number of empty and multi-cell droplets, while increasing the number of droplets containing single cells.

6.4.2 Characterization of the microfluidic chip - cell ordering

The curved microchannels for the cell-based experiments are 50 µm wide and 29 µm high, with 100 µm spacing between two successive loops. The initial radius of the spiral is 1500 µm and the total length is 7.2 cm. Three different types of droplet generators were tested, referred to as type A-C.

Table 6.3 shows how the flow rate (U_f) and the channel dimensions influence the Reynolds number (Re), the Reynolds particle number (Re_p), the Dean number (De), and the apparent Dean (F_D) and lift forces (F_L).

Table 6.3: Summary of the Dean force (F_D), lift force (F_L) and Re_p acting on 13 µm cells for varying Dean numbers.

w x h (µm)	**50 x 29 (µm)**		
R (µm)	1500		
a_p (µm)	13		
U_f (µL/min)	10	15	20
Re	4.2	6.3	8.4
Re_p	0.53	0.79	1.06
De	0.46	0.7	0.93
F_L (N)	5.6×10^{-10}	1.3×10^{-9}	2.2×10^{-9}
F_D (N)	6.4×10^{-12}	1.2×10^{-11}	2×10^{-11}

The Dean forces acting on the 13 µm cells at the three flow rates are less than the corresponding lift forces. Thus, the lift forces dominate, which predicts that ordering will occur and the cells will focus along the one equilibrium position at the inner wall, as previously illustrated in figure 6.3.

Cell ordering

Cell ordering was observed in the continuous curved microchannel, when flow rates approached 15 µL/min or higher. The observed cell ordering is classified as two types of self-organization. Firstly, cells were focused in one streamline along the inner wall (figure 6.9). Secondly, cells were arranged in an array that alternated in the x-y direction (figure 6.9). These self-organization patterns shared three distinctive characteristics with cell ordering in straight microchannels[10, 20]: (1) cells moved as a group in the direction of the flow, (2) cells were separated from their nearest neighbor by an uniform spacing, and (3) cells were always found near a channel wall.

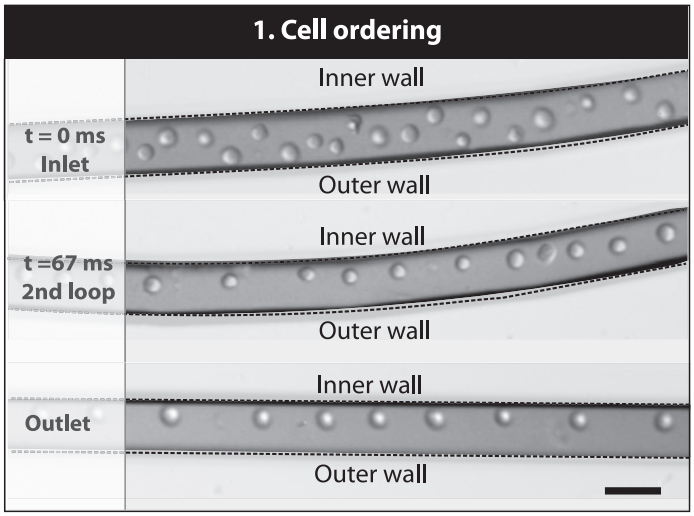

Figure 6.9: Pictures of cell ordering in the curved microchannel. Scale bar is 50 µm.

Cell ordering was observed, in the second loop in the direction of the flow (longitudinal), after 9400 µm, corresponding to 67 ms, at a flow rate of 15 µL/min as shown in figure 6.9. Thus, curved microchannels cause faster ordering to a predicted equilibrium position than straight microchannels[20]. To support this, we also performed experiments regarding cell ordering in straight microchannels with similar dimensions. Then cell ordering was observed after several cm. Cell ordering was demonstrated at flow rates over 30 µL/min. However, clogging occurred regularly. This disturbed or even stopped the flow and therefore negatively influenced the ordering capacity of the straight microchannel.

The observed channel length required for ordering in a curved microchannel is ~0.9 cm. The channel length, required for all the particles to travel to an equilibrium position at the inside of the microchannel wall is described by different formulas in literature. One presented by Di Carlo et al.[25] results in a required length of 0.6 cm. Nevertheless, when using a formula presented by Bhagat et al[30]. the required length would be 8.6 cm. Indicating that the required length is difficult to predict using the available formulas. It could give an indication when creating the chip design to ensure that the channel length is sufficient. A short channel length required for ordering offers a critical advantage because fluidic resistance decreases and hence, the pressure and power required to drive the flow decreases. In fact, it seems that fluidic resistance is the limiting factor for increasing the throughput of ordering, because high pressure leads to leakage at fluid inlets[18]. Therefore, our system is more practical for single cell encapsulation compared to straight channels devices**.** Additionally, channel clogging hardly occurred in the device, making the system more compact for particle ordering compared to the necessary several cm's in a straight channel.

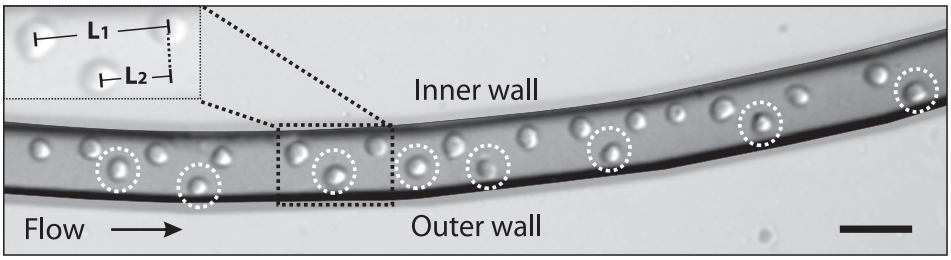

Figure 6.10: Double equilibrium position of HL60 cells observed in the focal plane, in the second loop of the curved microchannel. Insert showing the longitudinal distance measurement L1 for cells at the single equilibrium position at the inner wall and L2 for the longitudinal distance of cells in the alternating pattern. Scale bar is 50 µm.

The longitudinal distance, between adjacent cells on the same side of the channel (figure 6.10, insert L_1), at flow rates of 15 µL/min was 52 ± 6 µm (n=20). This flow rate corresponded to velocities of 14 ± 0.4 cm/s. Furthermore, figure 6.11 shows that when the flow rate increased from 15 to 50 µL/min (Re_p= 0.8-2.7), the longitudinal distance was not significantly influenced. This is mainly due to the large standard deviations in longitudinal distance between cells. The longitudinal distance for cells varied from 39 to 52 µm, corresponding to ~3-4 times the cell diameter (13 ± 1.6 µm HL60 cells (n=25) and 13.8 ± 2.2 µm K562 (n=25) cells). This observation has not been reported for a continuously symmetrically curved microchannel. For comparison, as stated previously, we also determined the longitudinal distance (L1) of 10 µm beads at different flow rates. The average longitudinal distance between beads was lower than that between cells as shown in figure 6.11; however this decrease is not significant. Moreover, the standard deviation of the distance between beads was lower than that between cells. One possible explanation is that the coefficient of variation of the cell diameter (CV) for both HL60 and K562 cells is higher (n=25, CV 13% and 16%) compared to that of the bead diameter (n=25, CV 10%).

Cell ordering into an alternating pattern, across the channel, was observed in the focal plane of the second loop at 15 µL/min. Hence, the longitudinal distance between cells was reduced to 28.3 ± 3.3 µm (n=20) (figure 6.10 insert L_2). Here, the velocity is similar to that used to obtain the one equilibrium position.

One of the key factors causing the double equilibrium position in the continuous curved microchannel was the volume fraction of the suspended cells. When the volume fraction reached 2.2%, an increasing number of double equilibrium positions was observed (m=1.4 vs m=1.1 with 1.7%), suggesting a similar relationship for curved microchannels as for straight microchannels as previously described in equation 6.6 and in section 6.4.2 for bead ordering. Hence, the volume fraction provides increased control regarding a single or double equilibrium position, whereas in straight channels there is always a minimum of two equilibrium positions. Furthermore, the longitudinal spacing (L1) between cells remains unaffected when changing the volume fraction between 1.7–2.2%. Additionally, due to cell-cell interactions, increasing the volume fraction above

2.2% decreases the distance between cells. However, no ordering occurs at that point. Moreover, increasing the flow rate from 15 to 50 µl/min did not influence the double equilibrium position. Finally, as extensively discussed in section 6.4.2, an intermediate R_f (R_f=10.4) could lead to interesting new ordering modes, as shown here, for a continuous curved microchannel. However, we still lack a complete explanation of why this geometry, in combination with specific volume fractions of cells, caused the single equilibrium position of cells in continuous curved microchannels to shift to two equilibrium positions. To conclude, the single equilibrium position is most stable and prominent during experiments when using the appropriate volume fraction of cells (1.7%) and flow rate (15 µL/min) in a chip of 50 x 29 µm.

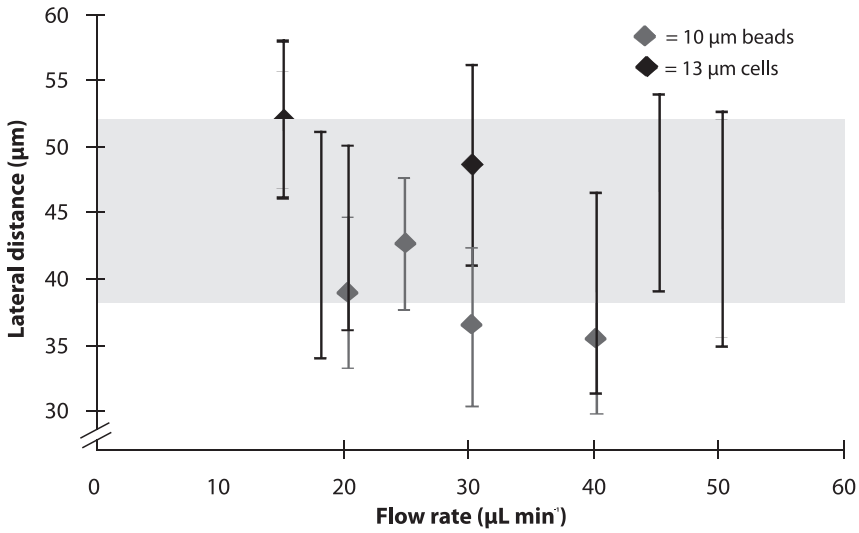

Figure 6.11: Longitudinal distance between cells (HL60) at different flow rates and 10 µm beads (± SD) (n=25).

Overall, this microfluidic device was capable of ordering beads and cells with dimensions down to 6 µm, demonstrating a dynamic range, which has not been shown in straight channels[10, 18]. Moreover, no difference in ordering capability between the two different cell types was observed.

6.4.3 Cell encapsulation

The curved microchannel presented here generates a cell train with a precise longitudinal spacing. The longitudinal distance and the corresponding velocity at one equilibrium position resulted in a cell frequency of 2700 cells/s. This is critical for controlled loading of single cells into droplets. To demonstrate this, we analyzed the use of three different flow-focusing geometries (table 6.4) for emulsifying concentrated suspensions of HL60 or K562 cells, immediately after they passed through the curved microchannel.

Table 6.4: Overview of the droplet generator type A-C and the corresponding values of droplet frequency (kHz) and volume (pL) observed for the flow rate range of interest (cells 15 µL/min; oil 30-43 µL/min). Scale bars are 50 µm.

	requency (kHz)	Volume (pL)
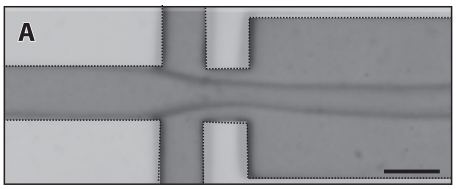	No droplet formation	x
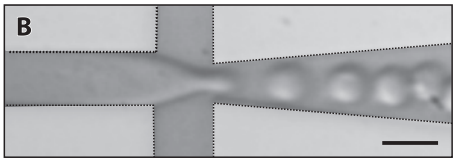	>18	<24
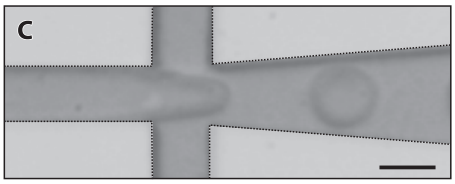	2.1-2.75	73-99

Type A, a regular junction, showed no droplet formation at the flow rates of interest. The second design, type B, generated droplets at 18 kHz or higher, which was too high compared to the cell frequency (2700 cells/s). Type C generated 73-99 pL droplets between 2.1-2.75 kHz. Hence, encapsulation experiments were performed with type C.

To ensure that the droplets contained only single cells , we adjusted the oil flow to generate droplets with a frequency comparable to, or higher than, the frequency of the cells. Thus, the oil flow rate was set at 43 µL/ min and generated 73 pL droplets at 2.7 kHz (figure 6.12).

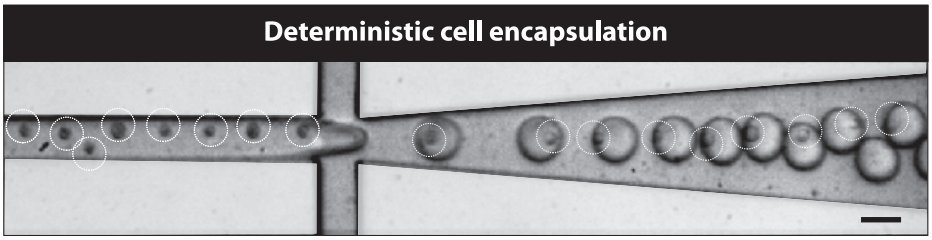

Figure 6.12: Deterministic cell encapsulation. showing simultaneous efficient single cell alignment and encapsulation.

We compared the cell encapsulation efficiency in our device with that determined by the Poisson distribution equation 6.1 in figure 6.13. The percentage of droplets containing single cells was significantly increased using the curved microchannel for cell ordering. The efficiency of encapsulating single cells approached 80%; the percentage of droplets containing multiple or no cells remained low. A Poisson distribution yielded a similar percentage of droplets containing multiple cells, but far more empty droplets. The efficiency of producing droplets with single cells using a Poisson distribution was around 37%. From these results, using curved microchannels leads to over a 100% increase in single cell encapsulation.

The cell volume fraction (1.7%) is an important factor controlling the efficiency of single cell encapsulation. Long empty spaces between the cells are undesirable, requiring values greater than 1.5% in this device. By contrast, when the volume fraction is greater than 2%, cell ordering is disturbed due to cell-cell contact and double equilibrium positions. This can be compensated to some extent by adjusting the droplet frequency. The optimal volume fraction in our experiments corresponds to $\lambda=1.1$, which may explain the percentage of droplets containing two cells. However, decreasing λ results in an increased percentage of empty droplets.

Finally, the viability of the encapsulated cells was assessed. The cells were stained with calcein AM and propidium iodide to determine cell viability and membrane integrity after encapsulation. Results showed that 92% of the cells retained their membrane integrity, compared with 97% in control samples.

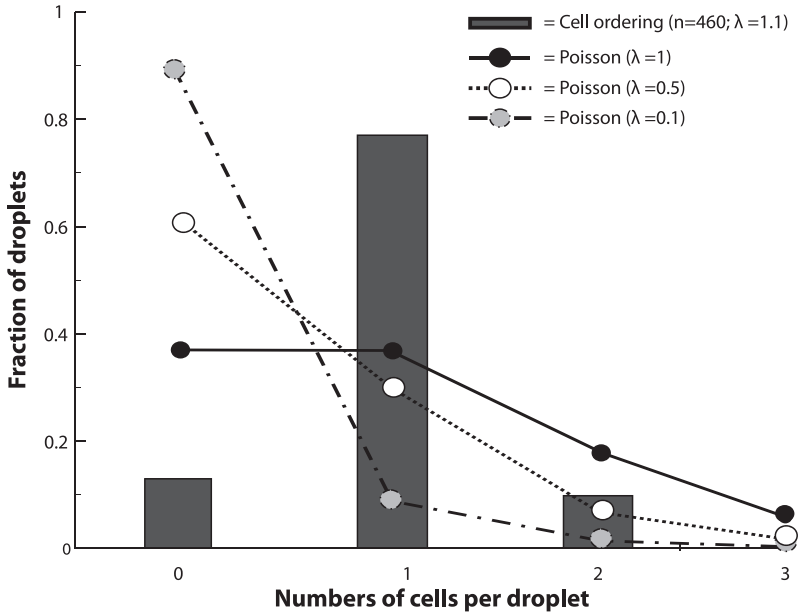

Figure 6.13: Deterministic cell encapsulation showing cell ordering vs. Poisson distributed cell encapsulation.

The device presented here is able to generate up to 80% single cell containing droplets. In addition, when using the curved microchannel the ratio between droplets containing one and two cells is 8:1. To establish this ratio with a Poisson distribution, the cell suspension would have to be diluted to a λ of 0.25, which would lead to less than 20% of the droplets containing single cells (a decrease of nearly a factor of four).

6.5 Conclusion

In this chapter, we presented a microfluidic device with a curved microchannel which is capable of cell ordering based on Dean coupled inertial ordering. Calculations were performed to characterize and understand the forces influencing the bead and cell ordering in this curved microchannel.

Firstly, bead ordering was studied experimentally to gain insight in the ordering capacity of the curved microchannels with different dimensions. Next, cell ordering was studied experimentally and two equilibrium positions were observed after traveling through the curved microchannel for less than 1 cm. The observation of double equilibrium positions, in both the bead and cell experiments, was profoundly discussed in detail. Subsequently, single cell encapsulation was successfully demonstrated by achieving single cell encapsulation efficiencies approaching 80%, while multiple and empty droplets remained low. Furthermore, cell viability was maintained (92%).

This microfluidic chip can perform efficient encapsulation of single cells on a relatively small device footprint (~0.4 cm^2), which offers easy integration in droplet-based microfluidic LOCs. Moreover, the short ordering distance decreases fluidic

resistance and, thus, lowers the required pressure and power to drive the flow. Additionally, the microfluidic design is versatile and capable of ordering beads and cells over a wide dynamic range (6-13 µm), which has not been shown in straight channels[10, 18]. Thus, the presented device can contribute to a variety of biomedical or manufacturing applications that involve rapid, low-cost and continuous encapsulation of single cells.

Due to the large standard deviation in the longitudinal spacing between cells, it not possible to obtain 100% encapsulation efficiency of single cells using this approach. This can be corrected by coupling this device to an integrated impedance analyzer. Therefore, the next chapter focuses on the label-free, electrical detection of cells in droplets for sorting purposes.

6.6 References

1. Teh, S.Y., et al., *Droplet microfluidics.* Lab Chip, 2008. **8**(2): p. 198-220.
2. Wheeler, A.R., et al., *Digital microfluidics for cell-based assays.* Lab on a Chip, 2008. **8**(4): p. 519-526.
3. Whitesides, G.M., *The origins and the future of microfluidics.* Nature, 2006. **442**(7101): p. 368-73.
4. Gelinck, G., et al., *Charge transport in high-performance ink-jet printed single-droplet organic transistors based on a silylethynyl substituted pentacene/insulating polymer blend.* Organic Electronics, 2011. **12**(8): p. 1319-1327.
5. Chao, S.H., et al., *Real-time PCR of single bacterial cells on an array of adhering droplets.* Lab on a Chip, 2011. **11**(13): p. 2276-2281.
6. Wheeler, A.R., et al., *Digital microfluidics with in-line sample purification for proteomics analyses with MALDI-MS.* Anal Chem, 2005. **77**(2): p. 534-40.
7. Koltay, P., et al., *Inkjet-like printing of single-cells.* Lab on a Chip, 2011. **11**(14): p. 2447-2454.
8. Whitesides, G.M. and *What comes next?* Lab Chip 2011. **11**(2): p. 191-193.
9. Clausell-Tormos, J., et al., *Droplet-based microfluidic platforms for the encapsulation and screening of Mammalian cells and multicellular organisms.* Chem Biol, 2008. **15**(5): p. 427-37.
10. Edd, J.F., et al., *Controlled encapsulation of single-cells into monodisperse picolitre drops.* Lab on a Chip, 2008. **8**(8): p. 1262-1264.
11. Koster, S., et al., *Drop-based microfluidic devices for encapsulation of single cells.* Lab Chip, 2008. **8**(7): p. 1110-5.
12. Um, E., S.G. Lee, and J.K. Park, *Random breakup of microdroplets for single-cell encapsulation.* Applied physics letters, 2010. **97**(15).
13. Courtois, F., et al., *Controlling the retention of small molecules in emulsion microdroplets for use in cell-based assays.* Anal Chem, 2009. **81**(8): p. 3008-16.
14. Papoulis, A., *Estimation of Average Density of a Nonuniform Poisson Process.* Ieee Transactions on Communications, 1974. **Co22**(2): p. 162-167.

15. Joensson, H.N., et al., *Detection and analysis of low-abundance cell-surface biomarkers using enzymatic amplification in microfluidic droplets.* Angew Chem Int Ed Engl, 2009. **48**(14): p. 2518-21.
16. He, M.Y., et al., *Selective encapsulation of single cells and subcellular organelles into picoliter- and femtoliter-volume droplets.* Analytical Chemistry, 2005. **77**(6): p. 1539-1544.
17. Chabert, M. and J.L. Viovy, *Microfluidic high-throughput encapsulation and hydrodynamic self-sorting of single cells.* Proc Natl Acad Sci U S A, 2008. **105**(9): p. 3191-6.
18. Lin, R., J.L. Prieto, J.S. Fisher, A.P.Lee, *high efficiency cell encapsulation utilizing novel on-demand droplet generation scheme and impedance-based detection*, in *14th international conference on miniaturized systems for chemistry and life sciences* H.A.-S. S. Verpoorte, J. Emineus, N. Pamme, Editor. 2010: Groningen, The Netherlands. p. 2135-2137.
19. Berger, S.A., L. Talbot, and L.S. Yao, *Flow in Curved Pipes.* Annual Review of Fluid Mechanics, 1983. **15**: p. 461-512.
20. Gossett, D.R. and D. Di Carlo, *Particle focusing mechanisms in curving confined flows.* Anal Chem, 2009. **81**(20): p. 8459-65.
21. Bhagat, A.A.S., S.S. Kuntaegowdanahalli, and I. Papautsky, *Inertial microfluidics for continious particle filtration and extraction.* microfluid Nanofluid, 2009. **7**(2): p. 217-226.
22. Di Carlo, D., et al., *Equilibrium separation and filtration of particles using differential inertial focusing.* Analytical Chemistry, 2008. **80**(6): p. 2204-2211.
23. Kuntaegowdanahalli, S.S., et al., *Inertial microfluidics for continuous particle separation in spiral microchannels.* Lab Chip, 2009. **9**(20): p. 2973-80.
24. Russom, A., et al., *Differential inertial focusing of particles in curved low-aspect-ratio microchannels.* New J Phys, 2009. **11**: p. 75025.
25. Di Carlo, D., *Inertial microfluidics.* Lab Chip, 2009. **9**(21): p. 3038-46.
26. Di Carlo, D., et al., *continious inertial focusing, ordering and seperation of particles in microchannels.* Proc Natl Acad Sci U S A, 2007. **104**(48): p. 18892-7.
27. Di Carlo, D., et al., *Particle segregation and dynamics in confined flows.* Phys Rev Lett, 2009. **102**(9).
28. Humphry, K.J., et al., *Axial and lateral particle ordering in finite Reynolds number channel flows.* Physics of Fluids, 2010. **22**(8).
29. Ookawara, S., D. Street, and K. Ogawa, *Numerical study on development of particle concentration profiles in a curved microchannel.* Chemical Engineering Science, 2006. **61**(11): p. 3714-3724.
30. Bhagat, A.A., S.S. kuntaegowdanahalli, and I. Papautsky, *continuous particle seperation in spiral microchannels using Dean flows and differential migration.* Lab Chip, 2008. **8**(11): p. 1906-1914.

31. Ookawara, S., et al., *Feasibility study on concentration of slurry and classification of contained particles by microchannel*. Chemical Engineering Journal, 2004. **101**(1-3): p. 171-178.
32. Bhagat, A.A., et al., *Inertial microfluidics for sheath-less high-throughput flow cytometry*. Biomed Microdevices, 2010. **12**(2): p. 187-95.

LABEL-FREE, HIGH-THROUGHPUT ELECTRICAL DETECTION OF CELLS IN DROPLETS*

CHAPTER 7

The previous chapter showed a new efficient high-throughput single cell encapsulation method using a curved channel. However, it was not possible to obtain 100% encapsulation efficiency of single cells using this approach. This stimulates the need for sorting droplets of interest. Conventionally, this involves cell labeling, which is labourious and not suitable for long-term culture. Hence, label-free detection of cells in droplets is desired. Till now, no label-free, integrated single cell detection method in droplets is available. In this chapter, a microfluidic set-up for fast (>100Hz), novel and label-free impedance-based detection of cells in droplets is presented. At a measurement frequency of 100 kHz, we demonstrated that the presence of a viable cell in a droplet decreased the electrical impedance. Additionally, no impedance change was detected when empty droplets or droplets containing non-viable cells passed the electrode pair. Therefore, droplets containing viable cells can be discriminated from empty droplets, as well as droplets containing non-viable cells. These results provide us with a valuable method to label-free detect and select (viable) cells in droplets.

*modified from: E. Kemna, F. Wolbers, I. Vermes, A. van den Berg. Analyst, 2013, 138 (16), 4585 - 4592

7.1 Introduction

Analysing single cells and perform biological studies on a single cell basis is of increasing interest[1,2]. Droplet-based microfluidics has become a standard platform for high-throughput single cell experimentation and analysis[3,4,5]. However, till now, label-free characterization and identification of cells in droplets, which is of great importance for cell analysis in droplets and selecting the droplets of interest, has not been demonstrated.

Single cell encapsulation has developed into an integral part in droplet microfluidics. Therefore, deterministic encapsulation of single cells in droplets receives growing interest. We have demonstrated high-yield (77%) and high-speed (2700 cells/s) single cell in droplet encapsulation using Dean-coupled inertial ordering in a simple curved continuous microchannel[6] (chapter 6). However, 100% efficiency was not obtained, and is difficult to reach due to the significant standard deviation in the longitudinal spacing between the cells. This inefficiency has stimulated us to develop a label-free method, using impedance, for the downstream selection of single cell containing droplets, to finally obtain 100% efficiency. Microfluidic impedance measurements are used to assess the dielectric properties of single cells passing an integrated electrode pair in a microchannel[7]. Since the dielectric properties of cells are frequency dependent, information about several cell characteristics can be obtained with electrical impedance measurements at different frequencies (impedance spectroscopy)[8, 9]. Furthermore, since no cell labelling is required, the use of external optical equipment is avoided [10].

Although fluorescent labelling permits molecular-level detection, this technique is expensive, laborious and time consuming. Moreover, fluorescence detection is not easily integrated on chip[11]. Label-free on-demand impedance based cell encapsulation has been demonstrated by Lin et al., but with relatively low throughput (10 Hz) and with the need to use valves[12]. Additionally, a droplet platform for cell detection in droplets has never been used[13 14].

Here a fast, novel and label-free impedance based approach to detect cells in droplets is presented. A microfluidic glass-PDMS device is developed, consisting of two main components – the droplet generator and the impedance sensor. The droplet generator has a flow focusing structure for stable droplet generation and cell encapsulation. The impedance sensor comprises two planar electrodes, patterned on glass, positioned in the main channel. In this chapter, we demonstrate the differentiation between empty and cell encapsulated droplets, with the use of electrical impedance measurements at a single frequency.

Firstly, the chip design and the measurement set-up is described with a theoretical explanation. Secondly, the impedance spectra of single cells (viable vs. non-viable), empty droplets and cell-containing droplets are shown, in either conducting (PBS) or isoosmolar low-conducting (LC) buffer. We demonstrate that low conducting droplets encapsulating viable cells can be discriminated from empty droplets or droplets with

non-viable cells, using high-speed impedance measurement analysis. To validate the impedance measurements, simultaneous high-speed camera recordings were taken of each measurement to ensure cells were actually encapsulated and compared with the electrical signal.

7.2 Materials and methods

7.2.1 Chip design

The microfluidic chip consists of two main components – the droplet generator, with one inlet for the cell suspension and one inlet for the oil, and the impedance sensor. The droplet generator has a flow focusing junction with a width of 30 or 40 µm and a focus-width of 25µm. Hence, the main channel is 30 or 40 µm wide. The impedance sensor comprises two planar platinum (Pt) electrodes with a width of 20 µm and an inter-electrode distance of 30 µm patterned on glass. The total chip depth is 26 µm.

A silicon master design was drawn in Clewin (version 4.0.1) and fabricated using standard UV-lithography. SU-8 2-25 (Microchem, Berlin, Germany) was spun on the silicon master with a thickness of 26 µm. The chip was made in PDMS (Sylgard 184, Dow Corning, Midland, MI, USA). Curing and base agent were mixed at a ratio of 1:10 and degassed. PDMS was poured onto a silicon wafer, degassed, and cured at 60°C for 24 hours. After curing, in- and outlets were punched using a dispensing tip (Nordson EFD, Maastricht, the Netherlands, ID 1.36 mm and OD 1.65 mm). Subsequently, the PDMS chip was sealed to a Pyrex glass slide with the patterned Pt electrodes using oxygen plasma (Harrick PDC-001, NY, USA). After sealing, the chip was placed at 60°C for a minimum of 30 minutes.

7.2.2 Materials

Isoosmolar low conducting (LC), based on Steenbakkers et al.[15], buffer consisted of deionized water, supplemented with 280 mM inositol (Sigma, St. Louis, USA), 0.1 mM calcium acetate (Sigma), 0.5 mM magnesium acetate (Sigma) and 1 mM l-histidine (Sigma,). The conductivity was adjusted, using deionized water, to 0.009 S m^{-1}. For the continuous phase, hexadecane (Sigma) with 1% Span80 (Sigma) was used. Polystyrene beads (Thermo scientific, Breda, The Netherlands) with a diameter of 11 µm were used in control experiments.

7.2.3 Cell culture

The mouse myeloma cell line NS-1 was a kind donation from ModiQuest, The Netherlands. Cells were grown in DMEM/F12 medium (Invitrogen, Grand Island, NY, USA), supplemented with 10% (v/v) fetal bovine serum (FBS; Invitrogen), 100 U ml^{-1} penicillin (Invitrogen), 2 mM L-glutamine (Invitrogen) (= $DMEM^{+}$ medium). Cell cultures

were sustained in a 5% CO_2 humidified atmosphere at 37°C. NS-1 cells were split every 3-4 days at a ratio of 1:10. In the experiments, cells were suspended in PBS or LC buffer at the desired concentration prior to use. To induce cell death, NS-1 cells were put at 56°C in LC buffer for 30 minutes. After washing and resuspension in LC buffer, viability was checked in an aliquot of the sample using propidium iodide (PI) (Sigma) at a final concentration of 10 µg ml^{-1} and Calcein AM (Sigma) at a final concentration of 2.5 µM.

7.2.4 Experimental set-up

The cell suspension and the oil were separately introduced into the microfluidic chip using two glass Hamilton syringes (Sigma), and connected to the two inlets with PEEK tubing (Vici, Schenkon, Switzerland, ID 0.5 mm and OD 1.59 mm). PEEK tubing was also connected to the outlet of the device and routed into a collection tube. Flow was driven at a constant volume rate by a syringe pump (neMESYS dosing units, Cetoni GmbH, Germany). A magnetic stir bar was inserted to the syringe containing the cell suspension, to prevent suspension settling during injection.

When conducting measurements on empty droplets only, flowrates of 0.15-0.5 µL min^{-1} for water and 1.8-8 µL min^{-1} for the continuous phase, where used. The droplets where generated ranging from 20-475 Hz at a frame rate of 3000 fps.
Secondly, for experimentation regarding cell containing droplets, the flow rate of the continuous phase varied between 0.2-2 µL min^{-1}. The aqueous flow rate, containing the cells, varied between 0.05-1 µL min^{-1} and the frame rate was set to 125-500 fps, to be able to increase the recording time

The microfluidic chip was mounted on a X-Y-Z translation stage of an inverted wide fluorescence microscope (Leica DM IRM, Leica Microsystems, Wetzlar, GmbH, Germany). Illumination was supplied by a fiber optic illuminator (Leica KL 1500 LCD). A computer-controlled high-speed camera (Photron SA-3, West Wycombe, United Kingdom), with accompanied Photron software (Photron Fastcam Viewer), was used for image recording of droplets passing the electrode pair. All videos and images captured were analyzed with the image-processing program ImageJ (National Institute of Health, MD, USA) and compared with the obtained electrical signal.

7.2.5 System overview

The electrodes on the glass slide of the chip were connected to a printed circuit board using wire bonding, enabling a stable electrical connection.

A frequency sweep of the chip was performed such that the influence of the different components of the equivalent circuit were identified at frequencies ranging from 1000 Hz to 40 MHz. Using an impedance/gain phase analyser (Hewlard Packard 4194A) a bode plot of the chip filled with PBS or LC buffer, with or without (non)viable cells at high concentrations, was generated. During the frequency sweep, flow was induced using different sized droplets on both inlets.

The Zurich impedance system (HF2IS, Zurich instruments). An AC signal of 100 kHz and 6-14 V_{pp} was generated by the Zurich system and transferred to one electrode on the chip. At the other electrode, a home-made current amplifier was placed, to measure the current in order to determine the impedance. This signal was fed back to the Zurich system and captured with a sample frequency of 899-3700 Hz at the laptop. For data analysis to calculate the impedance, Matlab (R2010B, version 7.11.0.854, 2010, the Mathworks Inc) was used. The peaks heights were detected and calculated, with respect to the baseline, such that the drift of the signal did not influence the analysis.

7.2.6 Matlab simulation

A model was used to determine the influence of the viability of the cell, suspended in low conducting buffer, on the frequency behavior of the impedance. Three different situations were modeled: (1) only electrolyte present between the electrodes; (2) a viable cell between the electrodes and; (3) a polystyrene bead between the electrodes. The cell was represented in the model as a single-shell model [16 17 18], while the influence of the suspended bead was calculated using the Maxwell-Wagner theory[16 17 19].

Using Matlab (R2010B, version 7.11.0.854, 2010, the Mathworks Inc), a bode plot of the three different situations were made. The conductivity and permittivity of the low conducting buffer were set to 0.009 S m^{-1} and 80 * ε_0, respectively (ε_0 = 8.854 * 10^{-12} F m^{-1}). Based on the data of Sun and Morgan 2010 [18], the parameters used for the cell were 7.5 µm for the cell radius, $1 \cdot 10^{-8}$ S m^{-1} for the conductivity membrane, 0.4 S m^{-1} for the conductivity cytoplasm, and 5 * ε_0 and 60* ε_0 for the relative permittivity of the cell membrane and cytoplasm, respectively (ε_0 = 8.854 * 10^{-12} F m^{-1}). For the polystyrene beads (radius 5.5 µm) the values were 2.5 * ε_0 and $1 \cdot 10^{-16}$ S m^{-1} for the relative permittivity and conductivity. The membrane thickness was set to 5 nm.

7.3 Results and discussion

7.3.1 Equivalent circuit model and system overview

Electrical impedance spectroscopy measures the AC electrical properties of particles (in suspension) from which the dielectric parameters of the particles can be obtained[18]. Impedance analysis is a widely used method for label-free analysis of cells[13 14].

The chip was connected with the Zurich impedance system (HF2IS, Zurich instruments) using a home-made current amplifier, to measure the current in order to determine the impedance. The setup is shown in figure 7.1.

The chip was glued on a printed circuit board (figure 7.2 A). A simplified equivalent circuit model for three different situations is given in figure 7.1b. In all situations, there are two double layer capacitances (C_{dl}), caused by the electrode-fluid interface, a parasitic capacitance (C_{par}) and a lead resistance (R_{lead}). When a droplet passes the electrode pair the double layer present in the oil changes to a double layer present in

the buffer. Also the R_{oil} is interchanged for R_{drop}, consisting of the used buffer and C_{drop} is added. When the droplet contains a cell, an additional circuit for the cell is implemented. This is represented by the addition of an equivalent circuit model for a cell (capacitance of the cell membrane (C_{mem}) and resistance of the cell interior (R_{cell})).The components of the cell are frequency dependent. Primarily due to the presence of the cell membrane, the cell presents a different impedance measurement when compared to the surrounding fluid. This change is detected by the sensing electrodes and is used to indicate the presence of a cell inside a droplet. The membrane of a cell, suspended in conducting buffer, forms a barrier to the current flow at frequencies below 1-3 MHz. Below these frequencies, the cell can be seen as an insulating sphere, which causes an impedance change depending on the size of the cell[12]. However, for a cell suspended in LC buffer, the frequency at which the current flows through the interior of the cell is lower. For example for a buffer with conductivity of 0.0016 S m^{-1} the frequency is expected around 10 kHz[18].

A typical bode plot of the equivalent circuit model is shown in the down right corner of figure 7.1b. At low frequencies, the spectrum is influenced by the double layer capacitances. A resistive plateau is seen at intermediate frequencies, which is primarily caused by the resistances in the channel due to the buffer, droplet and/or cell. The parasitic capacitance plays a role at higher frequencies.

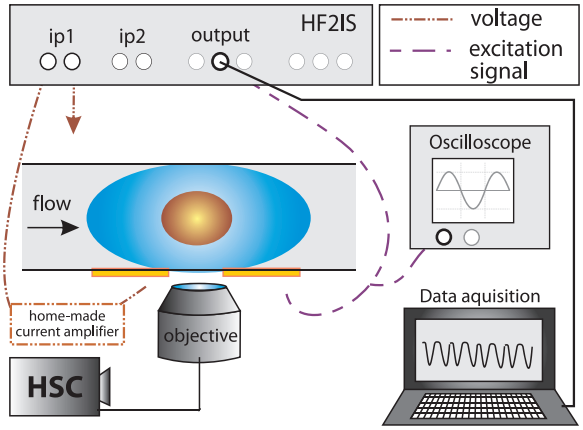

Figure 7.1: A schematic overview of the set-up with the Zurich impedance system (HF2IS). The side view of the channel with a cell containing droplet passing the electrode pair is shown, with connections to the high-speed camera and the home-made current amplifier.

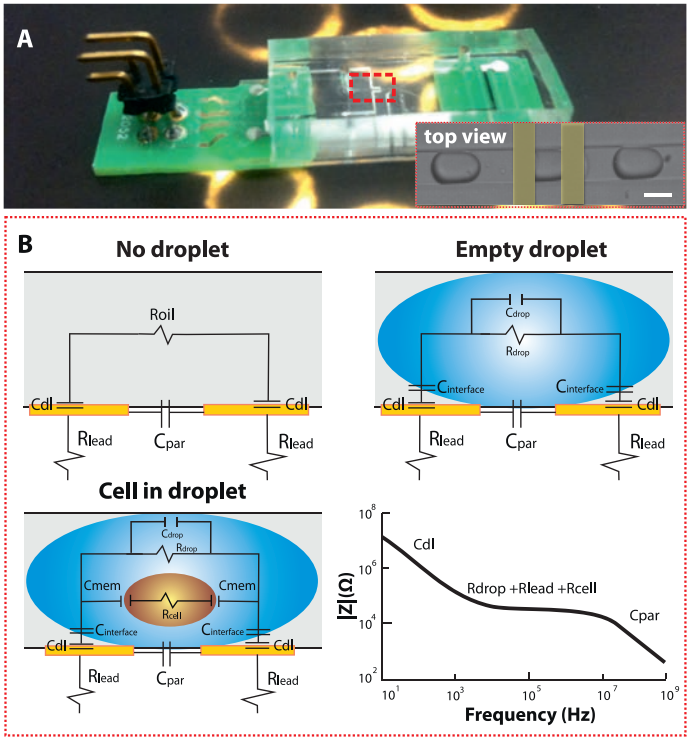

Figure 7.2: A) Photo of the microfluidic device glued on a printed circuit board. Insert shows the impedance sensor. Scale bar is 30 µm. B) Simplified equivalent circuit model of the microfluidic device w/o droplet, or cell in droplet. The interface between the two planar electrodes and the buffer in oil droplet is represented by the double layer capacitance (C_{dl}). R_{drop} is the buffer resistance C_{drop} is the buffer capacitance. R_{lead} the lead resistance and C_{par} is the parasitic capacitance. The schematic bode plot shows a typical frequency response of the electrical impedance of the equivalent circuit model for the situation of a cell containing droplet.

7.3.2 Characterization of the microfluidic device

The frequency behavior of the microfluidic chip with PBS or LC buffer, with and without (non-)viable cells was determined, to ensure that the electrical impedance measurements were performed at a frequency within the resistive plateau. Figure 7.3 A and B shows the averaged results of 50 individual impedance measurements of a chip filled with PBS or LC buffer for frequencies from 1 kHz to 40 MHz. The bode plot for PBS shows a clear influence of the double layer capacitance and parasitic capacitance. The electrolyte resistance is represented in the shaded area, nevertheless the double layer and parasitic capacitance are almost interlaced. In the bode plot of the LC buffer, the influence of the double layer capacitance, electrolyte resistance and parasitic capacitance can be clearly distinguished. Again the shaded area represents the resistive area. The cutoff frequencies, F_1 and F_2, of the resistive area have been estimated using

F_1~$1/(\pi*R_{el}*C_{dl})$ and F_2~$1/(2\pi*R_{el}*C_{par})$ by Langereis et al[20]. Where, F_1 and F_2 of solely PBS are respectively, 129 kHz and 395 kHz. For LC buffer, F_1 and F_2 were respectively, 663 Hz and 2 MHz. These values where combined with the visual inspection of the obtained bode plots of the different buffers with or without viable and non-viable cells. The obtained bode plots are in correspondence with the previous described theory and show at lower frequencies the influence of the double layer capacitance, at higher frequencies the parasitic capacitance and in the middle the influence of the buffer between the electrodes in the channel. The addition of cells to the LC buffer changes the frequency behavior. The presence of non-viable cells in LC buffer between the electrodes increased the impedance. However, a decrease in impedance was observed when viable cells were suspended in LC buffer. These data suggest that when using LC buffer, the behavior of viable cells with respect to the LC buffer alone is opposite to the behavior of non-viable cells. Similar results were obtained when comparing these results with our model. Due to the presence of viable cells in LC buffer, the impedance decreases, compared to solely LC buffer between the electrodes, indicating that a viable cell acts as a conducting sphere in low conducting buffer around 100 kHz. This different electrical behavior of the cells is due to presence of LC buffer instead of conducting buffer, where cells behave as insulating spheres below 3 MHz[22] .

Additionally, the influence of a solid sphere in the LC buffer was simulated, which resulted in a higher impedance at the resistive plateau. Beads were used in this simulation, since it was unclear what exactly happens with the equivalent electrical circuit model of a dead cell. Cell death was induced by heat and the compromised membrane allowed for cytoplasm leakage, leaving only a resistive membrane with denatured proteins. Therefore it was assumed that a non-viable cell can be represented as non-conducting membrane 'debris'. The modeled bead showed comparable results as non-viable cells, indicating that non-viable cells indeed act as resistive particle in LC buffer around 100 kHz.

When performing the frequency sweep measurements there was a highly concentrated cell containing solution present. This was transported through the device as described in 7.2.5. Therefore, the frequency sweep is based on a NS1 cell population. Moreover, the cells pass by at different positions in the channel. Hence, this induces moderate variation in the measured impedance, therefore 50 measurements were performed, averaging the effect.

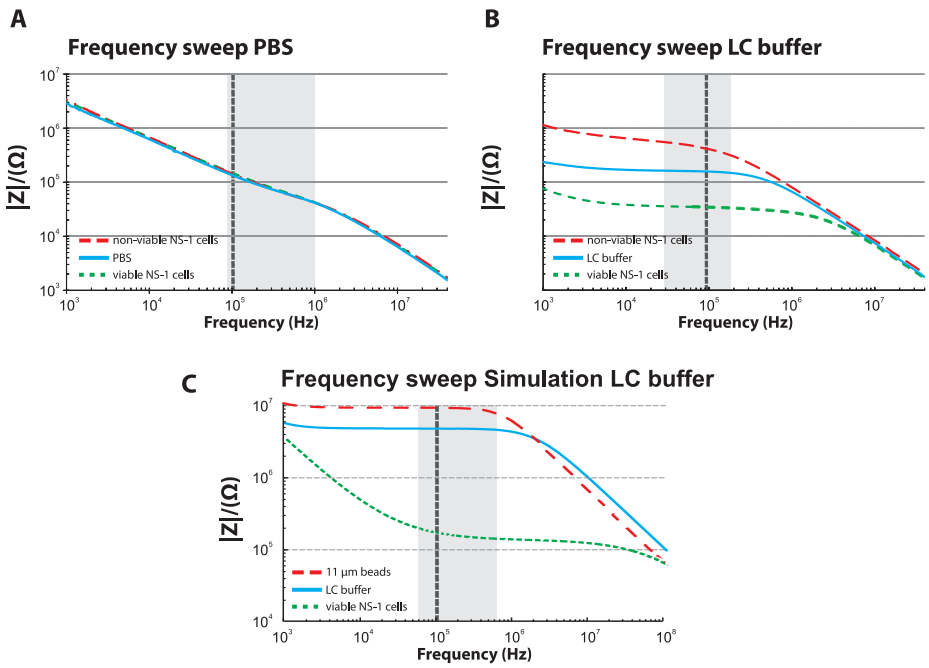

Figure 7.3: The measured frequency behavior of the microfluidic chip. (A and B) The lines in the graph show the average of 50 measurements obtained with the impedance/gain phase analyses using either PBS or LC buffer with or without (non)viable NS-1 cells. The shaded area indicates the resistive plateau and the dashed line represents the measurement frequency used during all subsequent experiments. C) Simulation of the frequency response of the electrical impedance of the equivalent circuit model with viable NS-1 cells, beads and only LC buffer.

The difference between viable and non-viable cells was not shown around 100 kHz, using a conducting buffer (PBS), which makes the use of LC buffer favorable, offering the discrimination based on viability. Lowering the buffer conductivity, therefore changing the buffer properties and electrical behavior of cells, lowers the frequencies at which discrimination between viability can be performed. Next, the frequency ranges in the shaded areas were examined and the optimal measurement frequency was shown to be at 100 kHz, for both PBS and LC buffer. So in further experiments, an actuation frequency of 100 kHz was used.

7.3.3 Droplet generation and detection

Droplets where generated using a flow focusing junction. Figure 7.4 A shows that the droplet generation frequency was determined with a maximum 475 Hz and visually confirmed using high-speed recordings. The length and the frequency of the droplets

varied using a range of flow rates. In our measurement system, we were able to relate electrical amplitude to droplet length (figure 7.4 B). Hence, the impedance change can be used to define an approximation of the droplet volume and detect changes in the droplet volume.

A quadratic power relation between droplet length and the measured impedance change is shown. This is due to the use of a first-order low-pass filter by the Zurich system. This filter suppresses the changes caused by the fast events, such as the passage of the droplet. For a long droplet, these changes occur at a lower frequency than for shorter droplets, and therefore the effect is less, resulting in a larger impedance peak. Another reason of the relation between droplet length and impedance change could be the RC-time of the setup or the wetting of the electrodes. Furthermore, figure 7.4 B shows that the measurement change of empty droplets passing one electrode pair can be used to determine the droplet length up till 185 µm. If the droplet length continuously increases the signal will saturate. At this point it is similar to measuring in solely (low) conducting buffer. Nevertheless, a passing cell will still result in a impedance change and can be detected. However, at a certain point there is plug flow and for our experiments and applications measuring cells in droplets is of main interest.

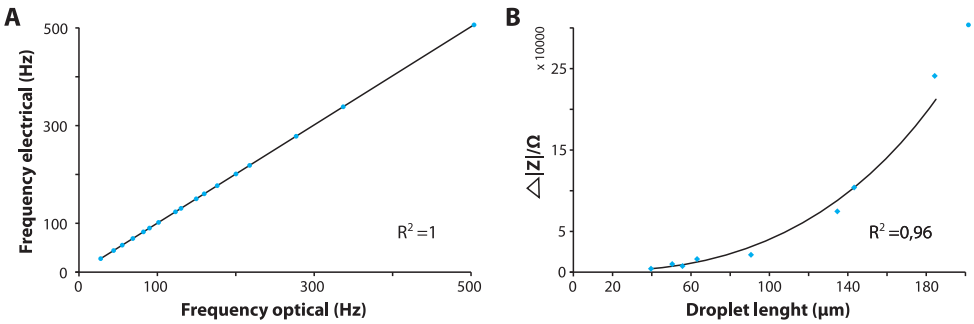

Figure 7.4: A) Optical versus impedance based droplet frequency determination B) Droplet length versus electrical amplitude. Obtained with Zurich impedance system. Sample rate 899 Hz, F_{act}=100 kHz 16V_{pp}

7.3.4 Cell detection in different conducting buffers

NS-1 cells were suspended in LC buffer and measured at a frequency of 100 kHz and 6V_{pp}. Both positive and negative peaks were observed, as shown in figure 7.5 A.

When suspending solely non-viable cells, only positive peaks were observed, with an average impedance change of 24400 ±12500 Ω (figure 7.5 C). This indicates that non-viable cells in LC buffer give an increase in impedance, as described previously (figure 7.3). The opposite effect, an impedance decrease, was observed when a viable cell passed the electrode pair with an average of -60400 ±37600 Ω (figure 7.5C). This peak

height also corresponds to the cell volume, as shown in figure 7.5A, peak number 1 and 2 corresponds to cell 1 and 2 in the insert. The decrease in resistance of viable cells in LC buffer can be explained by the presence of the conducting cytoplasm compared to the surrounding LC buffer. This results in an increase in the conductivity at the applied measurement frequency. As a consequence, the impedance decreases, giving rise to a negative peak. This effect is also confirmed by the simulations using Maxwell-Wagner theory (figure 7.3 C). Cell death was induced by heat. After this the cells were washed and suspended in fresh LC buffer, thereby replacing the cytoplasm with LC buffer. The induced heat denatures proteins and changes the membrane properties. Hence, it is likely the present membrane 'debris' adds to the impedance as a resistance at the measurement frequency, resulting in positive peaks. This observation is supported by the results shown in figure 7.5 A and figure 7.5 C. Where non-viable cells show similar impedance changes, unrelated to the (original) cell volume, and the membrane 'debris' is measured.

This hypothesis is supported by the observation that 11 µm beads suspended in LC buffer behave similar to non-viable cells as shown in figure 7.5 C. In conclusion, by using LC buffer it is possible to differentiate between viability based on the peak appearances. This is not possible when using more conducting buffer (PBS, 1.4 S m^{-1}). Data showed, for both viable and non-viable cells, positive peaks at frequencies ranging from 10 kHz - 3 MHz (figure 7.5 B). Hence, NS-1 cells suspended in PBS at an actuation frequency of 100 kHz, behave as insulating spheres, as expected.

To underline the possibility to detect a change in impedance when a cell containing droplet passes by, we have calculated that the R_{cell} has a relative contribution of 9.6% to the total R (R_{cell} +R_{lead} + R_{drop}, see figure 7.2 B). This is at a measurement frequency of 100 kHz in LC buffer, suggesting that it would be possible to detect an impedance change in a cell containing droplet compared to an empty droplet.

LC buffer is not a standard buffer to use in cell experiments, therefore the viability of NS-1 cells in LC buffer was evaluated. The viability of NS-1 cells, kept for 90 minutes in LC buffer, was ~95%. After two hours, the viability decreased significantly to 85%.

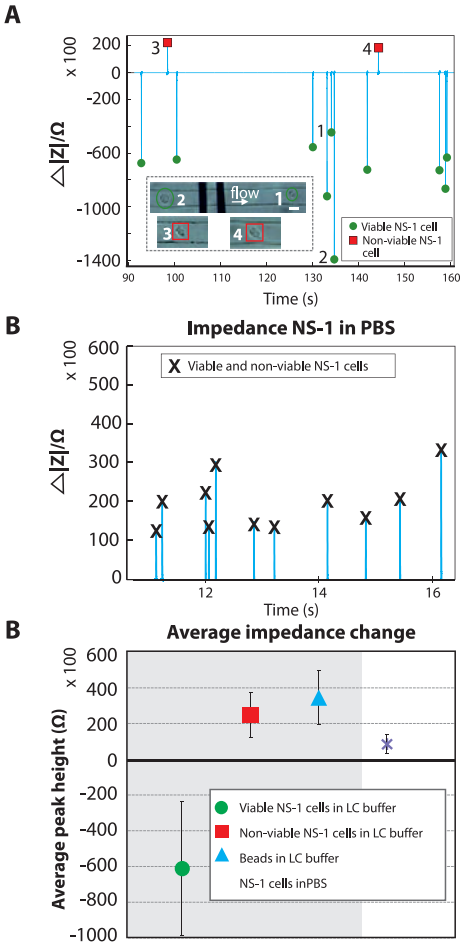

Figure 7.5: A) The processed signal with the peak heights and discrimination between viable and non-viable cells in buffer (Zurich impedance system sample rate 899 Hz, Fact=100 kHz 6V_{pp}). The insert is a microscopic image of a viable small (1) and a viable large (2) NS-1 cell passing the electrode pair (black bars) and two non-viable cells (3) and (4). Scale bar is 20 µm B) The processed signal with the peak heights of NS-1 cells in PBS (Zurich impedance system sample rate 899 Hz, F_{act}=100 kHz 6V_{pp}) C) The average impedance change of viable cells (n=68), non-viable cells (n=154) and beads (n=12) in either LC buffer (shaded area) or PBS(n=38).

7.3.5 Cell encapsulation and detection

Final experiments were focused on the detection of cells in droplets. Due to the best discriminating potency, NS-1 cells were suspended in LC buffer. Since LC buffer is more conducting than the continuous phase, the resistivity reduces when a droplet passes and thus the impedance signal decreases. As a result, empty droplets generate negative peaks.

Figure 7.6 shows the detection of two cell containing droplets using the impedance measurement data. When a droplet contained a viable cell, a decrease in impedance was shown. Different signal data were generated, however it was observed that the real part of the obtained signal was the most stable and the change due to a cell containing droplet was most significant. When the combined impedance signal was used, the signal contained more noise due to adding the phase information, making it more difficult to differentiate between the base line (empty droplets) and peaks (cell containing droplets).

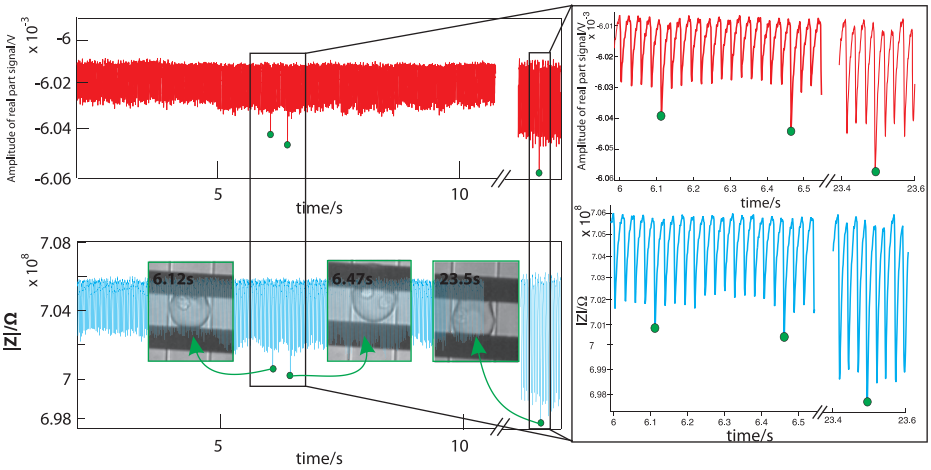

Figure 7.6: NS-1 cell in droplet detection using RMS voltage signal (top) and the final impedance change (bottom). NS-1 cells in LC buffer at F_{act} = 100kHz, sample rate is 899Hz and 6 V_{pp}.

Cells in LC droplets were detected up to a droplet frequency of 112 Hz. Additionally, non-viable cells and beads encapsulated in LC droplets could not be detected based on impedance change. Moreover, it was not possible to differentiate between empty and cell containing PBS droplets, using frequencies ranging from 10 Hz - 5 MHz.

As mentioned in paragraph 7.2.2, the impedance change is related to the droplet length (therefore volume), so for discrimination based on the presence of a cell, it is of utmost importance to generate homogeneous droplets. This length or volume effect can also be observed in figure 7.6 right part (23.5 s), where the base line has a larger amplitude compared to the left part (6 s). At 6 s the volume of the droplets is 43 pL (n=20) and at 23.5 s the volume of the droplets is 45.8 pL (n=20).

To eliminate a possible effect of droplet volume on the impedance change of a cell encapsulating droplet, the length of empty droplets was measured (n=20) and compared to the length of cell encapsulating droplets. The real part of the generated signal was used and the measurement of the empty and cell encapsulating droplet lengths using the corresponding frames, showed no significant difference. However, the change in amplitude of signals generated by cell encapsulating droplets compared to empty droplets did significantly differ ($p<0.01$). This finding eliminates the influence of the droplet length on the impedance change of the cell containing droplet, concluding that the measured change is solely based on the presence of a viable cell inside the droplet.

The sensitivity of the performed impedance measurements is 80%, hence 80% of the cell containing droplets are classified as a cell containing droplet using three times the standard deviation of empty droplets. Not all cell containing droplets were detected, which could be due to the cell position in the droplet or the sensitivity of the measurement setup. Finally, it could be due the presence of non-viable cells instead of viable cells, because the viability of the cells in the LC buffer after encapsulation has shown to be 90%. Furthermore, 99.98%, of the empty droplet were correctly identified. Finally a positive predictive value of 89% and a negative predictive value of 99.95% was shown (total amount of measured droplets is 8188).

Finally, the viability of the encapsulated cells was examined. The cells were stained with calcein AM and propidium iodide to determine cell viability and membrane integrity after encapsulation. Results showed that 90% of the cells retained their membrane integrity after 90 minutes, compared with 95% in control samples (data not shown). When putting on the electrical field of 100 kHz and $20V_{pp}$, the viability decreased to 91% (data not shown). So, there is no significant effect of the electric field on the viability of the cells when passing, for several milliseconds, an AC field of 100 kHz[21]. Furthermore, the LC buffer prevents localized heating.

7.4 Conclusion

Today, the analysis of single cells in droplets is of increasing interest. However, till now, it is not possible to label-free characterize and identify cells in droplets, which is of utmost importance if you need to select the droplets of interest, but do not want interference of any cell labeling Here, a microfluidic device for the label-free detection of cells in droplets, based upon electrical measurements, was presented. To our knowledge, this is the first time that label-free detection of cells in droplets is shown. Future experiments are focused on increasing the operating droplet frequency to several kilohertz, using a dedicated lock-in-amplifier. Furthermore, we want to detect cells in PBS or culture medium droplets, which is a better environment regarding the viability of cells, and favors (long-term) cell culture in droplets. The sensitivity of the impedance measurement data can be increased by using parallel electrodes instead of planar ones

and selection of the droplets of interest can be performed by incorporating a dielectrophoresis module.

In conclusion, these results provide us with a valuable method to label-free detect and select (viable) cells in droplets. Furthermore, the proposed method provides a usable method for increasing the efficiency of all kinds of cell-based applications, downstream of the encapsulation module. Even though the variety of applications of label-free cell detection in droplets is large, it is at the moment most suitable for applications around 100 Hz. Therefore, it is not suitable for usage in our current electrofusion platform. Hence the electrofusion platform discussed in chapter 8 involves only the use of the curved microchannels, operating at several kHz with an encapsulation efficiency of 77%.

The next chapter focuses on further development of the electrofusion platform, which entails different multi-usable components. The main goal of the next chapter is to achieve electrofusion of cells in droplets and utilize this finding for developing a high-throughput and efficient electrofusion platform.

7.5 References

1. Weitz, D.A., et al., *Drop-based microfluidic devices for encapsulation of single cells.* Lab on a Chip, 2008. **8**(7): p. 1110-1115.
2. Um, E., S.G. Lee, and J.K. Park, *Random breakup of microdroplets for single-cell encapsulation.* Applied physics letters, 2010. **97**(15).
3. Bhagat, A.A., et al., *Inertial microfluidics for sheath-less high-throughput flow cytometry.* Biomed Microdevices, 2010. **12**(2): p. 187-95.
4. Edd, J.F., et al., *Controlled encapsulation of single-cells into monodisperse picolitre drops.* Lab on a Chip, 2008. **8**(8): p. 1262-1264.
5. Koster, S., et al., *Drop-based microfluidic devices for encapsulation of single cells.* Lab Chip, 2008. **8**(7): p. 1110-5.
6. Kemna, E.W., et al., *High-yield cell ordering and deterministic cell-in-droplet encapsulation using Dean flow in a curved microchannel.* Lab Chip, 2012.
7. Segerink, L.I., et al., *On-chip determination of spermatozoa concentration using electrical impedance measurements.* Lab Chip, 2010. **10**(8): p. 1018-24.
8. Cheung, K.C., et al., *Microfluidic Impedance-Based Flow Cytometry.* Cytometry Part A, 2010. **77A**(7): p. 648-666.
9. Sun, T. and H. Morgan, *Microfluidic Impedance Cytometry: Measuring Single Cells at High Speed.* Microfluidics Based Microsystems: Fundamentals and Applications, 2010: p. 507-527.
10. Tang, S.K.Y., et al., *A multi-color fast-switching microfluidic droplet dye laser.* Lab on a Chip, 2009. **9**(19): p. 2767-2771.

11. Bao, N., J. Wang, and C. Lu, *Recent advances in electric analysis of cells in microfluidic systems.* Anal Bioanal Chem, 2008. **391**(3): p. 933-42.
12. Lin, R., et al., *Novel on-demand droplet generation for selective fluid sample extraction.* Biomicrofluidics, 2012. **6**(2).
13. Holmes, D., et al., *Leukocyte analysis and differentiation using high speed microfluidic single cell impedance cytometry.* Lab on a Chip, 2009. **9**(20): p. 2881-2889.
14. Holmes, D. and H. Morgan, *Single cell impedance cytometry for identification and counting of CD4 T-cells in human blood using impedance labels.* Anal Chem, 2010. **82**(4): p. 1455-61.
15. Steenbakkers, P.G., H.A. Hubers, and A.W. Rijnders, *Efficient generation of monoclonal antibodies from preselected antigen-specific B cells. Efficient immortalization of preselected B cells.* Mol Biol Rep, 1994. **19**(2): p. 125-34.
16. Morgan, H., et al., *High speed multi-frequency impedance analysis of single particles in a microfluidic cytometer using maximum length sequences.* Lab on a Chip, 2007. **7**(8): p. 1034-1040.
17. Foster, K.R. and H.P. Schwan, *Dielectric-Properties of Tissues and Biological-Materials - a Critical-Review.* Critical Reviews in Biomedical Engineering, 1989. **17**(1): p. 25-104.
18. Sun, T. and H. Morgan, *Single-cell microfluidic impedance cytometry: a review.* Microfluidics and Nanofluidics, 2010. **8**(4): p. 423-443.
19. Maxwell, J.C., *A treatise on electricity and magnetism.* 1873, Oxford,: Clarendon press.
20. Langereis, G.R., *an integrated sensor system for monitoring wahsing processes.* 1999, University of Twente.
21. Archer, S., et al., *Cell reactions to dielectrophoretic manipulation.* Biochem Biophys Res Commun, 1999. **257**(3): p. 687-98.

ELECTROFUSION OF CELLS IN DROPLETS*

CHAPTER 8

In this chapter, we present an integrated device for high-throughput electrofusion realized in a microdroplet platform. Four different components are described; droplet pairing, droplet fusion, droplet shrinkage and cell electrofusion in a droplet. Besides the latter one, these components are earlier described in literature. Our goal is to optimize these components for optimal integration in the electrofusion system. First, cells are deterministically encapsulated, and the droplets subsequently paired and fused. High-throughput, (>1000 Hz) droplet fusion is obtained (efficiency of 95%) using electrocoalescence. Stable volume reduction, to initiate cell-cell contact in the droplet, is demonstrated using three separate side channels or 'pitch fork structure'. Electroporation of the cell membrane is evaluated. Results show that after six successive pulses of 166 µs at 4 kV/cm, 86% of the cells in the droplets are PI+, which indicates that the membrane was (ir)reversibly electroporated. Finally, for the first time, successful electrofusion of two HL60 cells in a droplet is shown in detail using fluorescent membrane and nuclear dyes. Using six successive pulses of 4 kV/cm and pulse lengths ranging from 50-300 µs. These results ascertain the feasibility of electrofusion of cells in droplets, albeit with low efficiency (<0.1%). There are opportunities for improvement, regarding droplet shrinkage, electrode configuration and pulse settings.

*Parts are published in: R.M. Schoeman, E.W.M. Kemna, F. Wolbers and A. van den Berg, Electrophoresis accepted manuscript

8.1 Introduction

Droplet-based microfluidics for biological experiments received increasing interests over the last years[1-3]. It has earned his popularity due to several reasons. Firstly, the generation of monodisperse reaction vessels at high frequencies (kHz). Secondly, the encapsulation possibilities are enormous, ranging from bacteria to multicellular organisms[4] and this directly relates to all the possible biological assays which can be performed in a high-throughput manner. Thirdly, the droplet can be manipulated by fusion, splitting and sorting[5-7]. Due to all these possibilities regarding droplet-based cell experimentation, it is a small step to explore the possibilities of performing electrofusion in droplets. Since, the current method has very low efficiency, also due to random cell pairing. We believe the droplet platform can greatly improve the current method for hybridoma generation and selection.

Electrofusion in a droplet is a new approach for performing electrofusion between cells and has not been demonstrated before. In figure 8.1 the electrofusion of B-cells and myeloma cells in droplets is schematically represented.

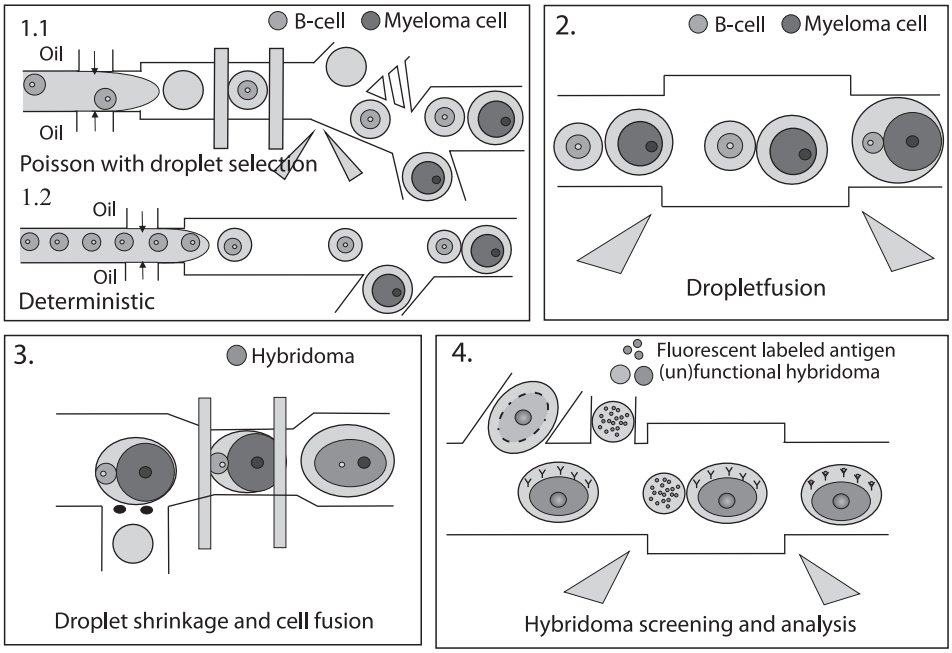

Figure 8.1: Schematic overview of electrofusion in a droplet platform.

In order to generate hybridomas in high-throughput and with high efficiency, a microfluidic system with several properties is needed. This microfluidic system should contain high-throughput single cell encapsulation, droplet pairing, droplet fusion to obtain one droplet containing two cell types (step 1). Subsequently, droplet shrinkage

should be incorporated, followed by cell in droplet electrofusion (step 2 and 3) and hybridoma selection (step 4). Previous chapters showed the first part of this system. In chapter 6 and 7, single cell encapsulation with high-efficiency and the label-free detection of (viable) cells in a droplet was demonstrated. In this final chapter, we present an integrated microfluidic device that combines a variety of functions, to analyze the feasibility of electrofusion of cells in droplets. Our ultimate aim is to realize a system for high-throughput hybridoma formation.

In figure 8.2 A, the complete design of the electrofusion system with its four components is shown. The different components are described (8.2 B-E); droplet pairing, droplet fusion, droplet shrinkage and cell electrofusion in a droplet. All components, besides the latter one, are earlier described in literature. Our goal is to improve these components for optimal integration in our electrofusion device, in order to assess the feasibility of electrofusion of cells in a droplet.

First, the previously mentioned curved microchannel is responsible for the single cell encapsulation. A second curved microchannel is incorporated for droplet pairing (figure 8.2 B). The generated droplet pairs are fused. For this, two methods were explored, either passive fusion based on Nui et al.[8], or an active method using a pair of sunken platinum on-chip electrodes, to initiate the electrocoalescence of droplets (figure 8.2 C). If the droplets are in close proximity of each other, the induced dipoles of both droplets align, which leads to an attractive Coulomb force between the two droplets, causing them to coalesce[7]. Electrocoalescence of droplets was first demonstrated by Chabert et al.[9] and showed multiple applications in microfluidics over the past years[10-14]. Standard settings for electrocoalescence apply a homogeneous or inhomogeneous AC field across droplets in the range of 0.01–10 kV/cm[9, 10]. Importantly, the gradient of the electric field produced by the electrodes must be perpendicular to the tangent of the two droplets.

Subsequently, the droplets pass a number of side channels, that are placed perpendicular to the microchannel, to reduce the droplet volume (figure 8.2 D). Generally, the side channels can either reduce or increase the volume of the fused droplet with cells. Increasing the volume can be achieved by applying a positive pressure (liquid flow), hence adding to the volume of the droplet. For electrofusion of cells in droplets, the cells need to be in close contact.

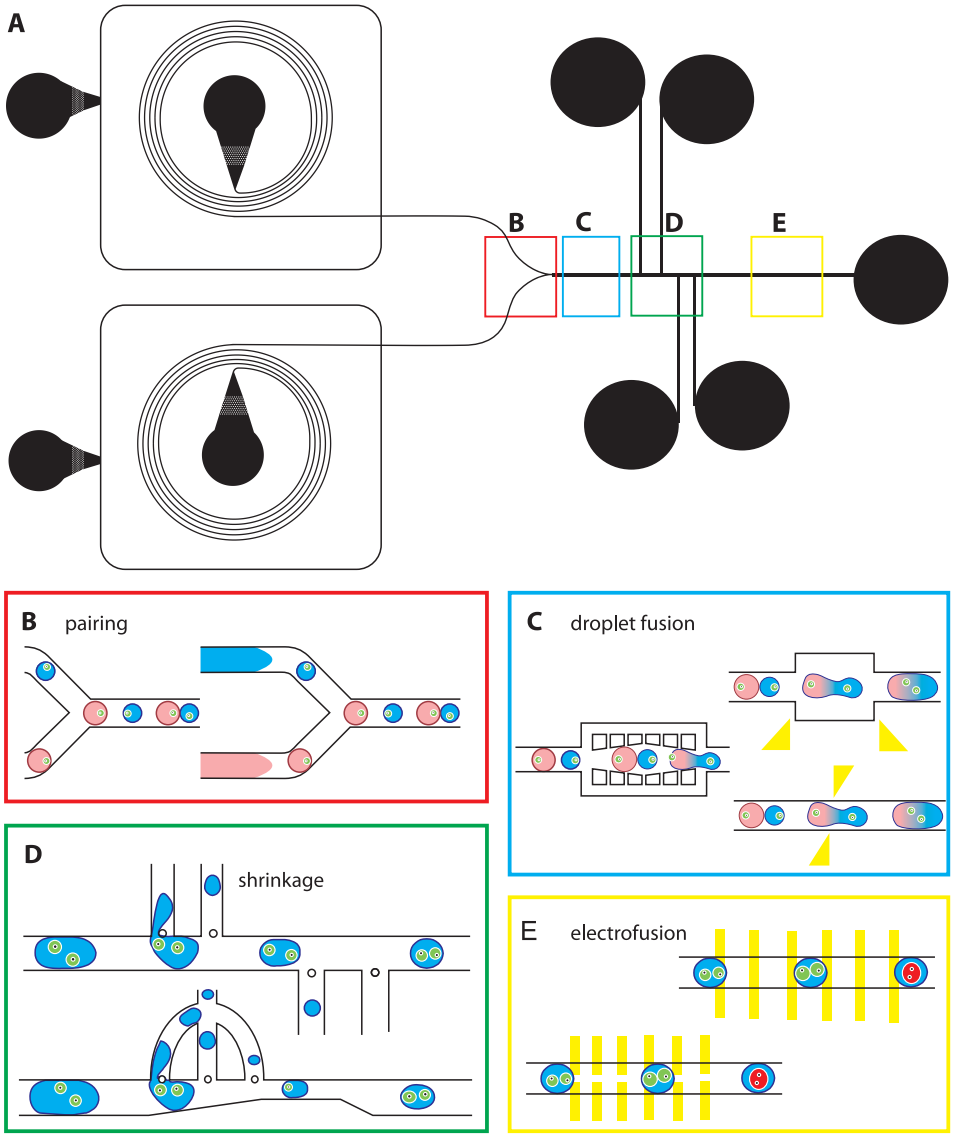

Figure 8.2: Schematic representation of the different components of the droplet-based microfluidic system/platform. A) Complete overview of the platform with all the different components. B) Single cell encapsulation in picoliter droplets followed by droplet pairing. C) Fusion of two droplets. D) Droplet shrinkage via side channels. The open circle defines a pillar, to prevent cell loss form the droplet. E) Cell fusion due to one or more electrodes pairs across the microchannel. Electrodes are depicted in yellow.

Therefore, the droplet volume ought to be reduced. It is shown in literature that T-junctions[15] or side channels[16] can be used to split a droplet. In this device, the side channels have the same length as the remainder of the microchannel and half the width

of the main microchannel. As a consequence, part of the droplet is split causing the volume of the droplet to reduce. One key element in our device, which differs from general splitting geometries, is the placement of small pillars at the inlet of the side channels, in order to prevent cells from entering the side channel.

Lastly, the key element in our device is the electrofusion component. These cell electrofusion experiments in a droplet are performed by passing the droplets, containing a cell pair, past an electrode array (figure 8.2 E). To achieve electrofusion of cells in a droplet, one needs to gain insight in the effect and behavior of the electric field inside a droplet. Therefore, COMSOL simulations are performed. Subsequently, to ensure that there is an electric field present inside a droplet and an encapsulated cell (or cells) experiences this electric field, initial electroporation experiments are performed. In the past few years, there have been some reports on electroporation in microfluidic droplets[17-19].

Finally, our focus is on the electrofusion of cells in droplets using downstream placed electrode pairs. Within our experiments, the feasibility of cell electrofusion in a droplet is shown using HL60 cells instead of B-cells and myeloma cells. Hence, droplets are generated containing predominantly two differently stained HL60 cells. Due to the fluorescent staining, the process of electrofusion can be assessed in detailed at a cellular level.

Concluding, the main goal of our device is to show the feasibility of cell fusion in a droplet. This involves research regarding the optimization of known components for droplet pairing, fusion and shrinkage for integration in the electrofusion device. And finally asses the feasibility of the electrofusion of cells in droplets evaluating different parameters, like electrode configuration, pulse strength and length. Furthermore, the presented platform is not constricted to cell fusion and is applicable for various other cell-based assays such as single cell analysis and differentiation assays[20].

8.2 Materials and methods

8.2.1 Chip design

The microfluidic chip consists of a one or two 5-loop curved microchannel, with in each curved microchannel one inlet for the cell suspension and one inlet for the oil. Several chip designs were used with varying parameters, which are specified when discussing the results.

A silicon master design was drawn in Clewin (version 4.0.1) and fabricated using standard UV-lithography. SU-8 (Microchem, Berlin, Germany) was spun on the silicon master with a thickness of 25 µm. The chip was made in PDMS (Sylgard 184, Dow Corning, Midland, MI, USA). Curing and base agent were mixed at a ratio of 1:10 and degassed. PDMS was poured onto the silicon wafer, degassed, and cured at 60 °C for 24 hours. After curing, in- and outlets were punched using a dispensing tip (Nordson EFD,

Maastricht, the Netherlands, inner Ø 1.36 mm and outer Ø 1.65 mm). Subsequently, the PDMS was sealed to a printed circuit board (VWR, Leuven, Belgium) using an oxygen plasma (Harrick PDC-001, NY, USA). After sealing, the chip was placed at 60 °C for a minimum of 30 minutes. Before use, Aquapel (Vulcavite, the Netherlands) was introduced into the channels to ensure hydrophobic channel walls.

8.2.2 Chip fabrication

The platinum electrodes were sputtered on a glass wafer using standard sputtering technique and the glass wafer was diced into individual chips. The glass chip was bonded with UV-glue onto a PCB. The electrode pads on both the PCB and the glass chip were connected via a double wirebond, which was sealed off with a drop of two component glue (Heisel). Onto the PCB, a plug was soldered, to make the electrical connection with the pulse generator (Agilent 33250A, Amstelveen, The Netherlands) and amplifier (Trek model 2210, Medina NY, USA). For droplet electrocoalescence experiments, an AC signal of 1 to 3 kHz and 2 to 4 Vpp was generated by the pulse generator. This generated signal was fed to the amplifier, giving rise to a 100 times amplified signal. For electroporation and electrofusion in droplets, a DC voltage was applied, varying from 3 to 8 Vpp.

8.2.3 Materials

HL60 (human promyelocytic leukemic) cells were grown in RPMI medium (Invitrogen, Grand Island, NY, USA), supplemented with 10% (v/v) fetal bovine serum (FBS; Invitrogen), 100 IU/ml penicillin (Invitrogen), 100 µg/ml streptomycin (Invitrogen) and 2 mM L-glutamine (Invitrogen) (=RPMI+ medium). Cell cultures were sustained in a 5% CO2 humidified atmosphere at 37°C. Cell cultures were split every 3 - 4 days at a ratio of 1:10. Prior to the experiments, the cells were counted, to establish the correct volume fraction of 1.7 - 2.2% in electrofusion buffer. This is a isoosmolar low conducting (LC), based on Steenbakkers et al.21, buffer consisted of deionized water, supplemented with 280 mM inositol (Sigma, St. Louis, USA), 0.1 mM calcium acetate (Sigma), 0.5 mM magnesium acetate (Sigma) and 1 mM l-histidine (Sigma,). The conductivity was adjusted, using deionized water, to 0.009 S/m.These cell containing solutions were used as the dispersed phase. For the continuous phase, HFE 7500 (3MTM NOVECTM) or FC-40 (3M™, St. Paul, MN, USA) was used, with a 1% (w/w) oil-phase biocompatible fluorosurfactant. This surfactant was a kind donation of dr. Ralph Sperling (Harvard).

8.2.4 Experimental set-up

The HL60 cell suspension was introduced into the microfluidic chip using plastic syringes (Hamilton, Bonaduz, Switzerland). The oil suspension was introduced into the microfluidic chip using a 5 mL glass syringe (Hamilton). All syringes were connected to their matching inlets with PEEK tubing (Vici, Schenkon, Switzerland, inner Ø 0.5 mm and

outer Ø 1.59 mm). Pipette tips were placed in the outlets of the chip and used as a waste bin or as a collection vessel for the main outlet. The fluid collected at the shrinkage side channels was discarded after the experiments.

Fluorescent staining using PI [10 µg/ml] and Calcein AM (Sigma; 2.5 µM/ml) was performed to determine the viability of the cells after electrocoalescence and shrinkage of droplets.

The flow was driven at a constant volume rate by a syringe pump (neMESYS dosing units, Cetoni GmbH, Germany). A magnetic stirrer bar was inserted into the cell containing syringes, to prevent the suspension from settling during the injection. The dispersed phase flow rates, containing the cell suspensions, were set at 5 - 25 µL/min, the flow rate of the continuous phase was 43 - 71 µL/min. The microfluidic chip was mounted onto the X–Y–Z translation stage of an inverted wide fluorescence microscope (Leica DM IRM, Leica Microsystems, Wetzlar, GmbH, Germany). Additionally, a computer-controlled high-speed camera (Photron SA-3, West Wycombe, United Kingdom) was mounted onto the microscope for image recording, using the accompanied Photron software (Photron Fastcam Viewer). Illumination was supplied by a Leica lamp 12V/100W in combination with a condenser.

Electroporation studies were performed using PI [10 µg/ml]. For the electrofusion experiments, half of the HL60 cell suspension was stained with a blue fluorescent nuclear dye (NucBlue, Invitrogen, Bleiswijk, The Netherlands), according to the provided protocol. The remaining half of the HL60 cell suspension was stained with a yellow/orange fluorescent nuclear staining [5 µM] (Cyto82 Invitrogen, Bleiswijk, The Netherlands). A green [5 µM] (Vybrant green Invitrogen, Bleiswijk, The Netherlands) and a red fluorescent membrane dye [5 µM] (Vybrant red Invitrogen, Bleiswijk, The Netherlands) was used in a few experiments, as well as a green fluorescent nuclear staining [1 µM] (SYBR green, Bleiswijk, The Netherlands).

After electroporation and electrofusion experiments, the droplets were collected and loaded on an microscope slide with single shallow depression (Corning, NY, USA). This allowed for a monolayer which could be scanned and analyzed.

8.2.5 Image acquisition and analysis

Images and videos were captured using the high-speed camera, at a frame rate of 1000 to 5000 frames per second and a shutter time of 2.5 - 5 µs. The captured images and videos were analyzed with the image-processing program ImageJ (National Institute of Health, MD, USA). To determine the droplet electrocoalescence efficiency, the number of passing droplet pairs was divided by the total number of generated droplet pairs. In order to determine the shrinkage percentage, the size of the droplet after passing the shrinkage structures was divided by the size of the same droplet before it passed this shrinkage module. The electrofusion images of the fluorescently labeled cells in droplets

were captured using an Olympus microscope (IX51; Olympus Europa Holding GmbH, Tokyo, Japan) with the required filters.

8.2.6 COMSOL simulation

Using COMSOL 4.3.0.184 Multiphysics, a 2D electric field profile of a droplet containing two cells, contacting both sides of the electrodes, was simulated. The module, which was used, was electric currents (ec). In addition, the conductivity of the droplet was set at 0.009 S/m and the oil at 4.5 $*10^{-7}$ S/m. One electrode was set as ground, the other was set to a potential of 8 V. The cell cytoplasm was modeled with a conductivity of $0.4*10^{-4}$ S/m and the cell membrane was modeled as insulating.

8.3 Results and discussion

In this section, the different components of the cell electrofusion platform are discussed. Starting with droplet electrocoalescence, two different approaches are shown and analyzed for their efficiency and operating frequency. Following droplet electrocoalescence, the shrinkage of droplets is discussed. We end this chapter with demonstrating what the behavior is of an electric field in a droplet and show the first results of electrofusion of cells in a droplet.

8.3.1. Droplet pairing

For two different droplets to fuse, they need to be paired and in contact. To obtain droplet pairing, two individual operating droplet channels were combined, as shown in figure 8.3 A. This did result in droplet pairing, however it was not a stable and efficient droplet pairing method.

The next approach for obtaining droplet pairing was achieved using a double T-junction (figure 8.3 B) based on previous work of Frenz et al.[11]. This did results in droplet pairing of 100% at a frequency >1.5 kHz[22].

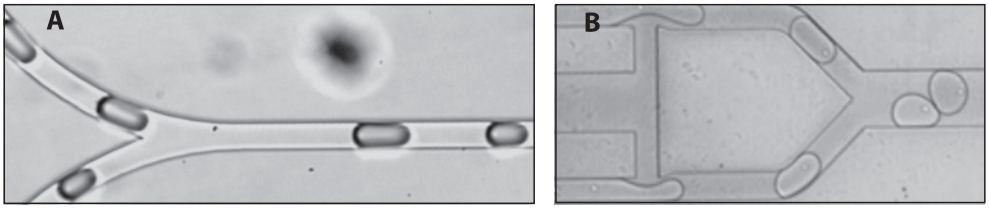

Figure 8.3: Droplet pairing methods. A) Droplet pairing in which the two individual operating droplet generators combine to one main channel. B) Droplet paring using a double T-junction.

8.3.2. Droplet fusion

For two different droplets to fuse, they need to be paired and in contact. Our first approach for obtaining droplet fusion was based on the passive fusion method of Nui et al.[8]. At flow rates to 1.8 µl/min for the oil and 0.25 µl/min for the water (10 Hz), full droplet contact was observed, but this did not result in passive fusion (figure 8.4).

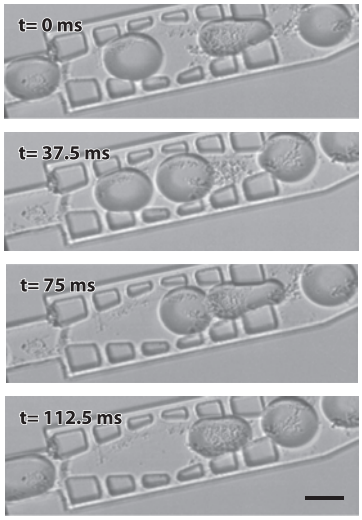

Figure 8.4: Passive fusion design with microfluidic pillars. Scale bar is 50 µm.

As passive fusion was not successful, droplet fusion was established by the use of an electric field, referred to as electrocoalescence. Droplets pass a pair of on-chip platinum electrodes, placed either on the similar side of the channel (figure 8.5 A), or diagonally on either side of the channel (figure 8.5 B), to initiate the electrocoalescence of droplets.

The first approach, shown in figure 8.5 A, is based on a design by Brouzes et al.[23]. Droplets were generated and paired at the main channel (figure 8.3 A). The electrodes were placed beneath the channel, at the position where the channel widens. This locally reduced the flow rate and droplets paired up. In combination with an AC field of 5 kV/cm at 1 kHz, fusion/electrocoalescence of droplets was observed. Even though the electrocoalescence/droplet fusion using this method was successful, the efficiency was not over 50%. This was due to the sub-optimal droplet pairing, as this was a combination between the method as shown in figure 8.3 A and the droplet pairing at the locally wider channel section. However, also correctly paired droplets did not always electrocoalescence, even when increasing the voltage this did not increase the efficiency. Moreover, the flow rate and subsequent maximum fusion frequency of 200 Hz, did not match the frequency needed for the deterministic ordering in the curved microchannel. Therefore, we optimized the electrocoalescence process using another configuration.

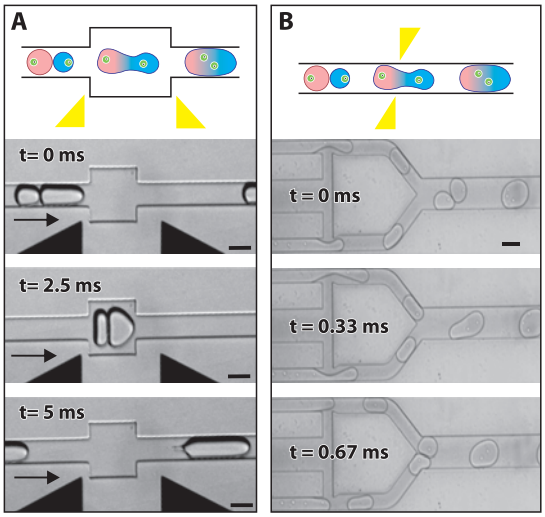

Figure 8.5: Active droplet fusion methods. A) Droplet fusion using widening of the channel and an electrode pair on similar side of the channel. AC 5 kV/cm at 1 kHz. Scale bar 40 µm. B) Droplet fusion using two oppositely located electrodes (electrodes not within resolution of capturing image, therefore not shown) AC of 18 kV/cm at 1 kHz. Scale bar 100 µm.

In this design, the droplet pairing was achieved using a double T-junction (figure 8.5 B). The electrodes were placed opposite of each other. This electrode configuration (the electric field is perpendicular to the droplets) showed electrocoalescence of droplets at higher frequencies (>1000 Hz) with 95% efficiency, using an electrical field strength of 18 kV/cm at a frequency of 1 kHz. The remaining 5% is due to suboptimal droplet contact.

8.3.3. Droplet shrinkage

The first electrofusion of cells in a droplet experiments are based on the electrofusion of HL60 cells (diameter 13 ± 1.6 µm). For electrofusion to occur, cells need to be in contact in the droplet. Hence, for two HL60 cells to be in contact, the droplet should have a final diameter of about 25-30 µm (~10-22.5 pL). When generating droplets using the curved microchannel, as discussed in chapter 6, the droplet volume of a single droplet ranges from 73-99 pL (50-65 µm). After droplet fusion, the volume would be approximately 150-200 pL (100-130 µm). The volume reduction should therefore need to be 90-95%, to obtain 20 pL droplets. To reduce the volume of a (fused) droplet, one to four side channels were punched and the droplet volume was reduced to a certain percentage of its original volume. The schematic overview of the design is shown in figure 8.6. The side channels have the same length as the remainder of the channel, but half the width. Thus the side channel has double the resistance and therefore splits a part of the passing droplet.

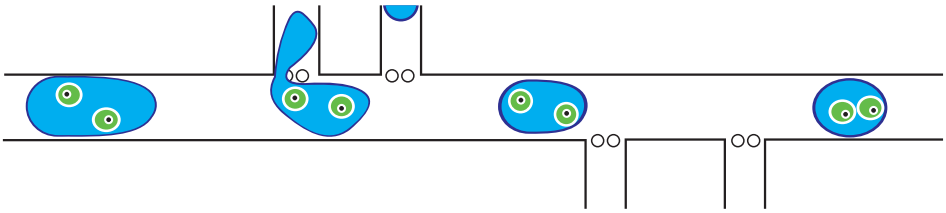

Figure 8.6: Schematic representation of the four individual shrinkage channels with pillars.

All these side channel contain pillars (black dashed circles in figure 8.7). In figure 8.7 the working mechanism of the pillars is shown. Using these pillars, in the majority of the experiments, the cells did not pinch of. In some cases, small cells were squeezed through or the pillars collapsed and malfunctioned.

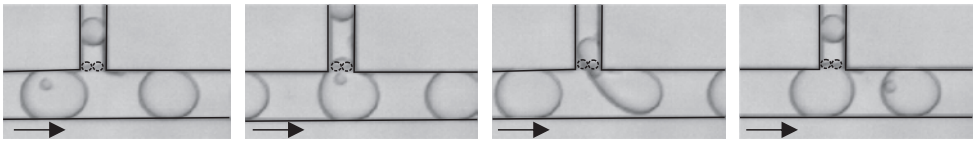

Figure 8.7: Pillars in the side channel to prevent cells from entering the side channel. Scale bar is 50 µm.

First, one side channel was punctured. Droplets were generated using one curved microchannel at similar speeds for cell ordering to occur. The droplet volume reduction using one channel was not sufficient, as it reached 22% volume reduction (figure 8.8 situation 0-1). The flow rates applied varied from 10-15 µl/min for water and 43-71 µl /min for oil. Using the lowest flow rate ratio (water 15 µl/min and oil 43 µl/min), a 22% volume reduction was obtained (100 pL to 78 pL). At the higher flow rates (water 15 µl/min and oil 66 µl/min), a similar volume reduction was observed. Nevertheless, a droplet volume reduction of 22% is too low to achieve sufficient cell-cell contact in the droplet.

When using two shrinkage channels, the average volume reduction was 37 ±3 % at flow rates ranging from 10-15 µl/min for water and 43-71 µl/min for oil (figure 8.7 situation 0-2.). In a situation using flow rates of water 10 µl/min and oil 71 µl/min, the droplet volume reduced to 45 pL, which is still too high.

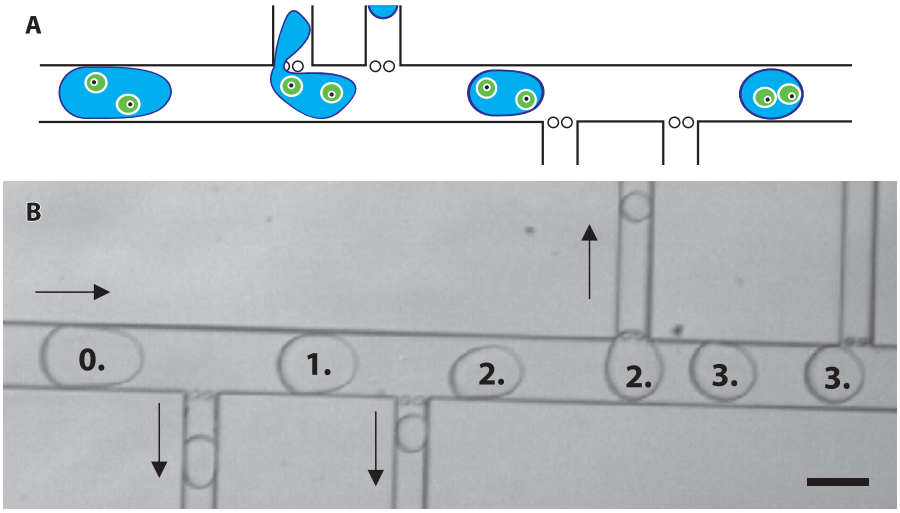

Figure 8.8: Droplet shrinkage at a water flow rate of 15 µl/min and an oil flow rate of 43 µl/min, when three shrinkage channels were punched. Scale bar is 50 µm.

The volume reduction was further increased by opening a third side channel (figure 8.7 situation 3). The volume reduction reached 45 ±3% of its original volume. The flow rates applied varied from 10-15 µl/min for water and 43-71 µl/min for oil. Using the lowest flow rate ratio (water 15 µl/min and oil 43 µl /min), a 45% volume reduction was shown (100 pL to 55 pL). At the higher flow rates (water 15 µl/min and oil 71 µl/min), a similar volume reduction was observed (48%). However, due to the higher flow rate ratio, the volume of the original droplet was smaller, hence after three side channels, the volume changed from 75 pL to 39 pL. Unfortunately, the percentage of volume shrinkage remains too low.

Lastly, four side channels were used for shrinkage at flow rates of water 15 µl/min and oil 43 µl/min. However, this resulted in unstable shrinkage effect, shown in the large variation of droplet volume reduction (dashed circles in figure 8.9).

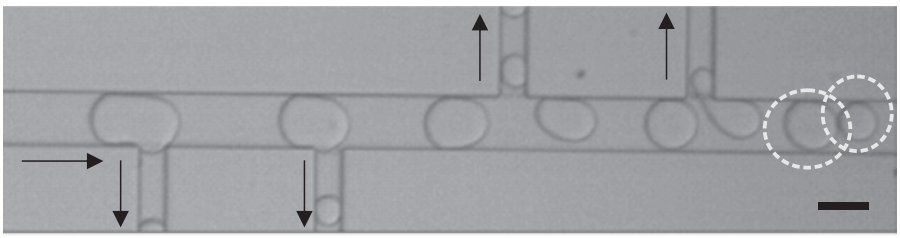

Figure 8.9: Droplet shrinkage using four open side channels. Scale bar is 50 µm.

When using similar channel lengths, than the remainder of the channel, the shrinkage of droplets using three side channels, goes up to 48%. However, the desired volume of 10-22.5 pL was not reached. Next, we changed the resistance by shortening

the length of four side channels by punching the outlet at ~1/2 of the channel length. A volume reduction of 67% was observed. In this situation the third and fourth channel did not add to the volume reduction, the droplet did not contact the third and fourth channel. Hence, only oil was flowing into the last two side channels, reducing the flowrate. The original droplet was 67.5 pL and the shrunken droplet was 22.5 pL (figure 8.10). This final volume is suitable to induce cell-cell contact. Hence, to reach the desired droplet volume using a reproductive and stable method, the resistance of the side channels and the design should be optimized.

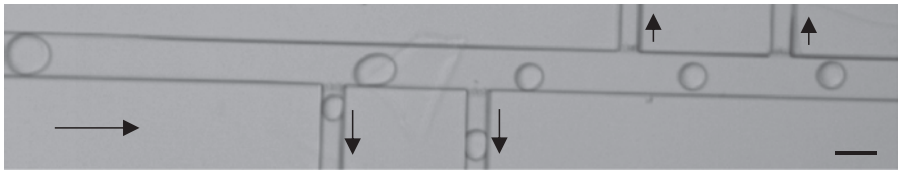

Figure 8.10: Droplet shrinkage with four open side channels, in which the channels are half of the original length. Scale bar is 50 µm.

Subsequently, we tried another shrinkage device. This design is based on a pitch fork structure (figure 8.11 A) and the main channel narrowed at the point where the pitch forks entered the main channel. This design combines the results of three open side channels, as shown above, to one side channel, branching into three side channels.

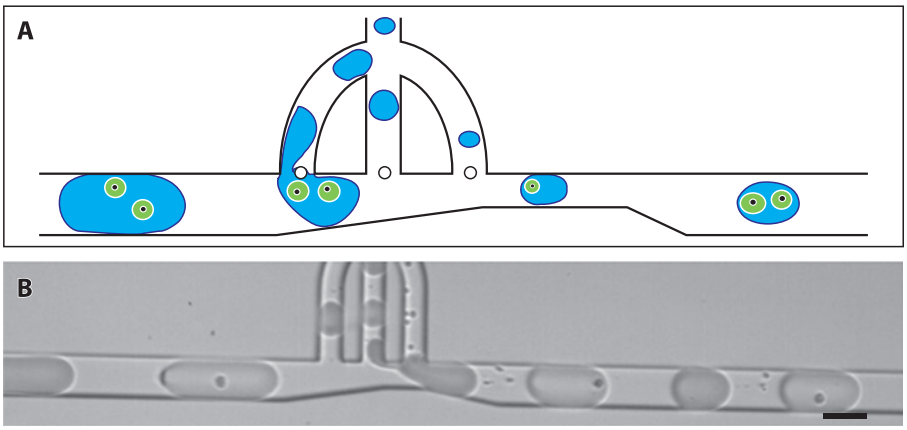

Figure 8.11: Droplet shrinkage. A) Schematic representation of the pitchfork structure. B. One pitchfork. The cumulative flow rate was 75 µL/min, the volume reduction 40 %. Scale bar is 50 µm.

With one pitchfork, the reduction was 40 % (figure 8.11 B). This reduction was further increased by adding two more pitchforks to a volume reduction of 75%. This 75% volume reduction of the droplet is in the range of the volume reduction required (90-95%). However, the narrowing in the main channel induces blockage and obstruction.

Overall, the droplet shrinkage results of both designs are summarized in table 8.1. The obtained results show that the volume reduction is not sufficient using the tested designs. The pitch fork structure shows promising results in stable volume reduction, however the narrowing increases the obstruction chances (impeding stable volume reduction). To achieve sufficient volume reduction, the resistance in the side channel should be optimized, as well as the number and design of the side channels. The four singular side channels with half the width and half the length of the remainder of the channel seem the most promising for achieving sufficient droplet shrinkage. Even though the volume reduction was 66%, a higher volume reduction should be possible when ensuring the droplet contact between the third and fourth channel.

Table 8 1: Overview of the percentage of volume reduction in the used shrinkage devices

	Number of open side channels						
	1	2	3	4	4_half length	1xPF	3xPF
Reduction (%)	22	37	45	unstable	66	45*	75*

PF: pitch fork, *blockage and obstruction of the main channel due to narrowing.

Finally, after droplet pairing, droplet electrocoalescence and droplet shrinkage, the feasibility of the electrofusion component needs to be assessed. Hence, the next paragraph focusses on the effect of an electric field on cells in a droplet.

8.3.4. Effect of electric field in a droplet on a cell

The idea of electrofusion of cells in a droplet addresses the critical question whether the voltage generated by the external applied electric field is sufficient for electrofusion in a droplet to be successful. Therefore, it is first important to characterize the electric field inside a droplet. This was performed with the simulation program COMSOL and with electroporation experiments.

Cells in the droplet can pass the electrode pair in different modes, as schematically represented in figure 8.12. There are two main electrode configurations as shown in figure 8.12 A and B. These electrode designs were tested for electroporation and electrofusion ability. Since planar electrodes are used, the cell will not always pass the electric field in the ideal position. The main different modes are depicted in figure 8.12 A and B for both designs. The black structures represent the electrodes and the lines represent the electric field present in the droplet. The gray circles symbolize the encapsulated cells. It can be seen that in the second situation in 8.12 A and in the first situation in 8.12 B, the cells are placed ideally perpendicular with regard to the electric field lines. This is the optimal situation for achieving electrofusion between cells. However, as can be seen, there are many different other positions possible, which do not have the ideal field line orientation. This is very important to realize for analyzing the results and improving the system.

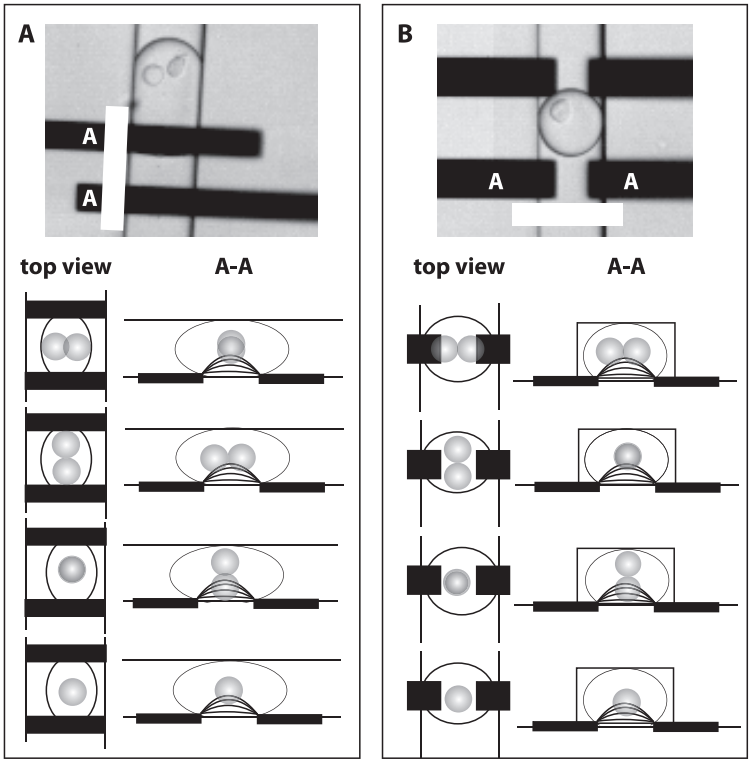

Figure 8.12: Overview of different cell in droplet situations regarding the applied electric field. A) Interlaced electrode pair. B) Oppositely placed electrode pair. A-B) Four different situations are shown, 1-3: Two encapsulated cells for electrofusion, 4: Electroporation of a single cell.

COMSOL simulation

The droplet experiences an electric field, when passing the electrode pair. This electric field was modeled using COMSOL at t=0. The second situation as depicted in figure 8.12 A, was used to model the electric field. This cell position is ideal for achieving electrofusion, since the electric field is perpendicular to the contacting membranes. The electrode distance and width in the simulation experiments were 20 µm, comparable to the dimensions in our microfluidic device. The droplet encapsulated two HL60 cells with a diameter of 13 µm and was in contact with both electrodes at this point (t=0). Figure 8.13 shows the result of the simulation of the electric field in a droplet. The electric field in the droplet can be estimated using this simulation, however, it has to be kept in mind that this is at t=0, so the double layer did not play a role and was not imbedded in the model. One electrode was set to ground, the other electrode had a potential of 8 V. The field strength in the area of the cells was ~2-3.5 kV/cm, depending on the position regarding the y-axis. This indicated that the field strength experienced by the encapsulated cells at t=0, is theoretically sufficient for electrofusion to occur, based on previous results.

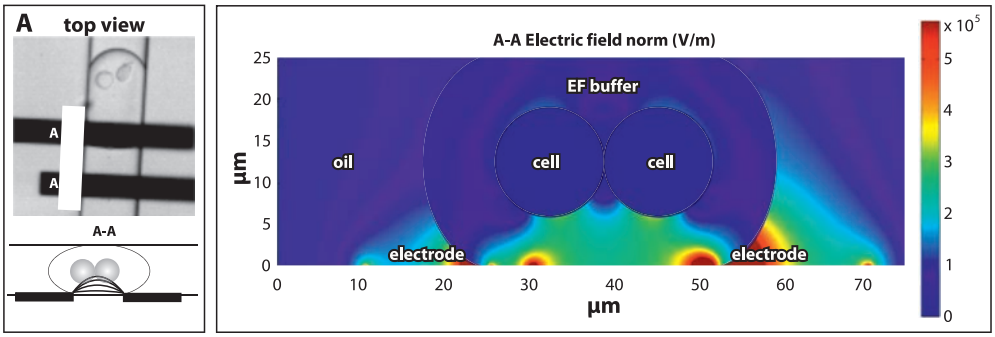

Figure 8.13: Simulation results of interlaced electrode pair. Left insert shows the simulated situation A-A. The right figure is a COMSOL simulation of the electric field in a droplet passing one electrode pair at t=0. The side view, in which the electrodes are placed at the bottom, is shown. The voltage of one electrode is 8 V, the other electrode is grounded.

Electroporation in a droplet

In addition to the COMSOL simulation, we did some initial electroporation experiments to ensure that there is an electric field present inside a droplet and an encapsulated cell (or cells) experiences this electric field. The HL60 cells were suspended in EF buffer with PI. Electroporation is the phenomenon that induces (ir)reversible breakdown of the cell membrane, which results in the formation of pores in the membrane. Molecules can enter and leave the cell during this permeabilized state. The electroporation process results in increased permeability and conductance of the membrane and PI can enter the cell. Subsequently, PI binds to the present DNA in the cell, and when bound, its fluorescence increases 1000 times and as results the cell becomes red fluorescent. This is in both reversible (cells remains viable) and irreversible electroporation. Hence, no discrimination between those two situations, purely based on PI fluorescence, can be made. Furthermore, PI is toxic for the cell and eventually enters in a non-permeabilized dead cell as well. We performed a control study and found that longer than 90 minutes in EF buffer with PI, results in an 10% PI+ cells. Hence, EF buffer permeabilizes the membrane and PI enters the cell without the need for an electric pulse. So it is important to keep in mind that, all the measurements must be finished in less than 90 minutes.

Electroporation occurs when the cell membrane experiences a strong electric pulse, typically 1-4 kV/cm for several micro- to milliseconds[24]. Using equation [4.3], one can determine the critical field strength E_{crit} (V/cm) for HL60 cells (diameter 13 ±1.6 µm). The calculated E_{crit} value for HL60 cells is 1.03 kV/cm. Based on the observations that the most favorable field strength for breakdown is 1 to 3 times E_{crit}[25], the electroporation experiments were performed ranging from 1-4 kV/cm, with pulse lengths ranging from 1000 µs to 7 ms.

Electroporation experiments were performed with two electrode designs as shown in figure 8.12 A and B. However, the results of the array depicted in 8.12 B did not show successful electroporation, when compared to the other design. Hence, we will continue

with the interlaced electrode array, as shown in figure 8.14. The cell in the droplet experienced two successive pulses of different strengths and lengths. The obtained results are shown in the graph (middle figure 8.14). If no electric field was applied, 5% of the cells were PI+, which indicates that 5% of the cells were electroporated or already death at the start of the experiment.

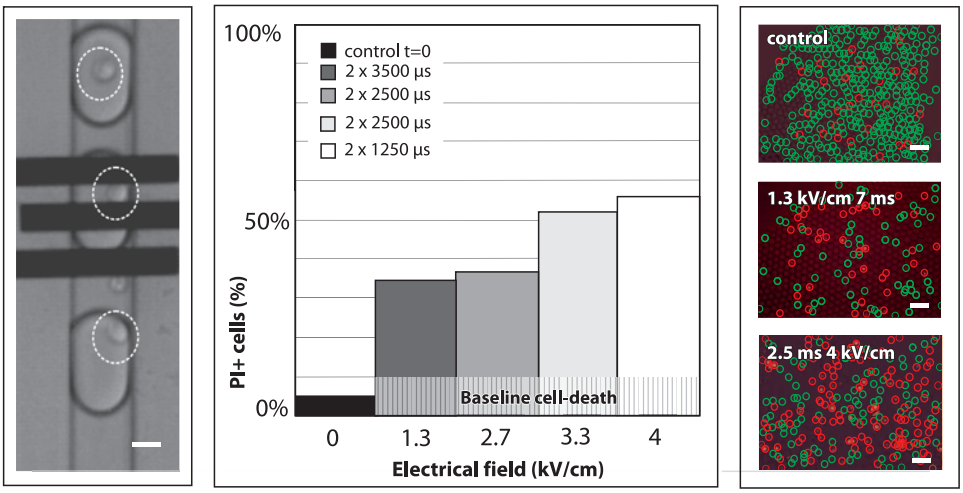

Figure 8.14: Overview of electroporation results using two pulses. Left insert shows the electrode array with droplets containing HL60 cells (dashed circles) passing the electrode structure (black lines). Scale bar 25 µm. The graph shows the electric field in combination with the pulse length, consisting of two successive pulses, and the percentage of PI+ cells. The left dark grey bar represents the control where 5% of the HL60 cells are PI+ at start of experiment. The horizontal transparent grey bar at 10% represents the PI+ cells after 90 minutes of EF followed by encapsulation. The right figures show, by using red and green circles, the PI+ (red) and PI- (green) cells. Scale bar 200 µm.

A substantial increase in PI+ positive cells, 36% and 52%, was observed when increasing the field strength from 2.7 kV/cm to 3.3 kV/cm, respectively. Moreover, cells did become increasingly positive with increasing field strength (2.7 kV/cm vs. 4 kV/cm), requiring lower pulse lengths (5 ms vs. 2.5 ms). When applying 4 kV/cm, the percentage PI+ cells rose to 56 %, the pulse length was 2.5 ms. Furthermore, applying multiple pulses resulted in higher percentages of PI+ cells. Electric field strengths of respectively 2 and 2.7 kV/cm and pulse lengths of 3.4 and 3.1 ms, resulted in 48 and 53 % PI+ cells (figure 8.14). These percentages were not reached when applying less pulses of similar field strengths and longer pulse lengths (36 %, figure 8.15). This indicates that multiple pulses is an important factor to increase the percentage of PI+ cells. The highest percentage of PI+ cells demonstrated was 86%, with a field strength of 4 kV/cm and a total pulse length of 1 ms (6 x 160 µs). However, it is important to keep in mind that there is no discrimination between reversible and irreversible poration. It is likely that at

high electric fields and/or long pulse lengths, a certain percentage of the cells is irreversibly damaged and therefore not applicable/usable for electrofusion.

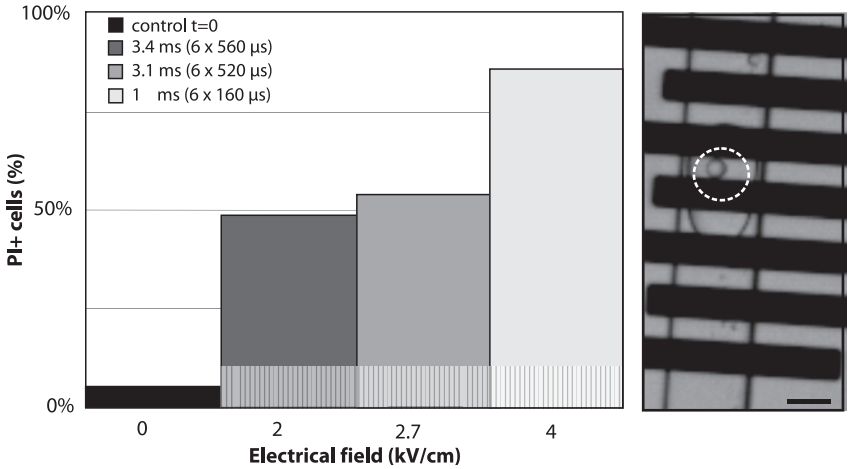

Figure 8.15: Overview of electroporation results using six pulses Right insert shows a droplet passing the electrode structure. The left graph shows the electric field in combination with the pulse length, consisting of six successive pulses, and the percentage of PI+ cells. The black bar represents the control. The horizontal transparent grey bar at 10% represents the PI+ cells after 90 minutes of EF followed by encapsulation. Scale bar 25 µm.

When an electrode is in contact with the dispersed phase, here EF buffer, there is interaction with the buffer and its contents. These interactions include for example cell lysis, hydrolysis and droplet sticking.

In contrast to others[18], we did not encounter easy droplet adherence to the channel wall, probably because we applied a hydrophobic coating before the start of the experiment. Hence, our continuous electroporation experiments were well and precise controlled. The adherence of membrane debris to the electrode surface was observed (figure 8.16 A). As a result, the electroporation process was disturbed. This effect only occurred when the electric field exceeded 6 kV/cm for longer periods of time (>15 min) and long pulse lengths (>500 µs).

Another effect which can appear is electrolysis at the electrodes (figure 8.16 B), due to a direct contact between the aqueous droplets and the electrodes. This occurred when the droplet contact was >5 ms and the electric field more than 3 kV/cm.

Finally, 'electrode sticking' was observed (figure 8.16 C). Droplets elongated and were 'stuck' at the electrode for a short period of time. This slowed the droplet down and the contact with the last electrode increased. This effect was also observed with impedance measurements (chapter 7) and could interfere with the cell-cell contact in the droplet.

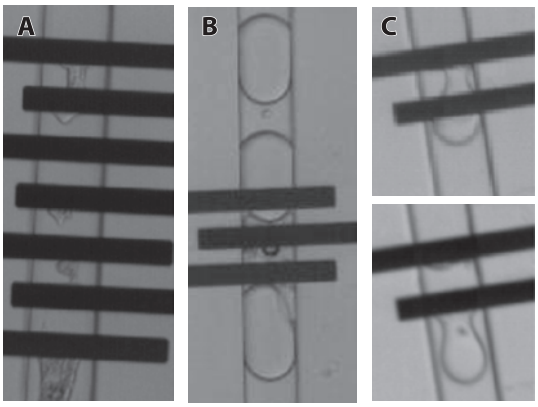

Figure 8.16: Electrode interactions, black bars represent the electrodes. A) Membrane and cell membrane debris due to cell lysis. B) Electrolysis at the electrodes due to long contact times and high electric DC field. C) Droplet sticking at 4 kV/cm, 150 µs pulses.

Overall, we ascertain the presence of an electric field in a droplet and electroporation of HL60 cells in droplets was assessed using PI. However, for electrofusion of HL60 cells in a droplet, the parameters are not known. We have shown static electrofusion of HL60 cells with multiple (1-3 pulses) of 40-100 µs and 2.5 kV/cm (chapter 2). Electrofusion of B- and NS-1 cells was shown using 6 pulses of 100 µs at 2.5 kV/cm (chapter 4). The next paragraph focuses on the electrofusion of HL60 cells in droplets.

8.3.5 Electrofusion in a droplet

To determine if electrofusion inside a droplet is feasible, the electrofusion experiments were based on electrofusion of the same cell type, namely HL60 cells. In these first experiments, it was sufficient to make droplets encapsulating two HL60 cells, hence only one curved microchannel was used. To encapsulate two cells in a droplet, the cell volume concentration was increased to 2.2% and the majority of the generated droplets contained two cells (more double equilibrium positions), as shown in figure 8.17 situation 2. In this way, the electrocoalescence of droplets was circumvented and less volume reduction was required to initiate cell-cell contact in a droplet.

For successful electrofusion to occur, various factors play a role. A crucial factor is the traveling droplet speed. The droplet speed, in combination with the electrode width and droplet length, defines the length of the applied fusion pulse. The droplet speed is adjustable by widening the channel, which slows down the droplet and hence increases the pulse length or adding oil, which accelerates the droplet and thus reduces the pulse length. The droplet volume is fixed to ~10-22.5 pL. The electrode width can also be adjusted, but should not be more than the droplet length, as the droplet must be in contact with both electrodes to ensure the effect of the electric field on the encapsulated cells.

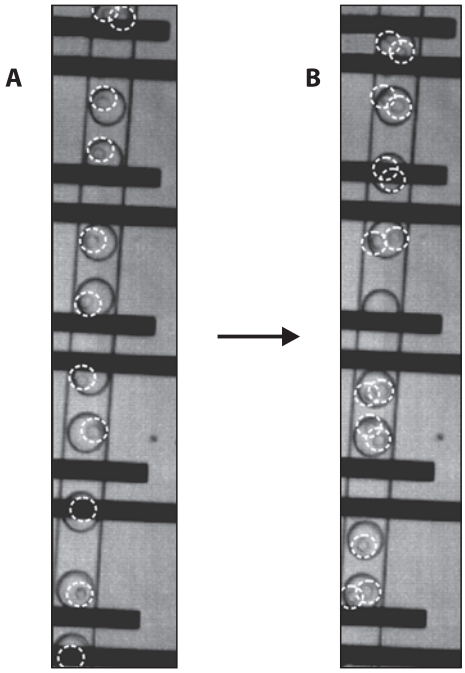

Figure 8.17: Single and double HL60 cell encapsulation. Situation 1 shows droplets containing single cells (volume fraction 1.7%) and situation 2 shows that the majority of the droplets contained two cells. This was due to increasing the volume fraction to 2.2 %, which caused double equilibrium positions. Scale bar is 50 µm.

In combination with the pulse length, the electric field is very important. The electroporation results demonstrated that an electric field of 2.7 - 4 kV/cm had an substantial effect on the encapsulated cells. Apart from the pulse length and applied electric field, we are also interested in applying multiple pulses, since our previous results have shown that multiple pulses achieve higher fusion efficiencies.

The first electrofusion results were obtained when performing the electroporation experiments. The white dashed circles in figure 8.18 show PI+ cells which seem to be fused, because more than one nucleus within one cell is visible The cell in the lower right corner in figure 8.18 C (orange dashed circle) is a cell undergoing mitosis.

These initial fusion results suggest that the droplet size does not have to be as small as the volume of the two cells to be fused. It seems that the HL60 cells inside a droplet also make cell-contact without the restriction of the droplet volume. In culture there is also the observation of cell adherence. Hence, for our goal this is beneficial, since cell-cell contact is critical for cell fusion to occur.

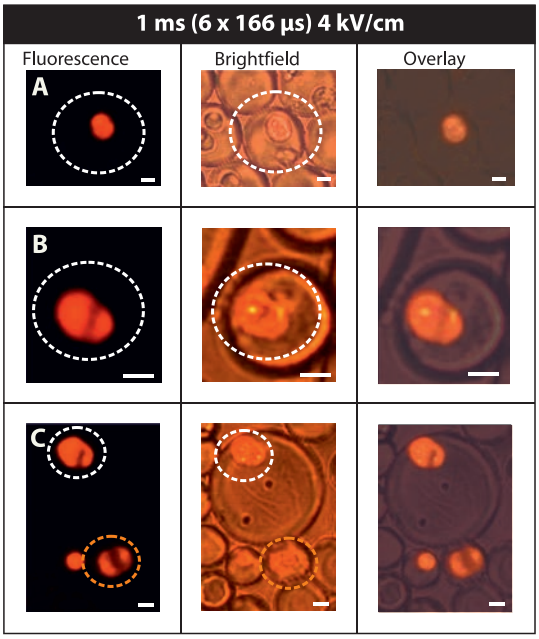

Figure 8.18: A-C) Cell fusion in a droplet after applying six successive pulses of 166 µs of 4 kV/cm (white dashed circles) Cells are red fluorescence due to PI staining. Cell in orange dashed circle is undergoing mitosis. Scale bars are 10 µm.

In our initial electroporation and electrofusion experiments, PI was a good marker. However, to definitively asses cell fusion in a droplet, different dyes should be used, which individually and differently stains the cell membrane and cell nucleus of the cells to be fused. In every image, the dyes which were used are specified. Furthermore, two electrode geometry and different settings were tested. The two electrode geometries involve the pairs next to each other or the electrode pairs opposite to each other (figure 8.2 E). The settings which were tested for both designs are ranging from 100 - 300 µs, 1 – 2 – 3 - 6 pulses and 2.5 - 4 kV/cm. The only successful electrofusion experiments inside a droplet were achieved with six successive pulses using the electrode structure as shown in figure 8.15, with an electric field of 4 kV/cm. Hence, the other mentioned geometry and settings which were tested did not result in cell electrofusion in a droplet. The difference with the electroporation study is the distance (and therefore time) between the pulses. The electrode pairs are placed further apart (105 µm) to induce separate, successive pulses.

In figure 8.19, half of the HL60 cells were stained with a green nuclear staining and a red membrane dye. The remaining half of the HL60 cells were fluorescently labeled with a blue nuclear stain. Figure 8.17 A and B both show one HL60 cell containing two nuclei. Even though the images suggest cell fusion, this is difficult to conclude as the blue and green nuclear dye are not clearly discriminative.

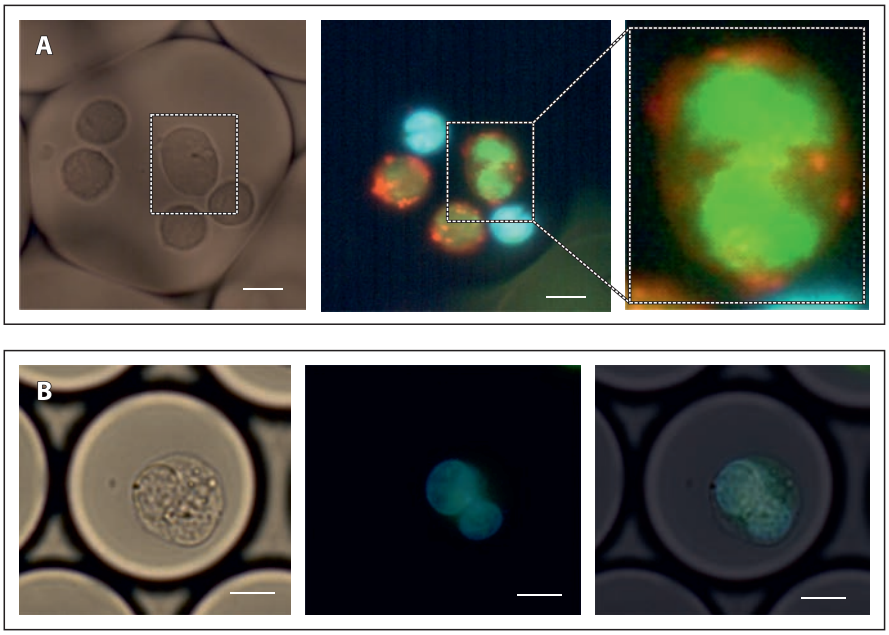

Figure 8.19: Bright field (left), fluorescent (middle) and overlay (right) images of HL60 cells in a droplet. A and B) Green nuclear staining in combination with red membrane staining, and blue nuclear staining. Images were taken after applying 6 x 300 us pulses at 4 kV/cm. Scale bar is 10 µm.

Moreover, at the time of electrofusion experiments, the HL60 cells were in the exponential growth phase, and thus the suspension also contains polynucleated cells (0.8 %; 4/492) To account for this phenomenon, electrofusion can only be stated if there are two differently (and clearly distinctive) labeled nuclei and/or membranes.

Therefore, in the next electrofusion experiment, half of the HL60 cells were stained with a yellow nuclear dye, the other half with a blue nuclear dye. Initiative fusion was observed between two differently labeled HL60 cells (figure 8.20). We refer to this as initiative, as the cell membranes were fully connected, however no rearrangement took place and the cells remained separate. However, in the most right image, cytoplasmic/nuclear exchange occurred, because the cell with the blue nucleus also clearly contains the yellow dye. Since there are no other cells in proximity and the membranes are attached, this suggests initiative electrofusion.

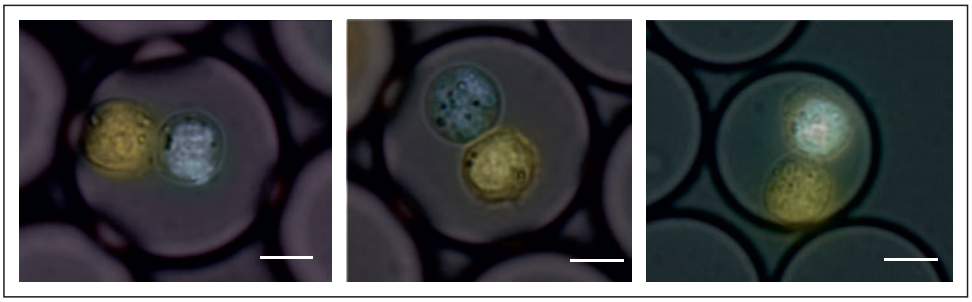

Figure 8.20: Initiative fusion between two differently labeled HL60 cells. One yellow labeled nucleus and one blue labeled nucleus. Images shows 3 separate HL60 pairs after applying 6 pulses of 300 µs at 4 kV/cm. Scale bar is 10 µm.

To visualize advanced fusion, which is defined as a fused HL60 cell (hence one rearranged cell membrane) with two nuclei, a green membrane dye instead was added, to the yellow nuclear dye. If a green cell with a blue nucleus is observed, cell-cell fusion has occurred. In figure 8.21 (different successful electrofusion events are shown using different pulse lengths (50-300 µs). In the left the fluorescence images are shown, in the middle the bright field images and the right images are the overlay between the both. Figure 8.21 B, shows electrofusion of two HL60 cells, one with a blue nucleus, with a HL60 cell having a green membrane. However, the yellow nuclear dye is difficult to observe. Nevertheless this suggest electrofusion, since this are two separately dyed cell populations and no blue nucleus with a green membrane was observed on forehand, or with control (no electric field).

Figure 8.21 A and C show electrofusion of two cells with a blue and yellow nucleus, here no green membrane dye was used. These results state that the droplet volume is not critical for electrofusion to occur, since the droplet was not as small as the volume of two HL60 cells. However, inducing cell-cell contact by decreasing the droplet volume has the potential to increase the percentage of successful fusion events.

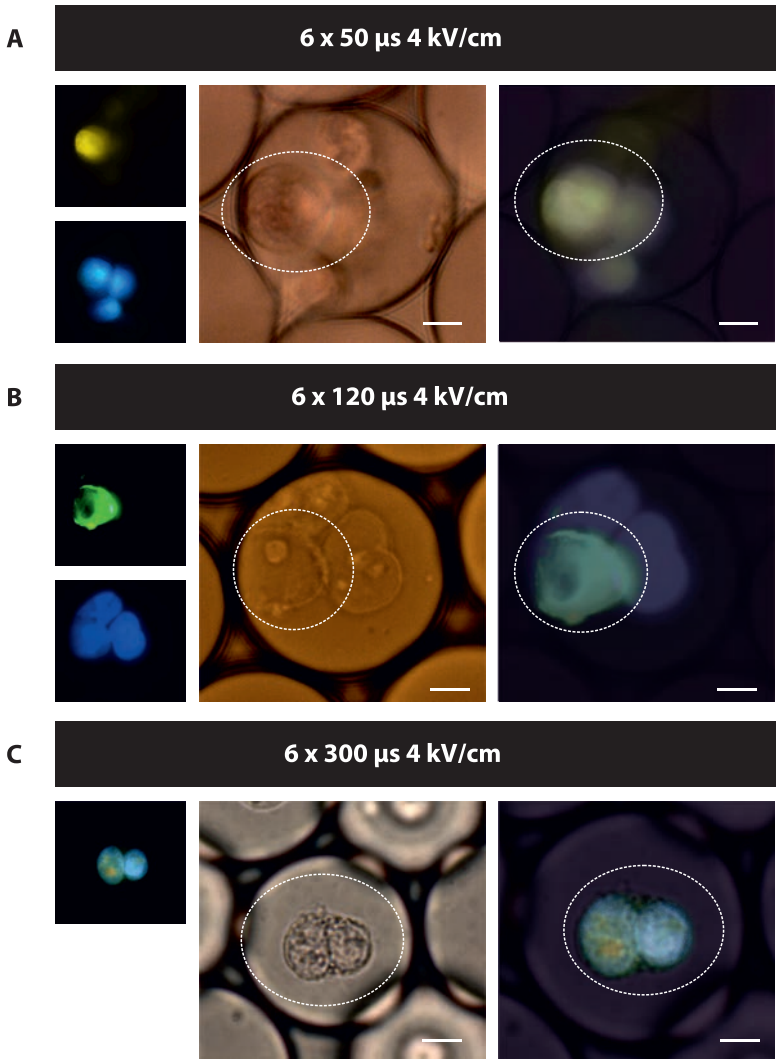

Figure 8.21: Electrofusion of HL60 cells in droplet after 6 successive pulses. Individual fluorescent (left), bright field (middle) and overlay (right) images are shown. A) pulses of 50 µs at 4 kV/cm. B) 120 µs pulses at 4 kV/cm. C) 300 µs pulses at 4 kV/cm. Scale bars are 10 µm.

To conclude this result section, we have shown for the first time electrofusion of cells in droplets. Before encapsulation, there were no cells with two differently fluorescently labeled nuclei. This indicates fusion of cells occurred inside the droplet. Furthermore, a negative control, so no pulse application, did not result in detectable cell fusion.

As shown in figure 8.21 different pulse lengths ranging from 50-300 µs at a constant field strength of 4 kV/cm resulted in electrofusion. These preliminary results do not give information about the influence of the pulse lengths on the electrofusion efficiency. Even though electrofusion in a droplet was established, our efficiency is still low (<0.1%;

<1 successful fusion out of 1000 counted cell containing droplets; n=3). And lower than both, commercially available methods (5 - 10%, different cell types or 40% cell fusion of similar cells) as well our static on-chip method, efficiency of 51 % [26] (chapter 4) and other on-chip methods[27-29] (up to 90% with similar cell types). However, it has to keep in mind that these electrofusion results are not performed in a droplet.

The main advantage of our method is the high-throughput aspect. Yet, to compete with existing methods, the electrofusion efficiency should be at least 10%. This 10% is based on the following method of argumentation.

Our ultimate aim is to fuse a B-cell with a myeloma cell in a droplet, to generate a hybridoma in a droplet. For this, we need two droplet generators. Two droplet generators with both one cell type (either a B-cell or a NS-1 cell) are encapsulating single cells at 77% efficiency at 2700 Hz (chapter 6). So, 5400 droplet are generated per second, of which 1620 droplets are correctly paired (60%=77% * 77%). As a result, 1500 droplets remain after droplet electrocoalescence and shrinkage. If in the next step, the electrofusion of the two encapsulated cells has an efficiency of 10%; this would result in 150 successful fusions per second. Running the device for 15 minutes, will result in 135.000 hybridomas. For this, we will need at the start of the experiment, two times 225 µl of cell suspensions (15 minutes at 15 µl/min) with a concentration for B-cells of around 9.5 x 10^7 cells/ml (1.7 % volume fraction, which ensures single cell encapsulation) and NS-1 cells of 9.7 x 10^6 cells/ml. These amounts of cells are feasible. If one would isolate B-cells from human peripheral blood the average amount of B-cells, in a normal population, is 7 x 10^5 cell/ml. So ~35 ml of peripheral blood is needed to isolate the desired amount of B-cells. If you then compare our droplet platform with the standard conventional fusion chamer, our method has great potential. In the conventional method using a fusion chamber, the volume ranges from 20 - 250 µl[30] with cell concentrations of 2 x 10^5 – 1 x 10^6 cells/ml of the fusion partner and 1 x 10^5 – 1 x 10^6 B-cells/ml.[21, 30-32]. Assuming that a total of 250 µl cell suspension is loaded in the fusion chamber, a maximum of 1.25 x 10^5 B-cells undergoes the electrofusion protocol. With a fusion efficiency approximately 10% for electrofusion of different cell types, 12.500 B cells would succesfully fuse. However, statistically 50% of these fusions would be with another B-cell, hence 6.250 hybridomas are generated. Additionally, the fusion process takes also about 15 minutes.

Hence, in theory, our droplet platform will, in the same time, result in a 21 times higher number of successful electrofused cells of different origin, in our case B-cells with NS-1 cells, and has therefore great potency.

8.4 Conclusion

In this chapter, a platform towards high-throughput electrofusion of cells in droplets was presented. HL60 cells were separately encapsulated, and subsequently paired and fused with respectively 100% and 95% efficiency, at a frequency over 1000 Hz. Additionally,

the droplet volume was reduced up to 75%. However, the shrinkage module needs to be optimized to ensure the desired volume reduction of 90-95%. To ensure that there is an electric field in a droplet, the electric field in the droplet was modeled with COMSOL and assessed by performing electroporation experiments. After six successive pulses of 166 µs at 4 kV/cm, 86% of the cells in the droplets were PI+, which indicates that the membrane was (ir)reversibly electroporated. To assess the viability, and state that the pulses do not harm the cells, one should use fluorescently labeled plasmids, for example GFP labeling

Finally, for the first time, electrofusion of HL60 cells in a droplet was demonstrated. Even though, the efficiency was still very low (<0.1%), the feasibility of electrofusion in a droplet was shown. There are opportunities for improvement and optimization, for example improving the shrinkage module and hence enhancing the cell-cell contact in the droplet. Moreover, the electrode configuration can be optimized. As shown in figure 8.12, there are many cell positions possible, in which the cells are not perpendicularly positioned in the electric field, and therefore not optimal for cell fusion to occur Instead of using planar electrodes, a 3D electrode structure can be used to generate a homogeneous electric field along the channel wall. Or a combination of arrays (interlaced; oppositely placed: 3D along channel wall), to ensure that the cell pair does undergo the electric field in optimal position. Overall, the obtained results provide a valuable tool to realize a platform for efficient high-throughput electrofusion of cells in droplets, which can definitely compete with the existing conventional methods. Moreover, this platform is not restricted to cell fusion and is applicable for various other cell-based assays such as single cell analysis and differentiation assays.

8.5 References

1. Joensson, H.N. and H.A. Svahn, *Droplet Microfluidics-A Tool for Single-Cell Analysis.* Angewandte Chemie-International Edition, 2012. **51**(49): p. 12176-12192.
2. Qu, B., et al., *Droplet electroporation in microfluidics for efficient cell transformation with or without cell wall removal.* Lab on a Chip, 2012. **12**(21): p. 4483-4488.
3. Clausell-Tormos, J., et al., *Droplet-based microfluidic platforms for the encapsulation and screening of mammalian cells and multicellular organisms (vol 15, pg 427, 2008).* Chemistry & Biology, 2008. **15**(8): p. 875-875.
4. Clausell-Tormos, J., et al., *Droplet-based microfluidic platforms for the encapsulation and screening of mammalian cells and multicellular organisms.* Chemistry & Biology, 2008. **15**(5): p. 427-437.
5. Yang, Y.J., et al., *Generation of sub-femtoliter droplet by T-junction splitting on microfluidic chips.* Applied Physics Letters, 2013. **102**(12).

6. Hung, L.H., et al., *Controlled droplet fusion in microfluidic devices.* Micro Total Analysis Systems 2004, Vol 2, 2005(297): p. 539-541.
7. Seemann, R., et al., *Droplet based microfluidics.* Reports on Progress in Physics, 2012. **75**(1).
8. Niu, X., et al., *Pillar-induced droplet merging in microfluidic circuits.* Lab on a Chip, 2008. **8**(11): p. 1837-1841.
9. Chabert, M., K.D. Dorfman, and J.L. Viovy, *Droplet fusion by alternating current (AC) field electrocoalescence in microchannels.* Electrophoresis, 2005. **26**(19): p. 3706-3715.
10. Ahn, K., et al., *Electrocoalescence of drops synchronized by size-dependent flow in microfluidic channels.* Applied Physics Letters, 2006. **88**(26).
11. Frenz, L., et al., *Microfluidic Production of Droplet Pairs.* Langmuir, 2008. **24**(20): p. 12073-12076.
12. Gu, H., et al., *A microfluidic platform for on-demand formation and merging of microdroplets using electric control.* Biomicrofluidics, 2011. **5**(1).
13. Zagnoni, M., G. Le Lain, and J.M. Cooper, *Electrocoalescence Mechanisms of Microdroplets Using Localized Electric Fields in Microfluidic Channels.* Langmuir, 2010. **26**(18): p. 14443-14449.
14. Zagnoni, M., C.N. Baroud, and J.M. Cooper, *Electrically initiated upstream coalescence cascade of droplets in a microfluidic flow.* Physical Review E, 2009. **80**(4).
15. Song, H., J.D. Tice, and R.F. Ismagilov, *A microfluidic system for controlling reaction networks in time.* Angewandte Chemie-International Edition, 2003. **42**(7): p. 768-772.
16. Menetrier-Deremble, L. and P. Tabeling, *Droplet breakup in microfluidic junctions of arbitrary angles.* Physical Review E, 2006. **74**(3).
17. Luo, C.X., et al., *Picoliter-volume aqueous droplets in oil: Electrochemical detection and east electroporation.* Electrophoresis, 2006. **27**(10): p. 1977-1983.
18. Xiao, K., et al., *Electroporation of micro-droplet encapsulated HeLa cells in oil phase.* Electrophoresis, 2010. **31**(18): p. 3175-3180.
19. Zhan, Y.H., et al., *Electroporation of Cells in Microfluidic Droplets.* Analytical Chemistry, 2009. **81**(5): p. 2027-2031.
20. Barbulovic-Nad, I., et al., *Digital microfluidics for cell-based assays.* Lab on a Chip, 2008. **8**(4): p. 519-526.
21. Steenbakkers, P.G.A., H.A.J.M. Hubers, and A.W.M. Rijnders, *Efficient Generation of Monoclonal-Antibodies from Preselected Antigen-Specific B-Cells - Efficient Immortalization of Preselected B-Cells.* Molecular Biology Reports, 1994. **19**(2): p. 125-134.

22. Schoeman, R.M., et al., *High-throughput deterministic single cell encapsulation and droplet pairing, fusion and shrinkage in a single microfluidic device.* Electrophoresis, 2013.
23. Brouzes, E., et al., *Droplet microfluidic technology for single-cell high-throughput screening.* Proceedings of the National Academy of Sciences of the United States of America, 2009. **106**(34): p. 14195-14200.
24. Fox, M.B., et al., *Electroporation of cells in microfluidic devices: a review.* Analytical and Bioanalytical Chemistry, 2006. **385**(3): p. 474-485.
25. Zimmermann, U., et al., *Electromanipulation of mammalian cells: Fundamentals and application.* Ieee Transactions on Plasma Science, 2000. **28**(1): p. 72-82.
26. Kemna, E.W.M., et al., *On chip electrofusion of single human B cells and mouse myeloma cells for efficient hybridoma generation.* Electrophoresis, 2011. **32**(22): p. 3138-3146.
27. Kirschbaum, M., et al., *Highly controlled electrofusion of individually selected cells in dielectrophoretic field cages.* Lab on a Chip, 2012. **12**(3): p. 443-450.
28. Skelley, A.M., et al., *Microfluidic control of cell pairing and fusion.* Nature Methods, 2009. **6**(2): p. 147-152.
29. Techaumnat, B., et al., *High-yield electrofusion of cells using electric-field constriction.* 2007 International Symposium on Micro-Nano Mechatronics and Human Science, Vols 1 and 2, 2007: p. 38-43.
30. Sukhorukov, V.L., et al., *A biophysical approach to the optimisation of dendritic-tumour cell electrofusion.* Biochemical and Biophysical Research Communications, 2006. **346**(3): p. 829-839.
31. eppendorf, *operating manual multiporator basic*. 2006, eppendorf AG, Hamburg.
32. White, K.L., *Animal Cell Electroporation and Electrofusion Protocols* in *Methods in Molecular Biology* J.A. Nickoloff, Editor. 1995.

SUMMARY AND OUTLOOK

CHAPTER 9

This chapter contains the summary of the main results obtained during this PhD project. Subsequently, recommendations regarding new experimental designs are given and the potential of the droplet-based electrofusion platform is discussed.

9.1 Summary

In this thesis, the results of the development of two microfluidic devices (static and high-throughput) for efficient electrofusion of cells were described and evaluated. Electrofusion of cells is an important tool for generating antibody producing hybridomas. These hybridomas are the result of the fusion between a B-cell and a myeloma cell. The conventional method for generating hybridomas has a very low efficiency (typically around 0.001%). In combination with the increasing need for antibodies, this has motivated us to explore a more efficient method for generating hybridomas. In our opinion, microfluidic chips offer several advantages compared to the conventional systems.

First, the fundamentals of electrofusion and the behavior of cells in an electric field were discussed, followed by a review of the current status of on-chip electrofusion devices (chapter 2). Different electrofusion efficiencies in microfluidic devices were reported, ranging from 3 – 90%. However, only two studies showed fusion between myeloma cells and B-lymphocytes[1] or B-lymphoblast[2]. The latter shows a fusion efficiency of 30% and cell survival of 22%, after 3 days. No antibody production or nuclear fusion was assessed, leaving room for improvement. Criteria and requirements were set regarding our electrofusion chip for hybridoma generation. To generate hybridomas, it is of utmost importance to fuse exactly one B-cell with one myeloma cell. This means that the device has to be designed with an optimal electric field distribution regarding different sized cell fusion. Additionally, appropriate cell pairing is needed to promote cell fusion. In the static approach cell pairing is be achieved using cell traps (chapter 4) while the high-throughput droplet based method, focuses on deterministic cell encapsulation (chapter 6). Moreover, the fusion process has to be followed at a cellular level, with the use of fluorescent dyes, and the successful fusion products need to be harvested for further analysis

In chapter 3, different microfluidic designs and approaches were evaluated to select the methods and parameters, which best fit our criteria. Low-throughput electrofusion of HL60 cells was shown using a glass plate with two oppositely located electrodes. These initial experiments provided us already with a few insights into our set critical parameters. Platinum electrodes provided the DC pulses which, if needed, could be combined with an AC field. Furthermore, the use of a low conducting buffer prevents electrode degradation and heating during experiments. The use of a cytoplasmic dye is a good trade-off between being able to visualize the cell fusion and avoiding interference with the fusion process. The most critical part of the electrofusion device was the controlled cell pairing combined with the electric field distribution.

A microfluidic chip was designed, meeting the above mentioned criteria (chapter 4). The design, a static cell trap approach, was based on the work of Skelley et al.[1]. The cell traps were optimized for the electrofusion of single human peripheral blood B-cells and mouse myeloma (NS-1) cells. Moreover, the trap structure was designed such that it provides an optimal electric field distribution regarding cell fusion of different sized cells.

6 DC pulses of 100 µs (2.5 kV/cm) combined with an AC field (30 s, 2 MHz, 500 V/cm) and pronase treatment resulted in the highest electrofusion efficiency of paired cells (51 ± 11 %). Furthermore, hybridoma formation was observed after culturing the fused cells for 14 days in conditioned medium. Even though this is a good approach for characterization and optimizing B- and myeloma cell fusion on chip, it is not a high-throughput approach. Therefore, we choose to move to the microfluidic droplet platform to obtain high-throughput cell fusion (chapter 5-8).

The basis of a droplet microfluidic platform is the formation of monodisperse droplets using two immiscible fluids. In chapter 5, an overview was given of the different droplet generation geometries and manipulation techniques. Subsequently, the recent advances of the droplet platform for cell experimentation and analysis were discussed. Finally, the potential of using droplet microfluidics for cell electrofusion was assessed. We believe the droplet platform can greatly improve the current method for hybridoma generation and selection, while it also enables high-throughput single cell analysis within micrometer-sized droplets. Furthermore, droplets are physically and (bio)chemically isolated and can be generated, merged, and sorted at kHz rates, enabling high-throughput single cell experimentation and analysis.

The first component of the droplet-based platform for electrofusion of cells is cell encapsulation. To obtain high fusion efficiencies, it is important to generate large amounts of single cell containing droplets (chapter 6 and 7). Next, droplet fusion needs to be established to obtain a single droplet containing one B-cell and one myeloma cell. Subsequently, the most critical part of the electrofusion platform is the cell fusion inside a droplet using electrodes placed inside the main channel (chapter 8). For this, droplet shrinkage is applied to promote cell-cell contact during pulsing (chapter 8). The final part of the electrofusion platform is the culture of the fused cells (hybridomas) followed by selection of the functional hybridomas (outlook).

Random encapsulation, dictated by the Poisson distribution, has a low encapsulation efficiency of single cells (37%). To overcome this problem, a curved microchannel for efficient single cell encapsulation was designed. The curved microchannel utilizes inertial forces in combination with Dean forces to push the cells into equilibrium positions. Combining this cell ordering module with a droplet generator resulted in high-throughput (2700 Hz) single cell encapsulation with efficiencies towards 77%. However with this method, it was (till now) not possible to obtain 100% encapsulation efficiency of single cells. To obtain only droplets containing one cell, the droplets of interest need to be sorted. Conventionally, this involves cell labeling, which is laborious and not suitable for long-term culture. Hence, label-free detection of cells in droplets is desired. Thus far, no label-free, integrated single cell detection method in droplets is available. In chapter 7, a microfluidic set-up, for novel, fast (>100Hz) and label-free impedance based detection of cells in droplets, was presented. At a measurement frequency of 100 kHz, we demonstrated that the presence of a viable cell in a droplet containing low-conducting buffer decreased the electrical impedance. Additionally, no

impedance change was detected when empty droplets or droplets containing non-viable cells passed the electrode pair. Therefore, droplets containing viable cells can be discriminated from empty droplets, as well as droplets containing non-viable cells. These results provide us with a valuable method to label-free detect and select (viable) cells in droplets.

Chapter 8 focuses on the modules needed for cellular electrofusion in a droplet: droplet pairing, droplet fusion, droplet shrinkage and cell electrofusion in a droplet. All components, besides the latter one, were previously described in literature. Our goal is to optimize these components for optimal integration in our electrofusion platform. First, cells were deterministically encapsulated, and the droplets subsequently paired and fused. High-throughput droplet electrocoalescence (>1000 Hz) was obtained, with an efficiency of 95%. The droplet volume needs to be reduced with 90 - 95% of its original volume to ~10-22.5 pL, to initiate cell-cell contact in the droplet. Stable volume reduction was demonstrated using either three separate side channels (volume reduction of 48%) or using a 'pitch fork structure' (volume reduction of 75%). Simulation experiments were performed to gain insight in the behavior of the electric field in a droplet at t=0. The electric field in the droplet can be estimated using this simulation. One electrode was set to ground, the other electrode had a potential of 8 V. The field strength in the area of the cells was ~3.5 kV/cm. This indicated that the field strength experienced by the encapsulated cells at t=0, is theoretically sufficient for electrofusion to occur, based on previous results. Next, the process of electroporation of the cell membrane in a droplet was evaluated. Results showed that after six successive pulses of 166 µs at 4 kV/cm, 86% of the cells in the droplets were positive for the fluorescent dye propidium iodide (PI), which states that the membrane was (ir)reversibly electroporated. Moreover, this confirmed that the electric field applied outside the droplet, could pass the droplet and affect the cells inside the droplet.

Finally, for the first time, successful electrofusion of two HL60 cells in a droplet was shown, in detail, using fluorescent membrane and nuclear dyes. For this, six successive pulses of 4 kV/cm with pulse lengths ranging from 50-300 µs were applied These results ascertain the feasibility of electrofusion of cells in droplets, albeit so far with low efficiency (<0.1%). There are opportunities for improvement, such as droplet shrinkage, electrode configuration and pulse settings (outlook).

Overall, we have demonstrated, to our knowledge for the first time, that successful single cell electrofusion is principally possible in the droplet platform. The obtained results presented in this thesis provide a basis to realize a platform for efficient high-throughput electrofusion of cells in droplet-based microfluidic devices, which can definitely compete with the existing conventional fusion methods.

9.2 Outlook

Based on the results shown in this thesis, it can be concluded that microfluidic devices are extremely useful tools for performing and characterizing cell electrofusion.

Moreover, the use of droplets for achieving high-throughput electrofusion of cells seems promising.

The experiments described in this thesis can be improved and/or adapted in a variety of ways to obtain better results. Below several issues are discussed.

Pre-selection of B-cells

Literature suggest a role for preselection of the right B-cells. This can result in increased functional hybridoma efficiency[3]. This part of the electrofusion process is a new area with a broad scala of possibilities. Instead of general a-specific stimulation, one can choose specific stimulation before on-chip electrofusion to increase hybridoma generation efficiency[3]. Furhtermore, specific B-cells (generating the desired antibodies) could be directly isolated from peripheral blood on chip, for subsequent on-chip electrofusion.

Cell treatment

Another parameter to optimize in future experiments would be the cell treatment before the electrofusion experiment. For example, a (short) hypotonic treatment of the cells before electrofusion can result in higher fusion efficiencies[4]. In theory the hypotonic buffer can be added using a pico-injector, incubate in a reservoir to subsequently move the droplet to the main channel and remove the buffer using a shrinkage module.

Single cell encapsulation

The flow rates, which are used in the continious curved microchannel (chapter 6) are relativly high and combined with a high volume fraction. For certain applications (*e.g.* low abundancy of cells), it is desired to use lower flow rates, while keeping the high single cell encapsulation efficiency. When using a discontinious curved microchannel, results showed that cells order at flow rates of 5-10 µl/min[5], which is a factor 1.5-3 lower.

Droplet pairing

Droplet pairing using the double T-junction (chapter 8) should be incorporated in future devices aiming for combining two droplets with different content. Another option would be to generate and subsequently reinject one droplet population. However, when using low conducting electrofusion buffer, this would time-wise not be optimal (after 90 minutes cell degradation).

Electrofusion in a droplet

The droplet shrinkage module should be optimized regarding the resistance of the main channel compared to the singular side channels, to obtain the desired droplet volume for electrofusion of cells. Also the number of side channels needs to be optimized (more side channels). As shown in figure 8.12, it is of importance to have an optimal electric field distribution for successful electrofusion. Therefore it would be of interest to use 3D

electrode structures, in the next generation of electrofusion devices, for a better distribution of the electrical field in the droplet.

Hybridoma selection

If efficient and successful electrofusion of cells in droplets is realized, it would be of great interest to combine it with on-chip selection of hybridomas. After electrofusion of cells in droplets, the electrofusion buffer needs to be removed or diluted using selection medium. This can be accomplished by adding 5 times the original droplet volume using a pico-injector. The cells in the droplet should be incubated in this medium for 30 min. Subsequently, cells could be retrieved from the droplet to continue conventional off-chip culturing, or cultured in droplets. This method offers the possibility to add a detection module using fluorescence[6], or impedance (chapter 7), to detect and subsequently select the functional hybridomas.

After this label-free or fluorescence based detection of the droplets of interest, it is of importance to select the droplets of interest. This selection module is a significant contribution of the microfluidic technology to the electrofusion device. Currently the sorting module is mostly based on the application of DEP force[7]. It would be of interest to use micro patterning for the precise location of these DEP inducing electrodes at the junction to allow for high-throughput droplet selection.

Overall, there are opportunities to culture the fused cells in droplets and combine this with detecting the antibody production[6] and select those droplets containing the hybridomas of interest.

Additional applications

The described platform in chapter 8 (without the electrofusion component), has many future applications in all other kinds of single cell related research. Especcialy in research areas were it is desired to mix cell types in droplets in a deterministic fashion. For example in applications were cells are not abundant (e.g. stem cell research) or were single cell encapsulation is of high importance (e.g. cell loaden microgels[8]).

Concluding, on-chip electrofusion of cells was demonstrated in both a static and high-througput fashion. The obtained results provide a valuable tool to realize a platform for efficient high-throughput electrofusion of cells in droplets. In the outlook different leads and starting points are described for improving the current electrofusion efficiency. The principal advances regarding electrofusion efficiency, lie within the pretreatment of the cells, the droplet shrinkage and the electrode configuration. Therefore, complementary research is necessary before high-throughput fusion in droplet will be able to compete with existing conventional fusion techniques.

9.3 References

1. Skelley, A.M., et al., *Microfluidic control of cell pairing and fusion*. Nature Methods, 2009. **6**(2): p. 147-152.
2. Kirschbaum, M., et al., *Highly controlled electrofusion of individually selected cells in dielectrophoretic field cages*. Lab on a Chip, 2012. **12**(3): p. 443-450.
3. Steenbakkers, P.G.A., H.A.J.M. Hubers, and A.W.M. Rijnders, *Efficient Generation of Monoclonal-Antibodies from Preselected Antigen-Specific B-Cells - Efficient Immortalization of Preselected B-Cells*. Molecular Biology Reports, 1994. **19**(2): p. 125-134.
4. Usaj, M., et al., *Cell-cell electrofusion: optimization of electric field amplitude and hypotonic treatment for mouse melanoma (B16-F1) and Chinese Hamster ovary (CHO) cells*. J Membr Biol, 2010. **236**(1): p. 107-16.
5. Schoeman, R.M., et al., *High-throughput deterministic single cell encapsulation and droplet pairing, fusion and shrinkage in a single microfluidic device*. Electrophoresis, 2013.
6. Mazutis, L., et al., *Single-cell analysis and sorting using droplet-based microfluidics*. Nature Protocols, 2013. **8**(5): p. 870-891.
7. Agresti, J.J., et al., *Ultrahigh-throughput screening in drop-based microfluidics for directed evolution*. Proceedings of the National Academy of Sciences of the United States of America, 2010. **107**(9): p. 4004-4009.
8. S.J. Henke, J.C.H.L., G. Marchioli, E.W.M. Kemna, A. van den Berg, P.J. Dijkstra, A.A. van Apeldoorn and M. Karperien. *Microgels for Tissue Engineering*. in *Dutch Biomaterials and Tissue Engineering Association*. 2012.

Samenvatting

Antilichamen spelen een belangrijke rol in het leven. Niet alleen binnen ons lichaam, als afweer tegen ziekteverwekkers zoals bacteriën en virussen maar ook buiten ons lichaam voor de preventie en behandeling van allerlei ziektes, zoals reuma en kanker. Door de vele toepassingen is er een grote en steeds toenemende vraag naar antilichamen. Er is dus behoefte om technieken te ontwikkelen voor efficiënte antilichaam productie. Normaliter kunnen antilichaam-producerende cellen (B-cellen) niet lang overleven in kweek. Om deze reden is er een methode ontwikkeld in de jaren '70, namelijk het fuseren van een B-cel met een kanker cel (myeloma cel). Na cel fusie ontstaat er een hybridoma met de eigenschappen van de oorspronkelijke cellen en hebben na fusie 'the best of both worlds': 1. Ongeremde celdeling 2. Antilichaamproductie. Dit antilichaam kan dan o.a. voor therapeutische doeleinden gebruikt worden. De fusietechniek die het meeste wordt toegepast is de elektrofusie van cellen. Hierbij worden twee cellen dicht bij elkaar gebracht en krijgen dan een of meerdere korte DC pulsen van hoge intensiteit. Als gevolg ontstaan er poriën in het celmembraan (electroporatie) en zullen de twee cellen fuseren (hybridoma). Met de huidige elektrofusie-technieken in fusiekamers is het mogelijk om B-cellen met kankercellen te fuseren, echter de fusie-efficiëntie is erg laag (~0.001%), dat wil zeggen dat er weinig hybridoma's gevormd worden. Eén van de redenen daarvoor is de willekeurigheid waarmee de cel paring optreedt. Naar onze mening kan een lab-on-a-chip systeem deze fusie-efficiëntie sterk verbeteren vergeleken met het conventionele systeem. In dit proefschrift worden de resultaten besproken van de ontwikkeling van twee microfluidische systemen (statisch en high-throughput) voor efficiënte electrofusie van cellen.

Eerst wordt de basis van de electrofusie techniek en het gedrag van cellen in een elektrisch veld besproken, gevolgd door een review over de huidige status van on-chip electrofusie systemen (hoofdstuk 2). Er worden criteria en eisen gesteld aan de electrofusie chip en bijbehorende parameters zoals buffers voor hybridoma generatie (hoofdstuk 3). Voor het genereren van hybridoma's is het erg belangrijk om één B-cel met één kanker cel te fuseren. Daarnaast moet de verdeling van het elektrische veld ook optimaal zijn, mede doordat het cellen zijn van verschillende grootte. Dit betekent dat het systeem moet worden ontworpen met optimale cel paring en goede elektrische veld verdeling. Het eerste, statische, ontwerp maakt gebruik van traps voor cel paring (hoofdstuk 4) en de high-throughput methode is gebaseerd op het gebruik van druppels voor cel paring (hoofdstuk 6-8). Daarnaast moet het fusie proces worden gevolgd op cellulair niveau met het gebruik van fluorescerende kleuringen en is het van belang om de succesvolle fusieproducten te kunnen vergaren voor verdere analyse.

In hoofdstuk 3 worden verschillende ontwerpen en aanpakken geëvalueerd om de beste methodes en parameters te selecteren. Low-throughput electrofusie van HL60 cellen is bewerkstelligd met behulp van een glas plaatje en twee tegenoverliggende elektrodes. Deze voorlopige experimenten gaf inzicht in een aantal parameters, zoals veldsterkte en buffer samenstelling. DC pulsen kunnen worden gegenereerd met platina

elektrodes, indien nodig gecombineerd met een AC veld. Daarnaast wordt er gebruik gemaakt van een laag geleidende buffer en is het gebruik van een cytoplasmatische kleuring een goede balans tussen visualisatie en minimale interferentie met het fusie proces. Het meest kritische onderdeel van het electrofusie systeem is de gecontroleerde cel paring in combinatie met de goede verdeling van het elektrische veld.
Het eerste systeem is ontworpen met behulp van traps (statisch) en voldeed aan de gestelde criteria (hoofdstuk 4). Het ontwerp was gebaseerd op het werk van Skelley et al. De cel-traps werden geoptimaliseerd voor electrofusie van één humane B-cel (uit perifeer bloed) en één muis kanker cel. Daarnaast geeft de trap structuur optimale verdeling van het elektrische veld. 6 DC pulsen van 100 µs (2.5 kV/cm) gecombineerd met een AC veld (30 s, 2 MHz, 500 V/cm) en pronase behandeling resulteerde in de hoogste electrofusie efficiëntie van gepaarde cellen (51 ± 11 %). Vervolgens was er hybridoma formatie geobserveerd na het kweken van de fusieproducten voor 14 dagen in geconditioneerd medium. Dit ontwerp is een geschikte methode om fusie te karakteriseren, maar het is geen high-throughput methode. Daarom is er voor gekozen om met behulp van het druppel platform high-throughput fusie te realiseren (hoofdstuk 5-8).

De basis van het druppel platform is de generatie van monodisperse druppels met behulp van twee niet-mengende vloeistoffen. Dit maakt high-throughput single cel experimentatie en analyse mogelijk. In hoofdstuk 5 wordt een overzicht gegeven van de verschillende methodes om druppels te genereren en manipuleren. Vervolgens worden de laatste resultaten besproken met betrekkong tot het druppel platform en cel experimentatie. Als laatste wordt de potentie van het druppel platform voor electrofusie van cellen geëvalueerd. Wij geloven dat het druppel platform de huidige methode van hybridoma generatie en selectie sterk kan verbeteren. Druppels zijn biochemisch gescheiden reactie containers en kunnen worden gegenereerd, gefuseerd en gesorteerd met kHz snelheden. Het eerste onderdeel van het druppel platform voor electrofusie van cellen is de cel encapsulatie. Om hoge fusie efficiënties te bereiken is het van belang om hoge percentages druppels te genereren welke één cel bevat (hoofdstuk 6 en 7). Vervolgens moeten druppels worden gefuseerd om één druppel te krijgen met beide cel types. Daarna komt het meest kritische onderdeel aan bod, de cel fusie in een druppel met behulp van elektrodes in het hoofdkanaal (hoofdstuk 8). Om cel fusie te bewerkstelligen wordt het volume van de druppel verkleind om cel-cel contact te bevorderen (hoofdstuk 8). Het laatste onderdeel is het kweken van de fusie producten (hybridoma's), gevolgd door de selectie van functionele hybridoma's (outlook).

Willekeurige encapsulatie van cellen wordt gedicteerd door Poisson distributie. Dit heeft tot gevolg dat het 37% van de druppels één cel bevat. Om dit probleem te tackelen, is er een circulerend ('curved') microkanaal voor efficiënte single cel encapsulatie ontworpen (hoofdstuk 6). In het circulerende microkanaal bestaan verschillende krachten, waaronder de netto lift kracht en de Dean kracht. De combinatie van deze krachten zorgt er voor dat de cellen worden geordend en in evenwichtsposities worden gedrukt. Het combineren van de cel ordening module met

een druppel generator resulteerde in high-throughput (2700 Hz) single cel encapsulatie efficiëntie van 77%.

Met de beschreven methode in hoofdstuk 6 was er geen 100% efficiëntie te bereiken. Om alleen maar druppels te verkrijgen met één cel, moeten de druppels worden geselecteerd. Conventioneel wordt dit gedaan met behulp van een laser. Maar hier is cel labeling voor nodig, dit is arbeidsintensief en niet optimaal voor celkweek op lange termijn. Daarom is label-free detectie van cellen in druppels gewenst. Tot nu toe is er geen label-free, geïntegreerde single cel detectie methode in druppels beschikbaar. In hoofdstuk 7 word de set-up voor een nieuwe, snelle (>100 Hz) en label-free impedantie gebaseerde detectie methode besproken. Bij een meet frequentie van 100 kHz, kan een levende cel in een druppel van laag geleidende buffer worden gedetecteerd door een verlaagde elektrische impedantie. Daarbij werd er geen impedantie verschil gemeten wanneer lege druppels of druppels met een dode cel de elektrodes passeerden. Hierdoor kunnen druppels met levende cellen worden onderscheiden van druppels die leeg zijn of een dode cel bevatten. Deze resultaten geven ons een waardevolle methode om met behulp van een label-free methode levende cellen in druppels te detecteren en selecteren.

Hoofdstuk 8 richt zich op de componenten die nodig zijn om cel fusie in een druppel te bewerkstelligen: druppel paring, druppel fusie, druppel krimping en electrofusie van cellen in een druppel. Alle componenten, behalve de laatste, zijn eerder beschreven in de literatuur. Ons doel is om de componenten te optimaliseren voor optimale integratie ons electrofusie systeem. Allereerst worden de cellen deterministisch ge-encapsuleerd (hoofdstuk 6), vervolgens worden de druppels gepaard en gefuseerd. High-throughput druppel fusie werd bereikt met electrocoalescence (>1000 Hz) met een efficiëntie van 95%. De druppel volume moet worden gereduceerd tot 5-10% (~10-22.5 pL) van het originele volume cel-cel contact in the druppel te verkrijgen. Stabiele volume reductie werd gedemonstreerd door gebruik van afzonderlijke zijkanalen (volume reductie van 48%) of met behulp van een 'hooivork structuur' (volume reductie van 75%). Simulaties zijn uitgevoerd om inzicht te krijgen in het verloop van het elektrische veld op t=0. Het aanwezige elektrische veld in de druppel kan op deze manier worden geschat. Vervolgens werd het electroporatie proces van de cel membraan in een druppel in een druppel geëvalueerd. Resultaten lieten zien dat na zes opeenvolgende pulsen van 166 µs en 4 kV/cm, 86% van de cellen in druppels PI positief waren. Dit laat zien dat de cel membraan (ir)reversibel geelectroporeerd was en dat het aangebrachte veld tussen de elektrodes een voldoende effect heeft op de ge-encapsuleerde cellen.

Als laatste is er, voor het eerst, succesvolle electrofusie van twee HL60 cellen in een druppel, in detail, met behulp van fluorescente kleuring, bewerkstelligd. Om dit te bereiken waren er zes opeenvolgende pulsen van 4 kV/cm met een puls lengte van 50-300 µs toegepast. Deze resultaten benadrukken de haalbaarheid van electrofusie van cellen in druppels, al is het tot nu toe met lage efficiëntie (<0.1%). Er is veel ruimte voor verbetering, zoals verbeterde druppel krimping, de electrode configuratie en puls instellingen (outlook).

Concluderend hebben we, naar ons weten, voor het eerst laten zien dat electrofusie in een druppel mogelijk is. De verkregen resultaten in dit proefschrift geven een basis om een electrofusie platform te realiseren met hoge efficiënties, welke zeker de competitie aankan met huidige conventionele methodes.

List of publications

Journal articles

E.W.M. Kemna, F. Wolbers, I. Vermes, A. van den Berg. "*On chip electrofusion of single human B cells and mouse myeloma cells for efficient hybridoma generation*". Electrophoresis. **2011** Nov 32 (22) 3138-46. (selected for Lab on a chip research highlight) (chapter 4)

E.W.M. Kemna, R.M. Schoeman, F. Wolbers, I. Vermes, D.A. Weitz, A. van den Berg. *"High-yield cell ordering and deterministic cell-in-droplet encapsulation using Dean flow in a curved microchannel"*. Lab Chip. **2012** Aug 21 (16) 2881-7. (top ten most accessed June 2012) (chapter 6)

R.M. Schoeman, E.W.M. Kemna, F. Wolbers, A. van den Berg. *"High-throughput deterministic single cell encapsulation and droplet pairing, fusion and shrinkage in a single microfluidic device"*. Electrophoresis. **2013** Jul 15. (chapter 8)

E.W.M. Kemna, L.I. Segerink, F. Wolbers, I. Vermes, A. van den Berg. *"Label-free, high-throughput, electrical detection of cells in droplets"*. **2013** Aug 21 (16) 4585-92. (chapter 7)

E.W.M. Kemna, R.M. Schoeman, F. Wolbers, A. van den Berg. *"Electrofusion of cells in droplets"*. Manuscript in preparation. (chapter 8)

S.J. Henke, J.C.H. Leijten, E.W.M. Kemna, A. van den Berg, P.J. Dijkstra, A.A. van Apeldoorn and M. Karperien. *"Enzymatically Crosslinked Dextran-Tyramine Microgels for Tissue Engineering"*. Manuscript in preparation.

Conference contributions

Oral

E.W.M. Kemna, L.I. Segerink, M. Odijk, F. Wolbers, I. Vermes and A. van den Berg. *"Label-free, high throughput electrical detection of cells in droplets"*. 16th International Conference on Miniaturized Systems for Chemistry and Life Sciences, October 28 - November 1, **2012**, Okinawa, Japan. ISBN: 978-0-9798064-5-2. (chapter 7)

R.M. Schoeman, E.W.M. Kemna, F. Wolbers, A. van den Berg. *"Deterministic single cell encapsulation and droplet fusion, shrinkage and sorting in a single microfluidic device"*. NanoBioTech Montreux **2012**. (chapter 8)

Poster

E.W.M. Kemna, F. Wolbers, I. Vermes and A. van den Berg. *"Electrofusion of cells on chip"*, MesaPlus, september **2010**, Enschede. (chapter 4)

E.W.M. Kemna, F. Wolbers, I. Vermes and A. van den Berg. *"Electrofusion of cells on chip"*, MicroNanoConference, November **2010**, Enschede. (chapter 4)

E.W.M. Kemna, R.M. Schoeman, L.I. Segerink, F. Wolbers, I. Vermes and A. van den Berg. *"Towards a high-throughput electrofusion platfrom using droplets: cell detection and deterministic encapsulation",* 15th International Conference on Miniaturized Systems for Chemistry and Life Sciences, October 2-6, **2011**, Seattle, Washington, USA. ISBN: 978-0-9798064-4-5. (chapter 6 and 7)

E.W.M. Kemna, R.M. Schoeman, L. M. Griep, F. Wolbers, B. de Wagenaar, P. M. ter Braak, J. -P. Frimat, E. Westein, M. J. E. Kuijpers, I. Vermes, A.D. van der Meer, V. V. Orlova, P. ten Dijk C. L. Mummery, D. A. Weitz, J.W. M. Heemskerk and A. van den Berg, *"Microfluidic technologies for organs-on-chip"*. Mesa plus, september **2013**, Enschede

S.J. Henke, J.C.H. Leijten, G. Marchioli, E.W.M. Kemna, A. van den Berg, P.J. Dijkstra, A.A. van Apeldoorn and M. Karperien. *"Microgels for Tissue Engineering"*, Jaarlijkse congres van de Nederlandse vereniging voor Biomaterialen en Tissue Engineering (Dutch Biomaterials and Tissue Engineering Association), dec **2012**, Lunteren.

R.M. Schoeman, E.W.M. Kemna, F. Wolbers, I. Vermes and A. van den Berg. *"Towards electrofusion on chip using droplets",* MicroNano Conference Ede **2013**

Lectures

F. Wolbers, E. Kemna *"Lab-on-a-chip for biomedical applications"*, Massachusetts Institute of Technology, June **2011**, Boston, VS.

E.W.M. Kemna, R.M. Schoeman, F. Wolbers, A. van den Berg. *"Towards A High-Throughput Electrofusion Platform For Antibody Production Using Droplets"*, University of Lyon, March **2012,** Lyon, France.

R.M. Schoeman, E.W.M. Kemna, F. Wolbers, A. van den Berg. "*Microfluidic platform towards electrofusion of cells in droplets",* Mesa plus September **2013,** Enschede**.**

Dankwoord

Ja, je bent bij de juiste pagina beland, het dankwoord. Volgens mij het meest gelezen gedeelte van (bijna) elk proefschrift. Dit is mijn kans om iedereen te bedanken die een bijdrage heeft geleverd aan dit proefschrift, op welke wijze dan ook, in de afgelopen jaren. En ik waarschuw je, dit zijn er veel en het is dus ook een flinke lap tekst. Ik weet niet waar ik moet beginnen en begin dus maar gewoon met schrijven.

Allereerst komt degene zonder wie dit proefschrift nooit tot stand was gekomen, namelijk mijn assistent-promotor Floor. Wat was je een rots in de branding tijdens de afgelopen jaren. Ik kon altijd bij je langskomen als ik er niet uit kwam en verwarde toestand het overzicht kwijt was. Je liet me m'n eigen beslissingen maken, maar stuurde aan waar nodig. Onze overleggen en discussies onder het genot van een kop thee of koffie waren gewoonweg leuk en goed! Je kunt mensen motiveren en het beste naar boven halen, dit is iets wat ik in de afgelopen jaren heb gewaardeerd. Jou positieve kijk op zaken maakte dat ik altijd weer met plezier richting de UT ging! Je hebt me zoveel geleerd, niet alleen binnen het onderzoek maar ook daarbuiten. En ik weet niet meer hoe vaak je de hoofdstukken van dit proefschrift wel niet hebt doorgelezen, maar je was onverwoestbaar (en bleef bovenal zeer perfectionistisch). Ongelooflijk bedankt voor alles!!

Beste Albert van den Berg, het is inmiddels bijna 5 jaar geleden dat ik jou BIOS leerde kennen. Ik ben erg blij dat ik de afgelopen jaren binnen deze groep mocht werken. De kansen en vrijheid die je me hebt geboden binnen het project en deze geweldige groep waardeer ik enorm. Tijdens overleggen kwam je vaak met de wildste en beste ideeën, waardoor ik weer maanden, dan wel jaren vooruit kon. Je enthousiasme en kritische blik op alles in de afgelopen jaren was enorm motiverend. Daarnaast waren er natuurlijk ook nog niet werk geralateerde bezigheden, zoals de jaarlijkse barbecue, kerstdiner, sinterklaasmiddag en bovenal de twee werkweken die ik mocht meemaken! Kortom bedankt voor alles!

István Vermes, jij hebt mijn passie voor onderzoek, biologie, chemie en techniek tijdens mijn studie flink aangewakkerd. Jou positiviteit en geloof in mij heeft me in de afgelopen jaren enorm gestimuleerd om het beste uit mezelf te halen. Eerst tijdens mijn stage in Budapest en het MST, daarna tijdens m'n PhD project en nu tijdens de opleiding tot klinisch chemicus nog steeds. Bedankt voor je enthousiasme en steun in de afgelopen jaren!

Loes, bedankt dat je m'n paranimf bent, het is een fijn gevoel dat je ook straks op het podium staat. En wat breng jij een eerlijkheid en vrolijkheid met je mee. Samen in het cel lab meezingen (nou ja bléren) of serieuze impedantie experimenten uitvoeren, karaoke in Japan, een daghap met Floor, alles was even gezellig! Bedankt voor de afgelopen jaren! Paul, de altijd goedgehumeurde goedlachse roomie en tevens paranimf tijdens de verdediging. Je ben altijd vrolijk en dat werkt aanstekelijk. Af en toe even lekker hard de muziek aan (misschien worden we ooit nog ontdekt als Roxette 2.0). Je hebt me altijd geholpen als cellen zich onverklaarbaar gedroegen, kleuringen onzichtbaar waren of ik ruzie had met de microscoop. Met name op het eind van het project en ik niet meer veel in het lab was, was de hulp erg welkom, bedankt! Mathieu, m'n andere roomie, altijd in voor een discussie of goed gesprek. Je was een luisterend oor de afgelopen jaren. Jou kennis van de electrotechniek en kritische kijk heeft geleid tot vele inzichten. Bedankt voor al je hulp! Ad ook jij hebt geholpen met de zware materie rondom hardcore electrotechniek, met name het 'kastje' voor de impedantie metingen was een schot in de roos, waarvoor dank! Dan Johan, de rustige, maar oh zo gedreven technicus binnen BIOS. Jij hebt in de clean room veel devices gemaakt voor mij en je had altijd tijd voor het doorspreken van een nieuw idee of ontwerp, dank hiervoor! De microscoop opstelling die ik alle jaren heb gebruikt is mede tot stand gekomen door Jan de microscoopman en door Hans, een creatieve duizendpoot. Jan, ik ga je verhalen missen... En hou de rust en eet geen mandarijnen uit blik of pijnboompitten ☺ Hans er is geen moppentapper zoals jou, de kip met de drie poten vergeet ik nooit meer! Jan E met jou kritische blik heb je mij in de afgelopen jaren vaak voorzien goede adviezen en ideeën, bedankt hiervoor! Dan is er natuurlijk nog Hermine, mijn dank is groot voor alle logistieke en administratieve dingen die je altijd maar weer regelt. Zonder jou was het een grote chaos!

Dan zijn er in de afgelopen jaren natuurlijk nog studenten geweest, bedankt Gerrit en Bastiaan. In het bijzonder wil ik Rogier bedanken, je hebt het project de duw gegeven die het nodig had toen je hier begon als master student. Ik hoop dat je toen net zo veel van mij hebt geleerd als ik van jou. Jij hebt een creatieve geest en denkt buiten de gezette paden. Deze eigenschappen kun je nu volop benutten tijdens je PhD bij BIOS. Ik wens je dan ook ontzettend veel succes! Sieger, het was leuk om samen te werken aan je project voor microgels, als masterstudent en nu als PhD student bij Developmental BioEngineering. Bedankt en succes in de toekomst!

Het organiseren van de werkweek was ook een bijzonder voorrecht. Samen met Maarten, Paul en Lingling was het een doel op zich om iedereen Amerika binnen te krijgen en bovenal, iedereen weer veilig terug. Dit is gelukt, zoals we vaak zeiden, 'we did not loose anyone!'. Het was een voorrecht om dit samen met jullie te organiseren, bedankt! (although I am still waiting for the beamer ☺)

A large part of the work is done in the office, behind the desk. Therefore I also would like to thank all the roommates during the past years. Georgette and Songyue in the Hogekamp, always fun with the Chinese lessons! After moving to Carré I shared a room with Justyna, Songyue, Lonneke and Maarten, thanks for being such good roommates! The last (packed) room I shared with Paul and Mathieu. Even though I was there half of the time, I had a great time, thanks!

Off course BIOS has many more group members (past and present) whom I would like to thank for the great time en work environment for the past years. Thanks, Eddy, Wouter O., Wouter S., Egbert, Laura, Lennart, Verena, Severine, Edwin, Yawar, Trieu, Mingliang, Lingling, Songyue, Sertan, Arpita, Allison, Wei-Shu, Fleur, Henriette, Loan, Rerngchai, Andries, Floris, Jean-Philippe, Adithya, Ganesh, Iris, Susan, Alexander, Natalja, Sourav, Wesley, Masood, Burcu, Liza, Zhenxia and Yanbo.

Also thanks to the group of Prof. Weitz at Harvard for giving me the opportunity to work in your group for a couple of months, it was an amazing experience. Moreover, it was great getting to know the people in your group and be part of the enthusiastic work environment, thank you!

Ook wil ik graag m'n nieuwe collega's bij het MST/Medlon bedanken voor de kans die ik heb gekregen om mijn laatste jaar van m'n onderzoek te combineren met de opleiding tot klinisch chemicus. In het bijzonder wil ik ook mijn vorige opleider Frank vd Bergh en huidige opleidster Jennita Slomp bedanken, het vergt ook wat van jullie om dit 2-jarige part time traject tot een goed einde te brengen, bedankt voor jullie begrip! Ik kijk uit naar de rest van de opleiding en de dingen wat ik allemaal nog kan, mag en ga leren!

Tijdens de afgelopen jaren is het op momenten, met name de laatste twee jaar, wel eens druk geweest en dan is het belangrijk om ook goed te ontspannen. Daarom wil ik ook iedereen bedankt die daar aan heeft bijgedragen.

Allereerst mijn studiegenoten, Marjolein Pieter en Corianne. Ook al zien we elkaar niet veel de laatste tijd is het altijd fijn als we bij elkaar zijn en tot diep in de nacht te praten over alles wat ons bezighoudt, bedankt! Dit moeten we ook vasthouden in de toekomst!

Els en Sjoerd, jullie wil ik ook bedanken voor de ontspannende avonden van de afgelopen jaren en niet te vergeten het kano avontuur! Wat is het fijn om met jullie af te spreken, heerlijk te eten en kletsen over van alles en nog wat, ik zie uit naar jullie huwelijk!!

Sinds de basis- en middelbare school is er al groep meiden waarvoor ik dankbaar ben dat ik er een deel van uitmaak. Dit is mijn kans om jullie en natuurlijk 'de aanhang', Anne H, Annemiek en Tom, Mirthe en Jente, Marloes, Anne Ol en Micha te bedanken voor de super leuke avonden, feestjes, vakanties en weekendjes weg van de afgelopen jaren! De belangstelling en interesse en welkome afleiding, heef iemand nog een roddel of verhaal ☺!! Het is altijd raak als we bij elkaar zijn en er gebeurd altijd wat, bedankt!!! Ook al woont iedereen door het hele land, deze avonden en weekenden blijven. Marloes ook bedankt voor de hardloopochtendjes op zondag, heerlijk ontspannen m'n hoofd leegmaken. Al lopen we te langzaam, aangezien we nog flink kunnen kletsen tijdens het rennen!

Ook wil ik iedereen bedanken die ik zo'n tien jaar geleden heb leren kennen via Leon. Wat een heerlijke groep vrienden, Emmy, Coen, Harold, Marieke, Adriana, David, Aniek, Rick, Bertine, Michiel, Danny, Mirella, Marloes, Aapje, Anne, Coen, Maaike, Tom, Jarno, Henri, Natasja, Robin, Herbert, Evelin, Mark, Rian, Claes en Frederique. Bedankt voor de belangstelling en nog meer voor welkome afleiding tijdens de weekendjes weg, verjaardagen en kroegavondjes! Hopelijk straks ook weer iets meer tijd voor een kop thee Aniek (die film moet er nu toch echt een keer van komen!!) en culinaire avonden met Marieke, Bertine en Emmy of natuurlijk de tapas/sinterklaasavonden met de hele club meiden, dank!!

Daarnaast, Robert en Jenny ook bedankt voor de ontspannen avondjes (en dank voor het daadwerkelijk lezen van een aantal hoofdstukken voor het Engels, top!) Thomas en Diana, bedankt voor het heerlijke weekend weg in Antwerpen (die broek kost wel 50 bollekes ☺) en m'n eerste echte Volendam ervaring!

En het laatste gedeelte van mijn dankwoord gaat uit naar m'n familie. Ik wil hier dan ook mijn (schoon) familie, ooms, tantes, neven en nichten bedanken voor de betrokkenheid tijdens de afgelopen jaren. De altijd terugkerende vraag: "Hoe het gaat met de studie en wanneer ben je klaar?" Bedankt voor de alle belangstelling en interesse! In het bijzonder wil ik ook natuurlijk mijn schoonouders bedanken, Annie en André. Wat bof ik met zo'n schoonvader en moeder, altijd belangstellend, lief en behulpzaam waar jullie maar kunnen. Bedankt daarvoor!!

Mijn grootste dank gaat uit naar mij ouders. Pap en mam, bedankt voor de onvoorwaardelijke steun en liefde die ik, zolang ik me kan herinneren, heb mogen ontvangen. Jullie hebben me altijd de vrijheid en de kansen gegeven om te doen wat ik leuk vond. Zo heb ik flink wat sporten beoefend, heel veel musea gezien, maar bleef muziek, techniek en gezondheid mijn passie. Bij de open haard nog even kletsen als ik terug kwam van werk of avondje uit. Jullie zaten dan nog beneden muziek van the Who, Moody blues, Elvis of noem maar op, te luisteren, heerlijke herinneringen! Jullie hebben me geleerd om niet op te geven, te geloven in jezelf en ergens voor durven gaan, bedankt!! Dan is er natuurlijk nog mijn lieve grote zus, Carlijn. Vroeger hadden we wel eens wat onenigheid als jonge meiden, maar wat ben je een schat van een zus, bedankt daarvoor! Samen met Roy zijn jullie altijd geïnteresseerd en betrokken! En dan nog mijn allerliefste neefje Pim en nichtje en Wieke. Jullie zijn nog te jong om het te beseffen, maar jullie vrolijkheid, onbezorgdheid en liefde is zo fijn, bedankt dat ik jullie peettante mag zijn!

Nu ben ik echt aan het einde gekomen van mijn dankwoord en hier komt de meest bijzondere man in mijn leven, Leon. Je hebt af en toe heel wat te verduren gehad met mij…Ik kan wel kantjes vol schrijven, maar hoop dat de volgende boodschap de lading dekt. Jij maakt mij gelukkig, kunt me geruststellen en weer een duw in de goede richting geven als ik de weg kwijt ben. Ik leer nog altijd van jou, je creatieve geest en perfectionisme, je stimuleert me om het beste te zijn wat ik kan zijn, bedankt lieve Leon, ik hou van je!

Liefs,

Evelien